New Reactivity and Syntheses of Titanium Imide Complexes

Martin Slusarczyk

Wolfson College



Thesis submitted to the University of Oxford for the degree of Doctor of Philosophy in Inorganic Chemistry, December 2018.

The work described in this Thesis was carried out in the Chemistry Research Laboratory, University of Oxford from October 2015 to December 2018 under the supervision of Professors Andrew S. Weller and Philip Mountford. All work is my own unless stated to the contrary, and has not previously been submitted for any degree at this or any other university.



Martin Slusarczyk

December 2018

Abstract

This Thesis reports the synthesis and reactivity of titanium imide complexes. The dehydrocoupling of amines with boranes was studied as novel catalytic application of transition metal imides. A particular focus lies on the mechanism of the dehydrocoupling of dimethylamine-borane (DMAB). Additionally, synthetic routes to novel titanium borylimides were explored, as well as their reactivity in the activation of small molecules.

Chapter Two describes the dehydrogenative coupling of amine-boranes using cyclopentadienyl-amidinate supported titanium imido catalysts Cp*Ti{MeC(NMe)$_2$}(NR). The substrate scope of the systems are described, and several differently substituted amine-boranes are shown to be coupled efficiently. For the dehydrocoupling of DMAB, catalyst Cp*Ti{MeC(NMe)$_2$}(N^{t}Bu) (**2.1**) featured a turnover frequency of $TOF_{90\%} = 1600\ h^{-1}$ (RT, toluene, $[DMAB]_0$=0.38 M), the highest TOF number for any group 4 system to date. The focus of this Chapter lies on a detailed mechanistic study of the dehydrocoupling process using DMAB as model substrate. The study suggests a mechanism with a constant oxidation state of Ti(IV), and in which Cp*Ti{MeC(NMe)$_2$}(NR) represents the active species. Significantly, the catalysis features two distinct kinetic regimes which can be exploited to isolate $Me_2NH{\cdot}BH_2NMe_2{\cdot}BH_3$ (and it's deuterium labelled isotopologues) directly and *catalytically* from DMAB in high yields on the preparative scale.

Chapter Three describes the reactivity of one of the first known transition metal borylimide complexes, namely Cp*Ti(HPP){NB(NDippCH)$_2$} (**1.83**). To begin, the chemistry with a variety of terminal and internal alkynes will be explored. Terminal alkynes exclusively reacted *via* C-H bond activation since [2+2] cycloaddition is sterically disfavoured. Next, [2+2] cycloadditions followed by cycloreversions with the heterocumulenes CO_2, and isocyanates ArNCO, as well as their heavier thio-congeners CS_2, and ArNCS will be presented. Finally, the reactivity with a variety of small organic carbonyls will be discussed, including aldehydes, ketones, esters, as well as amides. Tolylaldehyde was found to undergo initial [2+2] cycloaddition followed by cycloreversion to form titanium dioxo complex [Cp*Ti(HPP)(μ-O)]$_2$ (**3.22**) as well as borylimide N(CHTol){B(NDippCH)$_2$} (**3.29**). By contrast, *enolisable* ketones and esters RC(O)C$\underline{H}_3$ featuring protons in α-position were shown to form titanium enolate species of type Cp*Ti(HPP-H){NB(NDippCH)$_2$}{OC(CH$_2$)R}. In the case of esters, where R = OR', these

titanium enolate species rearranged to release ketenes and form titanium alkoxy/aryloxy species Cp*Ti(HPP)(NH{B(NDippCH)$_2$})(OR').

Chapter Four describes a novel synthetic protocol to access titanium borylimides, namely the oxidative addition of borylazides N_3BR to a Ti(II) precursor, namely (Cp"$_2$Ti)$_2$(μ_2:η^1,η^1-N_2) (**1.16**). Three different examples of highly reactive, base-free titanium borylimide complexes of type Cp"$_2$Ti=NBR$_2$ could be prepared this way, specifically Cp"$_2$Ti=NB{N(Me)$_2$C$_6$H$_4$} (**4.11**), Cp"$_2$Ti=NB(NDippCH)$_2$ (**4.12**) and Cp"$_2$Ti=NBMes$_2$ (**4.1**). In contrast to the vast majority of borylimide complexes that feature two nitrogen atoms adjacent to the boron centre, Cp"$_2$Ti=NBMes$_2$ (**4.1**) features two aryl groups. The solid state structure and MO DFT calculations suggest only negligible π-interactions between the aryl groups and the boron based p-orbital, thus pointing to significant "Ti=N=B" cumulene character. Preliminary reactivity studies suggest Cp"$_2$Ti=NBMes$_2$ (**4.1**) to be more reactive towards small molecule activation than the previously studied Cp*Ti(HPP)(NB(NDippCH)$_2$) (**1.83**). Significantly, dihydrogen is activated rapidly under ambient conditions to form the titanium hydride amide Cp"$_2$Ti(H)N(H)BMes$_2$ (**4.21**). This complex is characterised by X-ray crystallography, representing the first structurally authenticated example of a titanium hydride amide.

Appendix contains the Frontier Molecular Orbitals of the $[Cp_2Ti]^{2+}$ fragment.

CD Appendix contains CIF files for all new crystallographically characterised complexes.

Acknowledgements

Firstly, I would like to thank Prof. Andrew S. Weller and Prof. Philip Mountford for the opportunity to study in Oxford, and for their support during my studies. My stay in Oxford was truly enriching, and I am grateful to have met so many extraordinary and vibrant people.

To the members of the Mountford group, a massive thanks for their invaluable support during the past three years. In particular, I would like to thank Dr Ben Clough and Dr Bowen Xie for their help and deep expertise in organometallic chemistry, and for the many successful (and unsuccessful) attempts to run crystals! My special gratitude also goes to the previous postdocs for their continous help to keep the lab running: Dr Insun Yu and Dr Matthew Blake.

To the Weller and O'Hare groups for being fantastic neighbours, and for the Weller group in particular for their warm welcome, and the amazing conference in Florence.

To all my fellow PhD students, Archibald McNeillis, Theresa Scharbert, Natalia Reis, David Ryan, Wilf Diment, Bowen Xie, Ben Clough, Simona Mellino, Nichabhat Diteepeng, Helen Yin, Adan Reyes, Karen Gamero, Ross Green. I could not have asked for a better bunch of fellow PhD students, I enjoyed the many open market visits & Uni Club evenings. Massive thanks to Archi, David, Wilf & Bowen for all the banter, inside and outside the lab, and for making the PhD a fun experience. Lastly to Simona, without whom my stay in Oxford would not have been the same.

To all my fellow Wolfson and Clarendon friends, for the many pleasant evenings, trips, and rowing competitions!

To Dr Nick Rees for your endless humour and for keeping the NMR facilities running, and a special thanks to all the members of the CRL staff for keeping it running.

Finally, many thanks to my parents and my brother, as well as my close friends outside Oxford, for always supporting me.

Contents

	Declaration	i
	Abstract	ii
	Acknowledgements	iv
	Contents	v
	Abbreviations	viii

Chapter One: Introduction

1.1	General introduction	1
1.2	Transition metal Group 4 imido complexes	2
1.2.1	The imido ligand	2
1.2.2	Synthesis of titanium imido complexes	4
1.2.3	Structural features	7
1.2.4	Stoichiometric reactions	9
1.2.5	Catalytic hydroamination	12
1.2.6	Group 4 hydrazido complexes	13
1.2.6.1	Reactivity across the M=N_α bond	14
1.2.6.2	Reactivity across the N_α–N_β bond	16
1.2.7	Transition metal borylimido complexes	17
1.3	Dehydrocoupling of amine-boranes	22
1.3.1	Early examples	24
1.3.2	Mechanistic studies	25
1.3.2.1	Heterogeneous *vs* homogeneous dehydrocoupling	25
1.3.2.2	σ-complexes of amine-boranes and amino-boranes	27
1.3.2.3	Proposed mechanisms of the dehydrocoupling of amine-boranes	29
1.3.2.4	Generic mechanism for the dehydrocoupling of $Me_2NH{\cdot}BH_3$	46
1.4	Conclusion and outlook	48
1.5	References	49

Chapter Two: Titanium imide catalysed dehydrocoupling of amine-boranes

2.1	Overview	55
2.2	Definition of a suitable system	55

2.3	Mechanistic studies	61
2.3.1	Experimental details	61
2.3.2	Homogeneous or heterogeneous?	56
2.3.3	Active species and catalyst decomposition to Ti(III) species	64
2.3.4	Speciation and concentration-time plot analysis	69
2.3.4.1	Speciation	69
2.3.4.2	Concentration time-plot analysis	70
2.3.5	Catalyic synthesis of diborazane dimers	77
2.3.6	Investigation of the first kinetic regime	82
2.3.7	Investigation of the second kinetic regime	99
2.3.8	Proposed unified mechanistic model	108
2.4	Scope: Dehydrocoupling of amines and boranes and amine-boranes	111
2.5	Summary and outlook	114
2.6	References	115

Chapter Three: Reactivity of the titanium borylimide complex Cp*Ti(HPP){NB(NDippCH)$_2$} (1.83) with alkynes, heterocumulenes and carbonyls

3.1	Overview	118
3.2	Introduction	118
3.3	Reactions of Cp*Ti(HPP){NB(NDippCH)$_2$} (**1.83**) with alkynes	120
3.3.1	Reactions with terminal alkynes	120
3.3.2	Reactions with internal alkynes	130
3.4	Reactions of Cp*Ti(HPP){NB(NDippCH)$_2$} (**1.83**) with heterocumulenes	132
3.5	Reactions of Cp*Ti(HPP){NB(NDippCH)$_2$} (**1.83**) with organic small molecules featuring carbonyl groups	136
3.5.1	Reactions with aldehydes	136
3.5.2	Reactions with ketones	145
3.5.3	Reactions with esters	152
3.5.4	Reactions with amides	161
3.7	Miscellaneous substrates	164
3.8	Conclusions and outlook	164
3.9	References	166

Chapter Four: Synthesis and reactivity of base-free titanium sandwich complexes *via* an oxidative addition route

4.1	Overview	169
4.2	Introduction	169
4.3	Choice of a suitable synthetic route	171
4.4	Synthesis of borylazides	173
4.5	Synthesis and characterisation of novel titanium borylimide complexes	176
4.6	Preliminary reactivity studies using $Cp''_2Ti{=}NBMes_2$ (**4.1**)	189
4.6.1	Reactivity of $Cp''_2Ti{=}NBMes_2$ (**4.1**) with heat and Lewis bases	189
4.6.2	Reactivity of $Cp''_2Ti{=}NBMes_2$ (**4.1**) with carbonyl groups and dihydrogen	193
4.7	Conclusions and outlook	200
4.8	References	201

Chapter Five: Experimental details and characterising data

5.1	General methods and implemenation	203
5.2	Literature preparations	204
5.3	X-ray data collection and processing parameters	204
5.4	Computational details	205
5.5	Experimental details and characterising data for Chapter Two	205
5.6	Experimental details and characterising data for Chapter Three	217
5.7	Experimental details and characterising data for Chapter Four	237
5.8	References	244

Appendix 246

CD Appendix

Abbreviations

General

Å	Ångstrom
BDE	bond dissociation energy
ca	*circa*, about
cf.	*confer*, compared to
CSD	Cambridge Structural Database
^{o}	degrees
^{o}C	degrees Celsius
d	day(s)
DFT	density functional theory
g	grams
h	hour(s)
HOMO	highest occupied molecular orbital
η	hapticity
K	Kelvin
kcal mol^{-1}	kilocalorie(s) per mole
LUMO	lowest unoccupied molecular orbital
M	molarity, mol dm^{-3}
mbar	millibar(s)
min	minute(s)
mL	millilitre(s)
mmol	millimole(s)
MOCVD	Metal-Organic Chemical Vapour Deposition
RT	room temperature
s	second(s)
μ	bridging
μL	microlitre(s)
vs	versus

Chemical

9-BBN	9-borabicyclo[3.3.1]nonane
Ar	aryl group

Ar^{OMe}	4-C_6H_4OMe
Ar^{CF_3}	4-$C_6H_4CF_3$
Ar^{F}	C_6F_5
^{n}Bu	*n*-butyl
Cat	1,2-benzenediol
cent	ring centroid
Cp	C_5H_5
Cp*	C_5Me_5
Cp"	1,3-$C_5H_3(SiMe_3)_2$
Cy	Cyclohexyl
Dipp	2,6-$C_6H_3{}^{i}Pr_2$
DMAP	4-dimethylaminopyridine
E	generic chalcogen atom
Et	Ethyl
H_2Me_4taa	tetramethyl dibenzotetraaza[14]annulene
H-hpp	1,3,4,6,7,8-hexaydro-2*H*-pyrimido[1,2-*a*]pyrimidine
^{i}Pr	*iso*-propyl
KIE	kinetic isotope effect(s)
L	a supporting ligand (set)
Me	methyl
$Me_3[6]aneN_3$	1,3,5-trimethyltriazacyclohexane
Mes	2,4,6-$C_6H_2Me_3$
N_2N^{R}	generic diamide-amine ligand
N_2N^{py}	$MeC(2\text{-}C_5H_4N)(CH_2NSiMe_3)_2$
$N_2N^{SiMe_3}$	$Me_3SiN(CH_2CH_2NSiMe_3)_2$
$N_2{}^{TBS}N^{py}$	$MeC(2\text{-}C_5H_4N)\{CH_2N(Si^{t}BuMe_2)\}_2$
$N^{3,5\text{-}Xyl}N^{pyr}$	2-(3,5-dimethylphenylamino)pyrrolinato
$N_2{}^{pyr}N^{Me}$	*N*,*N*-di(pyrrolyl-α-methyl)-*N*-methylamine
Ph	phenyl
Pin	2,3-dimethyl-2,3-butanediol
py	pyridine
R	generic aryl or alkyl
^{t}Bu	*tert*-butyl
^{tBu}NacNac	$HC\{C(^{t}Bu)NAr\}_2$

THF	tetrahydrofuran
TMEDA	N,N,N',N'-tetramethylethylenediamine
Tol	4-C_6H_4Me
Xyl	2,6-$C_6H_3Me_2$
‡	transition state or activation parameter

Mass Spectrometry

EI	electron impact
FI	field impact
HR	high-resolution
m/z	mass to charge ratio
MS	mass spectrometry

Nuclear Magnetic Resonance Spectroscopy

$^{13}C\{^1H\}$	proton-decoupled ^{13}C
$^{11}B\{^1H\}$	proton-decoupled ^{11}B
$^{19}F\{^1H\}$	proton-decoupled ^{19}F
br.	broad
COSY	correlation spectrocopy
d	doublet
HMBC	heteronuclear multiple-bond correlation
HSQC	heteronuclear single quantum correlation
Hz	Hertz
i	*ipso*
J	coupling constant
m	*meta*
m	multiplet
MHz	Megahertz
NMR	nuclear magnetic resonance
NOE	nuclear Overhauser effect
o	*ortho*
p	*para*

ppm	parts per million
q	quartet
s	singlet
sept.	septet
t	triplet
VT	variable temperature
δ	chemical shift in ppm

Infrared Spectroscopy

br.	broad
FT-IR	fourier transform infrared
IR	infrared
cm^{-1}	wavenumber
m	medium
s	strong
w	weak
ν	frequency

Chapter One

Introduction

1.1 General introduction

For over four decades, transition metal complexes featuring metal–ligand multiple bonds have received sustained attention. Of particular interest is the formally dianionic ligand $\{NR_2\}^{2-}$.[1–5] Initially, this interest was sparked by the relevance of transition metal imido and hydrazido complexes (M=NR and $M=NNR_2$, respectively) to the mechanism of the catalytic reduction of dinitrogen to ammonia.[2,5] To date, transition metal imido compounds have been employed in numerous important transformations, including the aliphatic and aromatic C–H bond activation (including intermolecular activation of methane),[6–12] Ring Opening Metathesis or Ziegler Natta olefin polymerization,[13–17] MOCVD (Metal-Organic Chemical Vapour Deposition),[14,18,19] as well as new C–N bond forming reactions such as hydroamination (N–H bond addition across the CC bonds of alkynes and alkenes).[20–33]

Although catalytic formations of C–C and C–E (E = heteroatom) bonds have been studied in depth, the corresponding E–E bond formation for p-block elements is a relatively underdeveloped field.[34–37] Methods forming such E–E bonds are important tools to make new inorganic molecules which potentially feature interesting properties. Most recently, the dehydrocoupling of amine–boranes to furnish covalent N–B bonds under dihydrogen release has attracted intensive research efforts.[38–40] This Thesis (Chapter Two) describes transition metal imido complexes as novel and efficient catalysts for this transformation, specifically, the use of titanium imido compounds of type (L)Ti=NR (R = alkyl and aryl, respectively). The synthetic scope of this transformation, as well as the mechanism involving the Ti–N multiple bond is explored in detail.

This Thesis also describes the importance of heteroatom substituents, E, on the imido functionality, M=N–ER. Following our groups' efforts to investigate the chemistry of hydrazido and alkoxyimido complexes, $M=N–NR_2$[41–44] and M=N–OR[45,46], respectively, we

have extended these studies to borylimido functionalities, Ti=NBR_2. Previous to these studies, only a handful of borylimido complexes were known using metals from the entire periodic system. Given the lack of any study on their reactivity, it is important that underlying patterns of chemical behaviour are uncovered, and in Chapter Three this is described. Chapter Four explores the synthesis and reactivity of structurally and electronically different borylimido complexes. Aspects of this work has been published.[47]

The reader is referred to general reviews[1–5] on transition metal imido complexes for a general view of the field. The following sections in this Chapter will first focus more specifically on group 4 imido complexes, and subsequently present background and the state-of-the-art of the dehydrocoupling of amine-boranes.

1.2 Transition metal group 4 imido complexes

1.2.1 The imido ligand

Depending on the identity of the transition metal, the imido group may either function as inert spectator ligand or as centre of reactivity. Generally speaking, later transition metal imido moieties often act as innocent spectator ligands, whilst for low-coordination early transition metals the increased polarity of the $M^{\delta+}$–$N^{\delta-}$ multiple bond makes the imido group more reactive.[48,49] The imido group is a ligand often employed to stabilise high oxidation states by virtue of being an excellent π-donor. It is considered to form a σ-bond, and either one or two π-interactions, as shown in Figure 1.1.[3]

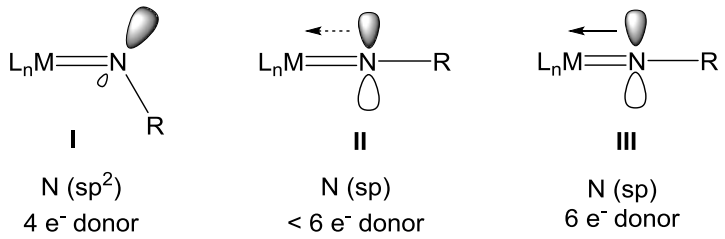


Figure 1.1 Bonding modes of the terminal imido ligand, as well as formal orbital hybridisation of the N atom, and the ionic valence electron count of the ligand.[3,50]

Structure **I** shows a bent M–N–R linkage with the nitrogen atom being sp^2 hybridised. The bonding situation here can be described as formal double bond M=NR ($\sigma^2\pi^2$) and with the lone pair of nitrogen residing in an sp^2 orbital. This situation is quite rare, with an example being found in the bis(imide) $Mo(NPh)_2(S_2CNEt_2)_2$ (**1.1**, Figure 1.2): The top phenylimido group features a bent structure (Mo–N–C = 139.4(4)°).[51] By contrast, the second phenylimido group is near-linear (Mo–N–C = 169.4(4)°) indicating sp hybridisation at nitrogen and the lone pair residing in a pure p-orbital. The majority of structurally characterised M–N–C linkages are near-linear, reflecting an sp-hybridised nitrogen as shown in scenarios **II** and **III**. Scenario **II** ($\sigma^2\pi^n$, $4 < n < 6$) arises when there is a lack of suitable metal-based acceptor orbitals for the nitrogen lone pair and can be due to symmetry or energy mismatch of the respective orbitals. A particularly relevant case-in-point represents the so-called "π-loaded" compound **1.2** (Figure **1.2**). What appears to be a 20 VE complex can be understood by considering that competition of the imido π-components against the π-donor orbitals of the Cp ligands prevents full donation of the lone pair to the metal.[52] Structure **III** depicts the case where lonepair donation of the nitrogen to the metal center is effective, giving rise to a triple bond M≡NR ($\sigma^2\pi^4$). The NR group is sp hydridised and represents a formal $6e^-$ donor. Thus, the dianionic $\{NR\}^{2-}$ moiety can be considered isolobal with $\{C_5R_5\}^{1-}$, and the terminal imido group M=NR is valence isoelectronic with the terminal oxo group M=O. For simplicity, throughout this Thesis imido linkages will be drawn as a double bond and the π-contribution is implicit from the M–N–R angle.

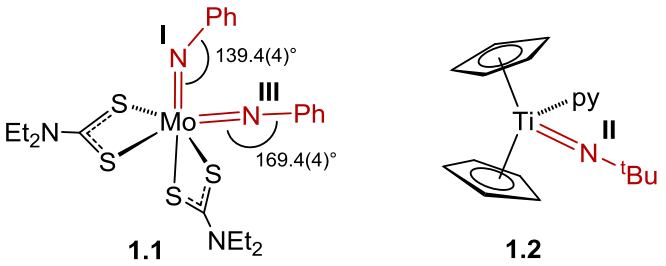
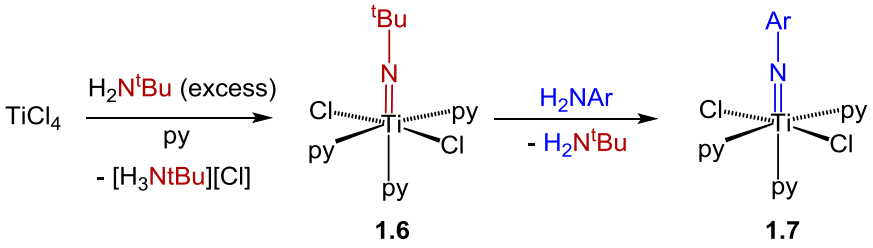


Figure 1.2 Example of a bent ($Mo(NPh)_2(S_2CNEt_2)_2$, **1.1**), and π-loaded ($Cp_2Ti(py)NtBu$, **1.2**) imido complex.

1.2.2 Synthesis of titanium imido complexes

In 1990, Roesky reported the first structurally authenticated terminal titanium imide by reaction of $TiCl_4$ with $(Me_3Si)_2NP(S)Ph_2$ to form $Ph_2PN{=}TiCl_2(py)_3$ (**1.3**).[53] In the same year, Rothwell found that the azobenzene complex $Ti(\eta^2\text{-}PhNNPh)(OAr)_2(py')_2$ (Ar) 2,6-i $Pr_2C_6H_3$) (**1.4**) was thermolysed to form the phenylimido compound $(Ti(Ar'O)_2(py')_2(NPh)$ (**1.5**, Ar' = 2,6-$C_6H_3{}^iPr_2$, py' = 4-pyrrolidinopyridine).[54] The X-ray structures of **1.4** and **1.5** revealed a significant shortening of the Ti–N bond distance from the amide (1.881(3) and 1.89(3) Å) to the final imide (1.719(3) Å).

Spurred by this initial success, various different synthetic strategies have been devised to assemble titanium imido complexes. Dehydrohalogenations and deprotonations are perhaps the most popular methods. Typically, $TiCl_4$ is treated with an excess of primary amine and in the presence of a donor ligand such as pyridine, as was demonstrated by Winter and Mountford (Scheme 1.1).[18,55,56] The excess of primary amine effects dehydrohalogenation to form titanium-amide linkages of type Ti–NHR under concomitant formation of $[H_3NR][Cl]$ ammonium salts.

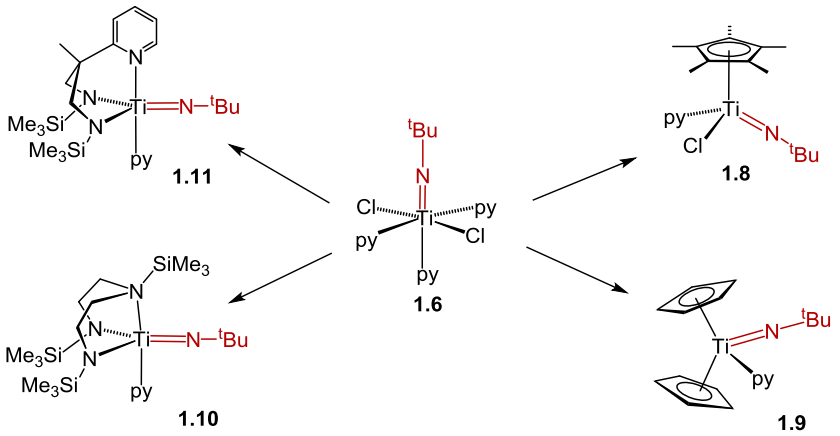


1.6 **1.7**

Scheme 1.1 Synthesis of $Ti(NtBu)Cl_2(py)_3$ (**1.6**) using the dehydrohalogenation and deprotonation metholodogy, and subsequent imide/amine exchange to form $Ti(NAr)Cl_2(py)_3$ (**1.7**).[55]

The employed donor ligands (e.g., pyridine, phosphineoxides, TMEDA) fulfill several roles: they abstract the Ti–NHR hydrogen atom to form the Ti=NR imide, coordinate to the metal center and thereby displace amines, as well as prevent oligomerisations.[57]

The higher Brønsted acidity of anilines (compared to H_2N^tBu) can be exploited to perform imide/amine exchanges giving a variety of arylimido complexes $Ti(NAr)Cl_2(py)_3$ (**1.7**, Scheme 1.1).[55,58] Crucially, these arylimido complexes could not be obtained by reaction of the relevant aniline with $TiCl_4$ and pyridine, due to difficulties in separating the anilinium salt side-products. These tris(pyridine) complexes of type $Ti(NR)Cl_2(py)_3$ represent important synthons for numerous novel compounds due to their capacity for ligand substitution and salt metathesis reactions (Scheme 1.2).[52,58–62]

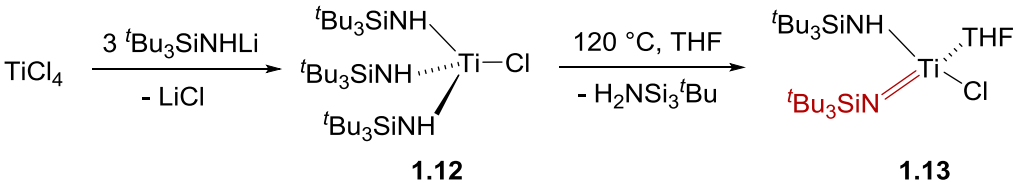


Scheme 1.2 Salt metathesis and ligand exchange reactions starting from $Ti(NtBu)Cl_2(py)_3$ (**1.6**).

In particular, salt metathesis reactions of **1.6** with sodiated or lithiated Cp-type ligands $M[C_5R_5]$ (M = Li or Na, R = H or Me) resulted in half-sandwich or sandwich complexes such as $Cp^*Ti(N^tBu)Cl(py)$ (**1.8**), and $Cp_2Ti(N^tBu)(py)$ (**1.9**), respectively.[52] Similarly, salt metathesis between **1.6** and lithiated diamide-amine ligands $Li_2N_2N^{SiMe_3}$ ($N_2N^{SiMe_3}$ = $Me_3SiN\{(CH_2)_2NSiMe_3\}_2$) and $Li_2N_2N^{py}$ (N_2N^{py} = $(2\text{-}C_5H_4N)CMe(CH_2NSiMe_3)_2$) produced the complexes and $Ti(N_2N^{SiMe_3})(N^tBu)(py)$ (**1.10**) and $Ti(N_2N^{py})(N^tBu)(py)$ (**1.11**), respectively.[63,64]

Another common route to furnish terminal titanium imides constitutes salt metathesis, where titanium halides are typically treated with primary amide salts such as LiNHR along with a base. Cummins and Wolczanski have used this strategy treating the bulky lithium silamide $LiNHSi^tBu_3$ with $TiCl_4$ to give $(^t BuSiNH)_3TiCl$ (**1.12**, Scheme 1.3).[65] Complex

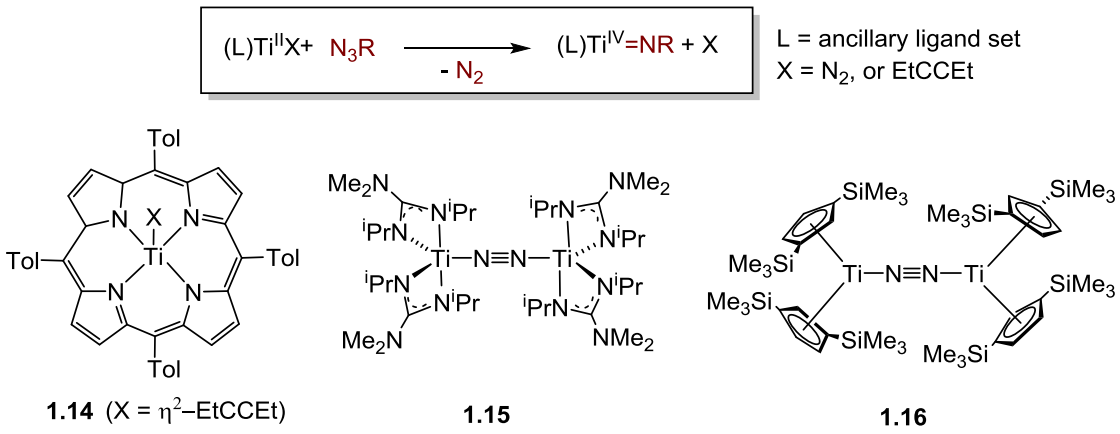
1.12 is subsequently thermolysed to form transient [(^{t}BuSiNH)Ti=NSi^{t}Bu$_3$(Cl)] (**1.12_int**) which was trapped with THF to give titanium imido complex **1.13** as THF adduct in 83% yield. In other cases the base can serve to deprotonate the α-hydrogen from the intermediate to form the imide, without the need of elevated temperatures.[3]



1.12 **1.13**

Scheme 1.3 Reaction of LiNHSi^{t}Bu$_3$ with TiCl$_4$ followed by thermolysis in THF.

There are also oxidative methods to assemble the imide functionality, using either Ti(II)[66–69] or Ti(III)[70,71] precursors. Of particular relevance to this Thesis is the oxidative addition of reactive, low-valent Ti(II) complexes with organic azides. To this end, Woo[72], Arnold[68] and Chirik[69] have prepared the suitable Ti(II) precursor complexes (TPP)Ti(η^2-EtCCEt) (TPP = meso-5,10,15,20-tetra-p-tolylporphyrinato dianion, **1.14**), ({(Me$_2$N)C(N^{i}Pr)$_2$}$_2$Ti)$_2$(μ_2,η^1,η^1-N$_2$) (**1.15**) and (Cp’’$_2$Ti)$_2$(μ_2,η^1,η^1-N$_2$) (Cp’’ = η^5-C$_5$H$_3$-1,3-(SiMe$_3$)$_2$), **1.16**), respectively (Scheme 1.4). In these cases, the titanium (II) centers are either bound to an alkyne or dinitrogen, which serve to stabilize the complex by partially accepting electron density from the metal. The resulting reduction in bond order of the dinitrogen can be measured by inspection of the X-ray structures of **1.15** and **1.16**, respectively. They feature N–N bond distances of 1.28(1) Å and 1.164 (5) Å, respectively, which is significantly elongated than the triple bond of free dinitrogen (1.0975(2) Å).[73]



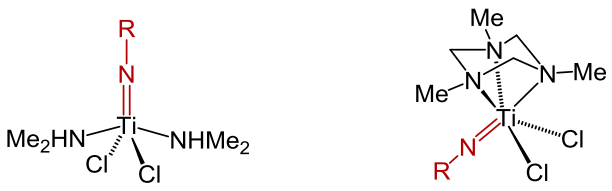
1.14 (X = η^2–EtCCEt) **1.15** **1.16**

Scheme 1.4 Oxidative addition of (L)TiX with N_3R to furnish (L)Ti=NR and free X. L = meso-5,10,15,20-tetra-p-tolylporphyrinato, TTP, and X = EtCCEt for **1.14**, L = $\{(Me_2N)C(N^iPr)_2\}_2$ and Cp''$_2$= (η^5-C_5H_3-1,3-$(SiMe_3)_2)_2$ and X = (μ_2,η^1,η^1-N_2 for **1.15** and **1.16**, respectively.[57]

It was shown that for all three complexes, the addition of azides N_3R effected the rapid conversion into the respective titanium(IV) imido complexes (L)Ti=NR. For example, (Cp''$_2$Ti)$_2$(μ_2,η^1,η^1-N_2) (**1.16**) reacted with N_3SiMe_3 or N_3Mes (Mes = 2,4,6-$C_6H_2Me_3$) to give the base-free complexes Cp''$_2$Ti=N$SiMe_3$ (**1.17**) and Cp''$_2$Ti=NMes (**1.18**) with concomitant release of dinitrogen, respectively.

1.2.3 Structural features

A number of experimental, structural and computational studies have been undertaken to understand the geometric and electronic structures of titanium imido complexes. Similar to what has been discussed in a previous DPhil Thesis,[50] a few key metrics are highlighted using the model complexes Ti(NR)$(NHMe_2)Cl_2$ (R = alkyl (**1.19**) or aryl (**1.20**)) and Ti(NR)$(Me_3[9]aneN_3)Cl_2$ (R = alkyl (**1.21**) or aryl (**1.22**), Figure 1.3).[55,74–76]



R = alkyl (**1.19**)
aryl (**1.20**)

R = alkyl (**1.21**)
aryl (**1.22**)

Figure 1.3 Structures of Ti(NR)$(NHMe_2)Cl_2$ (R = alkyl (**1.19**) or aryl (**1.20**)) and Ti(NR)$(Me_3[9]aneN_3)Cl_2$ (R = alkyl (**1.21**) or aryl (**1.22**)).

These complexes are all monomeric, and bear a terminal imido unit that formally represents a titanium-nitrogen triple bond ($\sigma^2\pi^4$ configuration). The very short Ti=N bond distances range from 1.672(2) – 1.7420(13) Å, and the Ti=N–R bond angles range from 164.46(17) – 180 °, which indicates sp hybridization, are all in line with triple bond character. Generally, alkyl imides feature shorter Ti=N bond lengths compared to their aryl congeners (avg. Ti–NR bond length, R = alkyl (1.690(1) Å), R = aryl (1.7183(7) Å)). A good example for this represents the two following series of compounds: $Ti(NR)Cl_2(NHMe_2)_2$ (R = ^{i}Pr (**1.19a**), Ph (**1.20a**), C_6F_5 = Ar^F (**1.20b**), 2,3,5,6-C_6HCl_4 (**1.20c**), 2-$C_6H_4CF_3$ (**1.20d**) and 2-$C_6H_4{}^t$Bu (**1.20e**))[74] as well as $Ti(NR)Cl_2(Me_3[9]aneN_3)$ (R = ^{t}Bu (**1.21a**), Xyl (**1.22a**), Ar' (**1.22b**), Ph (**1.27c**), and Ar^F (**1.22d**)),[76] where the Ti–N bonds lengths increased in the order R = alkyl < aryl < electron-withdrawing aryl group.

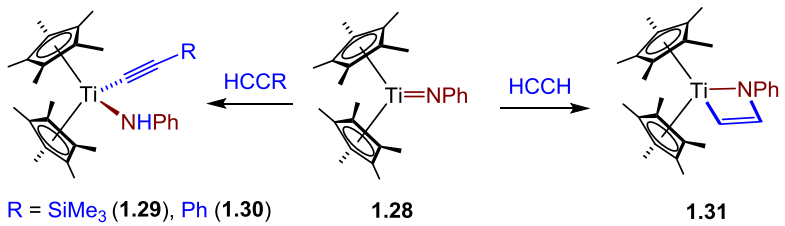
DFT computations have been used to elucidate how structure and bonding changes as a function of the imido substituent R, using the cyclopentadienyl-amidinate titanium imido systems of type $CpTi\{MeC(NMe)_2\}(NR)$ (R = alkyl, aryl or NR_2).[77] It was found that Ti=N bond length was significantly shorter when R = Me compared to R = Ph (1.688 *vs* 1.709 Å), which is consistent with the crystallographically obtained data discussed above. Inspection of the relevant molecular orbitals revealed that this can be explained by two effects. First, when R = Ph, there is significant interaction between a Ti=N π orbital with an electron accepting π* orbital of the phenyl ring. Secondly, there is also donation from a filled π orbital of the phenyl ring into the π* orbital of Ti=N. Both effects lead to a lengthening of the Ti=N linkage, and are absent in the case of R = Me. The corresponding R = NMe_2 and R = NPh_2 congeners featured Ti=N bond lengths of 1.705 Å and 1.713 Å, and are thus comparable to aryl compounds. It was shown that the lone pair on N_β (nitrogen in β position with respect to the metal) donates into the π* orbital of Ti=N, lengthening the

Ti=N bond distance compared to R = alkyl, similar to the case for R = Ph. Overall, the Ti=N bond lengths were shown to follow the trend alkyl < aryl ≈ hydrazido.

1.2.4 Stoichiometric reactions

Early studies by Bergman and Wolczanski showcased the highly reactive nature of group 4 imido complexes, in particular demonstrating the ability to activate C–H bonds for a variety of differently hybridized carbon atoms.[9,65,78] The transiently generated complexes [(^{t}Bu$_3$Si(H)N)$_2$M=NSi^{t}Bu$_3$] (M = Zr (**1.23**), Ti (**1.24**)) were shown to activate methane, as well as benzene, to form the amide complexes (^{t}Bu$_3$Si(H)N)$_2$M(R)NHSi^{t}Bu$_3$ (M = Zr, R = Ph or Me (**1.25**); M = Ti, R = Ph or Me (**1.26**)).[65,79] Similarly, the titanium siloxane congener [(^{t}Bu$_3$SiO)$_2$Ti=NSi^{t}Bu$_3$] (**1.27**), was shown to activate C–H bonds as well. In this report, a combination of kinetic and computational studies suggest a four-centered, concerted transition state in which the C–H bond is added across the Ti–N multiple bond.[78]

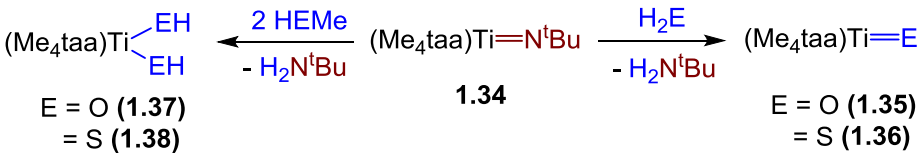
The reaction between Cp*$_2$Ti=NPh (**1.28**) with terminal alkynes HCCSiMe$_3$ and HCCPh afforded the C–H bond activation products **1.29** and **1.30**, respectively, while reaction with acetylide HCCH gave metallacycle **1.31** (Scheme 1.5). The preference for C–H bond activation is attributed to the increased steric bulk of HCCPh and HCCSiMe$_3$, which would lead to unfavourable steric interactions with the Cp* ligands in a metallacycle in analogy to **1.30**.



Scheme 1.5 C(sp)-H bond activation of HCCSiMe$_3$ and HCCPh, and [2 + 2] cyclometallation of HCCH with Cp*$_2$Ti=Ph (**1.28**).

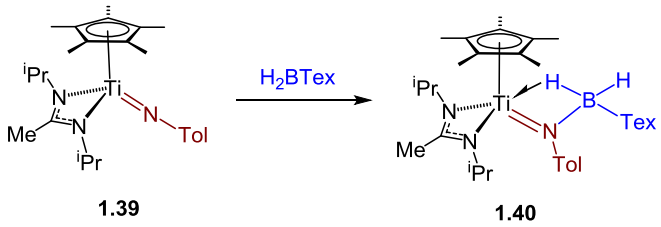
Titanium imido complexes were also shown to activate several other Element–H bonds, including E = H, OR, SR, BR$_2$. For example, dihydrogen adds across the Ti=N multiple

bond of Cp"$_2$Ti(NR) (R = SiMe$_3$ (**1.17**) or Mes (**1.18**)), affording the respective hydride-amide complexes Cp"$_2$Ti(H)(N(H)R) (R = SiMe$_3$ (**1.32**) or Mes (**1.33**)).[69] Treatment of [Ti(N^{t}Bu)(Me4taa)] (**1.34**, Me4taa = tetramethyldibenzotetraaza[14]annulene; Scheme 1.5) with H$_2$E protonated the imide unit to form [Ti(=E)(Me4taa)] (E = O (**1.35**), S (**1.36**), respectively), with concomitant release of H$_2$N^{t}Bu.[5] When 2 equivs of primary alcohols or sulfides HEMe (E = O, S) were added to **1.34**, the bis alkoxy/sulfido compounds [Ti(EMe)$_2$(Me4taa)] (E = O (**1.37**), S (**1.38**)) could be isolated.



Scheme 1.5 Reactions of [Ti(N^{t}Bu)(Me4taa)] (**1.34**) with H$_2$E (E = O, S; right), and two equivalents of HEMe (E = O, S; left).

In 2017, the Mountford group demonstrated that a variety of boranes HBR$_2$ react with Cp*Ti{MeC(NiPr$_2$)$_2$}(NTol) (**1.39**) to give borane adducts of type **1.40** (Eq. 1.2).[80] The examplar reaction with texylborane H$_2$BTex (Tex = 2,3-dimethyl-2-butyl) is depicted in Eq. 1.2. Interestingly, these adducts feature β-B agostic, 3-centre 2-electron interactions.[81]

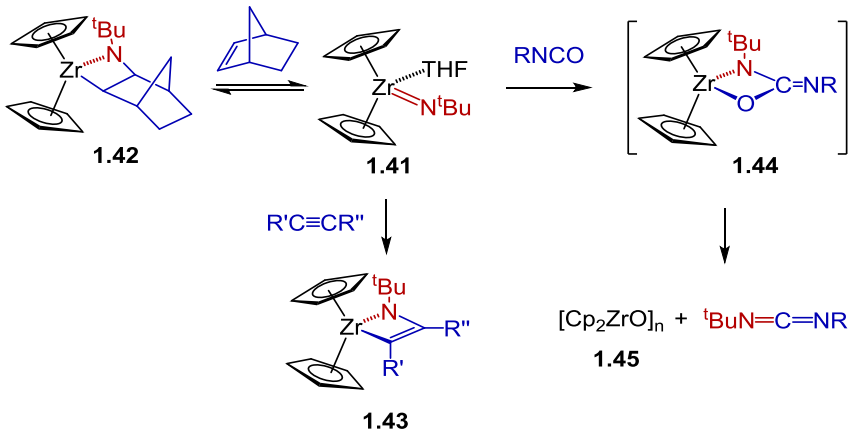


1.39 **1.40**

Equation 1.2

Although E–H bond activations have attracted considerable interest, especially for C–H bonds, the hallmark of group 4 imido complexes represents [2 + 2] cycloadditions of the M=N linkage with unsaturated substrates (where there is no E–H bond cleavage). Depending on the substrates, this reaction type has provided access to a variety of interesting metallacycle structures, as well as novel organic molecules which were formed

after cycloreversion. Bergman's $Cp_2Zr(N^tBu)(THF)$ (**1.41**) complex featured a particularly rich chemistry with a variety of small unsaturated substrates, and examplatory reactions are discussed in the following (Schemes 1.6 and 1.7). Ethene as well as norbornene were found to be in equilibrium with **1.41** and the corresponding [2 + 2] cycloaddition products (**1.42**).[82] By contrast, when subjected to a variety of internal alkynes the corresponding [2 + 2] cycloaddition products were formed irreversibly at RT, and only at elevated temperatures (85 – 110 °C) were equilibria observed.[83]

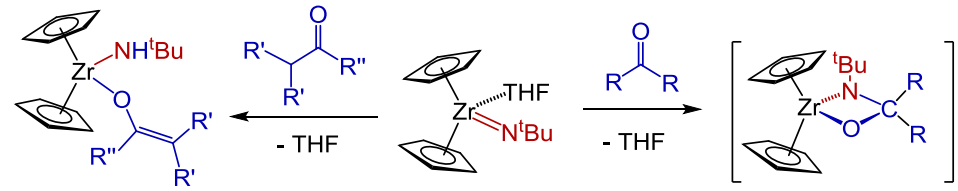


Scheme 1.6. [2 + 2] cycloaddition reactions of $Cp_2Zr(N^tBu)(THF)$ (**1.41**).[6,82]

Similarly, isocyanates RNCO (R = alkyl, aryl groups) initially formed the corresponding [2 + 2] metallacycles (**1.44**). However, they reacted further to complete the metathetical reaction[84] *via* cycloreversion, giving oligomeric $[Cp_2Zr{=}O]_n$ (**1.45**) and the carbodiimides $RNCN^tBu$. The Woo[67] and Mountford[95, 101] groups were able to isolate sufficiently stable κ^2 isocyanate cycloaddition adducts analogous to **1.44**, which were shown to undergo cycloreversion under forcing conditions.

The reaction of $Cp_2Zr(N^tBu)(THF)$ (**1.41**) with a variety of aldehydes and ketones also initially yielded metallacycles such as **1.46** and **1.47** before cycloreversion occurs (Scheme 1.7).[83] By contrast, when sterically more demanding (and enolisable) ketones were used the enolate complexes **1.48** and **1.49** were formed. Various other unsaturated subtrates are

reported to undergo [2 + 2] cycloadditions with group 4 imido complexes as well, including CO_2, CO,[85] azides,[83] and nitriles. [86]



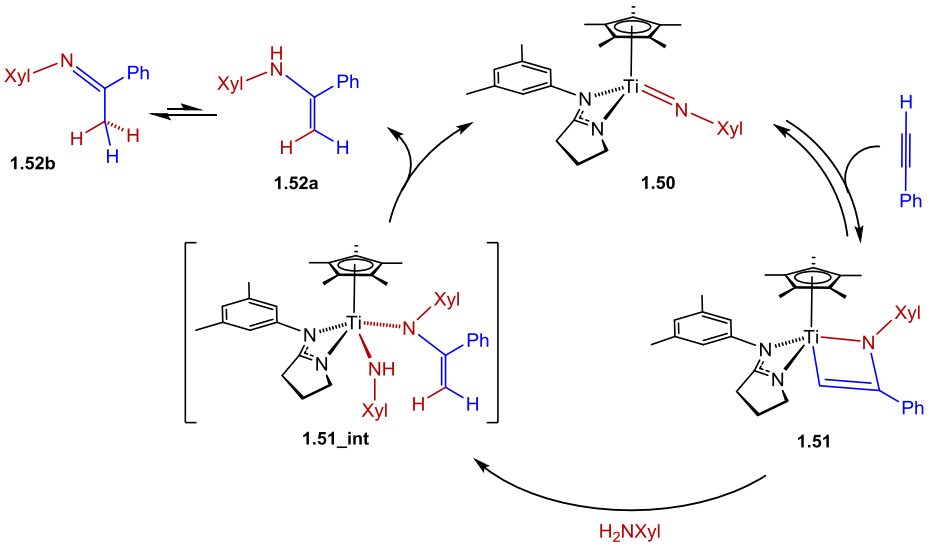
R' = R'' = cyclohexyl (**1.48**)
R' = Me, R'' = ^{i}Pr (**1.49**)

R = Me (**1.46**)
R = Ph (**1.47**)

Scheme 1.7 Reactions of **1.41** with ketones. Left: Enolate formation. Right: [2 + 2] cycloaddition.

1.2.5 Catalytic hydroamination

[2 + 2] cycloaddition reactions with group 4 imides are involved in various industrially relevant processes, such as ethene polymerization,[59,87] olefin metathesis[14] and carbonyl olefination.[59,83] Another important application of these catalysts represents the catalytic hydroamination of alkynes, alkenes allenes with amines.[16-19] In this transformation, N–H bonds are added across the carbon–carbon multiple bond forming N–C and C–H bonds in an atom-economic way. In many of these processes, the first step of the mechanism is the [2 + 2] cycloaddition of the alkyne or alkene across the metal–nitrogen multiple bond to yield an azametallacycle. For example, Scheme 1.8 depicts a catalytic cycle for the hydroamination of HCCPh with H_2NXyl using an titanium arylimido catalyst, Cp*Ti($N^{3,5\text{-}Xyl}N^{pyr}$)(NXyl) (**1.50**), as reported by Gade and co-workers.[25] Addition of HCCPh to **1.50** results in the azatitanacyclobutene **1.51** *via* a [2 + 2] cycloaddition. Next, H_2NXyl protonates the metallacycle to form the putative bisamido intermediate **1.51_int.** In this case, this compound could not be observed and an additional proton transfer reforms the imido catalyst **1.50** with concomitant release of enamine **1.50a**, which isomerizes to give imine **1.50b** as final product.



Scheme 1.8 Exemplar catalytic cycle of the hydroamination of a terminal alkyne using Cp*Ti($N^{3,5\text{-}Xyl}N^{pyr}$)(NXyl) (**1.50**) as catalyst. Xyl = 2,6-dimethylbenzene.[25]

The catalyst **1.50** was shown to efficiently couple aromatic and aliphatic primary amines with a variety of terminal and internal alkynes at 5% catalyst loading and 105 °C. Additionally, internal hydroaminations were performed as well, in which cyclisations to form secondary amines occured. Other titanium (pre)catalysts reported in the literature include $Cp_2Ti(\eta^2\text{-}Me_3SiC_2SiMe_3)$,[88] Cp_2TiMe_2,[89] $Ti(N_2^{pyr}N^{Me})(NMe_2)_2$ ($N_2^{pyr}N^{Me}$ = *N*,*N*-di(pyrrolyl-α-methyl)-*N*-methylamine)[28] as well as $Ti(NMe_2)_4$,[90–92] with the proposed catalytic cycles proceeding *via* imido intermediates in all cases.

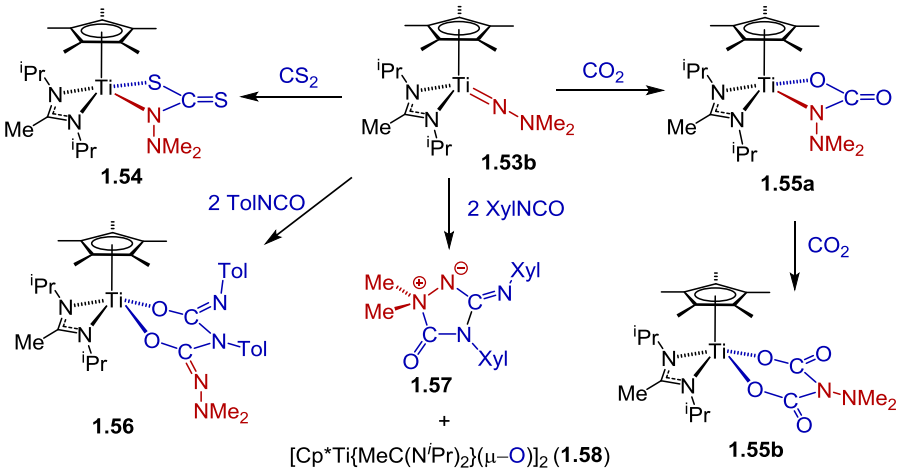
1.2.6 Group 4 hydrazido complexes

Early research into transition metal hydrazido complexes focused on the study of models for the biological fixation of molecular nitrogen, particularly using group 6 metals. By contrast, the more recent work on the chemistry of the group 4 $M{=}N_\alpha{-}N_\beta$ linkage focused on their rich chemistry in terms of small molecule activation more generally. The presence of a nitrogen atom in β-position has a profound effect on the reactivity. In general, reactivity can occur either on the $M{=}N_\alpha$, or the reducible $N_\alpha{-}N_\beta$ bond, which sets them apart from their imido congeners, and will be discussed in the following subsections.

1.2.6.1 Reactivity across the M=N$_\alpha$ bond

A wide variety of small molecules were shown to react with the M=N$_\alpha$ bond of hydrazido complexes, and, in analogy to their imido congeners, often the first step represents [2 + 2] cycloaddition. In many cases the resulting cycloaddition compounds can be isolated, and often undergo further reactions. These can include cycloreversion to extrude organic molecules, or insertion of a second substrate molecule into the, now single, M-N bond.

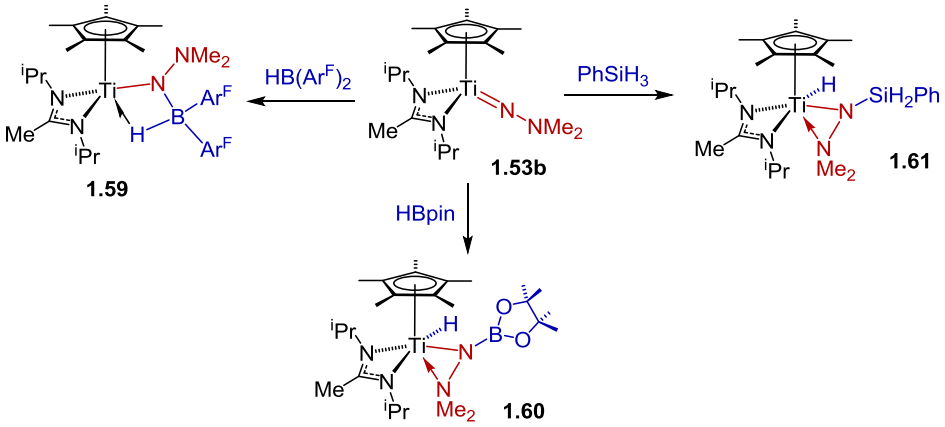
Cyclopentadienyl-amidinate ligand sets were shown to be robust platforms to study titanium imido chemistry. This ligand set was used extensively to study the corresponding reactions with hydrazide units using Cp*Ti{MeC(N^{i}Pr)$_2$}(NNR$_2$) (R = Ph (**1.53a**) or Me (**1.53b**)). Reactions starting from **1.53b** are illustrated in Scheme 1.9.



Scheme 1.9 Exemplar reactions of Cp*Ti{MeC(N^{i}Pr)$_2$}(NNMe$_2$) (**1.53b**) with heterocumulenes.

Subjecting **1.53b** to CS$_2$ and CO$_2$ first gave cycloaddition products **1.54** and **1.55a**, respectively, and in the latter case, a second CO$_2$ molecule inserted into the Ti-N$_\alpha$ bond resulting in the "double insertion" product **1.55b**.[77] Similarly, use of the related isocyanate TolNCO also gave a "double insertion" product, namely **1.56**. The analogous XylNCO (Xyl = 2,6-C$_6$H$_3$Me$_2$) isocyanate also reacted to form an initial [2 + 2] cycloaddition product, however, reacted further to give the cyclic N(Me)$_2$NC(NXyl)N(Xyl)C(O) (**1.57**)

as well as **1.58**. The additional bulk was reasoned to destabilize the initially formed cycloaddition adduct sufficiently to prevent a "double insertion" product analogous to **1.56**. In contrast to the variety of unsaturated small molecules investigated in their reactions with group 4 imides and hydrazides, the corresponding reactivity with silanes and boranes was only investigated very recently. These substrates generally react *via* 1,2-addition of the E–H bond across the M=N multiple bond to form metal hydride amides (Scheme 1.10).



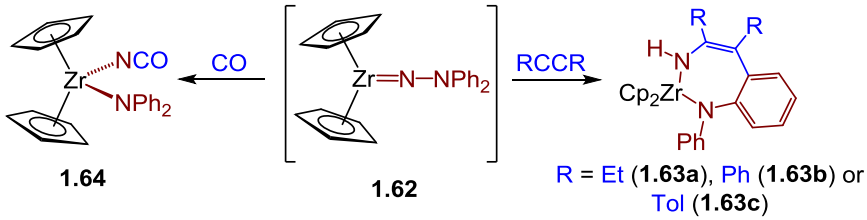
Scheme 1.10 Exemplar reactions of Cp*Ti{MeC(N^{i}Pr)$_2$}(NNMe$_2$) (**1.53b**) with boranes and silanes.

Depending on the substrate, the E–H bond might either break partially, or entirely. The reaction of HB(Ar^F)$_2$ (Ar^F = C_6F_5) with **1.53b** is an example of E–H bond activation, forming **1.59**. The less Lewis acidic HBPin reacts to cleave the B–H bond completely, forming a titanium hydride borylamide **1.60**, in which the N$_\beta$Me$_2$ moiety is coordinated to the metal.[80] The Si–H bond in PhSiH$_3$ is completely broken to form the analogous titanium hydride amidosilane species **1.61**, featuring N$_\beta$Me$_2$ coordination to the metal center as well.[93] By contrast, no reaction occurred with PhSiH$_3$ and the imido counterparts of **1.53b**. DFT calculations performed on these systems found that, without additional coordination of the β-NMe$_2$ group, 1,2-addition to Ti–N$_\alpha$ was thermodynamically unfavorable.[44,93]

1.2.6.2 Reactivity across the N_α–N_β bond

Despite the rich chemistry at the M=N_α bond in group 4 hydrazide compounds described in the previous section, it is with the discovery of many transformations at the N_α–N_β bond that group 4 hydrazide came to its own. The relatively weak N_α–N_β bond can be cleaved using a variety of formally oxidisable substrates such as alkynes or isonitriles.

Bergman and coworkers were the first to report such group 4 reductive N_α–N_β bond cleavage reactions.[94] The *in-situ* generated $Cp_2ZrNNPh_2$ (**1.62**) did not give the expected [2 + 2] cycloadditions with internal alkynes (as was observed for the imidozirconocene congeners),[83] but instead complexes of type **1.63** were observed (Scheme 1.11). These complexes feature seven-membered rings formed from initial N_α–N_β bond cleavage, followed by a C–H bond activation. **1.62** also reacted with CO at room temperature to afford the zirconium amide-isocyanate complex **1.64**.



Scheme 1.11. Reactions of $Cp_2Zr(NNPh_2)$ (**1.62**) with CO and internal alkynes.[94]

This initial report was subsequently followed by Gade *et al.* who reacted the bisamide-amine supported zirconium hydrazide $Zr(N_2{}^{TBS}N^{py})(NNPh_2)(py)$ (TBS = *tert*butyldimethylsilyl) (**1.65**) with isonitrile ^{t}BuNC to afford the amide carbodiimide compound **1.66** (Figure 1.4).[95] Related chemistry is observed when **1.65** is reacted with propylene sulfide or Ph_3PSe, forming the chalcogenide bridged dimers $\{Zr(N_2{}^{TBS}N^{py})(NPh_2)\}_2(\mu\text{-}N_2E)$ (E = S (**1.67a**) or Se (**1.67b**), Figure 1.4).[95] As in the case of **1.66**, N_α–N_β bond cleavage occured, and the $N_\beta Ph_2$ has migrated to the metal center in apical position.

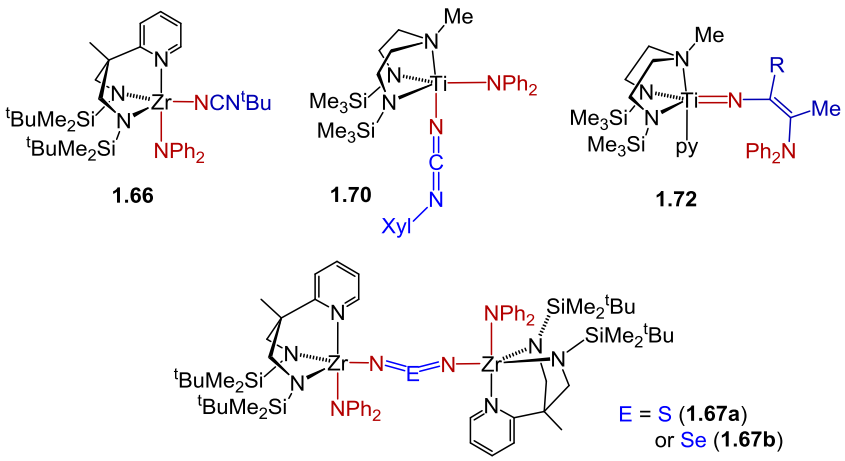


Figure 1.4 Exemplar reaction products of group 4 hydrazides after N_α–N_β bond cleavage.

Analogous isonitrile reactions with titanium hydrazide complexes were also reported, $Ti(N_2N^{py})(NNPh_2)(py)$ (**1.68**) and $Ti(N_2^{SiMe_3}N^{Me})(NNPh_2)(py)$ (**1.69**) both react with one equivalent of XylNC to give the N_α–N_β bond cleavage products $Ti(N_2N^{py})(NPh_2)(NCNXyl)$ (**1.70**) and $Ti(N_2^{SiMe_3}N^{Me})(NPh_2)(NCNXyl)$ (**1.71**, Figure 1.4) respectively.[96]

Previously, the possibility for alkynes to undergo [2 + 2] cycloadditions with imido (or hydrazido) complexes at the M=N bond has been discussed. When $Ti(N_2^{SiMe_3}N^{Me})(NNPh_2)(py)$ is treated with a variety of internal alkynes, indeed the respective azametallacycles were formed within a few hours at RT. However, after letting the reaction mixtures stand for 3 d at RT, full conversion to vinylimido complexes $Ti(N_2^{SiMe_3}N^{Me})\{NC(R)=C(Me)NPh_2\}$ (**1.72**, R = alkyl or aryl) was observed.[41]

1.2.7 Transition metal borylimido complexes

The wide range of group 4 imido and hydrazido compounds that have been prepared, and their rich reactivity with small molecules, prompted to study the effect of heteroatom substitution at the N_α site, M=N_α–ER (E = heteroatom).[1]

[1] Recently, the Mountford group has studied the synthesis and reactivity of alkoxyimido complexes M=N-OR, with E being an oxygen atom. Since the reactivity of these complexes did not dramatically differ from its imido and hydrazido counterparts, we will not cover them here for brevity. However, the interested reader is pointed to selected literature.[45,170,171]

Incorporation of a boron atom bound to the N_α gives borylimido complexes of type $M{=}N_\alpha{-}BR_2$. Only a handful of terminal borylimido complexes were reported across the entire periodic table, before the Mountford group started studies in this area (Figure 1.5). [47,97]

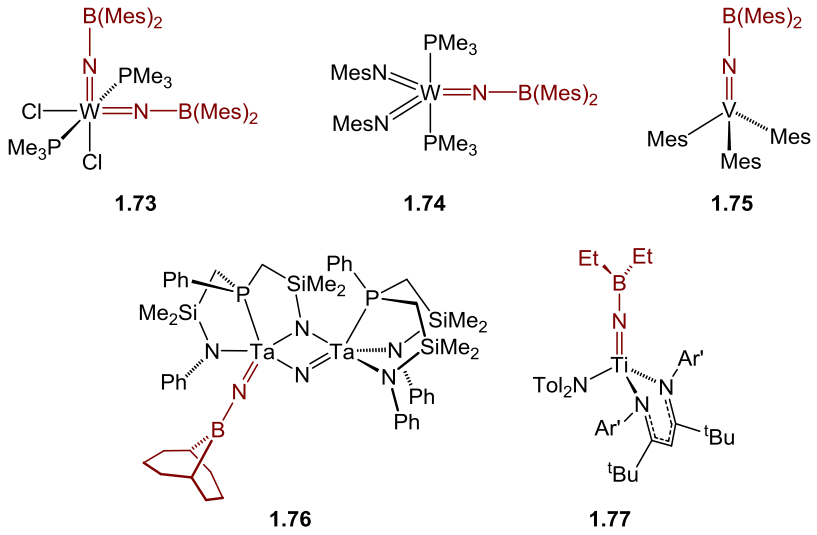
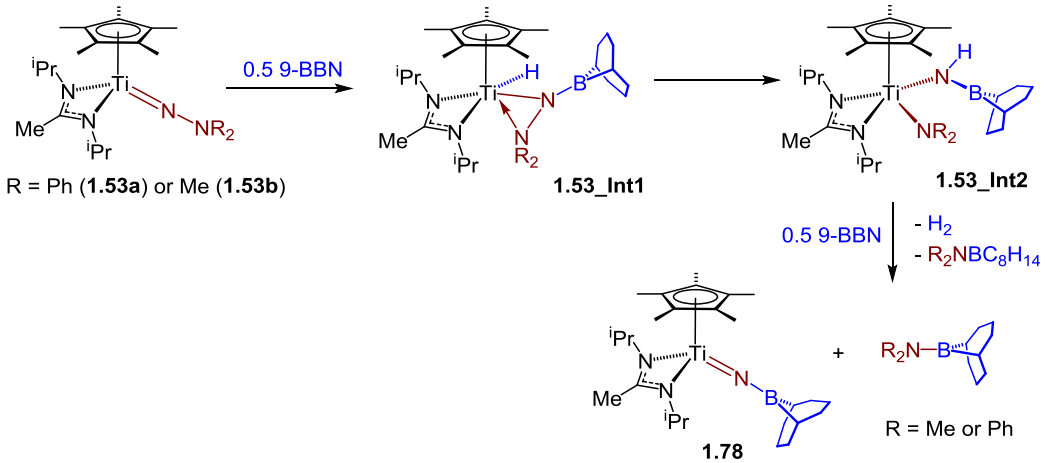


Figure 1.5 Previously reported terminal borylimido complexes.[44,98–101]

Wilkinson reported the first such compound, treating tungsten (II) complex $WCl_2(PMe_3)_4$ with 2 equivs of Mes_2BN_3 to afford the tungsten (VI) compound $W\{NB(Mes)_2\}_2Cl_2(PMe_3)_2$ (**1.73**).[100] This oxidative addition process is driven by the formation of two equivs of N_2. Similarly, the reactions of Mes_2BN_3 with the bis(imide) $W(NMes)_2(PMe_3)_3$ formed the mixed borylimido-bis(imido) complex $W\{NB(Mes)_2\}(NMes)_2(PMe_3)_2$ (**1.74**), and reacting it with vanadium(III) complex $V(Mes)_3(THF)$ formed the vanadium(V) imide $V\{NB(Mes)_2\}(Mes)_3$ (**1.75**, Figure 1.5).[101] Serendipitous rearrangement of an 9-BBN adduct of a ditantalum dinitrogen complex gave dimeric **1.76**. However, the addition of a second 9-BBN borane monomer did not form another borylimido moiety on the remaining metal center. The first group 4 borylimide was published by Mindiola in 2014, *via* formation of (^{tBu}NacNac)Ti($NBEt_2$)($NTol_2$) (**1.77**) from the parent imide (Ti=NH) with 2 equivs of $NaHBEt_3$ (Figure 1.5).[99]

Recently, the Mountford group has communicated the preparation of the second terminal titanium borylimido complex Cp*Ti{MeC(N^{i}Pr)$_2$}(NBC$_8$H$_{14}$) (**1.78**) through the reaction of terminal hydrazides (**1.53a**, or **1.53b**, respectively) with 1 equivalent of 9-BBN dimer (Scheme 1.12).[44]

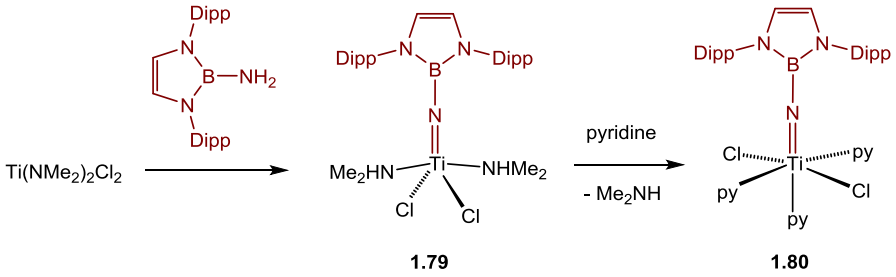


Scheme 1.12. Proposed reaction mechanism for Cp*Ti{MeC(N^{i}Pr)$_2$}(NNR$_2$) (R$_2$ = Ph (**1.53a**) or Me (**1.53b**)) + 9-BBN dimer.[102]

This reaction is proposed to proceed *via* initial 1,2-B–H addition to the Ti–N multiple bond to give a titanium hydride species **1.53_Int1**, followed by hydride transfer and N$_\alpha$–N$_\beta$ cleavage leaving a mixed amido-borylamido intermediate **1.53_Int2**. Finally, 1,2-elimination of HNR$_2$ (R = Ph or Me) forms the borylimido multiple bond, and the released amine undergoes dehydrogenation with the other half of the 9-BNN dimer forming R$_2$NBC$_8$H$_{14}$.[102] A computational study of **1.78** confirmed the presence of Ti–N triple bond character, and found the two Ti–N π interactions by MO and NBO analyses, one of which is significantly stabilised by delocalisation into the otherwise vacant 2p AO of boron.

However, this reaction was found to be not general, and could not be extended to form related borylimido complexes featuring different borylimido moieties, and purification difficulties limited its further use. Rational synthetic routes towards metal borylimido compounds were subsequently developed using a protonolysis methodology.[47,103] For example, borylamine H$_2$NB(NDippCH)$_2$ was shown to be sufficiently acidic to protonate

the (secondary) amides in $Ti(NMe_2)_2Cl_2$ to form $Ti\{NB(NDippCH)_2\}Cl_2(NHMe_2)_2$ (**1.79**; Scheme 1.13). Subsequent pyridine addition then replaced the $HNMe_2$ to generate $Ti\{NB(NDippCH)_2\}Cl_2(py)_3$ (**1.80**), borylimide analogue of the *tert*butylimido synthon $Ti(N^tBu)Cl_2(py)_3$ (**1.7**).

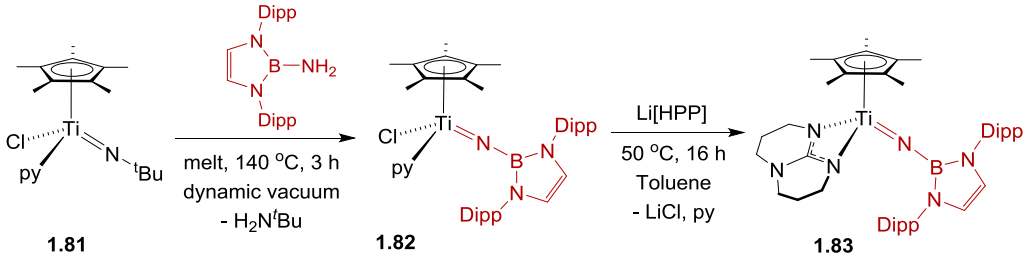


Scheme 1.13. Synthesis of borylimide synthon $Ti\{NB(NDippCH)_2\}Cl_2(py)_3$ (**1.85**).

1.80 was structurally characterised, and the Ti–N–B linkage was of particular interest. The Ti–N_α bond is short with 1.7118(9) Å, and the Ti–N_α–B angle of 177.85(9)° implying sp hybridisation at the N_α atom. The N_α–B bond length of 1.4216(14) Å falls within the range (*ca* 1.34 – 1.51 Å) of all N–B single bonds with sp hybridised N and three-coordinate B in the Cambridge Structural Database.[104] This data is in agreement with triple bond character in Ti–N_α, and only negligible π donation from the N_α lonepair to the boron atom. This can be explained by the two other nitrogen atoms bound to the boron atom, which both compete to donate their lone pair into the empty boron based p orbital. Formally, the boryl ring represents a 6-π electron aromatic ring which is isoelectronic to a phenyl moiety. In fact, the Ti–N_α bond length falls in the range of Ti–N_{im} distances in the previously structurally characterised arylimides $Ti(NAr)Cl_2(py)_3$ (avg. Ti–N_{im} = 1.718 Å, range 1.705(4) – 1.730(2) Å for six examples),[55,105–107] longer than in both the alkylimide $Ti(N^tBu)Cl_2(py)_3$ (**1.6**, average value of 1.701 Å),[55,108] and slightly shorter than in the hydrazide $Ti(NNPh_2)Cl_2(py)_3$ (1.727(2) Å).[109]

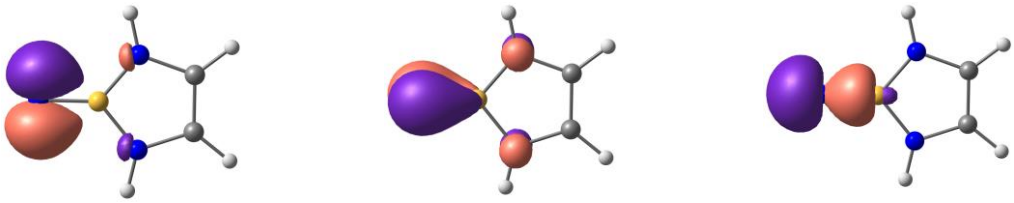
In analogy to their *tert*butyl- and arylimide counterparts, complexes **1.79** and **1.80** served as useful synthons, and a variety of (bis)amide-amine ligand sets were installed *via* salt

metathesis and ligand replacements.[110] The installation of a cyclopentadienyl ligand was attempted since this ligand proved to be a reliable and robust platform to study the small molecule activation chemistry of related titanium imide complexes.[50] However, side reactions precluded the installation of this ligand, and thus attention was turned to an alternative starting material, namely Cp*Ti(N^{t}Bu)Cl(py) (**1.81**) (Scheme 1.14). When titanium *tert*butylimide **1.81** was treated with $H_2NB(NDippCH)_2$, an equilibrium mixture was observed between the starting material, and the targeted borylimide complex Cp*Ti(NB(NDippCH)$_2$)Cl(py) (**1.82**). When the reaction was performed in neat melt of **1.81**, and dynamic vacuum, the free *tert*butylamine (bp = 43 °C)[111] was efficiently removed from the equilibrium mixture, and the reaction could be driven to the desired borylimide product **1.82** in moderate yield (60% isolated yield). From **1.82**, attempted installation of the amidinate [MeC(NiPr)$_2$], analogous to the previously discussed cyclopentadienyl-amidinate tolylimido complex Cp*Ti{MeC(NiPr$_2$)$_2$}(NTol) (**1.39**) and hydrazido complexes Cp*Ti{MeC(N^{i}Pr)$_2$}(NNMe$_2$) (**1.53b**), failed and is ascribed to insurmountable steric constraints. However, the sterically tied-back lithiated guanidinate Li[HPP] (Hhpp = 1,3,4,6,7,8-hexahydro-pyrimido[1,2-*a*]pyrimidine) successfully yielded Cp*Ti(HPP){NB(NDippCH)$_2$} (**1.83**, Scheme 1.14).



Scheme 1.14 Imide/borylamine exchange of **1.81** and subsequent ligand installations.

DFT calculations were used to compare the NB(NDippCH)$_2$ moiety with the isoelectronic and aromatic NPh. For this purpose, the σ- and π-type three highest energy frontier orbitals of the $[NB(NHCH)_2]^{2-}$ and $[NPh]^{2-}$ anions were compared to each other (Figure 1.6).



HOMO (π_h)	**HOMO-1 (π_v)**	**HOMO-2 (σ)**
7.38 (6.91) eV	7.06 (6.23) eV	5.00 (2.99) eV

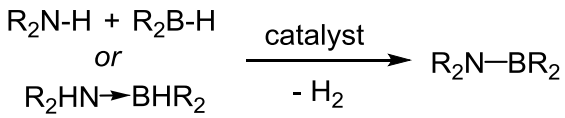
Figure 1.6 DFT computed σ- and π-type fragment molecular orbitals of the borylimido dianion $[NB(NHCH)_2]^{2-}$ with their energies (corresponding values for $[NPh]^{2-}$ are given in parentheses).

The electropositive nature of the boron atom, compared to the carbon atom, raises the average energies of the MOs containing this element. For example, the HOMO and HOMO-1 of the borylimide dianion is higher (less stable), suggesting that this borylimide is a better π-donor than phenylimide. This difference is even greater in the HOMO-2 of the anions. These represent the σ-donor orbitals and the borylimide orbital is *ca.* 2 eV less stable, suggesting an even greater improvement in σ-donor ability. Thus, the imido nitrogen atoms of borylimide complexes form stronger σ-bonds than their alkyl- or aryl imido analogues. For example, it was shown that C–H bond activations are more favourable in the borylimido case compared to arylimido complexes, due to the higher strength of the newly formed N–H bond formed from a borylimido ligand compared with an arylimido ligand.[103]

1.3 Dehydrocoupling of amine-boranes

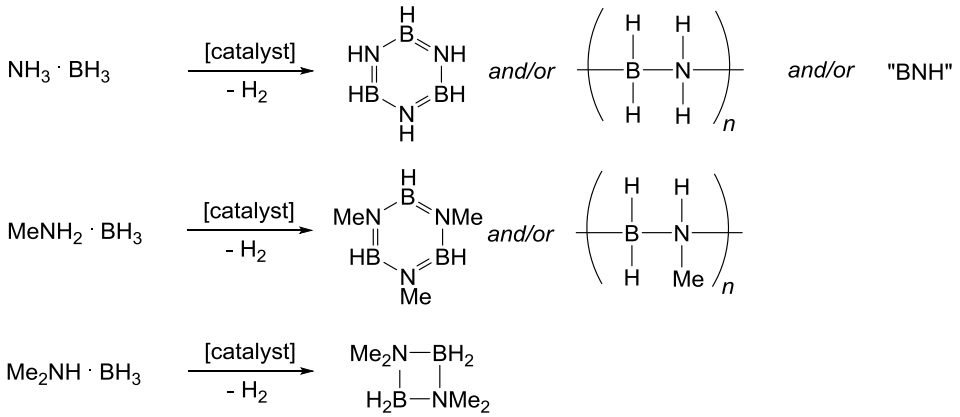
Catalytic processes that enable the formation of carbon-element C–E bonds (E = p-block element) have played a crucial role in organic chemistry over the past decades. By contrast, analogous processes forming p-block element-element bonds for inorganic materials are still in their relative infancy, and mainly rely on salt-metathesis reactions.[35] A particularly useful process is the dehydrogenative coupling of amines with boranes – an atom-economic

method forming new covalent N–B bonds, under the release of dihydrogen as sole side product (Equation 1.3).



Equation 1.3

This methodology has received intense interest due to various important applications, including the formation of BN-based ceramics and single-layer hexagonal BN thin films (white graphene),[112,113] hydrogen storage,[35,114] and inorganic polymers.[115–117] The dehydrocoupling of ammonia-borane $NH_3{\cdot}BH_3$ is the most interesting in light of its relative weight of hydrogen stored (ca. 19%). Despite progress in the regeneration of spent fuel from this process,[118,119] the resulting BN products (oligomers, polymers, cross-linked BN materials) are often ill-defined and insoluble (Scheme 1.15). The consequence is that the development of a mechanistic understanding of these dehydrocoupling reactions is hampered, which are crucially important to develop better reaction systems.



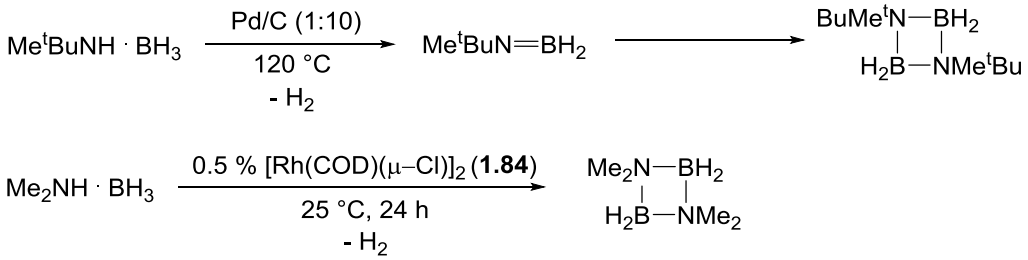
Scheme 1.15 Possible BN containing products from dehydrocoupling $NH_3{\cdot}BH_3$, $MeNH_2{\cdot}BH_3$, and $Me_2NH{\cdot}BH_3$. "BNH" denotes polyborazylene.

The next congener, $MeNH_2{\cdot}BH_3$, forms oligomeric and polymeric products upon dehydrocoupling as well, rendering mechanistic studies not straightforward (Scheme 1.15). By contrast, dehydrocoupling of the related $Me_2NH{\cdot}BH_3$ forms the cyclic $[Me_2N{=}BH_2]_2$ aminoborane as sole product (Scheme 1.15), which displays good solubility in common

organic solvents, as do potential reaction intermediates. These features facilitate mechanistic studies, and indeed $Me_2NH{\cdot}BH_3$ has been subject to numerous of different dehydrocoupling studies, allowing comparisons between systems as well.

1.3.1 Early examples

In 1989, Roberts reported the first example of a transition-metal catalysed dehydrocoupling of an amine-borane.[120] $Me^tBuNH{\cdot}BH_3$ was dehydrogenated using 10% Pd on charcoal to form the amino-borane $Me^tBuN{=}BH_2$, which dimerised to give $[Me^tBuN{=}BH_2]_2$ as final product (Scheme 1.16). It was not until 2001, when the next example of a transition-metal catalysed dehydrocoupling of an amine-borane was reported by Manners.[121] The rhodium complex **1.84** was employed at low loadings to dehydrocouple $Me_2NH{\cdot}BH_3$ to give $[Me_2N{=}BH_2]_2$ as sole product at room temperature (Scheme 1.16).



Scheme 1.16 Top: Dehydrocoupling of $Me^tBuNH{\cdot}BH_3$ to yield $[Me^tBuN{=}BH_2]_2$. Bottom: Dehydrocoupling of $Me_2NH{\cdot}BH_3$ to yield $[Me_2N{=}BH_2]_2$.

Further studies showed that the rhodium precatalyst operates *via* a heterogeneous mechanism, and that dehydrocoupling was not limited to $Me_2NH{\cdot}BH_3$ as substrate.[122] After these early examples, there have been many more reports on the dehydrocoupling of amine-boranes. In the following, key examples will be discussed with a focus on the mechanism using $Me_2NH{\cdot}BH_3$ as the substrate.

1.3.2 Mechanistic studies

1.3.2.1 Heterogeneous *vs* homogeneous dehydrocoupling

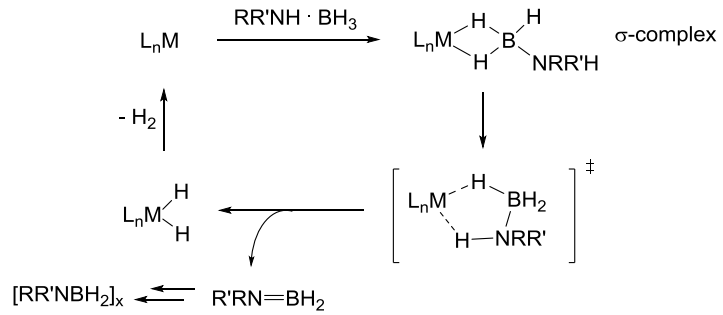
Both homogeneous as well as heterogeneous catalyst systems have been reported to be efficient in the dehydrocoupling of amine-boranes.[39] Heterogeneous systems are particularly attractive for industry, given the facile product separation, e.g., by filtration methods. Some heterogeneous systems are among the fastest reported dehydrocoupling catalysts. For example, Morris showed that a $[Fe(NCMe)_2(PNNP)[BF_4]_2/KO^tBu$ (PNNP = $Ph_2PC_6H_4CH=NCH_2)_2$) system is very active towards the dehydrogenation of $NH_3{\cdot}BH_3$, featuring a TOF (turnover frequency) of *ca*. 2400 h^{-1}.[123]

Finke developed a series of tests to distinguish homogeneous from heterogeneous catalysis, and critiqued them in a review to which the reader is referred to.[124] These tests were used by Manners to investigate the $[Rh(COD)(\mu\text{-}Cl)]_2$ (**1.84**) system.[122] For example, when an excess of Hg was added to the reaction mixture, turnover was stopped. Mercury is known to either form amalgams with nanoparticles or absorb to the metal surface, thus effectively poisoning the heterogeneous catalyst.[122,124] In an additional test, the catalytic mixture was poisoned with PPh_3. While an unpoisened blank reaction showed >60 % conversion of $Me_2NH{\cdot}BH_3$ after 2 minutes, a reaction mixture in which 0.5 equiv of PPh_3 are present featured less than 5% conversion. Substoichiometric amounts of strongly coordinating ligands (such as PPh_3) can completely poison a heterogeneous catalyst because only a fraction of the metal atoms are on the surface, whereas a homogeneous system would require >1 equivalent of ligands to poison the active site.[122,124] Furthermore, monitoring the reaction by ^{11}B NMR spectroscopy revelead the presence of an induction period during which the formation of a black precipitate was observed. This induction period was followed by significant dehydrocoupling, resulting in a sigmoidal shaped conversion-time plot, characteristic for metal particle formation reactions.[124–126] When all $Me_2NH{\cdot}BH_3$

substrate was consumed and more $Me_2NH{\cdot}BH_3$ was added, immediate dehydrocoupling was observed without an induction period. Finally, filtration of the catalytically active mixture also lead to almost complete suppresion of the reaction, and anlysis of the mixture by TEM (transmission electron microscopy) indicated the presence of metal particles.

All these tests suggest that the dehydrocoupling operates *via* a heterogeneous pathway. It is noted[126] that no single test is unambigious and that a combination of several tests is required to adequately assess whether a reaction is likely homogeneous or heterogeneous. For example, the Hg test does not work for all metals, while induction periods are also possible for homogeneous systems.

While the first examples of the dehydrocoupling of $Me_2NH{\cdot}BH_3$ were heterogeneous, homogeneous systems now dominate.[39] Homogeneous systems are particularly attractive with regard to mechanistic studies. These allow for the investigation of well-defined coordination sites and for the control of catalyst by tuning the ligand sets. There are two general mechanisms for homogeneous systems, outer-sphere and inner-sphere.



Scheme 1.17 Simplified inner-sphere dehydrogenation pathway.[39]

Outer sphere mechanisms induce dehydrogenations of amine-boranes without the direct coordination of the substrate to the metal-centre, by using metal-ligand cooperativity.[127–130] By contrast, inner-sphere mechanisms involve coordination of the amine-borane to the metal centre, forming a σ-complex, followed by dehydrogenation of the amine-borane

(Scheme 1.17). Several mechanistic pathways have been proposed for the dehydrogenation, and will be discussed in subsection 2.2.3.

1.3.2.2 σ-complexes of amine-boranes and amino-boranes

σ-complexes of amine- and amino-boranes often play an important role in the dehydrocoupling of amine-boranes operating *via* inner-sphere mechanisms. σ-complexes feature 3-centre, 2-electron M–H–B interactions, arising primarily from donation from the B–H σ-orbital to the metal (the σ*-orbital in amine-boranes is energetically high so that back-donation from the metal is often negligible).[131,132]

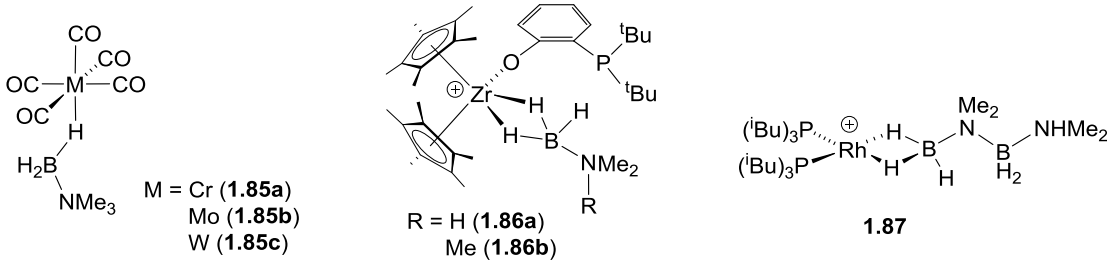


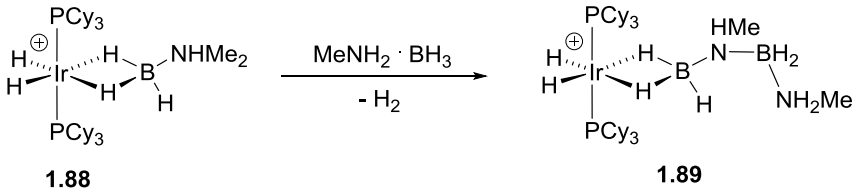
Figure 1.7 Examples of amine-borane σ-complexes. $[BAr^F_4]^-$ counterions not shown for complexes **1.91** and **1.92**.

Often, σ-complexes can be isolated using tertiary amine-boranes such as $Me_3N{\cdot}BH_3$, because the absence of N–H bonds generally prevents onward reactivity. In 1999, Shimoi reported the first examples of amine-boranes coordinated to transition metals using $Me_3N{\cdot}BH_3$.[132] When $M(CO)_6$ precursors were photolysed in the presence of $Me_3N{\cdot}BH_3$, the η^1 bound complexes $M(CO)_5(\eta^1\text{-}H_3B{\cdot}NMe_3)$ with M = Cr (**1.85a**), Mo (**1.85b**), W (**1.85c**) were formed (Figure 1.7).

Rather than being bound *via* a single M–H–B interaction, η^2 bound complexes are reported as well. Wass reported the crystallographically characterised Zr(IV) complex $[Cp^*_2Zr(\eta^2\text{-}H_3B{\cdot}NMe_3)(OC_6H_4P(^tBu)_2][BAr^F_4]$ (**1.86b)** as one such example, shown in Figure 1.6.[133] Using $Me_2NH{\cdot}BH_3$, spectroscopic evidence for the intermediacy of the secondary

dimethylamine borane adduct $[Cp^*_2Zr(\eta^2\text{-}H_3B{\cdot}NHMe_2)(OC_6H_4P(^tBu)_2]^+$ (**1.86a**) was also obtained, before dehydrocoupling proceeded to give $[Me_2N{=}BH_2]_2$ as final product.

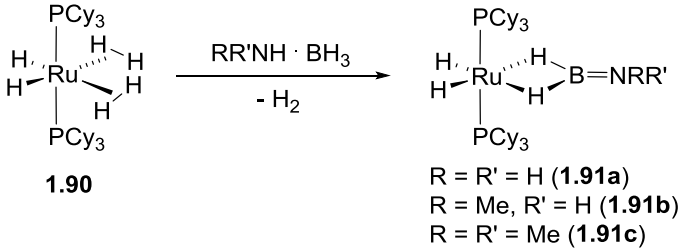
Diborazanes, $RR'_2NH{\cdot}BH_2NRR'_2{\cdot}BH_3$ (R, R' = H, and/or alkyl), are common intermediates observed during catalytic dehydrocoupling of amine-boranes. They can be thought of as simplest oligomeric species towards the formation of polyaminoboranes $[BH_2NR'R]_n$. Such diborazanes have been shown to bind to metal centres as σ-complexes. For example, the addition of one equiv. of $Me_2NH{\cdot}BH_2NMe_2{\cdot}BH_3$ to $[Rh(P^iBu_3)_2(\eta^6\text{-}C_6H_5F)][BAr^F_4]$ lead to formation of $[Rh(P^iBu_3)_2(\eta^2\text{-}H_3B{\cdot}NMe_2BH_2{\cdot}NHMe_2)][BAr^F_4]$ (**1.87**), which was crystallographically authenticated.[134] In 2011, Johnson and co-workers reported that the primary $MeNH_2{\cdot}BH_2NHMe{\cdot}BH_3$ diborazane could be isolated in a η^2-bound fashion to a metal centre.[135] When $[Ir(PCy_3)_2(H)_2(\eta^2\text{-}H_3B{\cdot}NMeH_2)][BAr^F_4]$ (**1.88**) was treated with one equivalent of $MeNH_2{\cdot}BH_3$ the new metal complex $[Ir(H)_2(PCy)_2(\eta^2\text{-}H_3B{\cdot}NHMeBH_2{\cdot}NH_2Me)][BAr^F_4]$ (**1.89**) could be isolated and structurally characterised (Scheme 1.18). This reaction can be thought of as first amine-borane oligomerisation event directly observed at a metal centre.



1.88 **1.89**

Scheme 1.18 $[BAr^F_4]^-$ counterions not shown.

Similarly, σ-complexes of amino-boranes, the products of dehydrocoupling, have also been isolated. Examples include systems of Rh, Ir, and Ru.[39] For example, Alcaraz reported the reaction of $[Ru(H)_2(H_2)_2(PCy_3)_2]$ with amine-boranes to yield $[Ru(H)_2(PCy_3)_2(\eta^2\text{-}H_2B{=}NR'R)]$ (Equation 1.4).[136] These metal-bound amino-borane species are of mechanistic interest since they have been suggested in a variety of dehydrocoupling mechanisms, despite often not being directly observed.[114,137,138]



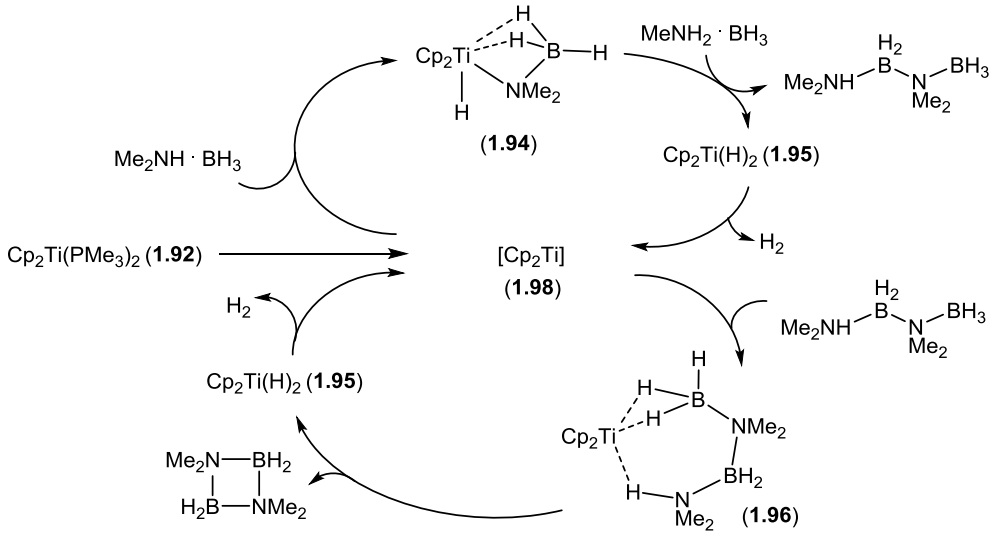
1.90

R = R' = H (**1.91a**)
R = Me, R' = H (**1.91b**)
R = R' = Me (**1.91c**)

Equation 1.4

1.3.2.3 Proposed mechanisms of the dehydrocoupling of amine-boranes

In 2006, Manners reported the Cp_2Ti^{II} (**1.93**) fragment as dehydrocoupling catalyst for $Me_2NH{\cdot}BH_3$.[139] The Cp_2Ti^{II} (**1.93**) fragment could be formed either *in-situ* from $Cp_2TiCl_2/^nBuLi$ or using $Cp_2Ti(PMe_3)_2$ (**1.92**). The catalysis was established to be homogeneous, and subsequent computational studies by Ohno and Luo suggested a stepwise mechanism.[140] In particular, initial N–H bond activation precedes B–H bond activation to form $Me_2N{=}BH_2$, which dimerises in an off-metal process to give $[Me_2N{=}BH_2]_2$ as final product. However, further kinetic mechanistic work by Manners and Lloyd Jones called this proposed mechanism into question.[141] Importantly, $Me_2NH{\cdot}BH_2NMe_2{\cdot}BH_3$ was identified as key intermediate, which is proposed to form $[Me_2N{=}BH_2]_2$ in a catalytic ring-closing process along with H_2, rather than formation of $[Me_2N{=}BH_2]_2$ *via* free $Me_2N{=}BH_2$. A mechanism with two cycles is proposed as illustrated in Scheme 1.19. $Cp_2Ti(PMe_3)_2$ (**1.92**) or Cp_2TiCl_2 / ^{n}BuLi served as sources for the "Cp_2Ti^{II}" fragment **1.93**.

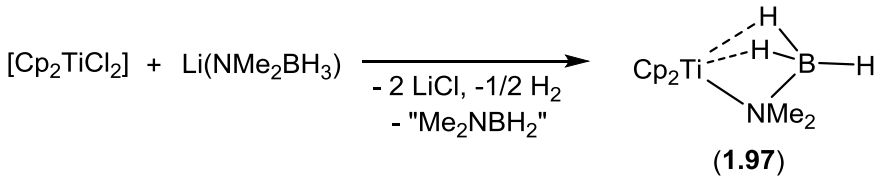


Scheme 1.19 Catalytic cycle proposed for the dehydrocoupling of $Me_2NH{\cdot}BH_3$ using $[Cp_2Ti]$.

The first step represents the oxidative N–H bond activation forming amidoborane $Cp_2Ti^{III}(\eta^2\text{-}H_3B{\cdot}NMe_2H)$ (**1.94**). It reacts with a second molecule of $Me_2NH{\cdot}BH_3$ to form $Me_2NH{\cdot}BH_2NMe_2{\cdot}BH_3$ and a transient titanium (bis)hydride (**1.95**), which reductively eliminates dihydrogen to reform the Cp_2Ti^{II} fragment. The second cycle proceeds *via* coordination of $Me_2NH{\cdot}BH_2NMe_2{\cdot}BH_3$ to form **1.96**, which undergoes catalysed ring formation to give $[Me_2N{=}BH_2]_2$ as well as titanium (bis)hydride (**1.95**). Loss of dihydrogen reforms $[Cp_2Ti]$ (**1.93**) to complete the cycle.

When independently synthesised $Me_2NH{\cdot}BH_2NMe_2{\cdot}BH_3$ was subjected to $[Cp_2Ti]$ (**1.93**), no $Me_2NH{\cdot}BH_3$ was detected, and only traces of $Me_2N{=}BH_2$ (<1%), suggesting that $Me_2NH{\cdot}BH_2NMe_2{\cdot}BH_3$ is the sole precursor of $[Me_2N{=}BH_2]_2$, contrary to Luo and Ohn's mechanism. Labelling experiments using $Me_2N\underline{D}{\cdot}BH_3$, $Me_2NH{\cdot}B\underline{D}_3$ and $Me_2N\underline{D}{\cdot}B\underline{D}_3$ established kinetic isotope effects (KIE) of 3.6(3) for N(H/D), 1.7(3) for B(H/D), and 4.5(3) for N(H/D) and B(H/D), during formation of the corresponding diborazanes. It was suggested that these KIE values are associated with the formation of $Cp_2Ti^{III}(\eta^2\text{-}H_3B{\cdot}NMe_2H)$ (**1.94**).

To support the proposed mechanism involving the Ti(II) and Ti(IV) manifolds ($Cp_2Ti(H)_2$ (**1.95**) is in oxidation state +4), a variety of Ti(0) and Ti(III) sources were tested for dehydrocoupling reactivity. Interestingly, no catalytic activity was found, and no other Ti(IV) sources were tested. However, more recent work suggested the importance of the paramagnetic titanium amidoborane $Cp_2Ti^{III}(NMe_2BH_3)$ (**1.97**) in this dehydrocoupling process. $Cp_2Ti^{III}(NMe_2BH_3)$ (**1.97**) was prepared by reacting $[Cp_2TiCl_2]$ with 2 equivalents of $Li(NMe_2BH_3)$ (Equation 1.5).[142,143]



Equation 1.5

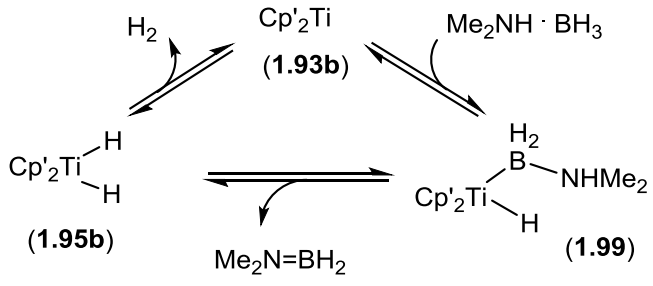
The catalytic activity of this paramagnetic Ti(III) complex was then compared with the one of *in-situ* generated $[Cp_2Ti^{II}]$. Both systems featured comparable conversions after 2 h (97% and 88%), and essentially the same turnover frequencies (10.7 h^{-1} and 11.1 h^{-1}), for **1.97** and $Cp_2Ti(PMe_3)_2$ (**1.92**), respectively. In both cases $Me_2NH{\cdot}BH_2NMe_2{\cdot}BH_3$ was observed to be formed as an intermediate, followed by formation of $[Me_2N{=}BH_2]_2$. Additionally, following the reaction mixtures by UV/VIS and EPR spectroscopy featured comparable spectra for the case of using $Cp_2Ti(PMe_3)_2$ (**1.92**) or $Cp_2Ti^{III}(NMe_2BH_3)$ (**1.97**), respectively. These results potentially suggest the importance of Ti(III) species during catalysis.

In 2018, Manners varied the substituents on the cyclopentadienyl ligands and achieved a maximum TOF of 141 h^{-1} (45% conversion of $Me_2NH{\cdot}BH_3$ after 5 min, 22 °C) using $Cp^*_2TiCl_2$ / ^{n}BuLi as precatalyst system.[115] Importantly, the substrate scope was extended to primary amine-boranes $RNH_2{\cdot}BH_3$ (R = Me, benzyl, phenylbutyl, thiophenylmethyl) giving polyamino-boranes in high molecular weight M_n of 4'000-54'000 g mol^{-1} with PDI

values ranging from 1.6-6.2. This represents the first early transition metal catalysed synthesis of high molar mass polyaminoboranes using primary amine-boranes such as $MeNH_2{\cdot}BH_3$.

Rosenthal and Beweries used the alkyne coordinated $[Cp_2M^{II}(\eta^2\text{-}Me_3SiCCSiMe_3)(L)]$ (M = Ti, no L, (**1.98a**); M = Zr, L = pyridine, (**1.98b**)) species as $[Cp_2M^{II}]$ sources and reported turnover frequencies of 3 (**1.98a**) and 1 h^{-1} (**1.98b**) for the dehydrocoupling of $Me_2NH{\cdot}BH_3$.[144] Moreover, titanium(IV) and zirconium(IV) complexes $M(NMe_2)_4$ (M = Ti, Zr) were also found to be suitable for dehydrogenating $Me_2NH{\cdot}BH_3$. Although no detailed mechanistic work has been conducted,[144] it was reported that there was no catalytic activity for the titanium(IV) compounds $TiCl_4$ and $Ti(O^iPr)_4$, indicating the importance of the amide group.

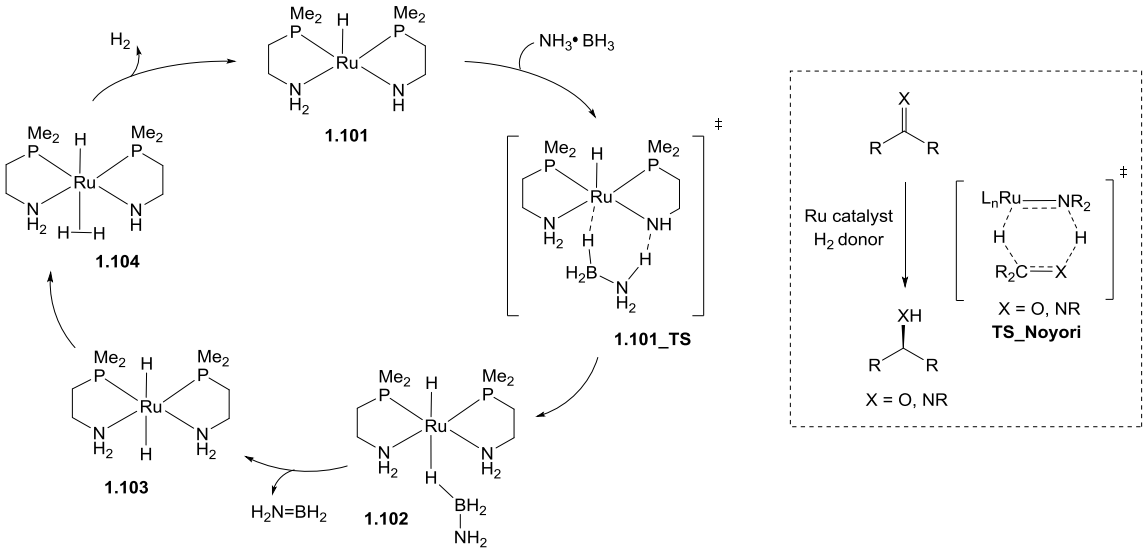
Chirik also reported the dehydrocoupling of amine-boranes with group 4 complexes.[145] In contrast to the mechanism proposed by Manners, initial B–H bond activation affording titanium hydride boryl species **1.99** is suggested (Scheme 1.20). When the catalysis is conducted under a D_2 atmosphere incorporation of deuterium is observed into the B–H positions of the $Me_2NH{\cdot}BH_3$ starting material, suggesting reversibility. Subsequently, β-hydride elimination is proposed to form $Me_2N{=}BH_2$ (dimerising to give dimeric $[Me_2N{=}BH_2]_2$), as well as titanium bis-hydride **1.95b** which loses hydrogen to regenerate Cp'_2Ti (**1.93b**). No $Me_2NH{\cdot}BH_2NMe_2{\cdot}BH_3$ was detected in this case.



Scheme 1.20 Proposed mechanism for the catalytic dehydrocoupling of $Me_2NH{\cdot}BH_3$ using sandwich complexes with Cp' = $\eta^5\text{-}C_5Me_4R$, R = $SiMe_2{}^tBu$, $SiMe_3$, ^tBu, ^iPr.

Tested catalysts included both titanium as well as zirconium based sandwich compounds. Generally, titanium based compounds featured higher activities, and the highest turnover number was achieved using the previously discussed Cp''_2Ti^{II}-N_2-$Ti^{II}Cp''_2$ (**1.16**, 420 h^{-1}). An anologous mechanism involving initial oxidative B–H bond addition, followed by β-hydride elimination to generate free $Me_2N{=}BH_2$ was also suggested for the dehydrocoupling of $NH_3{\cdot}BH_3$ using $Ni(NHC)_2$ (NHC = 2,2'-bis-(1,3,4-triphenyl-4,5-dihydro-1H-1,2,4-triazol-5-ylidene), as reported by Baker.[146,147]

In 2008, Fagnou reported the efficient dehydrocoupling of $NH_3{\cdot}BH_3$ (TOF ≈ 20'000 h^{-1}) as well as $Me_2NH{\cdot}BH_3$ using $[Ru(Cl)_2(^iPr_2PCH_2CH_2NH_2)_2]$ (**1.100**), activated by KO^tBu.[129] The mechanism was probed by DFT calculations on the model complex $[Ru(H)(Me_2PCH_2CH_2NH_2)(Me_2PCH_2CH_2NH)]$ (**1.1061** Scheme 1.20), the product of activation of $[Ru(Cl)_2(Me_2PCH_2CH_2NH_2)_2]$ with KO^tBu.



Scheme 1.20 Proposed mechanism of catalytic dehydrocoupling of $NH_3{\cdot}BH_3$ by **1.101**, with key transition state **1.101_TS**. Right: Asymmetric hydrogenation of ketones and imides *via* related transition state **TS_Noyori**.[148,149]

A cooperative inner-sphere mechanism was suggested by which the ruthenium amide is protonated to form complex **1.102**. This step was implicated to occur *via* concerted N–H/B–H bond activation as shown in transition state **1.101_TS**. The B–H bond remained

partially intact, involved in a 3-centered 2-electron interaction with the metal centre. Loss of $H_2N{=}BH_2$ forms bis(hydride) **1.103** which gives dihydrogen adduct **1.104** in a rate-determining step. Loss of dihydrogen reforms **1.101.** This mechanism is closely related to the bifunctional Noyori-Morris mechanism reported for the asymmetric hydrogenation of ketones and imides (Scheme 1.20, right).[148,149]

In 2009, the group of Schneider communicated the dehydrogenation of $NH_3{\cdot}BH_3$ using ruthenium pincer complex [Ru(H)(PMe_3)(PNP)] (**1.105**, PNP = $N(CH_2CH_2P^iPr_2)_2$).[150] This complex featured extremely high activities towards formation of polymeric $[H_2NBH_2]_n$ with only small amounts of borazine detected (TOF ≈ 12'000 h^{-1}). The mechanism of the dehydrocoupling of $Me_2NH{\cdot}BH_3$ using this complex was studied as well.[128]

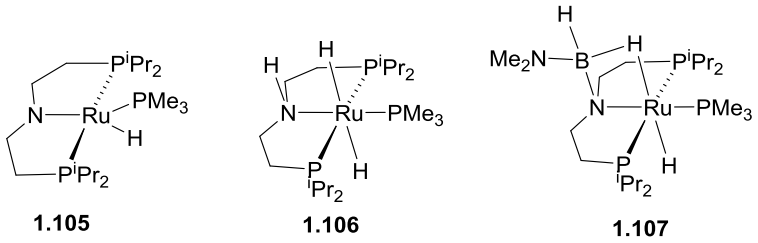
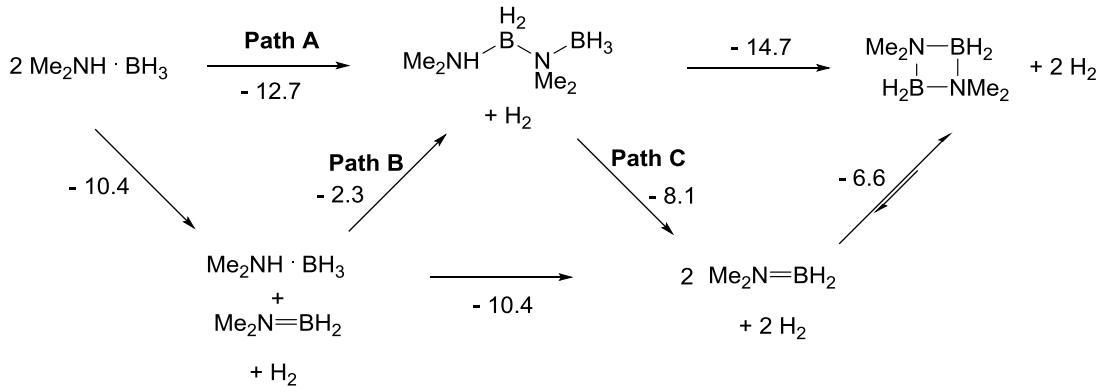


Figure 1.8 Schneider's ruthenium species investigated for the dehydrocoupling of $Me_2NH{\cdot}BH_3$.

Catalysis of $Me_2NH{\cdot}BH_3$ starting from 2% **1.105** proceeded to 70% conversion in a fast, initial kinetic regime (initial TOF ≈ 3'600 h^{-1}), followed by a slow, second regime (TOF ≈ 1.5 h^{-1}), suggesting a change in mechanism.[128] [Ru(H)$_2$(PMe_3)(PNP^H)] (**1.106**, PNP^H = $HN(CH_2CH_2P^iPr_2)_2$, Figure 1.8) was identified as resting state during the first kinetic regime, and featured very similar reaction kinetics compared to **1.105**. During late stages of catalysis, a second ruthenium complex was observed and identified as **1.107** (Figure 1.8). This complex can be isolated in 70% upon addition of 2.3 equiv of $Me_2NH{\cdot}BH_3$ to [Ru(H)(PMe_3)(PNP)] (**1.105**), and features a four-membered Ru–N–B–H metallacycle. Starting the catalysis with this metallacycle **1.106** gave very similar kinetic compared to the second, slow kinetic regime.[128]

Upon dehydrocoupling $Me_2NH{\cdot}BH_3$, the formation of both $Me_2N{=}BH_2$ as well as $Me_2NH{\cdot}BH_2NMe_2{\cdot}BH_3$ were detected as intermediates, and both experimental evidence and thermodynamic calculations were used to investigate their role during catalysis. Two possible pathways were considered for the formation of $Me_2NH{\cdot}BH_2NMe_2{\cdot}BH_3$ (Scheme 1.21): Metal-centered BN coupling of two $Me_2NH{\cdot}BH_3$ (Path A, -12.7 kcal mol^{-1}), and catalysed dehydrocoupling of $Me_2NH{\cdot}BH_3$, followed by uncatalysed rearrangement of $Me_2N{=}BH_2$ with $Me_2NH{\cdot}BH_3$ (Path B, -2.3 kcal mol^{-1}).

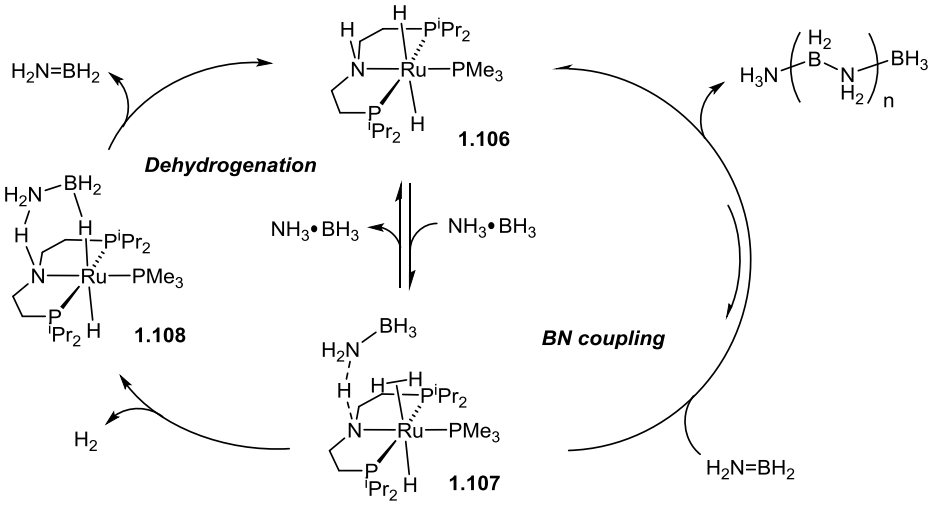


Scheme 1.21 Thermochemistry of the dehydrocoupling of $Me_2NH{\cdot}BH_3$. Free enthalpies in kcal mol^{-1}.[128]

$Me_2N{=}BH_2$ is known to be in rapid equilibrium with its dimeric form, although the position lies far on the side of the dimer (K_{eq} >> 100, 100 °C).[151] Pathway B was thus tested experimentally by dissolving both dimeric $[Me_2N{=}BH_2]_2$ and $Me_2NH{\cdot}BH_3$ in THF, in absence of catalyst. No formation of $Me_2NH{\cdot}BH_2NMe_2{\cdot}BH_3$ was observed at RT and thus Schneider concluded that although Path B is thermodynamically feasible (-2.3 kcal mol^{-1}), there is a high, insurmountable kinetic barrier. Thus, it is argued that $Me_2NH{\cdot}BH_2NMe_2{\cdot}BH_3$ is formed by metal-centered Path A. Notably, this is in line with DFT calculations by Zimmerman *et al*., who reported the barrier for the rearrangement of the related $H_3N{\cdot}BH_3$ and $H_2N{=}BH_2$ to form $H_3N{\cdot}BH_2NH_2{\cdot}BH_3$ at ΔG_{298K} = 31 kcal mol^{-1}.[152] This barrier would be inaccessible at room temperature, and the corresponding barrier with the more bulky methyl substituted congeners is likely even higher.

To account for the formation of $Me_2N{=}BH_2$, the initial concentrations of $Me_2NH{\cdot}BH_3$ was varied. At higher concentrations of $Me_2NH{\cdot}BH_3$, a greater proportion of diborazane relative to $Me_2N{=}BH_2$ was formed ($[Me_2NH{\cdot}BH_3]_0$=0.54 M, $Me_2NH{\cdot}BH_2NMe_2{\cdot}BH_3/Me_2N{=}BH_2$ = 0.44; $[Me_2NH{\cdot}BH_3]_0$=0.1 M, $Me_2NH{\cdot}BH_2NMe_2{\cdot}BH_3/Me_2N{=}BH_2$ = 4). This showed that $Me_2N{=}BH_2$ and $Me_2NH{\cdot}BH_2NMe_2{\cdot}BH_3$ are formed *via* different pathways, and that $Me_2NH{\cdot}BH_2NMe_2{\cdot}BH_3$ is indeed formed *via* a metal-catalysed path. When the reaction was started from $Me_2NH{\cdot}BH_2NMe_2{\cdot}BH_3$, $Me_2N{=}BH_2$ was detected as well, suggesting that the formation of $Me_2NH{\cdot}BH_2NMe_2{\cdot}BH_3$ is reversible (Path B). Similar observations were made previously by the groups of Hall and Weller, and are in line with the calculations suggesting a close to thermoneutral process (ΔG = 2.3 kcal mol^{-1}, Scheme 1.21).[134,153] Dehydrocyclisation from $Me_2NH{\cdot}BH_2NMe_2{\cdot}BH_3$ to $[Me_2N{=}BH_2]_2$ was not probed.

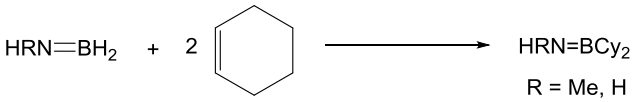
In 2013, a more detailed study established that catalysts [Ru(H)(PMe_3)(PNP)] (**1.105**) and [$Ru(H)_2(PMe_3)(PNP^H)$] (**1.106**) are likely to operate *via* two different mechanisms, rather than in the same catalytic cycle.[127] For example, both catalysts featured first order behaviour using $NH_3{\cdot}BH_3$. However, using the $N\underline{D_3}{\cdot}BH_3$ analogue as substrate led to first-order kinetics for catalyst **1.106**, and zeroth order behaviour with **1.95**, suggesting a change in the rate-determining step. Additionally, different degrees of cross-linking was observed in the resulting aminoborane $[H_2NBH_2]_n$ product distribution.



Scheme 1.22 Proposed mechanism for the dehydrocoupling of $NH_3{\cdot}BH_3$ using **1.106**.

For the catalysis using **1.106**, a combined experimental and computational study led to the proposed mechanism shown in Scheme 1.22. $[Ru(H)_2(PMe_3)(PNP^H)]$ (**1.106**) is proposed to be in equilibrium with complex **1.107**, *via* a reversible outer-sphere N–H bond activation process. The left half accounts for the dehydrogenation of $NH_3{\cdot}BH_3$, releasing free $H_2N{=}BH_2$. The right half describes the metal-mediated BN bond formation *via* insertion of the previously formed free $H_2N{=}BH_2$.

Amino-boranes $HRN{=}BH_2$ with R = H, or Me, are difficult to observe directly, and are generally transient species during catalytic dehydrocoupling. Cyclohexene can react with $HRN{=}BH_2$ to form the hydroborated species $HRN{=}BCy_2$ (Equation 1.6), and can thus serve as a useful marker for free amino-boranes (in case hydroboration is kinetically competitive to BN coupling reactions of $HRN{=}BH_2$).[39]

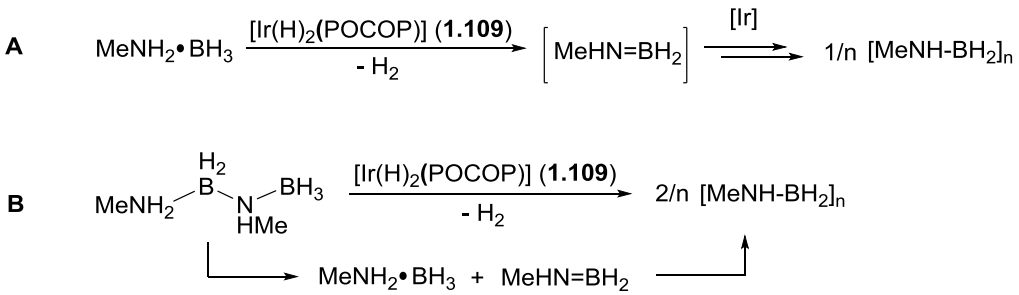


Equation 1.6

No $H_2N{=}BCy_2$ was detected during catalysis in Schneider's case, and it was suggested that this is due to BN coupling to be faster than hydroboration, as has been observed in many other cases.[39] DFT calculations showed that the barrier for insertion of free $H_2N{=}BH_2$ to

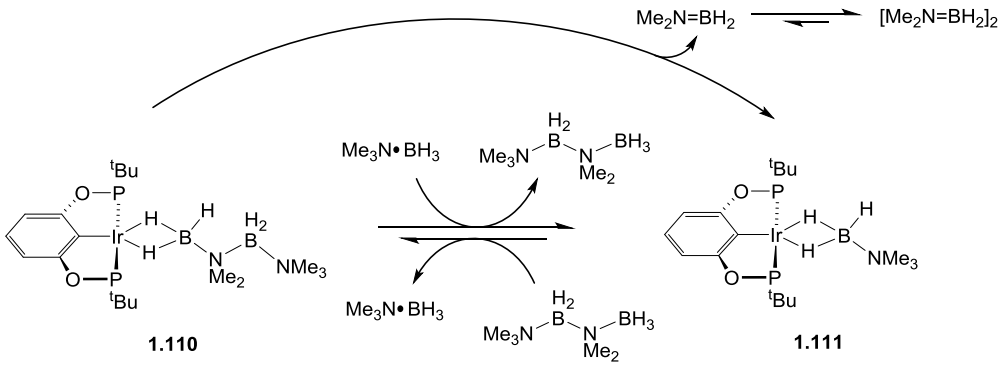
form polymeric $[H_2NBH_2]_n$ is indeed low, and comparable to dehydrogenation.[127] However, the formation of $H_2N{=}BCy_2$ was observed after the reaction was complete. This demonstrates the presence of free $H_2N{=}BH_2$ indirectly,[39] and suggests that BN coupling in the polymer is reversible. Since $NH_3{\cdot}BH_2NH_2{\cdot}BH_3$ is known to be stable under the employed reaction conditions, Schneider suggested that this polymer degradation, the reverse of BN coupling, is likely metal catalysed. Additionally, BN coupling was computed to be close to thermoneutral, and thus in line with a reversible process.

Similarly, Manners reported a case of reversible, metal-centered BN coupling using Brookhart's Ir catalyst $[Ir(H)_2(POCOP)]$ (**1.109**, POCOP = $[\mu_3\text{-}1,3\text{-}(OP^tBu_2)_2C_6H_3]$).[154] When **1.109** was subjected to $MeNH_2{\cdot}BH_3$ polymeric $[MeNH\text{-}BH_2]_n$ was formed, and the same product was observed when $MeNH_2{\cdot}BH_2NMeH{\cdot}BH_3$ was used as substrate (Scheme 1.23). Importantly, the parent amine-borane $MeNH_2{\cdot}BH_3$ was observed as intermediate, suggesting that $MeHN{=}BH_2$ is also formed, either remaining bound on-metal or free in solution. Trapping by cyclohexene did not lead to formation of $Cy_2B{=}NHMe$, presumably because Ir catalysed oligomerisation is kinetically outcompeting hydroboration. When $MeNH_2{\cdot}BH_2NMeH{\cdot}BH_3$ was heated to 70 °C both $MeNH_2{\cdot}BH_3$ as well as trimeric $[MeHN{=}BH]_3$ was observed. In this case, addition of cyclohexene lead to formation of $Cy_2B{=}NHMe$, strongly suggesting the presence of $MeHN{=}BH_2$.



Scheme 1.23 Proposed mechanism of polymerisation of A) $MeNH_2{\cdot}BH_3$, and B) $MeNH_2{\cdot}BH_2NMeH{\cdot}BH_3$ using Brookhart's catalyst **1.109**.

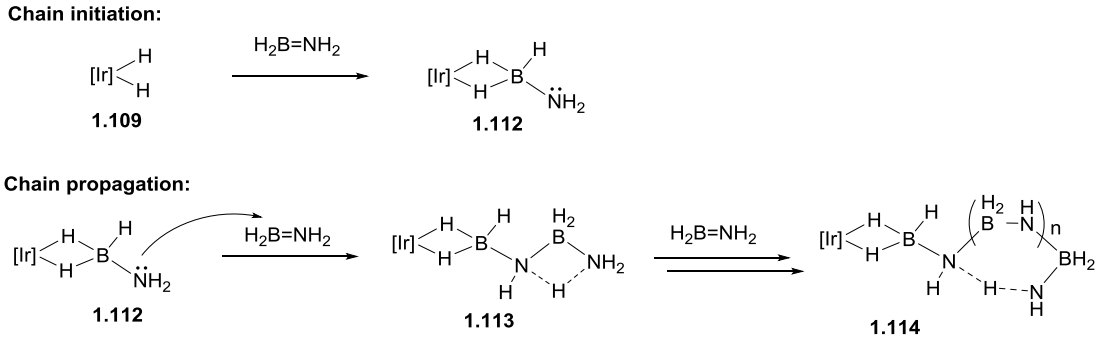
In a detailed follow-up paper, the thermal and metal-catalysed redistribution reaction of the model diborazane $Me_3N{\cdot}BH_2NMe_2{\cdot}BH_3$ (lacking N–H bonds) was studied both by experiment and kinetic simulations. $Me_3N{\cdot}BH_2NMe_2{\cdot}BH_3$ was experimentally found to form $Me_3N{\cdot}BH_3$ as well as $Me_2N{=}BH_2$.[155]



Scheme 1.24 Proposed kinetic model for the redistribution reaction of $Me_3N{\cdot}BH_2NMe_2{\cdot}BH_3$.

The kinetic model suggests that $[Ir(H)_2(POCOP)]$ (**1.109**) initially reacts with $Me_3N{\cdot}BH_2NMe_2{\cdot}BH_3$ to form σ-complex **1.110**, from which redistribution occurs to form the proposed σ-complex **1.111** as well as $Me_2N{=}BH_2$ (Scheme 1.24). $Me_3N{\cdot}BH_2NMe_2{\cdot}BH_3$ can then reversibly replace bound $Me_3N{\cdot}BH_3$ to reform **1.110**. Based on the dimerisation of $Me_2N{=}BH_2$ in absence of Ir metal catalyst, in the presence of it, as well as kinetic simulations, dimerisation of $Me_2N{=}BH_2$ is suggested to be metal-catalysed. Similarly, based on DFT calculations, Peruzzini *et al.* suggested that the dimerisation of $H_2N{=}BH_2$ is an on-metal process occuring during a Pd catalysed dehydrocoupling of $NH_3{\cdot}BH_3$.[156]

The dehydropolymerisation of $RNH_2{\cdot}BH_3$ (R = H, Me, ^{n}Bu) using $[Ir(H)_2(POCOP)]$ (**1.109**) was the first example of a well-defined, homogeneous polymerisation of amine-boranes.[157] A chain-growth mechanism was proposed to proceed *via* slow initial dehydrogenation of $RNH_2{\cdot}BH_3$ followed by rapid insertion of the resulting $RHN{=}BH_2$.[127] This experimental proposal was later followed by a recent computational study by Paul.[158] A low energy pathway for the chain initiation and propagation is shown in Scheme 1.25.

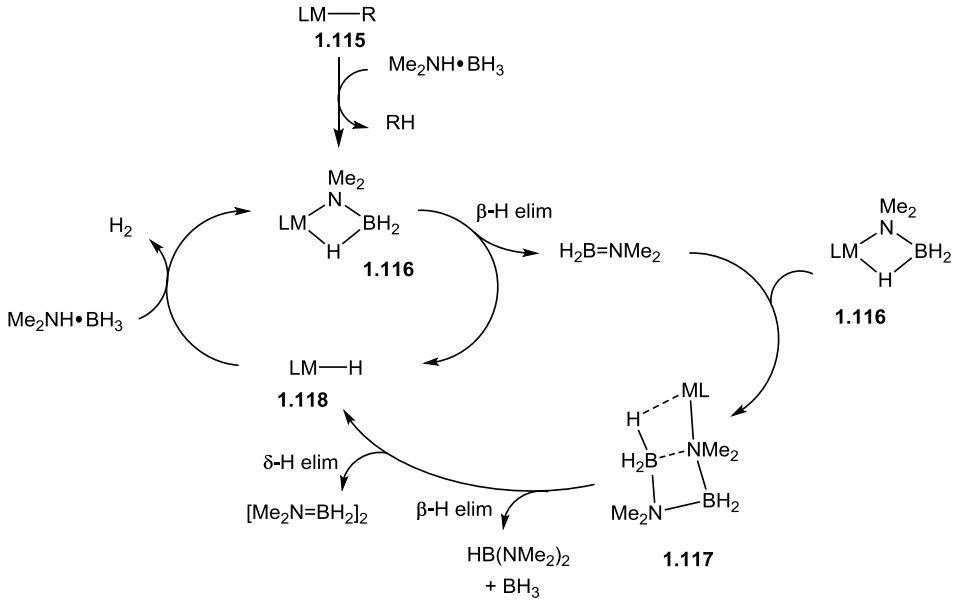


Scheme 1.25 Computationally proposed mechanism for the Ir catalysed dehydropolymerisation of $NH_3{\cdot}BH_3$.

Following dehydrogenation of $NH_3{\cdot}BH_3$ catalyst [Ir(H)$_2$(POCOP)] (**1.109**) reacts with the resulting $H_2N{=}BH_2$ to form σ-complex **1.112**, analogous to **1.111**. Frontier Molecular Orbital (FMO) analysis revealed that the HOMO of **1.112** is best represented as the lone pair residing on the terminal nitrogen atom. This lonepair is then postulated to attack the boron atom of free $H_2B{=}NH_2$ forming **1.113**. This process features an extremely low barrier of 3.6 kcal mol^{-1}. Complex **1.113** also exhibits a terminal nitrogen atom, and can undergo subsequent nucleophilic attack on another $H_2B{=}NH_2$ monomer to grow the polyaminoborane chain. The first three consecutive monomer additions were calculated to occur at very low barriers as well (4.6, 5.0 and 7.1 kcal mol^{-1}, respectively), in an overall process that is thermodynamically downhill (the corresponding thermodynamic stability gains are 8.8, 9.9 and 9.8 kcal mol^{-1}, respectively). The calculated mechanistic scenario is low in energy, and is in line with the experimentally proposed chain-growth mechanism by Manners *et al*.[127,158] Notably, the propagation occurs *via* nucleophilic attack of the terminal nitrogen based lone pairs, and thus differs from the insertion mechanism proposed for Ziegler-Natta ethylene polymerisation.

Catalytic dehydrocoupling of amine-boranes is not limited to transition metal complexes, and a number of main group catalysts has been reported in the literature.[159–163] For example, Hill investigated alkyl and amide Mg and Ca complexes (**1.115**) for the dehydrocoupling of $Me_2NH{\cdot}BH_3$.[161] Although the investigated complexes were sluggish,

and required several days at 60 °C to go to completion, the reactions were shown to be catalytic in the sense of showing several turnovers per metal centre. The observation of amidoborane LM(NMe_2BH_3) (**1.116**), $Me_2N{=}BH_2$, coordinated diborazane in the form of LM($NMe_2{\cdot}BH_2NMe_2{\cdot}BH_3$) (**1.117**, L = ligand set), as well as metal hydride LM-H (**1.118**) led to the proposed mechanism shown in Scheme 1.26.



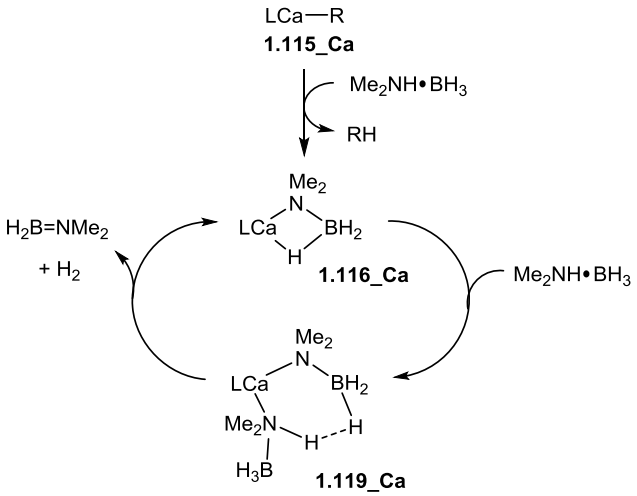
Scheme 1.26 Proposed mechanism for the dehydrocoupling of $Me_2NH{\cdot}BH_3$ using group 2 metal alkyl and amide complexes.

Initial N–H bond activation forms amidoborane complex LM(NMe_2BH_3) (**1.116**), which can undergo β-hydride elimination to release $Me_2N{=}BH_2$. This intermediate is proposed to insert into the M–B bond of **1.116** to form **1.117** containing the $[NMe_2{\cdot}BH_2NMe_2{\cdot}BH_3]^-$ anion. From **1.117**, two pathways are possible. First, β-B–H elimination can form $HB(NMe_2)_2$ and BH_3 as well as metal hydride LM–H (**1.118**). The second option is a relatively rare case of a δ-B–H elimination forming $[Me_2N{=}BH_2]_2$ as well as the same metal hydride species **1.118** as for the first option.

Hill found that Mg based catalysts are more efficient in the dehydrocoupling process than their Ca congeners. It was postulated that this could be explained by the difference in charge

density, and that an increase in charge or reduction in ionic radius leads to more stable amidoborane complexes of type **1.116** towards β-H elimination.

A computational study of the dehydrocoupling of secondary amine-boranes catalysed by group 2 metal complexes was later conducted by Sicilia.[164] For Mg as group 2 metal, DFT calculations support the mechanism proposed by Hill (Scheme 1.26). For the analogous Ca complexes, the β-H elimination from amidoborane **1.116** to form metal hydride LM-H (**1.118**) was not found to occur. Instead, it is proposed that a second equivalent of amine-borane is required to coordinate to the metal centre to form **1.119_Ca** (Scheme 1.27).



Scheme 1.27 Computationally invoked mechanism for the dehydrocoupling of $Me_2NH{\cdot}BH_3$ using Ca catalysts.

Subsequently, the hydridic BH of the amido-borane interacts with the protic NH of the coordinated amine-borane, and release dihydrogen as well as amino-borane, regenerating amidoborane **1.116_Ca**. It was argued that the two differing mechanisms are due to the larger radius of the Ca ion, as well as a relative instability of the calcium hydride compared to the amidoborane.

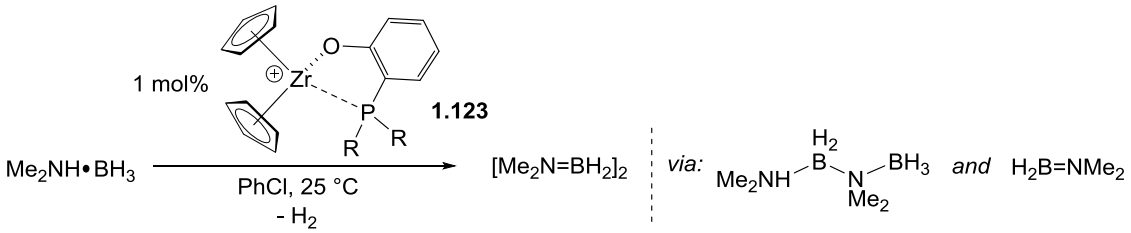
Both mechanisms (Scheme 1.26 and 1.27) have in common that the oxidation state of the d^0 early metal complexes remains unchanged throughout catalysis. Additionally, it is the N–H bond that is preferentially activated to form amido metal bonds, rather than initial B–

H bond activation. This contrasts with mid- and late metal mechanisms, in which a change in oxidation state is frequently invoked,[139,142,165–167] and B–H bond activation represents the first step of amine-borane activation.[39,145,154,155,158]

Additional studies extended the dehydrocoupling of amine-boranes to other d^0 metal catalysts and supported the charge-density theory: There is an increasing catalytic efficiency with greater electronic density on the metal centre.[159,160] Anticipating increased catalytic activity of d^0 group 3 metal catalysts compared to the previously studied group 2 congeners, Hill explored the dehydrocoupling of $Me_2NH{\cdot}BH_3$ using Y and Sc based catalysts.[159] Treatment of 3 mol% $[Y(N(SiMe_3)_2)_3]$ (**1.120**) lead to complete consumption of $Me_2NH{\cdot}BH_3$ to give 90% $[Me_2N{=}BH_2]_2$ and 10% after 12 h at 60 °C. When Sc congener $[Sc\{N(SiHMe_2)_2\}_3(THF)_2]$ (**1.121**) was employed, featuring a smaller M^{3+} radius compared to Y^{3+}, the same reaction was complete within 1 h under otherwise same conditions. In an attempt to elucidate the active species, 4 equiv of $Me_2NH{\cdot}BH_3$ were added to the Sc amided precatalyst (**1.121**), the Sc complex $[Sc\{N(SiHMe_2)_2\}(NMe_2{\cdot}BH_2NMe_2{\cdot}BH_3)_2]$ (**1.122**) was isolated and crystallographically authenticated. This species also contains the $[NMe_2{\cdot}BH_2NMe_2{\cdot}BH_3]^-$ anion, in analogy to **1.117**, and an analogous mechanism to the group 2 metal congeners was suggested as discussed previously (Scheme 1.26).

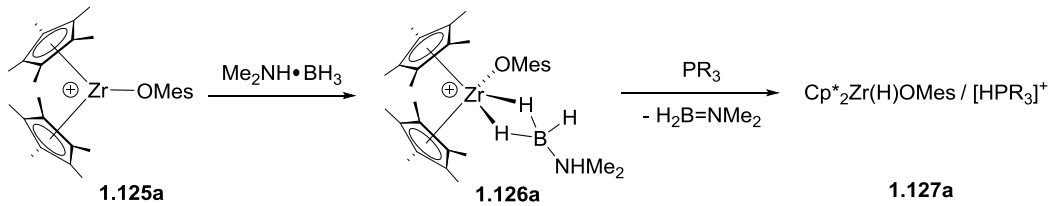
In 2010, Bercaw and Miller reported the non-catalytic dehydrogenation of $Me_2NH{\cdot}BH_3$ using a frustrated lewis pair (FLP), namely $P^tBu_3/B(Ar^F)_3$.[168] Wass replaced the electrophilic borane with an electrophilic transition metal centre, such as Zr(IV), and was able to effect the efficient dehydrocoupling of $Me_2NH{\cdot}BH_3$ (Scheme 1.28).[133,169] Using $[Cp_2Zr(OC_6H_4PR_2)]^+$ (R = $^tBu_2$, **1.123a**), a turnover frequency of 600 h^{-1} was reported, the highest for group 4 catalysts reported thus far. Both $Me_2N{=}BH_2$ as well as $Me_2NH{\cdot}BH_2NMe_2{\cdot}BH_3$ were detected as intermediates, and a detailed mechanistic study

was reported in 2016.[169] When less basic phosphines were used, such as with R = 3,5-CF_3-C_6H_3 (**1.123b**), only sluggish conversion was observed, suggesting that the phosphine is involved in N–H bond activation of the amine-borane substrate.



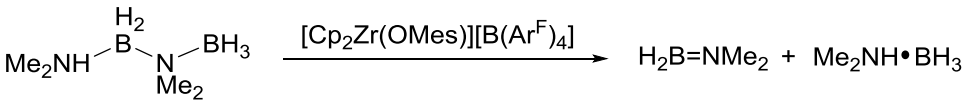
Scheme 1.28 Catalytic dehydrocoupling of $Me_2NH{\cdot}BH_3$ using $[Cp_2Zr(OC_6H_4PR_2)][B(Ar^F)_4]$ (**1.123**). R = alkyl, aryl. $[B(Ar^F)_4]^-$ counterion not shown.

The role of the aryl tether in **1.123** was probed. While *intermolecular* FLPs such as $[Cp_2Zr(OMes)]^+$ / P^tBu_3 (**1.124a**) were still found to dehydrocouple and give $Me_2N{=}BH_2$ as well as $Me_2NH{\cdot}BH_2NMe_2{\cdot}BH_3$ as intermediates, no catalysis was observed in absence of phosphines. Instead, η^2-$H_3B{\cdot}NHMe_2$ adducts were observed and in the case of $[Cp^*_2Zr(OMes)(\eta^2\text{-}H_3B{\cdot}NHMe_2)]^+$ (**1.126a**) the product was crystallographically characterised (Scheme 1.29). When basic phosphines (e.g., P^tBu_3) were added to these adducts, $Me_2N{=}BH_2$, zirconium hydrides such as **1.127a** and a phosphonium species $[HPR_3]^+$ were formed (Scheme 1.29). Subsequently, zirconium hydride reacts with $[HPR_3]^+$ to form dihydrogen. Importantly, no formation of diborazane was observed when an excess of $Me_2NH{\cdot}BH_3$ was added to **1.125a**. Hence, it was argued that both, the presence of a Lewis acid and Lewis base is required to effect dehydrogenation.



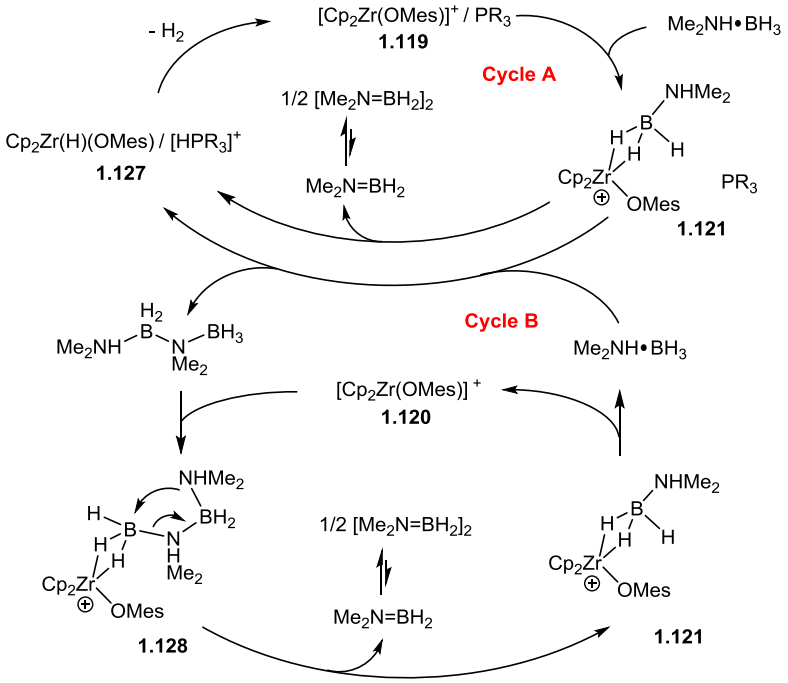
Scheme 1.29 Stoichiometric reaction of $[Cp^*_2ZrOMes][B(Ar^F)_4]$ (**1.125a**) with $Me_2NH{\cdot}BH_3$, followed by addition of phosphine PR_3. $[B(Ar^F)_4]^-$ counterion not shown.

When $Me_2NH{\cdot}BH_2NMe_2{\cdot}BH_3$ was added directly to $[Cp_2Zr(OMes)]^+$, the formation of both $Me_2NH{\cdot}BH_3$ as well as $Me_2N{=}BH_2$ was observed (Equation 1.7), similar to the redistribution reactions previously discussed by Manners.[154,155]



Equation 1.7

Importantly, there was no further dehydrogenation of $Me_2NH{\cdot}BH_3$. Only when a phosphine was added, further dehydrogenation was observed.



Scheme 1.30 Proposed mechanism for the catalytic dehydrocoupling of $Me_2NH{\cdot}BH_3$ using a Zr(IV) / P FLP.

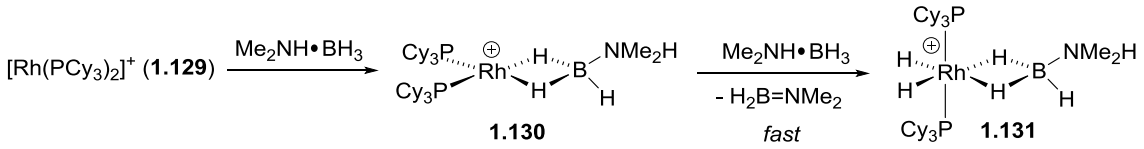
These observations led to the proposed mechanism shown in Scheme 1.30. Cycle A describes the dehydrogenation to form $Me_2N{=}BH_2$ which is thought to require both the Lewis acid and Lewis basic motif. By contrast, Cycle B describes the formation of diborazane and its redistribution which does not require the Lewis base motif (PR_3). In particular, $Me_2NH{\cdot}BH_2NMe_2{\cdot}BH_3$ is proposed to be formed *via* recombination of $Cp_2Zr(OMes)(\eta^2\text{-}H_3B{\cdot}NHMe_2)]^+$ (**1.121**) with $Me_2NH{\cdot}BH_3$. A transient $Cp_2Zr(OMes)(\eta^2$-

$H_3B{\cdot}NMe_2BH_2{\cdot}NHMe_2)]^+$ (**1.128**) is suggested to rearrange to release $Me_2N{=}BH_2$ and reform **1.121**.

1.3.2.4 Generic mechanism for the dehydrocoupling of $Me_2NH{\cdot}BH_3$

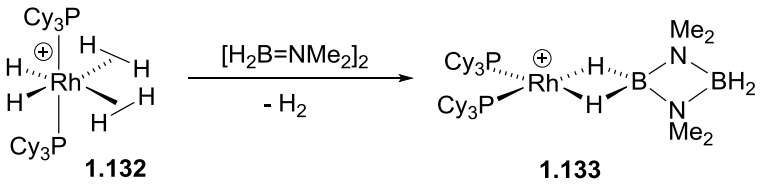
In 2012, Weller and Lloyd-Jones reported a detailed mechanistic study on the dehydrocoupling of $Me_2NH{\cdot}BH_3$ using $[Rh(PCy_3)_2][B(Ar^F)_4]$ (**1.129**). A rich mechanistic landscape has been observed, with both $Me_2NH{\cdot}BH_2NMe_2{\cdot}BH_3$ as well as $Me_2N{=}BH_2$ being observed as intermediates, and several Rh oxidation states manifolds playing a role. First, several key observations will be presented, before the derived mechanism will be discussed.

The addition of 2 equiv of $Me_2NH{\cdot}BH_3$ to **1.129** initially formed Rh(I) complex $[Rh(PCy_3)_2(\eta^2\text{-}H_3B{\cdot}NHMe_2)][B(Ar^F)_4]$ **1.130**, which rapidly released $Me_2N{=}BH_2$ to form Rh(III) species $[Rh(PCy_3)_2(H)_2(\eta^2\text{-}H_3B{\cdot}NHMe_2)][B(Ar^F)_4]$ **1.131** (Scheme 1.31).



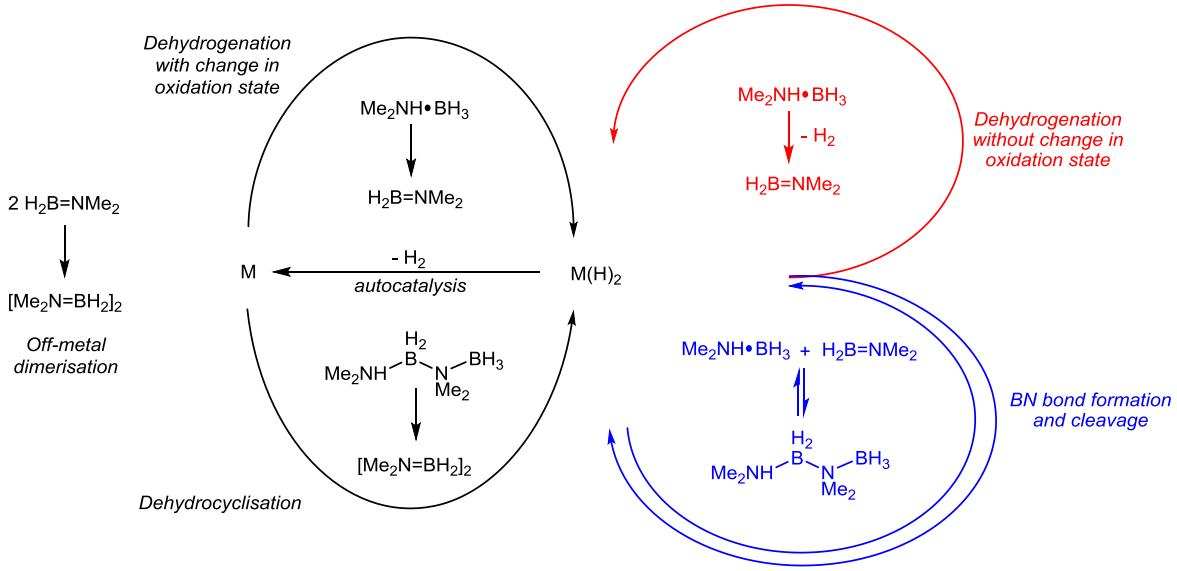
Scheme 1.31 Reaction of **1.129** with 2 equivalents of $Me_2NH{\cdot}BH_3$. $[B(Ar^F)_4]^-$ not shown.

Dihydrogen loss from **1.131** does not occur easily, and it is suggested that this Rh^{III} complex is the active catalyst, operating in a constant oxidation state after rapid formation from Rh^I. However, addition of $[Me_2N{=}BH_2]_2$ to Rh^{III} species **1.132** led to the immediate formation of Rh^I species **1.133** (Scheme 1.32). This demonstrates that $[Me_2N{=}BH_2]_2$ can promote the reduction of Rh^{III} to Rh^I, by facilitating the reductive elimination of dihydrogen. Indeed, it was found that $[Me_2N{=}BH_2]_2$ acted as a modifier under catalytic conditions by generating kinetically relevant amounts of Rh^I species. For example, when exogeneous $[Me_2N{=}BH_2]_2$ was added from the start of the catalysis of $Me_2NH{\cdot}BH_3$ using **1.129**, a faster reaction was observed.



Scheme 1.32 Reductive elimination of **1.132** upon addition of $[Me_2N{=}BH_2]_2$ to form Rh^I complex **1.130**. $[B(Ar^F)_4]^-$ not shown.

Thus, it was established that there are two parallel catalytic cycles: A slow cycle catalysed by Rh^{III} in constant oxidation state, and a second, faster cycle catalysed by a Rh^I/Rh^{III} manifold.



Scheme 1.33 Generic mechanism for the dehydrocoupling of $Me_2NH{\cdot}BH_3$. M = catalyst.

The observations made during the study led to the simplified, generic mechanism shown in Scheme 1.33. There are five main processes: 1) Off-metal dimerisation of $Me_2N{=}BH_2$, 2) Dehydrogenation of $Me_2NH{\cdot}BH_3$ to $Me_2N{=}BH_2$ with a change in oxidation state, 3) Dehydrocyclisation of $Me_2NH{\cdot}BH_2NMe_2{\cdot}BH_3$ to $[Me_2N{=}BH_2]_2$, 4) Dehydrogenation of $Me_2NH{\cdot}BH_3$ to $Me_2N{=}BH_2$ without change in oxidation state, 5) Potentially reversible B–N bond formation between $Me_2NH{\cdot}BH_3$, $Me_2N{=}BH_2$, as well as $Me_2NH{\cdot}BH_2NMe_2{\cdot}BH_3$. This scheme gives an overview in the mechanistic possibilities for the dehydrocoupling $Me_2NH{\cdot}BH_3$, and can be used as guide in the exploration of the mechanism of other transition metal or main group catalysts.

1.4 Conclusion and outlook

As outlined in section 1.3, the dehydrocoupling of amine-boranes is a relatively underdeveloped field. One challenge is to find more active catalysts, and to understand the mechanism of the polymerisation in order to harness the properties of the resulting inorganic polymers. Chapter 2 will therefore describe a new type of catalyst class, namely transition metal imides. In particular, titanium imide complexes of type Cp*Ti{MeC(NMe)$_2$}(NR) will be presented as efficient catalysts for the dehydrocoupling of amine-boranes, and the mechanism using DMAB as model substrate will be described in depth. The experimental results suggest a mechanism without change in oxidation state (*cf.* Scheme 1.30, right), differing from the majority of previously reported group 4 catalysts.

As outlined in section 1.2, the imido substituent R on transition metal imide systems M=NR had a profound effect on the bonding and reactivity of these complexes. However, there are only a handful examples of boryl substituted imide complexes across the entire periodic table, and their reactivity is virtually unexplored. Therefore, the Mountford group recently established the first synthetic protocols to furnish group 4 metal borylimide complexes of type LM=N{B(NDippCH)$_2$}. Hence, the aim of Chapters 3 and 4 will be to extend these studies. Chapter 3 will establish the first in-depth reactivity study of borylimido complexes using the model titanium borylimido complex Cp*Ti(HPP){NB(NDippCH)$_2$} (**1.83**) with a variety of small molecule classes, and benchmark it to related titanium imide complexes. Chapter 4 aims to extend the synthetic protocols which was limited by the fact that only the NB(NDippCH)$_2$} and closely related borylimides could be installed on to metal fragments. These suffered from the disadvantage to be very bulky, and the fact that the boron atom is flanked by two additional nitrogen atoms. Thus, an oxidative addition route was explored to access titanium borylimide complexes of general formula LTi=NBR$_2$.

1.5 References

1 W. A. Nugent and B. L. Haymore, *Coord. Chem. Rev.*, 1980, **31**, 123–175.
2 W. A. Nugent and J. M. Mayer, *Metal-Ligand Multiple Bonds*, Wiley-Interscience, New York, 1988.
3 D. E. Wigley, in *Progress in Inorganic Chemistry*, ed. K. D. Karlin, Wiley-Interscience, New York, 1994, vol. 42, pp. 239–482.
4 M. H. Chisholm and I. P. Rothwell, in *Comprehensive Coordination Chemistry*, Pergamon Press, Oxford, 1987, vol. 2, pp. 161–184.
5 P. Mountford, *Chem. Commun.*, 1997, 2127–2134.
6 A. P. Duncan and R. G. Bergman, *Chem. Rec.*, 2002, **2**, 431–445.
7 S. A. Blum, V. A. Rivera, R. T. Ruck, F. E. Michael and R. G. Bergman, *Organometallics*, 2005, **24**, 1647–1659.
8 S. Y. Lee and R. G. Bergman, *J. Am. Chem. Soc*, 1996, **118**, 6396–6406.
9 T. R. Cundari, A. Thomas R. Klinckman and P. T. Wolczanski, *J. Am. Chem. Soc*, 2002, **124**, 1481–1487.
10 J. de With and A. D. Horton, *Angew. Chem. Int. Ed.*, 1993, **32**, 903–905.
11 B. A. Arndtsen, R. G. Bergman, T. A. Mobley and T. H. Peterson, *Acc. Chem. Res.*, 1995, **28**, 154–162.
12 P. Royo and J. Sánchez-Nieves, *J. Organomet. Chem.*, 2000, **597**, 61–68.
13 N. Adams, H. J. Arts, P. D. Bolton, D. Cowell, S. R. Dubberley, N. Friederichs, C. M. Grant, M. Kranenburg, A. J. Sealey, B. Wang, P. J. Wilson, A. R. Cowley, P. Mountford and M. Schröder, *Chem. Commun. (Camb).*, 2004, 434–435.
14 P. D. Bolton and P. Mountford, *Adv. Synth. Catal.*, 2005, **347**, 355–366.
15 H. R. Bigmore, S. R. Dubberley, M. Kranenburg, S. C. Lawrence, A. J. Sealey, J. D. Selby, M. A. Zuideveld, A. R. Cowley and P. Mountford, *Chem. Commun.*, 2006, 436–438.
16 H. R. Bigmore, M. A. Zuideveld, A. M. Kowalczyk, A. R. Cowley, M. Kranenburg, E. J. L. McInnes and P. Mountford, *Inorg. Chem.*, 2006, **45**, 6411–6423.
17 P. J. Wilson, A. J. Blake, P. Mountford and M. Schroder, *Chem. Commun.*, 1998, 1007–1008.
18 C. H. Winter, P. H. Sheridan, T. S. Lewkebandara, M. J. Heeg and J. W. Proscia, *J. Am. Chem. Soc.*, 1992, **114**, 1095–1097.
19 T. S. Lewkebandara, P. H. Sheridan, M. J. Heeg, A. L. Rheingold and C. H. Winter, *Inorg. Chem.*, 1994, **33**, 5879–5889.
20 I. Bytschkov and S. Doye, *Eur. J. Org. Chem.*, 2003, **2003**, 935–946.
21 S. Doye, *Synlett*, 2004, **2004**, 1653–1672.
22 S. Banerjee, E. Barnea and A. L. Odom, *Organometallics*, 2008, **27**, 1005–1014.
23 K. Weitershaus, H. Wadepohl and L. H. Gade, *Organometallics*, 2009, **28**, 3381–3389.
24 P. D. Schweizer, H. Wadepohl and L. H. Gade, *Organometallics*, 2013, **32**, 3697–3709.
25 K. Weitershaus, B. D. Ward, R. Kubiak, C. Müller, H. Wadepohl, S. Doye and L. H. Gade, *Dalton Trans.*, 2009, 4586–4602.
26 A. V. Lee and L. L. Schafer, *Eur. J. Inorg. Chem.*, 2007, 2243–2255.
27 T. E. Müller, K. C. Hultzsch, M. Yus, F. Foubelo and M. Tada, *Chem. Rev.*, 2008, **108**, 3795–892.
28 Y. Li, Y. Shi and A. L. Odom, *J. Am. Chem. Soc.*, 2004, **126**, 1794–1803.

29 J. S. Johnson and R. G. Bergman, *J. Am. Chem. Soc.*, 2001, **123**, 2923–2924.
30 C. Cao, Y. Shi and A. L. Odom, *Org. Lett.*, 2002, **4**, 2853–2856.
31 L. Ackermann and R. Born, *Tetrahedron Lett.*, 2004, **45**, 9541–9544.
32 V. Khedkar, A. Tillack, M. Michalik and M. Beller, *Tetrahedron Lett.*, 2004, **45**, 3123–3126.
33 S. Banerjee, Y. Shi, C. Cao and A. L. Odom, *J. Organomet. Chem.*, 2005, **690**, 5066–5077.
34 T. J. Clark, K. Lee and I. Manners, *Chem. - A Eur. J.*, 2006, **12**, 8634–8648.
35 E. M. Leitao, T. Jurca and I. Manners, *Nat. Chem.*, 2013, **5**, 817–829.
36 R. Waterman, *Chem. Soc. Rev.*, 2013, **42**, 5629–5641.
37 R. J. Less, R. L. Melen and D. S. Wright, *RSC Adv.*, 2012, **2**, 2191.
38 A. Rossin and M. Peruzzini, *Chem. Rev.*, 2016, **116**, 8848–8872.
39 H. C. Johnson, T. N. Hooper and A. S. Weller, 2015, pp. 153–220.
40 A. Staubitz, A. P. M. Robertson and I. Manners, *Chem. Rev.*, 2010, **110**, 4079–4124.
41 A. D. Schofield, A. Nova, J. D. Selby, C. D. Manley, A. D. Schwarz, E. Clot and P. Mountford, *J. Am. Chem. Soc.*, 2010, **132**, 10484–10497.
42 A. D. Schofield, A. Nova, J. D. Selby, A. D. Schwarz, E. Clot and P. Mountford, *Chem. – A Eur. J.*, 2011, **17**, 265–285.
43 A. D. Schwarz, C. S. Onn and P. Mountford, *Angew. Chem. Int. Ed.*, 2012, **51**, 12298–12302.
44 L. C. Stevenson, S. Mellino, E. Clot and P. Mountford, *J. Am. Chem. Soc.*, 2015, **137**, 10140–10143.
45 A. D. Schwarz, A. Nova, E. Clot and P. Mountford, *Chem. Commun.*, 2011, **47**, 4926–4928.
46 L. R. Groom, A. D. Schwarz, A. Nova, E. Clot and P. Mountford, *Organometallics*, 2013, **32**, 7520–7539.
47 B. A. Clough, S. Mellino, A. V. Protchenko, M. Slusarczyk, L. C. Stevenson, M. P. Blake, B. Xie, E. Clot and P. Mountford, *Inorg. Chem.*, 2017, **56**, 10794–10814.
48 G. R. Giesbrecht and J. C. Gordon, *Dalton Trans.*, 2004, 2387–2393.
49 J. F. Berry, *Comments Inorg. Chem.*, 2009, **30**, 28–66.
50 B. Clough, DPhil Thesis, University of Oxford, 2016.
51 B. L. Haymore, E. A. Maatta and R. A. D. Wentworth, *J. Am. Chem. Soc.*, 1979, **101**, 2063–2068.
52 S. C. Dunn, P. Mountford and D. A. Robson, *Dalton Trans.*, 1997, **2**, 293–304.
53 H. W. Roesky, H. Voelker, M. Witt and M. Noltemeyer, *Angew. Chemie Int. Ed. English*, 1990, **29**, 669–670.
54 J. E. Hill, R. D. Profilet, P. E. Fanwick and I. P. Rothwell, *Angew. Chemie Int. Ed. English*, 1990, **29**, 664–665.
55 A. J. Blake, P. E. Collier, S. C. Dunn, W. Li, P. Mountford and O. V Shishkin, *Dalton Trans.*, 1997, 1549–1558.
56 S. C. Dunn, A. S. Batsanov and P. Mountford, *J. Chem. Soc. Chem. Commun.*, 1994, **724**, 2007–2008.
57 A. R. Fout, U. J. Kilgore and D. J. Mindiola, *Chem. Eur. J*, 2007, **13**, 9428–9440.
58 L. H. Gade and P. Mountford, *Coord. Chem. Rev.*, 2001, **216**–**217**, 65–97.
59 N. Hazari and P. Mountford, *Acc. Chem. Res.*, 2005, **38**, 839–849.
60 A. J. Blake, J. M. McInnes, P. Mountford, G. I. Nikonov, D. Swallow and D. J. Watkin, *Dalton Trans.*, 1999, 379–392.
61 D. Swallow, J. M. McInnes and P. Mountford, *J. Chem. Soc. Dalt. Trans.*, 1998, 2253–2260.
62 E. Müller, J. Müller, F. Olbrich, W. Brüser, W. Knapp, D. Abeln and F. T. Edelmann,

Eur. J. Inorg. Chem., 1998, 87–91.
63 P. E. Collier, S. M. Pugh, H. S. C. Clark, J. B. Love, A. J. Blake, F. G. N. Cloke and P. Mountford, *Inorg. Chem.*, 2000, **39**, 2001–2005.
64 A. J. Blake, P. E. Collier, L. H. Gade, P. Mountford, J. Lloyd, S. M. Pugh, M. Schubart, M. E. G. Skinner and D. J. M. Trösch, *Inorg. Chem.*, 2001, **40**, 870–877.
65 C. C. Cummins, C. P. Schaller, G. D. Van Duyne, P. T. Wolczanski, A. W. E. Chan and R. Hoffmann, *J. Am. Chem. Soc.*, 1991, **113**, 2985–2994.
66 R. Duchateau, A. J. Williams, S. Gambarotta and M. Y. Chiang, *Inorg. Chem.*, 1991, **30**, 4863–4866.
67 J. L. Thorman, I. A. Guzei, Young and L. K. Woo, *Inorg. Chem.*, 1999, **38**, 3814–3824.
68 Sarah M. Mullins, Andrew P. Duncan, R. G. Bergman and J. Arnold, *Inorg. Chem.*, 2001, **40**, 6952–6963.
69 T. E. Hanna, I. Keresztes, E. Lobkovsky, W. H. Bernskoetter and P. J. Chirik, *Organometallics*, 2004, **23**, 3448–3458.
70 Falguni Basuli, Brad C. Bailey, John Tomaszewski, A. John C. Huffman and D. J. Mindiola, *J. Am. Chem. Soc*, 2003, **125**, 6052–6053.
71 F. Basuli, J. C. Huffman and D. J. Mindiola, *Inorganica Chim. Acta*, 2007, **360**, 246–254.
72 Steven D. Gray, Joseph L. Thorman, L. M. Berreau and L. K. Woo, *Inorg. Chem.*, 1997, **36**, 278–283.
73 P. G. Wilkinson and N. B. Houk, *J. Chem. Phys.*, 1956, **24**, 528–534.
74 N. Adams, H. R. Bigmore, T. L. Blundell, C. L. Boyd, S. R. Dubberley, A. J. Sealey, A. R. Cowley, M. E. G. Skinner and P. Mountford, *Inorg. Chem.*, 2005, **44**, 2882–2894.
75 Aldo E. Guiducci, A. Catherine L. Boyd and P. Mountford, *Organometallics*, 2006, **25**, 1167–1187.
76 N. Adams, H. J. Arts, P. D. Bolton, D. Cowell, S. R. Dubberley, N. Friederichs, C. M. Grant, M. Kranenburg, A. J. Sealey, B. Wang, P. J. Wilson, M. Zuideveld, A. J. Blake, M. Schröder and P. Mountford, *Organometallics*, 2006, **25**, 3888–3903.
77 P. J. Tiong, A. Nova, L. R. Groom, A. D. Schwarz, J. D. Selby, A. D. Schofield, E. Clot and P. Mountford, *Organometallics*, 2011, **30**, 1182–1201.
78 J. L. Bennett and P. T. Wolczanski, *J. Am. Chem. Soc*, 1997, **119**, 10696–10719.
79 C. C. Cummins, S. M. Baxter and P. T. Wolczanski, *J. Am. Chem. Soc.*, 1988, **110**, 8731–8733.
80 S. Mellino, L. C. Stevenson, E. Clot and P. Mountford, *Organometallics*, 2017, **36**, 3329–3342.
81 M. Brookhart, M. L. H. Green and G. Parkin, *Proc. Natl. Acad. Sci. U. S. A.*, 2007, **104**, 6908–14.
82 P. J. Walsh, F. J. Hollander and R. G. Bergman, *Organometallics*, 1993, **12**, 3705–3723.
83 A. P. Duncan and R. G. Bergman, *Chem. Rec.*, 2002, **2**, 431–445.
84 J. F. (John F. Hartwig, *Organotransition metal chemistry : from bonding to catalysis*, .
85 A. E. Guiducci, C. L. Boyd, E. Clot and P. Mountford, *Dalton Trans.*, 2009, 5960–5979.
86 A. Bashall, P. E. Collier, L. H. Gade, M. McPartlin, P. Mountford, S. M. Pugh, S. Radojevic, M. Schubart, I. J. Scowen and D. J. M. Trösch, *Organometallics*, 2000, **19**, 4784–4794.
87 P. D. Bolton, E. Clot, A. R. Cowley and P. Mountford, *Chem. Commun.*, 2005,

3313–3315.
88 A. Tillack, H. Jiao, I. G. Castro, C. G. Hartung and M. Beller, *Chem. - A Eur. J.*, 2004, **10**, 2409–2420.
89 I. Bytschkov and S. Doye, *European J. Org. Chem.*, 2003, **2003**, 935–946.
90 L. Ackermann, R. G. Bergman and R. N. Loy, *J. Am. Chem. Soc.*, 2003, **125**, 11956–11963.
91 D. Duncan and T. Livinghouse, *Organometallics*, 1999, **18**, 4421–4428.
92 L. Ackermann and R. G. Bergman, *Org. Lett.*, 2002, **4**, 1475–1478.
93 P. J. Tiong, A. Nova, E. Clot and P. Mountford, *Chem. Commun.*, 2011, **47**, 3147.
94 P. J. Walsh, M. J. Carney and R. G. Bergman, *J. Am. Chem. Soc.*, 1991, **113**, 6343–6345.
95 H. Herrmann, J. L. Fillol, H. Wadepohl and L. H. Gade, *Angew. Chem. Int. Ed.*, 2007, **46**, 8426–8430.
96 A. D. Schofield, A. Nova, J. D. Selby, A. D. Schwarz, E. Clot and P. Mountford, *Chem. Eur. J*, 2011, **17**, 265–285.
97 L. C. Stevenson, S. Mellino, E. Clot and P. Mountford, *J. Am. Chem. Soc.*, 2015, **137**, 10140–10143.
98 M. D. Fryzuk, B. A. MacKay, S. A. Johnson and B. O. Patrick, *Angew. Chem. Int. Ed.*, 2002, **41**, 3709–3712.
99 R. Thompson, C.-H. Chen, M. Pink, G. Wu and D. J. Mindiola, *J. Am. Chem. Soc.*, 2014, **136**, 8197–8200.
100 A. A. Danopoulos, C. Redshaw, A. Vaniche, G. Wilkinson, B. Hussain-Bates and M. B. Hursthouse, *Polyhedron*, 1993, **12**, 1061–1071.
101 K. Weber, K. Korn, A. Schorm, J. Kipke, M. Lemke, A. Khvorost, K. Harms and J. Sundermeyer, *ZAAC*, 2003, **629**, 744–754.
102 L. C. Stevenson, S. Mellino, E. Clot and P. Mountford, *J. Am. Chem. Soc.*, 2015, **137**, 10140–10143.
103 B. A. Clough, S. Mellino, E. Clot and P. Mountford, *J. Am. Chem. Soc.*, 2017, **139**, 11165–11183.
104 D. A. Fletcher, R. F. McMeeking and D. Parkin, *J. Chem. Inf. Comput. Sci.*, 1996, **36**, 746 (Cambridge Structural Database version 5.37).
105 P. E. Collier, S. C. Dunn, P. Mountford, O. V Shishkin and D. Swallow, *Dalton Trans.*, 1995, **2**, 3743–3745.
106 C. T. Owen, P. D. Bolton, A. R. Cowley and P. Mountford, *Organometallics*, 2007, **26**, 83–92.
107 C. Lorber, R. Choukroun and L. Vendier, *Eur. J. Inorg. Chem.*, 2006, 4503–4518.
108 C. J. Carmalt, A. C. Newport, I. P. Parkin, A. J. P. White and D. J. Williams, *Dalton Trans.*, 2002, 4055–4059.
109 J. D. Selby, C. D. Manley, A. D. Schwarz, E. Clot and P. Mountford, *Organometallics*, 2008, **27**, 6479–6494.
110 B. A. Clough, S. Mellino, A. V Protchenko, M. Slusarczyk, L. C. Stevenson, M. P. Blake, B. Xie, E. Clot and P. Mountford, *Inorg. Chem.*, 2017, **56**, 10794–10814.
111 W. Haaf, *Chem. Ber.*, 1963, **96**, 3359–3369.
112 A. Staubitz, A. P. M. Robertson, M. E. Sloan and I. Manners, *Chem. Rev.*, 2010, **110**, 4023–4078.
113 Z. Liu, L. Song, S. Zhao, J. Huang, L. Ma, J. Zhang, J. Lou and P. M. Ajayan, *Nano Lett.*, 2011, **11**, 2032–2037.
114 Y. Jiang, O. Blacque and H. Berke, *Dalton Trans.*, 2011, **40**, 2578–2587.
115 T. Jurca, T. Dellermann, N. E. Stubbs, D. A. Resendiz-Lara, G. R. Whittell and I. Manners, *J. Am. Chem. Soc*, 2018, **9**, 3360–3366.

116 A. Staubitz, M. E. Sloan, A. P. M. Robertson, A. Friedrich, S. Schneider, P. J. Gates, J. S. auf der Günne and I. Manners, *J. Am. Chem. Soc.*, 2010, **132**, 13332–13345.

117 G. M. Adams, A. L. Colebatch, J. T. Skornia, A. I. McKay, H. C. Johnson, G. C. Lloyd−Jones, S. A. Macgregor, N. A. Beattie and A. S. Weller, *J. Am. Chem. Soc.*, 2018, **140**, 1481–1495.

118 B. L. Davis, D. A. Dixon, E. B. Garner, J. C. Gordon, M. H. Matus, B. Scott and F. H. Stephens, *Angew. Chem. Int. Ed.*, 2009, **48**, 6812–6816.

119 A. D. Sutton, A. K. Burrell, D. A. Dixon, E. B. Garner, J. C. Gordon, T. Nakagawa, K. C. Ott, J. P. Robinson and M. Vasiliu, *Science*, 2011, **331**, 1426–9.

120 I. G. Green, K. M. Johnson and B. P. Roberts, *J Chem Soc Perkin Trans 2*, 1989, 1963–1972.

121 C. A. Jaska, K. Temple, A. J. Lough and I. Manners, *Chem. Commun.*, 2001, 962–963.

122 C. A. Jaska and I. Manners, *J. Am. Chem. Soc*, 2004, **126**, 9776–9785.

123 J. F. Sonnenberg and R. H. Morris, *ACS Catal.*, 2013, **3**, 1092–1102.

124 J. A. Widegren and R. G. Finke, *J. Mol. Catal. A Chem.*, 2003, **198**, 317–341.

125 Katherine S. Weddle, A. John D. Aiken III and R. G. Finke, *J. Am. Chem. Soc*, 1998, **120**, 5653–5666.

126 Jason A. Widegren, Martin A. Bennett and R. G. Finke, *J. Am. Chem. Soc*, 2003, **125**, 10301–10310.

127 A. N. Marziale, A. Friedrich, I. Klopsch, M. Drees, V. R. Celinski, J. Schmedt auf der Günne and S. Schneider, *J. Am. Chem. Soc.*, 2013, **135**, 13342–13355.

128 A. Friedrich, M. Drees and S. Schneider, *Chem. Eur. J*, 2009, **15**, 10339–10342.

129 N. Blaquiere, S. Diallo-Garcia, S. I. Gorelsky, D. A. Black and K. Fagnou, *J. Am. Chem. Soc.*, 2008, **130**, 14034–14035.

130 C. Boulho and J.-P. Djukic, *Dalton Trans.*, 2010, **39**, 8893–8905.

131 C. J. Stevens, R. Dallanegra, A. B. Chaplin, A. S. Weller, S. A. Macgregor, B. Ward, D. McKay, G. Alcaraz and S. Sabo-Etienne, *Chem. - A Eur. J.*, 2011, **17**, 3011–3020.

132 M. Shimoi, S. Nagai, M. Ichikawa, Y. Kawano, K. Katoh, M. Uruichi and H. Ogino, *J. Am. Chem. Soc*, 1999, **121**, 11704–11712.

133 A. M. Chapman, M. F. Haddow and D. F. Wass, *J. Am. Chem. Soc.*, 2011, **133**, 8826–8829.

134 T. M. Douglas, A. B. Chaplin, A. S. Weller, X. Yang and M. B. Hall, *J. Am. Chem. Soc.*, 2009, **131**, 15440–15456.

135 H. C. Johnson, A. P. M. Robertson, A. B. Chaplin, L. J. Sewell, A. L. Thompson, M. F. Haddow, I. Manners and A. S. Weller, *J. Am. Chem. Soc.*, 2011, **133**, 11076–11079.

136 L. Euzenat, D. Horhant, Y. Ribourdouille, C. Duriez, G. Alcaraz and M. Vaultier, *Chem. Commun.*, 2003, **0**, 2280–2281.

137 H. C. Johnson, E. M. Leitao, G. R. Whittell, I. Manners, G. C. Lloyd-Jones and A. S. Weller, *J. Am. Chem. Soc.*, 2014, **136**, 9078–9093.

138 A. Kumar, H. C. Johnson, T. N. Hooper, A. S. Weller, A. G. Algarra and S. A. Macgregor, *Chem. Sci.*, 2014, **5**, 2546–2553.

139 M. E. Sloan, A. Staubitz, T. J. Clark, C. A. Russell, G. C. Lloyd-Jones and I. Manners, *J. Am. Chem. Soc.*, 2010, **132**, 3831–3841.

140 L. Yi and K. Ohno, *Organometallics*, 2007, **26**, 3597–3600.

141 M. E. Sloan, A. Staubitz, T. J. Clark, C. A. Russell, G. C. Lloyd-Jones and I. Manners, *J. Am. Chem. Soc.*, 2010, **132**, 3831–3841.

142 H. Helten, B. Dutta, J. R. Vance, M. E. Sloan, M. F. Haddow, S. Sproules, D. Collison, G. R. Whittell, G. C. Lloyd-Jones and I. Manners, *Angew. Chem. Int. Ed.*,

2013, **52**, 437–440.
143 D. J. Wolstenholme, K. T. Traboulsee, A. Decken and G. S. Mcgrady, *Organometallics*, 2010, **29**, 5769–5772.
144 T. Beweries, S. Hansen, M. Kessler, M. Klahn and U. Rosenthal, *Dalton Trans.*, 2011, **40**, 7689–7692.
145 D. Pun, E. Lobkovsky and P. J. Chirik, *Chem. Commun.*, 2007, **0**, 3297–3299.
146 Richard J. Keaton, J. M. Blacquiere and R. T. Baker, *J. Am. Chem. Soc*, 2007, **129**, 1844–1845.
147 X. Yang and M. B. Hall, *J. Am. Chem. Soc.*, 2008, **130**, 1798–1799.
148 C. A. Sandoval, T. Ohkuma, K. Muñ and R. Noyori, *J. Am. Chem. Soc*, 2003, **125**, 13490–13503.
149 R. Noyori and S. Hashiguchi, *Acc. Chem. Res.*, 1997, **30**, 97–102.
150 M. Käß, A. Friedrich, M. Drees and S. Schneider, *Angew. Chem. Int. Ed.*, 2009, **48**, 905–907.
151 H. Nöth and H. Vahrenkamp, *Chem. Ber.*, 1967, **100**, 3353–3362.
152 P. M. Zimmerman, A. Paul, Z. Zhang and C. B. Musgrave, *Inorg. Chem.*, 2009, **48**, 1069–1081.
153 A. B. Chaplin and A. S. Weller, *Inorg. Chem.*, 2010, **49**, 1111–1121.
154 A. P. M. Robertson, E. M. Leitao and I. Manners, *J. Am. Chem. Soc.*, 2011, **133**, 19322–19325.
155 A. P. M. Robertson, E. M. Leitao, T. Jurca, M. F. Haddow, H. Helten, G. C. Lloyd-Jones and I. Manners, *J. Am. Chem. Soc.*, 2013, **135**, 12670–12683.
156 A. Rossin, G. Bottari, A. M. Lozano-Vila, M. Paneque, M. Peruzzini, A. Rossi and F. Zanobini, 2013, **42**, 3533.
157 A. Staubitz, M. E. Sloan, A. P. M. Robertson, A. Friedrich, S. Schneider, P. J. Gates, J. S. auf der Günne and I. Manners, *J. Am. Chem. Soc.*, 2010, **132**, 13332–13345.
158 S. Bhunya, T. Malakar and A. Paul, *Chem. Commun.*, 2014, **50**, 5919.
159 M. S. Hill, G. Kociok-Köhn and T. P. Robinson, *Chem. Commun.*, 2010, **46**, 7587.
160 E. Lu, Y. Yuan, Y. Chen and W. Xia, *ACS Catal.*, 2013, **3**, 521–524.
161 D. J. Liptrot, M. S. Hill, M. F. Mahon and D. J. MacDougall, *Chem. - A Eur. J.*, 2010, **16**, 8508–8515.
162 J. Spielmann, M. Bolte and S. Harder, *Chem. Commun.*, 2009, **0**, 6934.
163 P. Bellham, M. S. Hill, G. Kociok-Köhn and D. J. Liptrot, *Chem. Commun.*, 2013, **49**, 1960.
164 V. Butera, N. Russo and E. Sicilia, *Chem. - A Eur. J.*, 2014, **20**, 5967–5976.
165 Y. Jiang, O. Blacque, T. Fox, C. M. Frech and H. Berke, *Organometallics*, 2009, **28**, 5493–5504.
166 Y. Kawano, M. Uruichi, M. Shimoi, S. Taki, T. Kawaguchi, T. Kakizawa and H. Ogino, *J. Am. Chem. Soc.*, 2009, **131**, 14946–14957.
167 R. Dallanegra, A. P. M. Robertson, A. B. Chaplin, I. Manners and A. S. Weller, *Chem. Commun.*, 2011, **47**, 3763.
168 A. J. M. Miller and J. E. Bercaw, *Chem. Commun.*, 2010, **46**, 1709.
169 O. J. Metters, S. R. Flynn, C. K. Dowds, H. A. Sparkes, I. Manners and D. F. Wass, *ACS Catal.*, 2016, **6**, 6601–6611.
170 L. R. Groom, A. D. Schwarz, A. Nova, E. Clot and P. Mountford, *Organometallics*, 2013, **32**, 7520–7539.
171 A. D. Schwarz, A. Nova, E. Clot and P. Mountford, *Inorg. Chem.*, 2011, **50**, 12155–12171.

Chapter Two

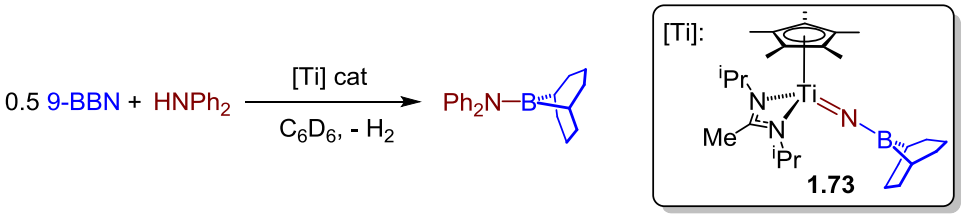
Titanium imide catalysed dehydrocoupling of amine-boranes

2.1 Overview

This Chapter describes the dehydrogenative coupling of amine-borane adducts using cyclopentadienyl-amidinate supported titanium imido catalysts. The efficiency of the systems is described, and several differently substituted amine-boranes are coupled. The focus of this Chapter lies on a detailed mechanistic study of the dehydrogenation process using dimethylamine-borane ($Me_2NH{\cdot}BH_3$) as model substrate. The study investigates the role of two key organic intermediates first, $Me_2N{=}BH_2$ and $Me_2NH{\cdot}BH_2NMe_2{\cdot}BH_3$, and focus on the role of the metal catalyst in a second step. Finally, the scope is further explored using amines and boranes that do not form amine-borane adducts in solution.

2.2 Definition of a suitable system

As discussed in Chapter One, the Mountford group recently studied the reactions between titanium imides and boranes. During these studies it was serendipitously found that during one of these reactions 9-BBN was coupled with diphenylamine to form the corresponding amino-borane and hydrogen gas, and that this reaction proceeded more quickly in the presence of a titanium borylimide **1.73** (Equation 2.1).



Equation 2.1

The majority of reported transition metal catalysed dehydrocoupling reactions of amines and boranes are based on often expensive mid- and late 4d and 5d metals such as rhodium. Early transition metal catalysts are less well-developed, and titanium represents an earth abundant metal. Notably, group 4 amine-borane dehydrocoupling catalysts are often based on metallocene systems, as reported by Manners,[1–4] Chirik,[5] Rosenthal,[6] Wass,[7,8]

Beweries,[9] and Baker.[10] Important for the context of this Chapter is that these ligand sets are able to support lower oxidation states. In fact, the majority of group 4 catalysed dehydrocoupling reactions are proposed to involve M(II) or M(III) species. Notable exceptions are the FLP incorporated systems reported by Wass, and the non-metallocene amide-supported Zr catalysts by Waterman.[11–13] Imido ligands such as in systems shown in Equation 2.1 are able to stabilise group 4 metals in their d^0 configuration. Therefore, it is interesting to investigate the mechanism of these systems in the dehydrocoupling of amine-boranes since it likely differs from those proposed to involve M(II) and M(III) species.

Cyclopentadienyl-amidinate supporting ligand sets such as in **1.73** (Equation 2.1) were shown in Chapter One to be versatile platforms for titanium imido mediated transformations. The robust cyclopentadienyl-titanium bond renders colloid formation unlikely which facilitates detailed mechanistic and kinetic studies. Although Ti(IV) to Ti(III) reduction is a fairly facile reduction, the nitrogen-based amidinate and imido moieties are both hard donors, as well as strong π-donors, and thus stabilise the titanium (IV) oxidation state particularly well. Cyclopentadienyl-amidinate supported imido catalysts are thus well-suitable to study homogeneous Ti^{IV} mediated chemistry.

In order to find a suitable and sufficiently active system, the imido substituent R was varied in these Cp*Ti{$MeC(NMe)_2$}(N<u>R</u>) catalysts. These screening reactions were performed jointly with Dr Simona Mellino. Hydrazide complexes (R = NMe_2 (**1.49b**), NPh_2 (**1.49a**), $NCPh_2$ (**2.1**)) proved to be sluggish towards dehydrocoupling of a variety of amine-boranes including $Me_2NH{\cdot}BH_3$. The borylimide congeners (R = $B(NDippCH)_2$ (**1.78**), BC_8H_{14} (**1.73**)) proved to be slow as well, and were easily protonated by virtue of being relatively Brøensted acidic. By contrast, good results were obtained using alkyl and aryl imides (R =

^{t}Bu (**2.1**), and R = tolyl (**1.36a**), Figure 2.1), both in terms of activity as well as scope (*vide infra*).

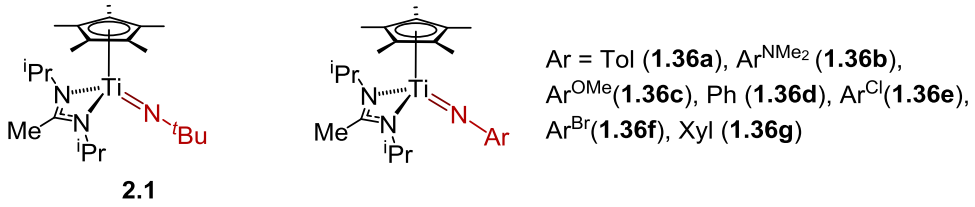
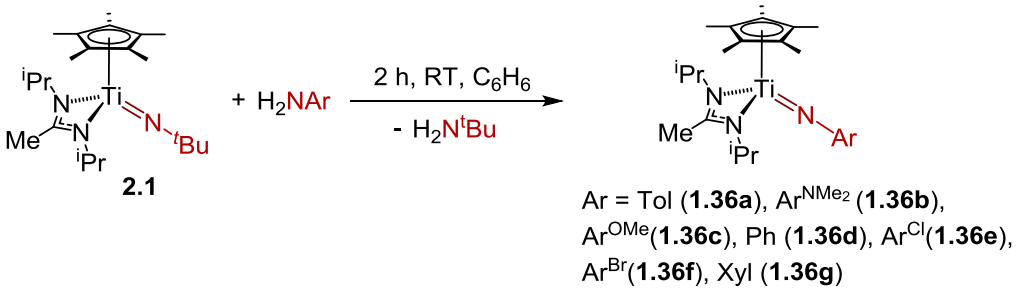


Figure 2.1 Titanium imide catalysts used in this study.

When complex **2.1** was added in equal amounts to toluene solutions of $Me_2NH{\cdot}BH_3$, the starting material was fully consumed by the time a NMR spectrum was recorded. Using a stock solution to perform the reaction at 1 mol% catalyst loading instead, 90% $Me_2NH{\cdot}BH_3$ was observed to be converted after 200 seconds on the NMR tube scale, corresponding to a $TOF_{90\%}$ = 1600 h^{-1} (RT, toluene, $[Me_2NH{\cdot}BH_3]_0$=0.38 M). Under the same conditions, a $TOF_{90\%}$ = 370 h^{-1} was determined using **1.36a**. While highly active catalysts are generally desirable, they make mechanistic investigations less straightforward. Therefore, we decided to use **2.1** to explore the synthetic value as well as the scope of the cyclopentadienyl-amidinate titanium imido systems, while we perform mechanistic studies using the slower tolyl catalyst **1.36a**.

The aryl moiety offers the possibility to tune the electronic as well as steric catalyst profile. Thus, the family of analogues **1.36a-g** were prepared using a simple imide/amine exchange methodology using the alkyl imide **2.1** as starting material (Equation 2.2).[14]



Equation 2.2

Generally, Cp*Ti{MeC(NMe)$_2$}(N^{t}Bu) (**2.1**) was dissolved in benzene to give a red solution to which pre-sublimed arylamine was added. The colour gradually changed to green within *ca.* 10 minutes, indicating formation of the arylimide. After 2 h stirring at RT, the volatiles (including the formed *tert*butylamine H$_2$N^{t}Bu) were removed *in vacuo*, and subsequent washing in cold hexanes (273 K) afforded the green aryl imide complexes **1.36** in 60-80% yield. Attempts to isolate the analogue featuring the more electron withdrawing Ar^{CF_3} group failed, due to difficulties to purify the compound to >95% purity as judged by ^{1}H NMR integration. Similarly, upon installation of the Ar^{NO_2} only marginal solubility in apolar solvents such as benzene was observed, presumably due to the polar nature of the NO$_2$ group. Thus, both compounds were not used for catalytic investigations. Overall, complexes **2.1** and **1.36a-g** can be readily prepared in 4-5 steps and high yields, starting from the commercially available TiCl$_4$.

Diffraction-quality crystals of complexes Cp*Ti{MeC(NMe)$_2$}(NAr), Ar = Ar^{NMe_2} (**1.36b**), Ph (**1.36d**), Ar^{Br} (**1.36e**) were obtained by slow vapour diffusion of the respective toluene solutions at RT (Figure 2.2 for **1.36d**, the fully analogous structures **1.36b** and **1.36e** are found in the CD Appendix). All three arylimides feature a three-legged piano stool geometry, and selected bond distances and angles are listed in Table 2.1, and fall within the previously reported ranges[14,15] for titanium(IV) complexes of the three types of ligands present. The para-substituents of the aryl rings increase in their electron donating ability in the series Ar^{Br} < Ph < Ar^{NMe_2}. However, there are no discernable structural trends that reflect this electron donating series. For example, the Ti(1)–N(1) bond lengths for **1.36b**, **1.36d, 1.36f** are 1.7374 Å (avg. of two crystallographically independent molecules), 1.743 (3) Å and 1.7391 (17) Å, respectively. These values are lower than the previously reported value of 2.094 Å for Cp*Ti{MeC(NMe)$_2$}(NXyl) (**1.36g**), due to steric repulsions.[14]

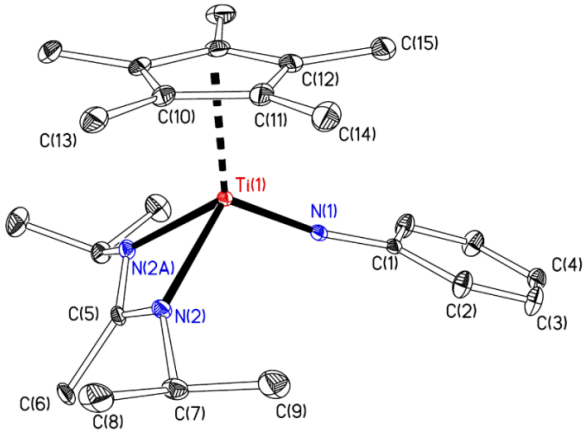


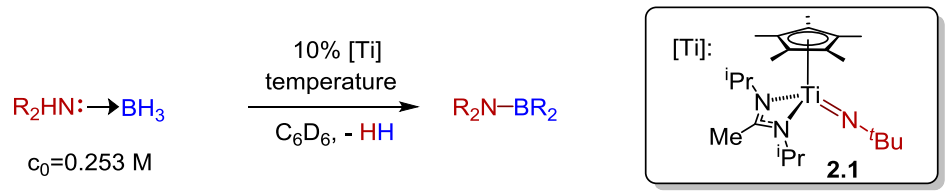
Figure 2.2 Displacement ellipsoid plot (20% probability) of Cp*Ti{MeC(NMe)$_2$}(NPh) (**1.36d**). H atoms are omitted. Atoms carrying the suffix 'A' are related to their counterparts by the symmetry operator x, y, $^3/_2$-z).

Table 2.1 Selected bond distances (Å) and angles (°) for Cp*Ti{MeC(N^{i}Pr)$_2$}(NAr), Ar = Ar^{NMe_2} (**1.36b**), Ph (**1.36d**), Ar^{Br} (**1.36f**). Cp$_{cent}$ refers to the computed η^5-Cp* ring centroid. Values in brackets are for the second crystallographically independent molecule.

Parameter	**1.36b**	**1.36d**	**1.36f**
Ti(1)–N(1)	1.7317(12) [1.7430(11)]	1.743(3)	1.7391(17)
Ti(1)–N$_{am,1}$	2.0951(12) [2.0807(11)]	2.095(2)	2.0975(12)
Ti(1)–N$_{am,2}$	2.0951(12) [2.0972(12)]	2.095(2)	2.0975(12)
Ti(1)–Cp$_{cent}$	2.06 [2.06]	2.06	2.06
Cp$_{cent}$–Ti(1)–N(1)	120.8 [121.2]	121.2	119.2
Cp$_{cent}$–Ti(1)–N$_{am,1}$	121.0 [120.5]	121.1	123.9
Cp$_{cent}$–Ti(1)–N$_{am,2}$	119.5 [120.0]	121.1	123.9
Ti(1)–N(1)–C(1)	166.85(10) [163.17(10)]	170.7(3)	166.65(14)

N$_{am}$ = Amidinate nitrogen atoms bonded to the titanium centre.

Next, the scope of the dehydrocoupling is investigated using five amine-borane adducts of type R$_2$HN·BH$_3$ with different R groups and using Cp*Ti{MeC(NMe)$_2$}(N^{t}Bu) (**2.1**, 10 mol%) as catalyst (Scheme 2.1, Table 2.2). The reactions were followed by ^{1}H and ^{11}B NMR spectroscopy and Table 2.2 shows the required reaction conditions on the NMR tube scale. The results of control reactions are shown as well, indicating that there is no conversion in the absence of catalyst.



Scheme 2.1 Dehydrocoupling of different amine-boranes (R = H, alkyl) catalysed by Cp*Ti{MeC(NMe)$_2$}(N^{t}Bu) (**2.1**).

Table 2.2 Amine-boranes tested in the dehydrocoupling catalysed by 10 mol% **2.1**, the corresponding temperature, and time to conversion of the substrates (*c.f.* Scheme 2.1).

Entry	Substrates	Temp	Time (h)	Conversion (%)[a)]	Conversion (no [Ti], %)[a)]
1	$NH_3{\cdot}BH_3$ [b)]	RT	<0.16	> 99	0
2	^{t}BuNH$_2{\cdot}$BH$_3$ [b)]	RT	2	> 99	0
3	MeNH$_2{\cdot}$BH$_3$ [b)]	RT	<0.16	> 99	0
4	Me$_2$NH$\cdot$BH$_3$ [b)]	RT	<0.16	> 99	0
5	^{i}Pr$_2$NH$\cdot$BH$_3$ [b)]	60 °C	24	> 99	0

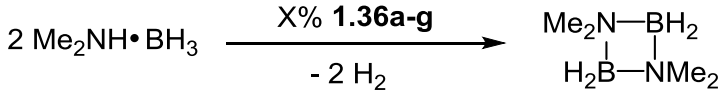
All reactions were carried out in a J-Young NMR tube under nitrogen atmosphere. [a)] Conversion measured by $^{11}B\{^1H\}$ NMR.

$NH_3{\cdot}BH_3$ (entry 1) is converted within less than 10 minutes at RT, and grey precipitate is observed after 20 min. The ^{11}B NMR revealed the presence of a variety of oligomeric species. In particular, trimeric borazine $N_3B_3H_6$ (30.2 ppm, d, $^1J_{BH}$ = 141 Hz, C_6D_6)[16] is detected early (10 min), and the signals corresponding to this species slowly decrease after 5 h as more precipitate is formed, indicating subsequent formation of oligomeric and polymeric species. Similarly, MeNH$_2{\cdot}$BH$_3$ (entry 3) is also quantitively consumed within less than 10 min at RT and 10 mol% catalyst loading. The ^{11}B spectra reveal the formation of a variety of oligomeric species as well, with cyclic [MeN=BH]$_3$ being detected as major product (^{11}B = 33.2, d, $^1J_{BH}$ = 132 Hz, C_6D_6).[16] The slightly more bulky ^{t}BuNH$_2{\cdot}$BH$_3$ (entry 2) requires longer times for conversion (2 h, 10% [Ti], RT), and the main product was identified as (^{t}BuNH)$_2$BH (26 ppm, d, $^1J_{BH}$ = 128 Hz, C_6D_6; lit: 25.8 ppm, d, $^1J_{BH}$ = 127 Hz, CH_2Cl_2) and the formation of grey precipitate indicates oligomerisation.[17] Notably, it was only in 2018 when Manners reported the first example of an early-transition metal catalysed polymerisation of primary alkylamine-boranes such as MeNH$_2{\cdot}$BH$_3$.[4] The secondary amine-borane Me$_2$NH$\cdot$BH$_3$ (entry 4) was converted quantitatively to the dimeric

$[Me_2N{=}BH_2]_2$ (4.5 ppm, t, $^1J_{HB}$ = 112, C_6D_6)[18] within less than 10 min at RT, while the bulkier $^iPr_2NH{\cdot}BH_3$ (entry 5) required heating to 60 °C to form $^iPr_2N{=}BH_2$ (34.8 ppm, t, $^1J_{HB}$ = 127.2 Hz, C_6D_6)[19] as the exclusive product.

These results show that steric bulk requires harsher reaction conditions (as can be seen by comparing entries 2 and 3). Overall, dehydrocoupling of these alkylamine-boranes proved to be efficient, and the required reaction conditions are relatively mild. For reference, primary and secondary amine-borane adducts generally require heating >100 °C to undergo thermally induced dehydrocoupling.[20]

In the following, we will use tolyl imide complex Cp*Ti{MeC(NMe)$_2$}(NTol) (**1.36a**), and aryl congeners **1.36b-g** with their differing electronic and steric profiles, and investigate the mechanism of dehydrocoupling amine-boranes. $Me_2NH{\cdot}BH_3$ was chosen as model substrate owing to the wide variety of comparisons available,[1–3,6–9] good solubility of potential intermediates, and the formation of a single product ($[Me_2N{=}BH_2]_2$). Additionally, it serves as a simple model for the related $MeNH_2{\cdot}BH_3$ and $NH_3{\cdot}BH_3$ congerners which are more interesting since they form polymeric materials (but are also more difficult to study). Overall, the reaction converts 2 equivalents of $MeNH_2{\cdot}BH_3$ to one equivalent of final product $[Me_2N{=}BH_2]_2$, under the release of dihydrogen (Equation 2.3).



Equation 2.3

2.3 Mechanistic studies

2.3.1 Experimental details

Catalytic and stoichiometric experiments are generally performed in a J. Young valve closed NMR tube, and followed by NMR spectroscopy, unless otherwise noted. To extract

kinetic concentration-time profiles of all boron containing species, the reactions were followed *via* $^{11}B\{^{1}H\}$ NMR spectroscopy. Performing the catalysis at RT lead to complete consumption of $Me_2NH{\cdot}BH_3$ within a few minutes, complicating analysis. Thus, we developed a protocol to set up the reactions at 0 °C in J. Youngs valve capped NMR tubes (detailed in the experimental section in Chapter Five). This protocol was used for all following reactions at 0 °C unless otherwise noted, and was shown to give excellent reproducibility. All reactions were run in duplicates with matching results.

2.3.2 Homogeneous or heterogeneous?

Finke has reviewed and critiqued a number of tests which help to guide whether a catalysis is homogeneous or heterogeneous, some of them will be used to investigate current system.[21] This is important to establish before considering kinetic studies. When a green stock solution of Cp*Ti{MeC(NMe)$_2$}(NTol) (**1.36a**) is subjected to a solution of 50 equivs of $Me_2NH{\cdot}BH_3$ (c_0=0.38 M, toluene, 273 K) immediate bubbling is observed, indicative of dihydrogen gas formation. The green colour of the reaction mixture is retained throughout the reaction, remains transparent, and no precipitate is observed. Next, we attempted phosphine poisoning.

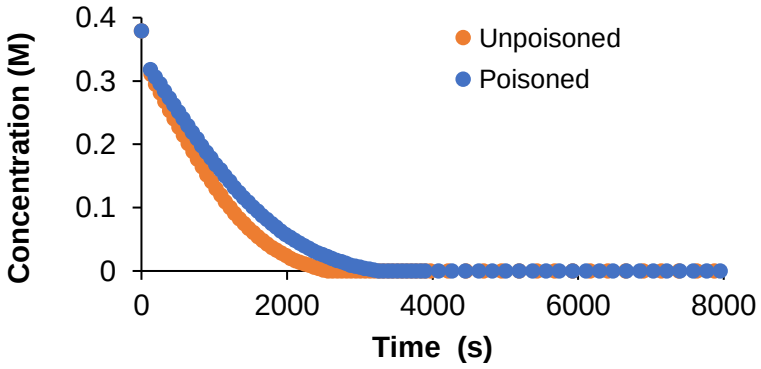


Figure 2.3 Orange: Conversion-time profile showing the catalytic conversion of $Me_2NH{\cdot}BH_3$ (c_0=0.38 M, toluene, 273 K) using Cp*Ti{MeC(NMe)$_2$}(NTol) (**1.36a**, 2 mol%). Blue: The same reaction is shown but in the presence of 10 mol% PPh_3 (relative to **1.36a**).

Figure 2.3 shows the conversion of an unpoisened catalysis of $Me_2NH{\cdot}BH_3$ (c_0=0.38 M, toluene, 273 K) with 2 mol% **1.36a**, compared to a reaction in which 10 mol% PPh_3 (relative to catalyst loading) was added from the start. The initial rate decreased from 3.4(3) x 10^{-4} mol dm^{-3} s^{-1} to 2.7(8) x 10^{-4} mol dm^{-3} s^{-1} for the unpoisoned and poisoned case, respectively. The decrease in activity indicates that the phosphine is able to bind to the titanium complex. It was previously observed that substioichiometric amounts of strongly binding ligands such as phosphines are efficient to block the active sites of heterogeneous metal catalysts, and essentially shut down catalysis completely.[21] Given that some amount of metal centres are buried within the clusters, substoichiometric amounts of strongly binding ligands are sufficient to entirely block the surface. Overall, the fact that some activity is decreased while the reaction is still comparable, featuring the same order of magnitude in initial rate and similar times to fully convert $Me_2NH{\cdot}BH_3$, points to the reaction being homogeneous. Notably, the conversion-time plot of $Me_2NH{\cdot}BH_3$ does not show a sigmaoidal shape or induction period which would point to the formation of nanoparticles.[22]

Heterogeneity was also probed with mercury poisoning. Hg(0) can poison metal particles by either amalgamating or adsorbing on the metal surface. If there is no poisoning detected, this is (negative) evidence for a homogeneous catalyst.[21] We added excess of elementary Hg (100 equivs) to a toluene solution of $Me_2NH{\cdot}BH_3$ (c_0=0.38 M, RT) and added the tolylimide catalyst **1.36a** at 1 mol% loading to start the reaction. The NMR tube was immediately fixed on a Fisher lab shaker to ensure vigorous shaking. The reaction showed conversion to 50% dimeric $[Me_2N{=}BH_2]_2$ after 18 min, which is the same time a blank reaction without excess Hg took for the same conversion.

Finally, a readdition experiment (shown in subsection 2.3.3) shows that upon readdition of more substrate, the catalysis is increasingly slowed. It is observed that titanium catalyst

Cp*Ti{MeC(NMe)$_2$}(NTol) (**1.36a**) slowly decomposes to paramagnetic species during the reaction (*vide infra*, Section 2.3.3). When the amount of intact Cp*Ti{MeC(NMe)$_2$}(NTol) (**1.36a**) is highest, the catalytic activity is highest. When all Cp*Ti{MeC(NMe)$_2$}(NTol) (**1.36a**) is converted to paramagnetic species, no further catalytic activity was observed. These results suggest that the active species is Cp*Ti{MeC(NMe)$_2$}(NTol) (**1.36a**).

Taken together, all observations presented in Section 2.3.2 strongly support the catalysis being homogeneous.

2.3.3 Active species and catalyst decomposition to Ti(III) species

After arguing that the catalysis is homogeneous, rather than heterogeneous, more attention is given to the nature of the active species in the following. When Cp*Ti{MeC(NMe)$_2$}(NTol) (**1.36a**) is subjected to a toluene solution of 50 equivs of $Me_2NH{\cdot}BH_3$ (c_0=0.38 M, 298 K), following the reaction by ^{1}H NMR spectroscopy confirmed that **1.36a** is observed throughout catalysis. However, the relative concentrations of the catalyst decrease slowly over time. When a readdition experiment was performed and 50 additional equivalents of $Me_2NH{\cdot}BH_3$ were added, the time to convert 90% of DMAB increased from 450 seconds to 1800 seconds for the second addition (Figure 2.4).

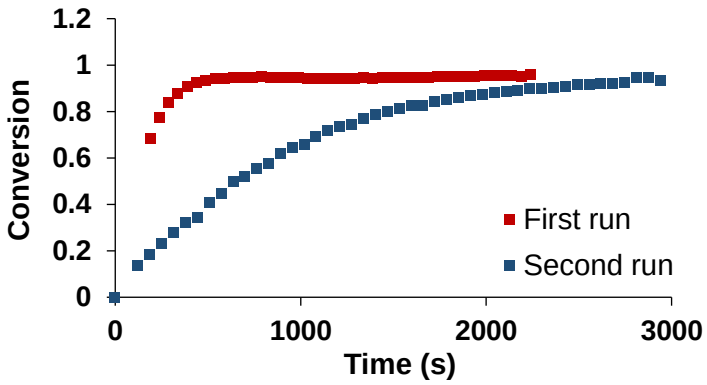


Figure 2.4 Two consecutive addition of 50 equivs of $Me_2NH{\cdot}BH_3$ to Cp*Ti{MeC(NMe)$_2$}(NTol) (**1.36a**) dissolved in toluene (298 K).

This decrease in catalyst activity indicates two points. First, there is catalyst decomposition. Secondly, catalytic activity is highest in the first run, when most titanium imide **1.36b** is still intact. This suggests that it is this imide which accounts for the catalytic activity, and not the compound(s) that are formed by decomposition. Importantly, when all Cp*Ti{MeC(NMe)$_2$}(NTol) (**1.36a**) was decomposed as judged by ^{1}H NMR integration, and more $Me_2NH{\cdot}BH_3$ was added, no further reaction was observed. When the catalyst loading was reduced to 0.1 mol% of **1.36a** (0 °C, toluene) only 80% of $Me_2NH{\cdot}BH_3$ was converted. This corresponds to a maximum turnover number TON_{MAX} of 800, indicating that **1.36a** is an efficient catalyst.

Surprisingly, the ^{1}H NMR spectra during and after catalysis, as well as after complete decomposition of Cp*Ti{MeC(NMe)$_2$}(NTol) (**1.36a**), did not reveal the formation of new titanium containing compounds. However, the appearance of several EPR active species can explain these observations. The EPR spectrum of the reaction mixture after catalysis (full conversion of $Me_2NH{\cdot}BH_3$ to final product $[Me_2N{=}BH_2]_2$) is shown in Figure 2.5.

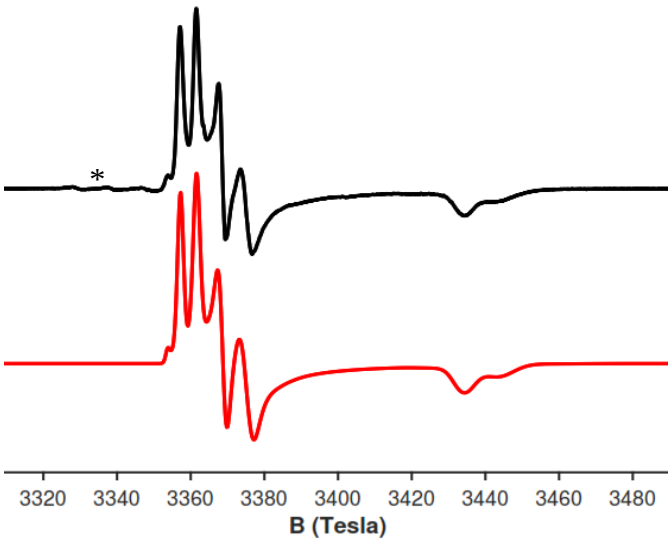


Figure 2.5 W-band EPR spectrum of the reaction mixture of Cp*Ti{MeC(NMe)$_2$}(NTol) (**1.36a**, 7%) and $Me_2NH{\cdot}BH_3$ (c_0=0.38 M, RT, benzene) after catalysis, recorded at 85 K (Frequency: 9.394594 GHz; modulation: 2.5 G; power: 0.317 mW). Simulated spectrum (red), original data (black). "*" denotes trace amounts of manganese impurities found in the cavity of the spectrometer.

The experimental spectrum (black line) reveals the presence of three different species, two

main species in ca. 1:1 ratio, and a third, minor one. A control EPR spectrum was recorded of the Cp*Ti{MeC(NMe)$_2$}(NTol) (**1.36a**) catalyst dissolved in benzene, without $Me_2NH{\cdot}BH_3$, and no signals were observed. A good model (red line) was fitted to the experimental spectrum, and the principal g tensors were extracted (Table 2.2). The model was developed by David Ryan and Dr William Myers.

The average g factors corresponding to the two main species (1.97863 and 1.98177) are consistent with Ti(III) metallocene complexes, and compare well with literature values. For example, McGrady[3] and Manners[23] reported the synthesis of the metallocene Ti(III) amidoboranes $Cp_2Ti(NH_2BH_3)$ (**2.2a**) and $Cp_2Ti(NMe_2BH_3)$ (**2.2b**), respectively, which featured average g-values of 1.9885 and 1.9903. However, direct comparisons are difficult to make, since g-tensors in EPR are very sensitive, and the amidinate imido ligands are largely unexplored. As discussed in Chapter One, Ti(III) species (**2.2b**) was proposed to be involved in the dehydrocoupling of $Me_2NH{\cdot}BH_3$ using the $Cp_2TiCl_2/{}^nBuLi$ system. Isolated **2.2b** featured a comparable TOF value towards $Me_2NH{\cdot}BH_3$ as compared to the *in-situ* generated catalyst from Cp_2TiCl_2 and ^nBuLi (2 equivs), specifically, 10.7 and 11.1 h^{-1}, respectively (2% [Ti] loading, 20 °C, toluene).[3]

Table 2.2 Principal g-values of the EPR spectra shown in Figure 2.5.

	Species 1	**Species 2**	**Species 3**
g_1	1.99500	1.99760	1.99970
g_2	1.98700	1.99080	1.99160
g_3	1.95270	1.94750	1.95400
g_{av}[a)]	1.97823	1.97863	1.98177

[a)] $g_{av} = (g_1 + g_2 + g_3)/3$

In an attempt to crystallise the EPR active decomposition products after catalysis, 1000 equivalents of $Me_2NH{\cdot}BH_3$ (benzene, RT) were subjected to Cp*Ti{MeC(NMe)$_2$}(NTol) (**1.36a**). The catalyst fully decomposed within 48 h, as indicated by ^{1}H NMR spectroscopy.

All volatiles (including $[Me_2N{=}BH_2]_2$) were removed *in vacuo* to give a brown solid which was dissolved in hexanes. After 2 weeks diffraction quality crystals of the dimeric Ti(III) complex $[Cp^*Ti\{HB(NTol)_2\}]_2$ (**2.3**) were grown (Figure 2.6). Given the application of vaccuum and the relatively long time required to grow these crystals, caution is required to interpret these results.

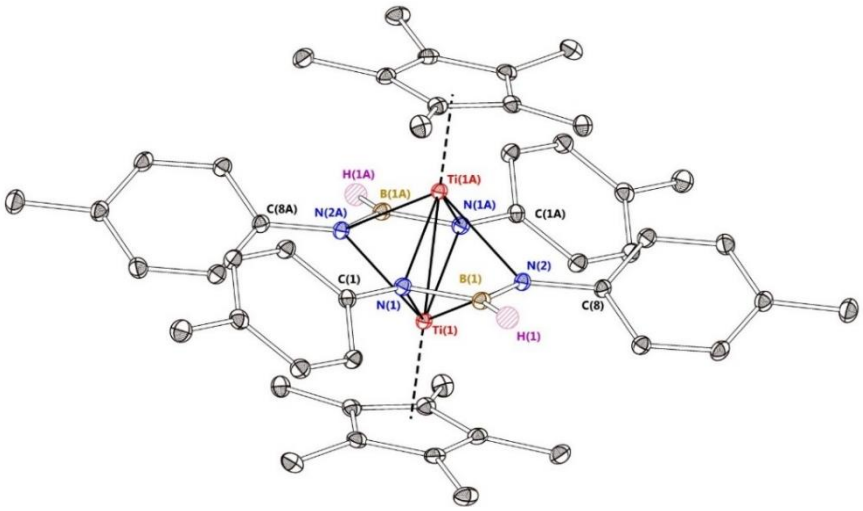


Figure 2.6 Displacement ellipsoid plot (20% probability) of $[Cp^*Ti\{HB(NTol)_2\}]_2$ (**2.3**). C-bound H atoms omitted. H(1) and H(1A) drawn as spheres of arbitrary radius. Atoms carrying the suffix 'A' are related to their counterparts by the symmetry operator x, 2-y, -z).

Table 2.3 Selected bond distances (Å) and angles (°) for $[Cp^*Ti\{HB(NTol)_2\}]_2$ (**2.3**). Cp_{cent} refers to the computed η^5-Cp* ring centroid.

Ti(1)–Ti(1A)	2.4537(4)	Cp_{cent}–Ti(1)–N(1)	122.4
Ti(1)–N(1)	2.2092(9)	Cp_{cent}–Ti(1)–N(2)	122.2
Ti(1)–N(2)	2.2036(9)	Ti(1)–N(1)–B(1)	88.24(7)
Ti(1)–B(1)	2.5466(12)	N(1)–B(1)–N(2)	106.98(9)
N(1)–B(1)	1.4294(15)		
N(2)–B(1)	1.4242(15)		
Cp_{cent}–Ti(1)	2.07		

The dimer consists of two different ligands coordinated to each metal centre, the cyclopentadienyl as well as a newly formed, dianionic bis(tolylamido)borane, $HB(NTol)_2$. Ligand frameworks of type $RB(NR')_2$ have previously been reported. For example, Nocera used the dilithiated $Li_2[PhB(N^tBu)_2]$ to form a variety of group 4 and 5 bis(tert-

butylamido)phenylborane complexes starting from the corresponding metal chloride precursors.[24] Spectroscopic and structural data showed that these are analogous to amidinate ligands. Compared to amidinates, $RB(NR')_2$ ligands were observed to have relatively shorter metal-nitrogen bonds, in part due to their dianionic nature.[24]

The four bis(tolylamido)borane nitrogen atoms are bridging two formal titanium(III) centres. The Ti–Ti distance was found to be 2.4537(4) Å, well below the sum of covalent radii of 3.2 Å.[25] In fact, the Ti–Ti bond distance in **2.3** is among the shortest found for any structurally characterised Ti–Ti bonded complexes (range: 2.41-3.33 Å, 90 examples in the CSD database).[26]

Despite formal Ti(III) oxidation state, the presence of a metal-metal bond would render complex **2.3** diamagnetic, and thus EPR silent.[27] The low solubility of this compound in common organic solvents (benzene, DCM, pyridine) precluded full characterisation *via* NMR spectroscopy. Mixtures of **2.3** in these solvents were EPR silent. Control reactions were performed in which 5 equivalents of $Me_2NH{\cdot}BH_3$ were added to these mixtures, however, no reaction was observed after 2 weeks at RT. Thus, there is no evidence for catalytic dehydrocoupling activity.

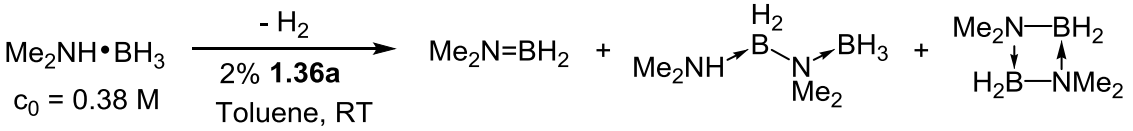
In summary, $Cp^*Ti\{MeC(NMe)_2\}(NTol)$ (**1.36a**) decomposes during catalysis and forms several Ti(III) species as shown by EPR spectroscopy. The crystal structure of dimeric $[Cp^*Ti\{HB(NTol)_2\}]_2$ (**2.3**) is further evidence for the formation of Ti(III) species. Despite **2.3** being diamagnetic, it might arise from EPR active, monomeric Ti(III) which dimerised and rearranged over time. Importantly, readdition experiments established that catalytic activity decreases as **1.36a** is decomposed. Highest catalytic activity is observed when highest amounts of **1.36a** are detected. The more **1.36a** is decomposed, as judged by NMR integration, the lower the catalytic activity. After **1.36a** is fully decomposed, there is no catalytic activity and $Me_2NH{\cdot}BH_3$ is not dehydrocoupled anymore. Notably, when a

mixture of [Cp*Ti{HB(NTol)$_2$}]$_2$ (**2.3**) in benzene is subjected to Me$_2$NH·BH$_3$, no dehydrocoupling was observed. Finally, there is no induction period observed during catalysis which would point to the formation of another active species. Taken together, these experiments strongly suggest that Cp*Ti{MeC(NMe)$_2$}(NTol) (**1.36a**) is the active species during dehydrocoupling catalysis.

2.3.4 Speciation and concentration-time plot analysis

2.3.4.1 Speciation

Next, we turn our attention to a detailed mechanistic analysis of the dehydrocoupling of Me$_2$NH·BH$_3$ using Cp*Ti{MeC(NMe)$_2$}(NTol) (**1.36a**) as catalyst, and focus on the involved organic intermediates first (Scheme 2.2).



Scheme 2.2 Main species formed during the catalytic dehydrocoupling of Me$_2$NH·BH$_3$ with **1.36a**.

When the reaction was followed by ^{11}B NMR spectroscopy, three main organic species were identified by comparison of their diagnostic chemical shift, and $^1J_{HB}$ coupling constants with literature values (Figure 2.7). A triplet at 37.4 ppm ($^1J_{HB}$ = 131 Hz) is identified as amino-borane Me$_2$N=BH$_2$ (Lit: 37.1 ppm, t, $^1J_{HB}$ = 136 Hz, C$_6$D$_6$),[28] and another triplet represents the final dimeric product [Me$_2$N=BH$_2$]$_2$ (4.9 ppm, t, $^1J_{HB}$ = 113 Hz; Lit: 4.5 ppm, t, $^1J_{HB}$ = 112 Hz, C$_6$D$_6$).[18] There are two additional peaks at 1.5 (t, $^1J_{HB}$ = 109 Hz) and -13.5 (q, $^1J_{HB}$ = 94 Hz). These correspond to the BH$_2$ and BH$_3$ groups of the linear dimer Me$_2$NH·BH$_2$NMe$_2$·BH$_3$ (Lit: 1.4 ppm, t, $^1J_{HB}$ =108 Hz (BH$_2$); -13.7, q, $^1J_{HB}$ = 94 Hz (BH$_3$), toluene).[16,29] Notably, the BH$_3$ group is overlapping with the BH$_3$ of starting material Me$_2$NH·BH$_3$.[16] Finally, trace amounts of amidoborane HB(NMe$_2$)$_2$ were also

detected (29 ppm, d, $^{1}J_{HB}$ = 133 Hz; Lit: 29 ppm, d, $^{1}J_{HB}$ = 130 Hz, toluene).[6] $HB(NMe_2)_2$ is a common side product in the dehydrogenation of $Me_2NH{\cdot}BH_3$, and can arise from various mechanisms.[30] However, due to the very low amounts formed during catalysis (<1%) species is neglected in the following discussions.

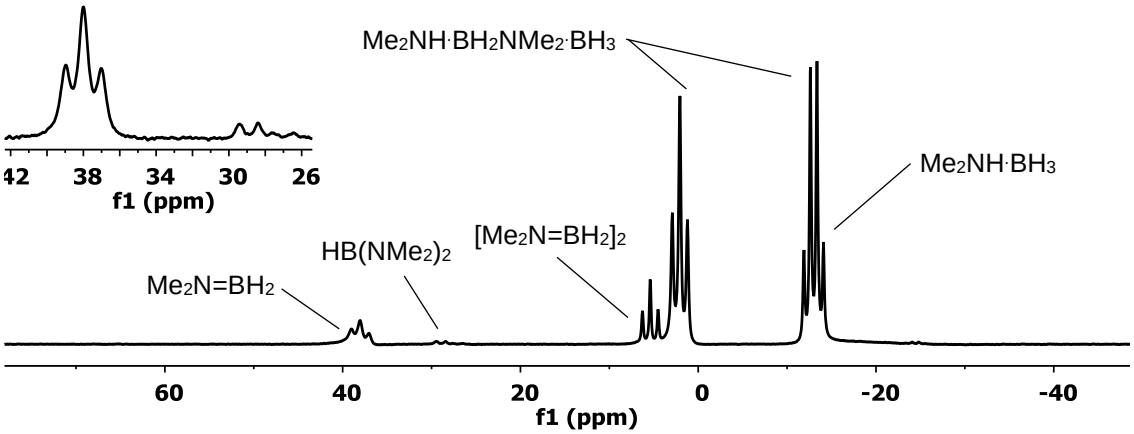


Figure 2.7 ^{11}B NMR spectrum (160 MHz) of **1.36a** with 14 equivs of $Me_2NH{\cdot}BH_3$ (c_0=0.38 M) in toluene at RT after 3 minutes.

2.3.4.2 Concentration-time plot analysis

The concentration-time profiles of the dehydrocoupling of $Me_2NH{\cdot}BH_3$ using 2 mol% Cp*Ti{$MeC(NMe)_2$}(NTol) (**1.36a**) at 0 °C is shown in Figure 2.8. The $Me_2NH{\cdot}BH_3$ starting material is fully consumed within 50 minutes. During this decay there is near-quantitative formation of the linear dimer $Me_2NH{\cdot}BH_2NMe_2{\cdot}BH_3$, which constitutes 96% of the reaction mixture at maximum (reached after *ca.* 50 min). Subsequently, the linear dimer reacts during this process slowly, and both $Me_2N{=}BH_2$ as well as dimeric $[Me_2N{=}BH_2]_2$ are observed.

Notably, $Me_2N{=}BH_2$ goes through a maximum (96 min) *after* the $Me_2NH{\cdot}BH_2NMe_2{\cdot}BH_3$ does (Figure 2.8). Both species decay again, and thus feature a typical concentration-time profile of intermediate species. Finally, $[Me_2N{=}BH_2]_2$ continously grows over time, representing the final product of the reaction (after *ca.* 2 days).

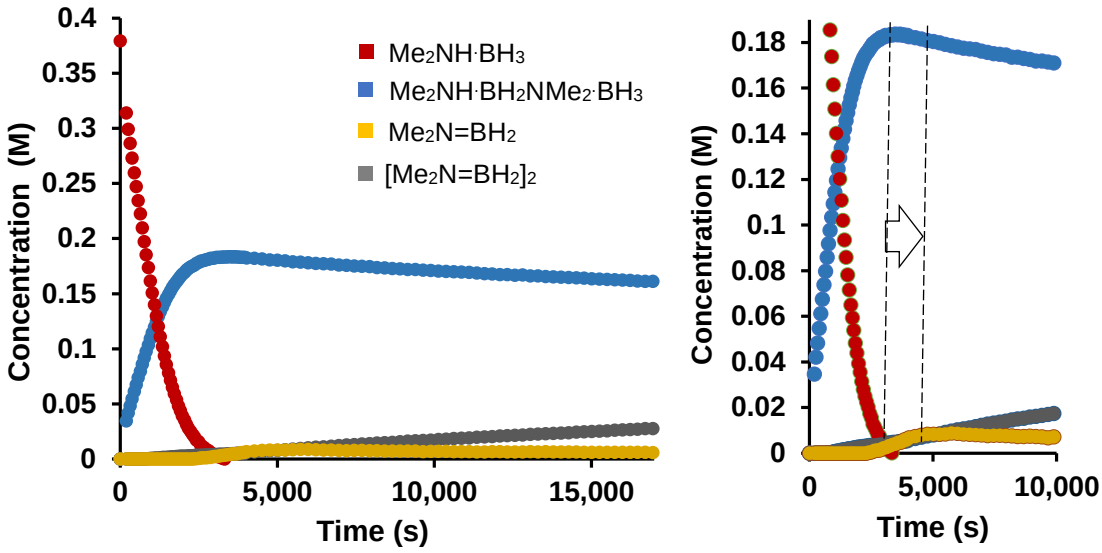
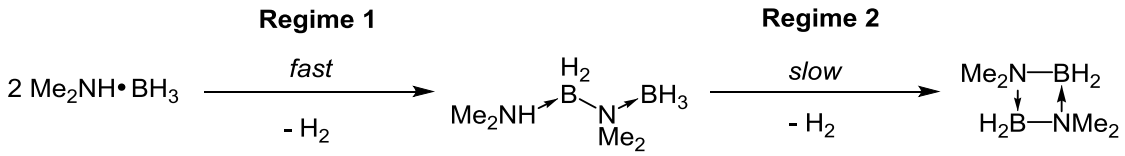


Figure 2.8 Catalytic dehydrocoupling of $Me_2NH{\cdot}BH_3$ (c_0=0.38 M, 273 K, toluene) by Cp*Ti{MeC(NMe)$_2$}(NTol) (**1.36a**, 2 mol%). Right: Dotted lines indicate the maxima of $Me_2NH{\cdot}BH_2NMe_2{\cdot}BH_3$ and $Me_2N{=}BH_2$ and help visualise that the former preceeds the latter in time.

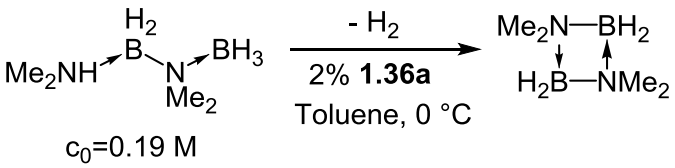
Overall, the concentration-time profiles indicate the presence of two main kinetic regimes. A first one, in which $Me_2NH{\cdot}BH_3$ is converted rapidly to form $Me_2NH{\cdot}BH_2NMe_2{\cdot}BH_3$ near-quantitatively. The regime that follows represents the slower conversion of this molecule to ultimately form $[Me_2N{=}BH_2]_2$ (Scheme 2.3).



Scheme 2.3 Two kinetic regimes in the catalysis of $Me_2NH{\cdot}BH_3$ using **1.36a**.

The intermediate species $Me_2NH{\cdot}BH_2NMe_2{\cdot}BH_3$ was synthesised independently for further investigation (the synthesis is discussed in the next subsection). Under otherwise identical conditions, the catalysis was started from this intermediate ("Set 1"), and compared the reaction profile with the one starting from $Me_2NH{\cdot}BH_3$ ("Set 2", Equation 2.4, Figure 2.9). It is pointed out that 2 equivalents of $Me_2NH{\cdot}BH_3$ are required to form 1 equivalent of $Me_2NH{\cdot}BH_2NMe_2{\cdot}BH_3$. Thus, the starting concentration of $[Me_2NH{\cdot}BH_3]_0$ = 0.38 M used

previously (conditions in Figure 2.8), corresponds to a starting concentration of $[Me_2NH{\cdot}BH_2NMe_2{\cdot}BH_3]_0$ = 0.19 M (Equation 2.4).



Equation 2.4

Overlapped concentration-time profiles are shown in Figure 2.9. The catalysis is well-behaved, in that the same species are formed in both catalytic runs, and their concentration-time profiles show good overlap. Importantly, $Me_2N{=}BH_2$ is formed as linear dimer decomposes, accummulates to *ca*. 0.009 M, and then decreases in concentration again. This shows that the $Me_2N{=}BH_2$ is formed directly from $Me_2NH{\cdot}BH_2NMe_2{\cdot}BH_3$.

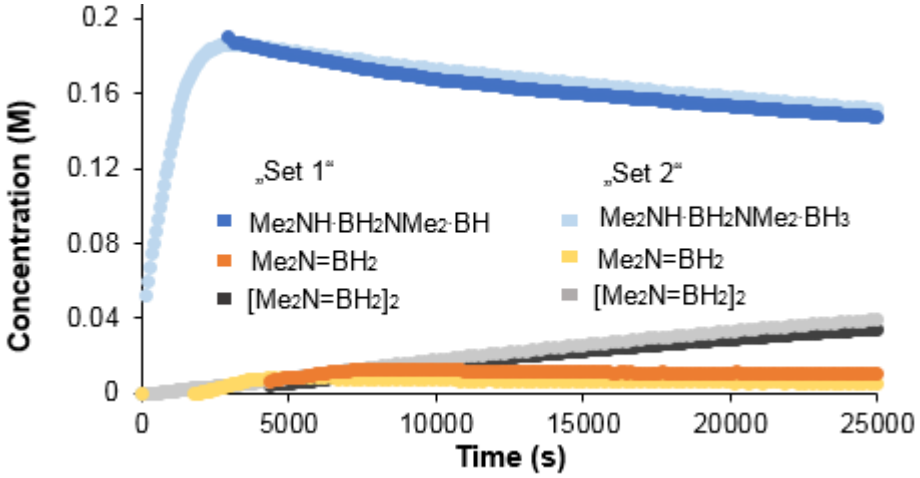


Figure 2.9 Overlap of the concentration-time profiles starting the catalysis from linear dimer $Me_2NH{\cdot}BH_2NMe_2{\cdot}BH_3$ ("Set 1"; c_0=0.19 M, 273 K, toluene, 2% **1.36a**) with the corresponding concentration-time profiles starting catalysis from $Me_2NH{\cdot}BH_3$ ("Set 2"; c_0=0.38 M, 273 K, toluene, 2% **1.36a**). The data points for Set 1 feature a time origin of 50 min, the time when $Me_2NH{\cdot}BH_2NMe_2{\cdot}BH_3$ of Set 2 is at its maximum.

Upon close inspection of the ^{11}B NMR spectra starting the catalysis from $Me_2NH{\cdot}BH_2NMe_2{\cdot}BH_3$, small amounts of $Me_2NH{\cdot}BH_3$ are also detected (both, at 0 °C and RT, Figure 2.11). The presence of this molecule was further confirmed by a doublet resonance at 1.81 ppm (^3J = 5.8 Hz, NHMe) in the ^{1}H NMR spectrum which was compared to an authentic sample of $Me_2NH{\cdot}BH_3$.

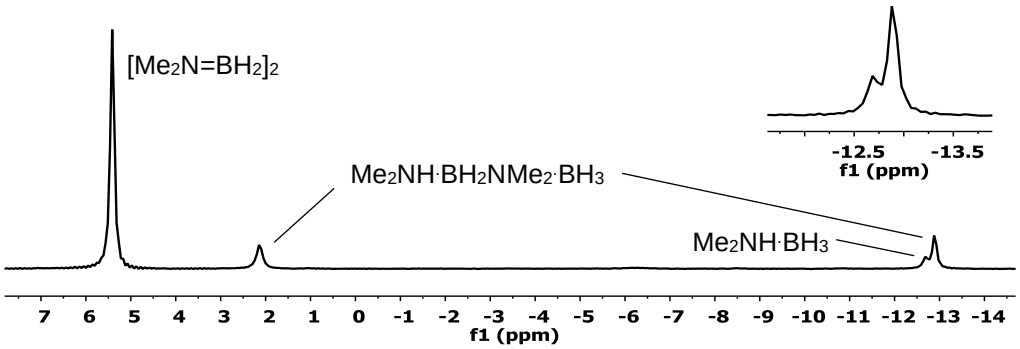


Figure 2.11 $^{11}B\{^{1}H\}$ NMR spectrum (160.4 MHz, toluene, 298 K) of catalytic starting the catalysis from linear dimer $Me_2NH{\cdot}BH_2NMe_2{\cdot}BH_3$ (c_0=0.09 M, 298 K, toluene, 21% **1.36a**) after 27 min. The inset shows the presence of peak corresponding to $Me_2NH{\cdot}BH_3$.

Since conversion of $Me_2NH{\cdot}BH_2NMe_2{\cdot}BH_3$ proceeds only slowly at 0 °C, the reaction was studied at RT, and at higher catalyst loadings of 21 mol% to achieve full conversion (Figure 2.12). Both $Me_2NH{\cdot}BH_3$ as well as $Me_2N{=}BH_2$ are formed from the start of the reaction, thus representing a redistribution. The low amounts of $Me_2NH{\cdot}BH_3$ compared to $Me_2N{=}BH_2$ could be explained by its relatively faster conversion to form $Me_2NH{\cdot}BH_2NMe_2{\cdot}BH_3$ (*c.f.* Figure 2.8).

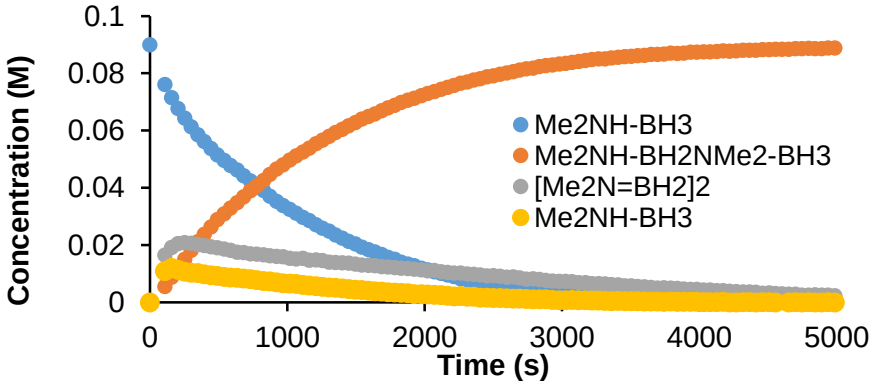
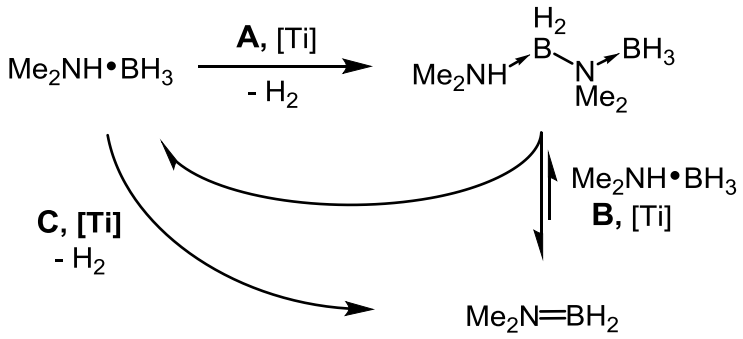


Figure 2.12 Concentration-time profiles starting the catalysis from linear dimer $Me_2NH{\cdot}BH_2NMe_2{\cdot}BH_3$ (c_0=0.09 M, 298 K, toluene, 21 mol% **1.36a**).

The rich mechanistic landscape is now discussed in more detail, starting with the role of $Me_2N{=}BH_2$. It was previously established that $Me_2NH{\cdot}BH_3$ reacts to form $Me_2NH{\cdot}BH_2NMe_2{\cdot}BH_3$ near-quantitatively during a fast, first kinetic regime (Scheme 2.4, pathway A). Subsequently, this linear dimer slowly drops in intensity during the second kinetic regime. Since $Me_2N{=}BH_2$ peaks after the linear dimer does, it suggests that titanium

imide **1.36a** converts linear dimer into $Me_2N{=}BH_2$ (Pathway B).



Scheme 2.4 Two parallel pathways to form $Me_2N{=}BH_2$.

Independently isolated $Me_2NH{\cdot}BH_2NMe_2{\cdot}BH_3$ confirmed formation of $Me_2N{=}BH_2$ on addition of **1.36a**, and revealed concomittant formation of $Me_2NH{\cdot}BH_3$. As discussed in Chapter One, these redistribution reactions have been previously reported. For example, a related and reversible redistribution reaction between $MeHN{=}BH_2$, $MeNH_2{\cdot}BH_3$ and $MeNH_2{\cdot}BH_2NHMe{\cdot}BH_3$ was previously observed for an Ir catalysed system by Manners.[31] It is noted that the majority of $Me_2N{=}BH_2$ formed during the presented catalysis starting from $Me_2NH{\cdot}BH_3$ is formed only during the second kinetic regime, after near-quantitative linear dimer formation. This suggests that the majority of free $Me_2N{=}BH_2$ is formed from linear dimer, and not directly from $Me_2NH{\cdot}BH_3$ (Scheme 2.4, pathway C). However, we cannot discount that pathway C plays a role. In fact, small amounts of $Me_2N{=}BH_2$ are detected from the start of $Me_2NH{\cdot}BH_3$ catalysis (Figure 2.10).

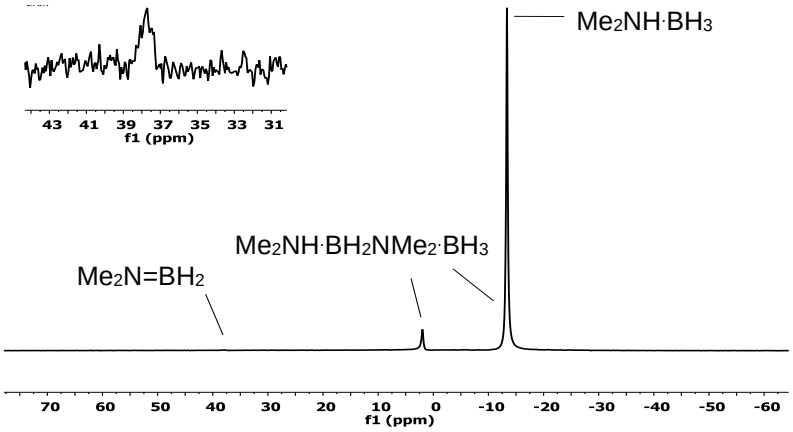
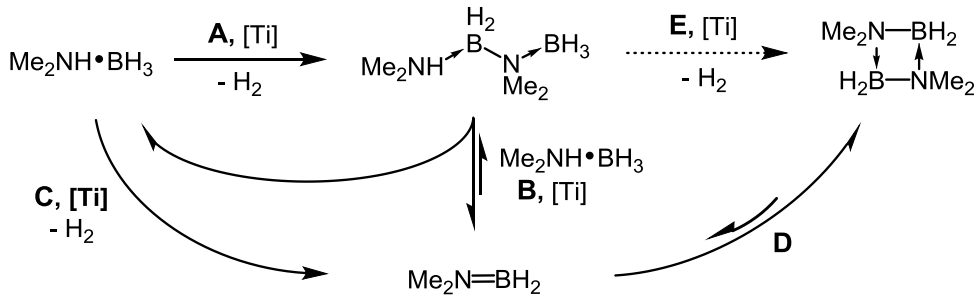


Figure 2.10 $^{11}B\{^1H\}$ NMR spectrum (160 MHz) of the dehydrocoupling of $Me_2NH{\cdot}BH_3$ (c_0=0.38 M, toluene, 273 K) with 2% **1.36a** after 2 minutes. The inset shows the presence of $Me_2N{=}BH_2$.

Schneider previously reported the ruthenium catalysed dehydrocoupling of $Me_2NH{\cdot}BH_3$ to form both $Me_2N{=}BH_2$, and $Me_2NH{\cdot}BH_2NMe_2{\cdot}BH_3$.[32] He noted a large dependence on overall concentration on the relative amounts of $Me_2N{=}BH_2$ and $Me_2NH{\cdot}BH_2NMe_2{\cdot}BH_3$ and thus argued that this is due to these two molecules being formed by two different, parallel pathways. In our case, under otherwise same reaction conditions, dropping the initial concentration of $Me_2NH{\cdot}BH_3$ by a factor of 3.5 led to a large increase of detected free $Me_2N{=}BH_2$. For example, after 5 min a ratio $Me_2N{=}BH_2/Me_2NH{\cdot}BH_2NMe_2{\cdot}BH_3$ of 0.16 was observed for $[Me_2NH{\cdot}BH_3]_0 = 0.11$ M, versus an observed ratio of only 0.01 for $[Me_2NH{\cdot}BH_3]_0 = 0.38$ M. Thus, higher concentrations favour formation of linear dimer. This experiment gives evidence that pathway C is proceeding in parallel to the main pathways A and B, analogous to Schneider's observations (Scheme 2.4).

In the same report, Schneider noted that the conversion of $Me_2N{=}BH_2$ and $Me_2NH{\cdot}BH_3$ to $Me_2NH{\cdot}BH_2NMe_2{\cdot}BH_3$ is almost thermoneutral ($\Delta G = -2$ kcal mol^{-1}), and can thus form an equilibrium if kinetically feasible (pathway B, Scheme 2.5).



Scheme 2.5 Mechanistic overview of the dehydrocoupling of $Me_2NH{\cdot}BH_3$ using catalyst **1.36a**.

In our case, we observed the formation of $Me_2N{=}BH_2$ and $Me_2NH{\cdot}BH_3$ from $Me_2NH{\cdot}BH_2NMe_2{\cdot}BH_3$, which is energetically uphill (but driven by the subsequent exothermic dimerisation of $Me_2N{=}BH_2$). Additionally, the formation of $Me_2NH{\cdot}BH_2NMe_2{\cdot}BH_3$ is observed when the catalysis is started from $Me_2NH{\cdot}BH_3$. Taken together these results strongly suggest the presence of an equilibrium. It should be noted

that this process must be catalysed in both directions. $Me_2NH{\cdot}BH_2NMe_2{\cdot}BH_3$ is stable in absence of catalyst **1.36a** for weeks in solution at RT. Similarly, experimental and computational work suggest that off-metal formation of $Me_2NH{\cdot}BH_2NMe_2{\cdot}BH_3$ from $Me_2NH{\cdot}BH_3$ and $Me_2N{=}BH_2$ is kinetically disfavoured.[32–34] In particular, when $[Me_2N{=}BH_2]_2$ and $Me_2NH{\cdot}BH_3$ were dissolved in toluene, no formation of $Me_2NH{\cdot}BH_2NMe_2{\cdot}BH_3$ was observed after 1 week. Since $[Me_2N{=}BH_2]_2$ is in rapid equilibrium with 2 equivalents of $Me_2N{=}BH_2$, this result suggests a kinetic barrier towards formation of $Me_2NH{\cdot}BH_2NMe_2{\cdot}BH_3$.[32]

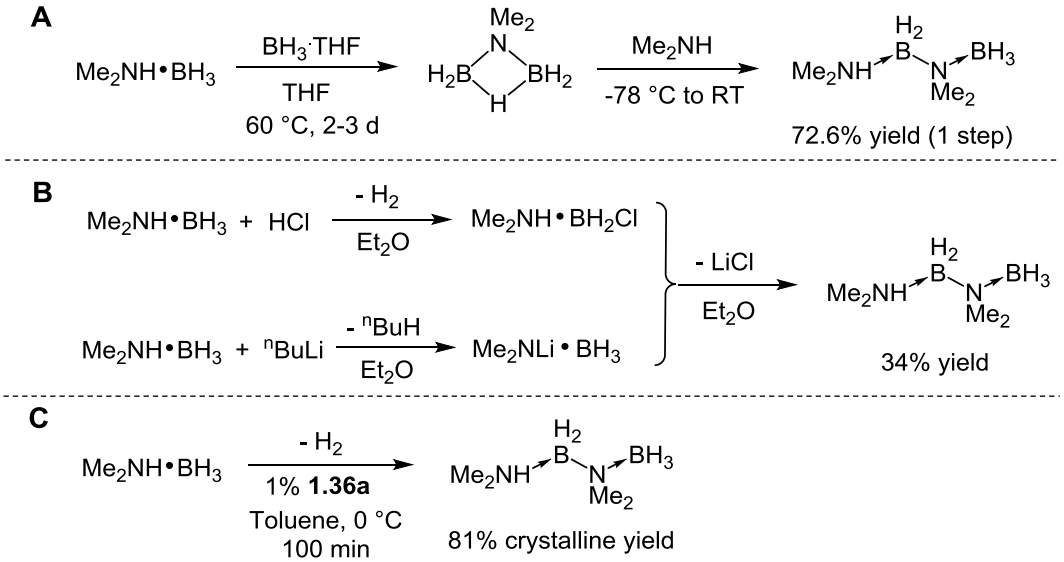
Finally, amino-borane $Me_2N{=}BH_2$ can react to form cyclic $[Me_2NH{=}BH_2]_2$ through off-metal self-dimerisation (Scheme 2.5, pathway D). These two species are known to be in rapid equilibrium, which lies heavily on the dimer-side.[35] Notably, Macgregor and Weller were able to study the self-dimerisation of $Me_2N{=}BH_2$, starting from $[Ir(PCy_3)_2(H)_2(H_2B\text{-}NMe_2)]^+$ (**2.4**), a latent source of free $Me_2N{=}BH_2$. The dimerisation was shown to be a second order process in $Me_2N{=}BH_2$, featuring a $\Delta G^{\ddagger}(298\ K) = 18 \pm 3$ kcal mol^{-1}.[34] This data is in line with our observations in that we see low, but significant accummulation of $Me_2N{=}BH_2$ at 0 °C (as well as RT), which then dimerises over time to yield $[Me_2NH{=}BH_2]_2$.

Another possibility to form $[Me_2N{=}BH_2]_2$ is from $Me_2NH{\cdot}BH_2NMe_2{\cdot}BH_3$ directly (Scheme 2.5, pathway E).[18,32,36] For example, in the $[Cp_2Ti]$ system reported by Manners, self-dimerisation of $Me_2N{=}BH_2$ is suggested to play only a minor role, while metal-bound linear dimer is converted to $[Me_2N{=}BH_2]_2$ in a dominating pathway (D, Scheme 2.5).[18] Although there is evidence for pathways B and C, we cannot discount the possibility for pathway E to play a minor role.

Cyclohexene was previously used to detect free amino-boranes $MeHN{=}BH_2$ and $H_2N{=}BH_2$ as it can be hydroborated forming Cy_2B-NHR (R = H, Me), thereby acting as marker for free amino-boranes.[37] An analogous hydroboration was thus attempted to trap and quantify the amount of $Me_2N{=}BH_2$ generated from $Me_2NH{\cdot}BH_2NMe_2{\cdot}BH_3$ to delineate pathways C, E and D. The reaction of $Me_2NH{\cdot}BH_2NMe_2{\cdot}BH_3$ with **1.36a** was performed in the presence of 3 equivs of cyclohexene at RT. However, no trace of hydroborated Cy_2B-NMe_2 was found by ^{11}B NMR ($^{11}B(C_6D_6)$ = 44.1ppm).[38] Similarly, the use of the more reactive terminal alkenes 1-hexene and styrene did not lead to hydroboration either. However, control reactions between $[Me_2N{=}BH_2]_2$, which is in rapid equilibrium with $Me_2N{=}BH_2$, showed no reaction with either of the three alkenes after 1 week at RT. Thus, reactions with alkenes are not suitable to trap $Me_2N{=}BH_2$ due to a decreased ability to hydroborate as compared to its $RHN{=}BH_2$ (R = Me, H) congeners.[37]

2.3.5 Catalytic synthesis of diborazane linear dimers

The clear kinetic distinction between the two regimes has previously not been observed in other systems, and offers the possibility to isolate $Me_2NH{\cdot}BH_2NMe_2{\cdot}BH_3$ from the catalytic reaction mixture (Scheme 2.6, C). As discussed for Figure 2.8, $Me_2NH{\cdot}BH_2NMe_2{\cdot}BH_3$ reached the maximum after *ca* 50 min on the NMR tube scale at 2% catalyst loading. Upon scale-up of $Me_2NH{\cdot}BH_3$ (2 g), keeping the same concentration but 1% catalyst **1.36a** loading, ^{11}B NMR analysis of an aliquot confirmed the presence of *ca* 90% $Me_2NH{\cdot}BH_2NMe_2{\cdot}BH_3$ after 100 min.



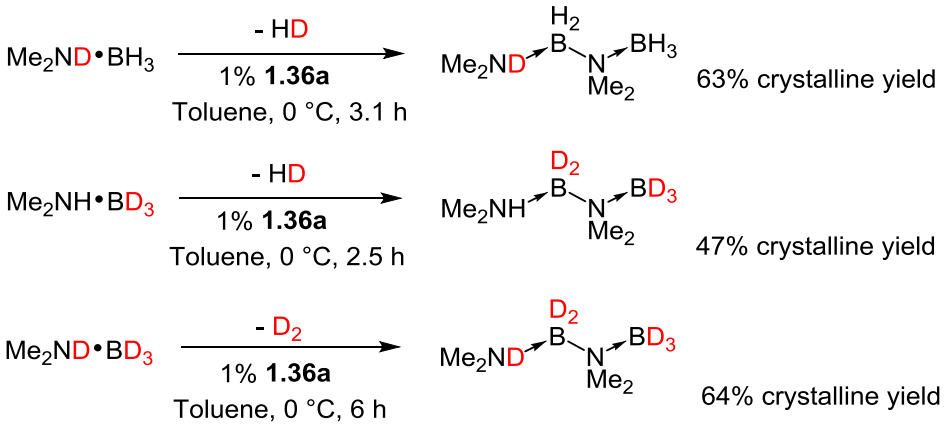
Scheme 2.6 Synthetic preparations of $Me_2NH{\cdot}BH_2NMe_2{\cdot}BH_3$. A and B represent stoichiometric literature preparations,[16,39] C shows our catalytic method.

Catalysis was quenched using 1 drop of distilled water (ca. 20 µL) upon which the green solution turned light yellow after *ca* 5 minutes of stirring. The yellow colour indicates formation of insoluble, dimeric $[Cp^*Ti\{MeC(NMe)_2\}(\mu\text{-}O)]_2$ (**2.5**), a known literature complex identified by ^1H NMR spectroscopy, which can easily be removed by canula filtration.[14] The volatiles were removed *in vacuo*, and the resulting off-white solid was dried by two consecutive recrystallisations at -80 °C in diethyl ether to give 1.59 g (81% yield) crystalline and analytically pure $Me_2NH{\cdot}BH_2NMe_2{\cdot}BH_3$.

The formation of this linear dimer was first reported by Hahn and Schaeffer, who reacted dimethylamine Me_2NH with dimethylaminodiborane $Me_2N(B_2H_5)$.[39] This methodology was later improved, and used for the synthesis of other diborazane analogues,[31] including $H_3N{\cdot}BH_2NH_2{\cdot}BH_3$ by Zhao and Shore (Scheme 2.6, A).[40] Subsequently, Manners reported a complementary, multi-step synthesis chlorinating the boron site of a batch of $Me_2NH{\cdot}BH_3$, lithiated the nitrogen site of a second batch of $Me_2NH{\cdot}BH_3$, and then reacting them together (Scheme 2.6, B).[16] By contrast, the protocol presented here is the first

catalytic synthesis of this molecule (Scheme 2.6, C). This protocol complements the previously reported, catalytic synthesis of the related $MeNH_2{\cdot}BH_2NHMe{\cdot}BH_3$ by Weller.[41]

Analogously, we were able to use our catalytic protocol for the synthesis of selectively labelled isotopologues of $Me_2NH{\cdot}BH_2NMe_2{\cdot}BH_3$ (Scheme 2.7), which were previously unknown compounds.



Scheme 2.7 Synthesis of isotopologues of the diborazane $Me_2NH{\cdot}BH_2NMe_2{\cdot}BH_3$.

On the preparative scale, the reaction conditions were analogous to the one used for $Me_2NH{\cdot}BH_2NMe_2{\cdot}BH_3$ (1% catalyst loading, 273 K, toluene). However, the kinetic isotope effects of the reactions need to be considered in order to quench the reaction when the corresponding linear dimer is at its maximum (the mechanistic significance of the KIEs will be discussed later). Mindful of the potential exchange between the hydrogen atoms of water and the amine hydrogens, 20 µL of D_2O was used to quench the reactions in the cases of $Me_2ND{\cdot}BH_2NMe_2{\cdot}BH_3$ and $Me_2ND{\cdot}BD_2NMe_2{\cdot}BD_3$.

Notably, diborazanes are insufficiently stable in neat water. When $Me_2NH{\cdot}BH_2NMe_2{\cdot}BH_3$ was dissolved in D_2O in an attempt to deuterate the amine functionality, the compound slowly decomposed before N(H/D) exchange could be effected. Various ^{11}B NMR resonances were observed, including $[Me_2N{=}BH_2]_2$, highlighting the synthetic value of the catalytic protocol shown in Scheme 2.7. All deutero-isotopologues could be isolated in good yields on the preparative scale (500-900 mg). The relatively lower yield compared to

the catalytic isolation of the $Me_2NH{\cdot}BH_2NMe_2{\cdot}BH_3$ analogue is likely due to a larger scale used in the latter case.

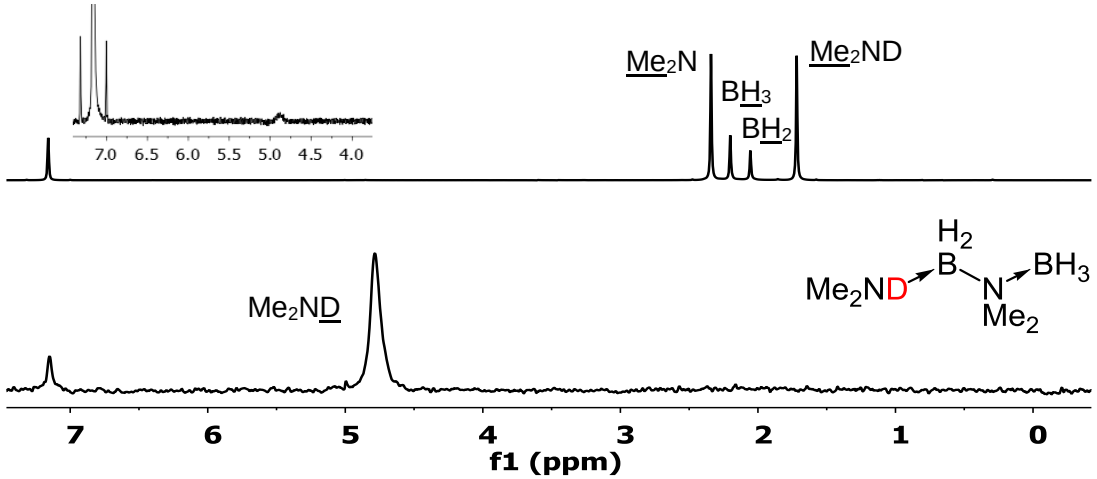


Figure 2.13 Top: $^1H\{^{11}B\}$ NMR spectrum (C_6D_6, 400 MHz, 298 K) of $Me_2N\underline{D}{\cdot}BH_2NMe_2{\cdot}BH_3$. The inset shows the residual NH peak at 4.9 ppm. Bottom: $^2H\{^{11}B\}$ NMR spectrum (C_6H_6, 61.4 MHz, 298 K).

^1H, ^2H and ^{11}B NMR as well as IR spectroscopy confirmed that the diborazanes were all labelled selectively, and the analytic results are discussed in the following. For $Me_2N\underline{D}{\cdot}BH_2NMe_2{\cdot}BH_3$, there is >98% deuteration at the nitrogen site, as estimated by integration of the ^1H NMR resonance against a methyl resonance (Figure 2.13). The deuteration on the nitrogen site was further confirmed in the $^2H\{^{11}B\}$ NMR spectrum, which showed no sign of deuteration of the boron moieties (Figure 2.13, bottom).

Infrared spectroscopy further confirmed the absence of both υ(N–H) and υ(B–D) stretch frequencies. The υ(N–H) stretch was found at 3195 cm^{-1} for $Me_2NH{\cdot}BH_2NMe_2{\cdot}BH_3$, compared to the appearance of a υ(N–D) stretch at 2248 cm^{-1} in this case, giving υ(N–D)/υ(N–H) = 0.74, in good agreement with the harmonic oscillator approximation υ(N–D)/υ(N–H) = 0.73.

Next, $Me_2NH{\cdot}B\underline{D}_2NMe_2{\cdot}B\underline{D}_3$ is discussed. The $^1H\{^{11}B\}$ NMR spectrum does not feature any sign of BH signals between 2.2 and 2.05 ppm, as was observed in the case of $Me_2ND{\cdot}BH_2NMe_2{\cdot}BH_3$ (Figure 2.14, Top). By contrast, the $^2H\{^{11}B\}$ NMR spectrum

features two broad BD signals corresponding to these shifts, and no ND signal could be detected.

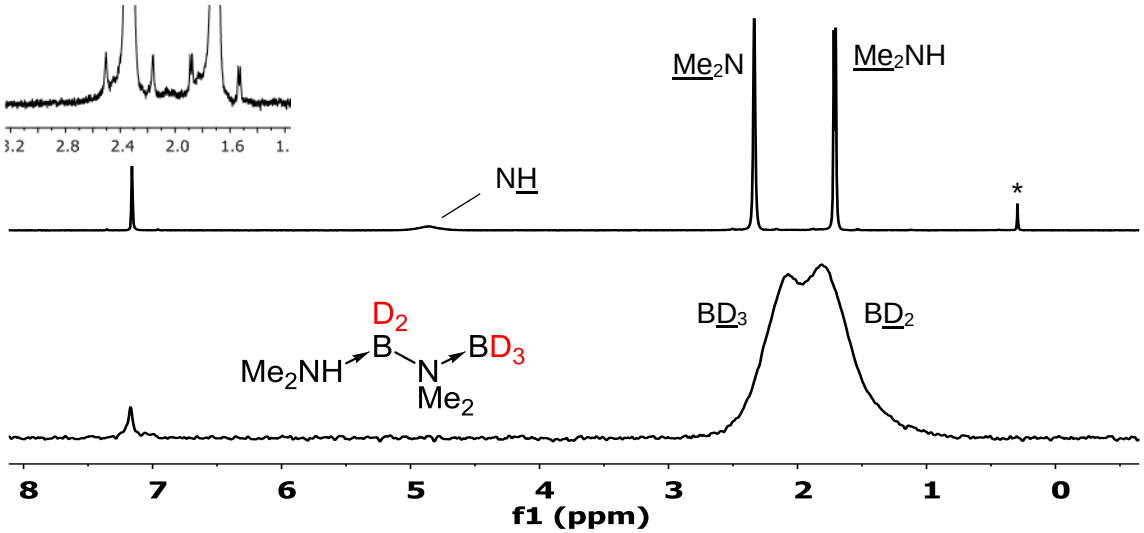


Figure 2.14 Top: $^{1}H\{^{11}B\}$ NMR spectrum (C_6D_6, 400 MHz, 298 K) of $Me_2NH{\cdot}B\underline{D}_2NMe_2{\cdot}B\underline{D}_3$. The inset shows the absence of BH resonances in region 3-1.4 ppm. Bottom: $^{2}H\{^{11}B\}$ NMR spectrum (C_6H_6, 61.4 MHz, 298 K). "*" denotes a grease impurity.

IR spectroscopy confirmed the absence of the four υ(B–H) stretch signals between 2450-2250 cm^{-1}, which were observed for the protio $Me_2NH{\cdot}BH_2NMe_2{\cdot}BH_3$ sample. Instead, four υ(B–D) stretches were detected between 1811-1636 cm^{-1}, giving υ(B-H)/ υ(B-D) of 0.73-0.75 which is in good agreement with the value obtained using the harmonic oscillator approximation (0.74). Additionally, a strong signal is detected at 3195 cm^{-1} corresponding to the υ(N–H) stretch, while there is no discernible signal between 2355-2365 cm^{-1} (expected for the corresponding υ(N–D) stretch). These results are all in agreement with selective and quantitative deuteration of the boron site, while there is no detectable sign of deuteration at the nitrogen site.

Finally, the $^{1}H\{^{11}B\}$ and $^{2}H\{^{11}B\}$ spectra for $Me_2N\underline{D}{\cdot}B\underline{D}_2NMe_2{\cdot}B\underline{D}_3$ are shown in Figure 2.15. In this case, the amine as well as boron functionalities are near-quantitatively deuterated. While no BH peaks were detected, a small amount of residual NH was observed. Nevertheless, ^{1}H NMR integration against the methyl resonances indicates >98%

deuteration on this site. Additionally, the IR spectrum confirms the near-quantitative deuteration on both the nitrogen and boron sites.

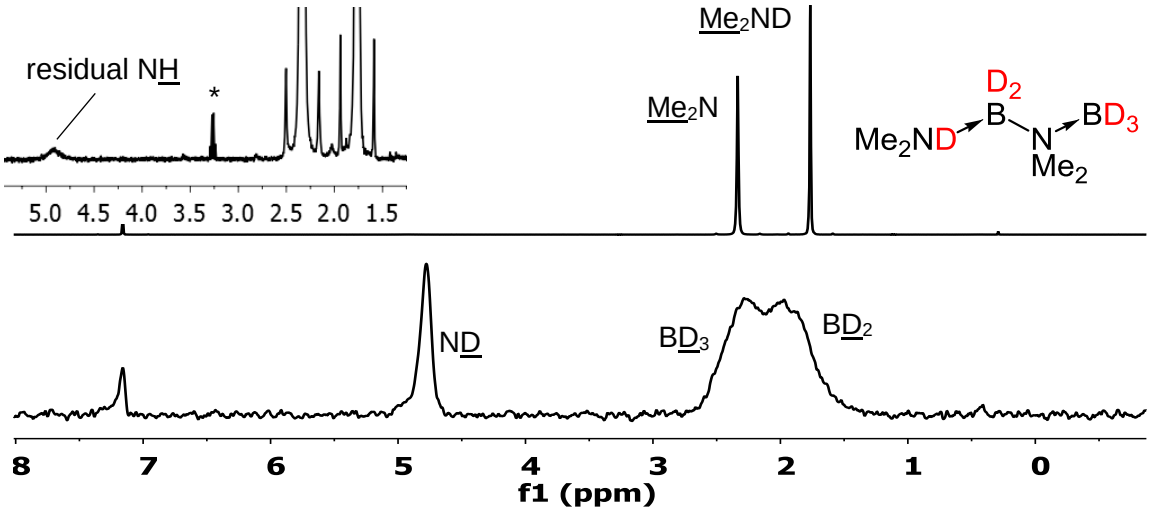
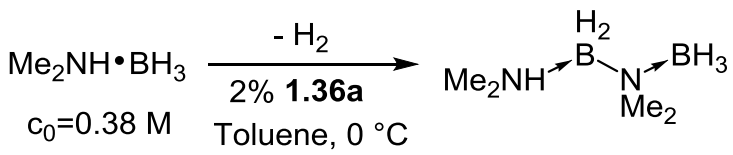


Figure 2.15 Top: $^{1}H\{^{11}B\}$ NMR spectrum (C_6D_6, 400 MHz, 298 K) of $Me_2ND{\cdot}BD_2NMe_2{\cdot}BD_3$. The inset shows the the presence of residual NH, and no discernible BH peaks. Bottom: $^{2}H\{^{11}B\}$ NMR spectrum (C_6H_6, 61.4 MHz, 298 K). "*" denotes residual diethyl ether impurity.

In conclusion, we developed a protocol for the *catalytic* preparation of $Me_2NH{\cdot}BH_2NMe_2{\cdot}BH_3$ and the corresponding isotopologues in high yields. The method enables near-quantitative, and selective deuteration at the nitrogen and boron sites, respectively. Importantly, there is no scrambling observed between hydrogens bound to nitrogen and boron.

2.3.6 Investigation of the first kinetic regime

The analysis of the concentration-time profiles led to the previously discussed mechanistic landscape shown in Scheme 2.5. In the following, more detailed mechanistic work is presented with the goal to understand the role of the catalyst Cp*Ti{MeC(NMe)$_2$}(NTol) (**1.36a**) itself. To start, the focus is on the first kinetic regime, the fast conversion of $Me_2NH{\cdot}BH_3$ to $Me_2NH{\cdot}BH_2NMe_2{\cdot}BH_3$ (Equation 2.6).



Equation 2.6

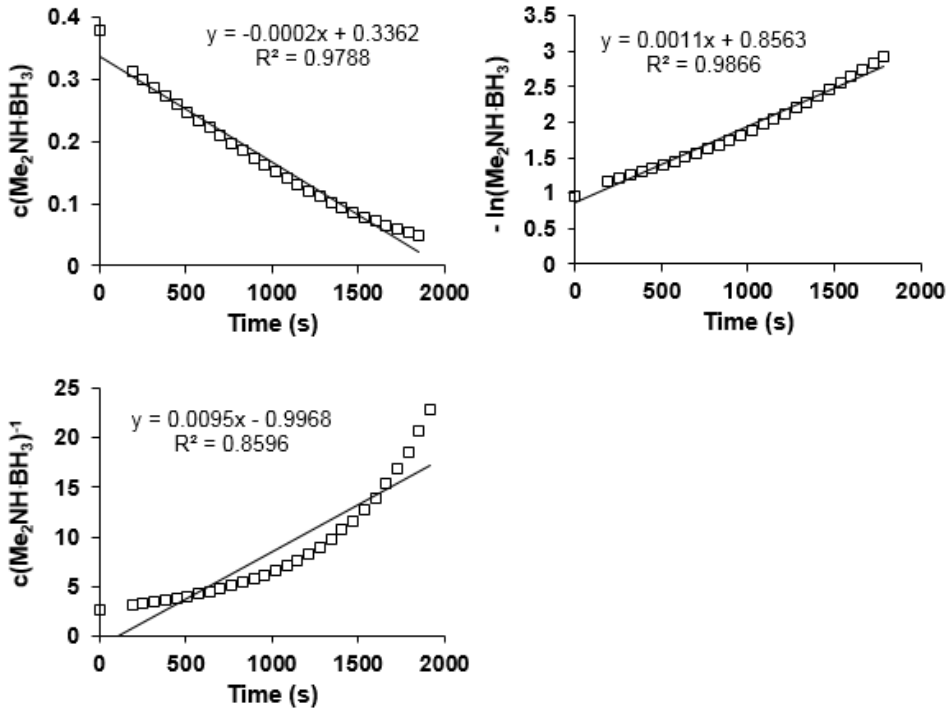


Figure 2.16 Order plots for the dehydrocoupling of $Me_2NH{\cdot}BH_3$ (c_0 = 0.38 M, toluene, 273 K) using 2 mol% **1.36a**, and corresponding least squares fit function.

Order plots for catalytic conversion of $Me_2NH{\cdot}BH_3$ (c_0 = 0.38 M, toluene, 273 K) using 2% **1.36a** are shown in Figure 2.16. From the inverse concentration-time plot it is clear that the reaction is not second order in substrate. By contrast, both the zeroth as well as first order plots (top left, and right, respectively) show reasonable least square fits to a linear function. Thus, the apparent order is not an unambigous integer value, reflective of a complex mechanistic landscape as illustrated in Scheme 2.5. However, a more distinct curved trend can be observed for the zeroth order plot. Additionally, small amounts of the formed linear dimer are converted at 0 °C (Figure 2.8). This means that small amounts of $Me_2NH{\cdot}BH_3$ are reformed during this process, therefore reducing the apparent order of $Me_2NH{\cdot}BH_3$.

Next, the order in catalyst **1.36a** was determined. To circumvent complications arising from catalyst decomposition the initial rates method was employed. The method effectively determines the rate of substrate consumption $d[Me_2NH{\cdot}BH_3]/dt$ at time = 0. The same experiment was repeated several times, keeping all conditions the same, varying only the

catalyst loading (initial catalyst concentration). Following the reactions by $^{11}B\{^{1}H\}$ NMR spectroscopy which gave concentration-time plots such as given in Figure 2.17.

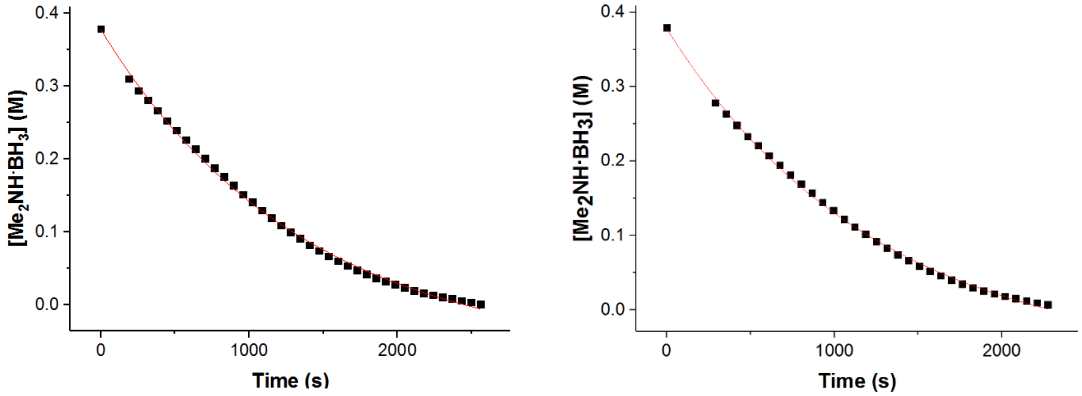


Figure 2.17 Left: Plot of $[Me_2NH{\cdot}BH_3]$ *vs.* time plotted in Origin. The best-fit line ($R^2 = 0.998$) shown gave $A_1 = 0.452$ (4), $B_1 = 1350$ (80) giving an initial rate of 3.3 (1) x 10^{-4} mol dm^{-3} s^{-1}. Right: A duplicate of the same reaction ($R^2 = 0.998$). $A_1 = 0.450$ (4), $B_1 = 1250$ (30) giving an initial rate of 3.7 (1) x 10^{-4} mol dm^{-3} s^{-1}.

The graphical software ORIGIN was used to fit these data points using a simple exponential function (Equation 2.7), where y_0, A_1 and B_1 are empirical parameters. The curve was then differentiated to give an equation for the gradient (Equation 2.8), and then the gradient was calculated at time = 0 s (Equation 2.9).

$$[Me_2NH{\cdot}BH_3] = [Me_2NH{\cdot}BH_3]_0 + A_1\, e^{t/B_1} \qquad (2.7)$$

$$\frac{d[Me_2NH{\cdot}BH_3]}{dt} = \frac{A_1\, e^{t/B_1}}{B_1} \qquad (2.8)$$

$$\left(\frac{d[Me_2NH{\cdot}BH_3]_0}{dt}\right)_{t=0} = \frac{A_1}{B_1} \qquad (2.9)$$

This allows the calculation of the initial rate of the reaction (Figure 2.15). It is noted that the method is accurate when the studied reaction is sufficiently slow.

As can be seen in Figure 2.18, the initial rate approximately doubles when the catalyst loading is doubled and in the absence of catalyst the substrate was stable in solution for weeks. Therefore, the reaction is likely first order in catalyst.

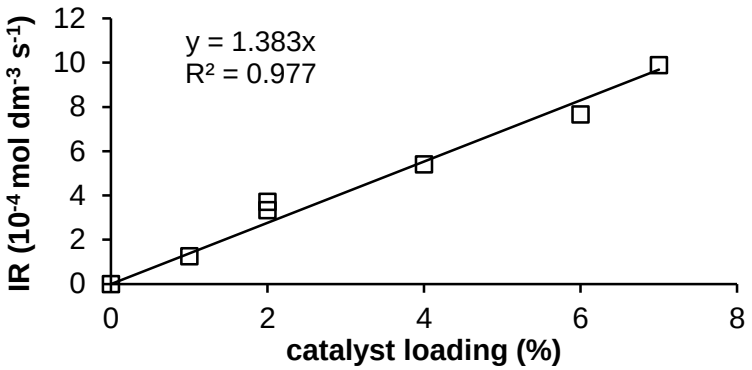
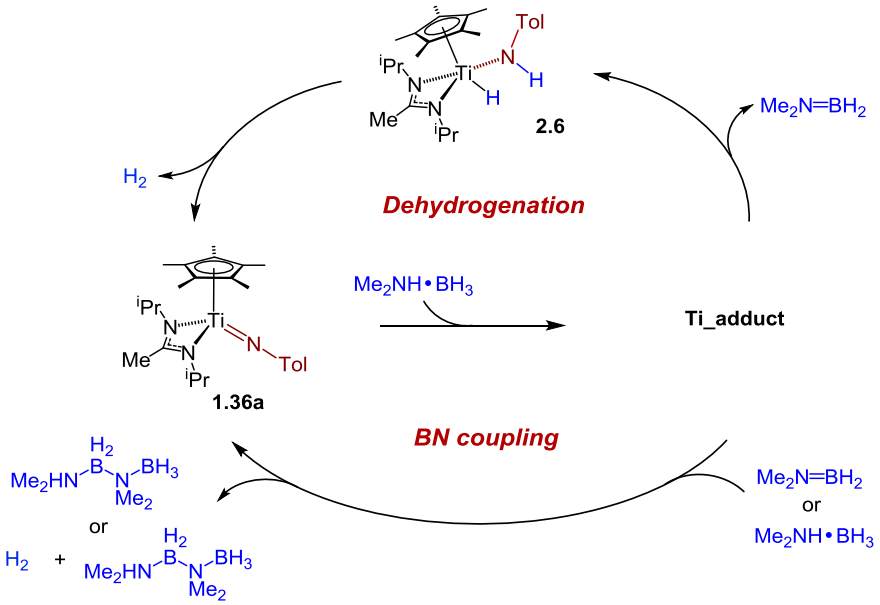


Figure 2.18 Initial rates (IR) as function of **1.36a** catalyst loading of the dehydrocoupling of $Me_2NH{\cdot}BH_3$ (c_0 = 0.38 M, toluene, 273 K), and corresponding least squares fit function. The data point at 2% catalyst loading was run in duplicate.

As discussed earlier, there is near-quantitative conversion of $Me_2NH{\cdot}BH_3$ to $Me_2NH{\cdot}BH_2NMe_2{\cdot}BH_3$ while there is only limited formation of free $Me_2N{=}BH_2$ at early stages of catalysis. Additionally, experimental and computational work suggest that off-metal formation of $Me_2NH{\cdot}BH_2NMe_2{\cdot}BH_3$ from $Me_2NH{\cdot}BH_3$ and $Me_2N{=}BH_2$ is kinetically disfavoured.[32–34] This suggests that B–N coupling to form linear dimer occurs at a metal-bound $Me_2NH{\cdot}BH_3$/$Me_2N{=}BH_2$ species (**Ti_adduct**).

This suggests that $Me_2NH{\cdot}BH_3$ remains bound to the metal centre after initial activation to form an adduct, **Ti_adduct**, which has two possible reaction pathways as is shown in Scheme 2.8. The first is for **Ti_adduct** to release $Me_2N{=}BH_2$ and form titanium hydride amide Cp*Ti(H){MeC(NMe)$_2$}(NHTol) (**2.6**). This pathway accounts for the detection of small quantities of free $Me_2N{=}BH_2$ from the start of catalysis, formed independently from diborazane. Titanium hydrides are highly reactive species, and have been implicated in a variety of catalytic processes; including olefin polymersation,[42] olefin hydrosilylation, dehydrocoupling of silanes and stannanes,[43,44] as well as the dehydrocoupling of $Me_2NH{\cdot}BH_3$.[18]



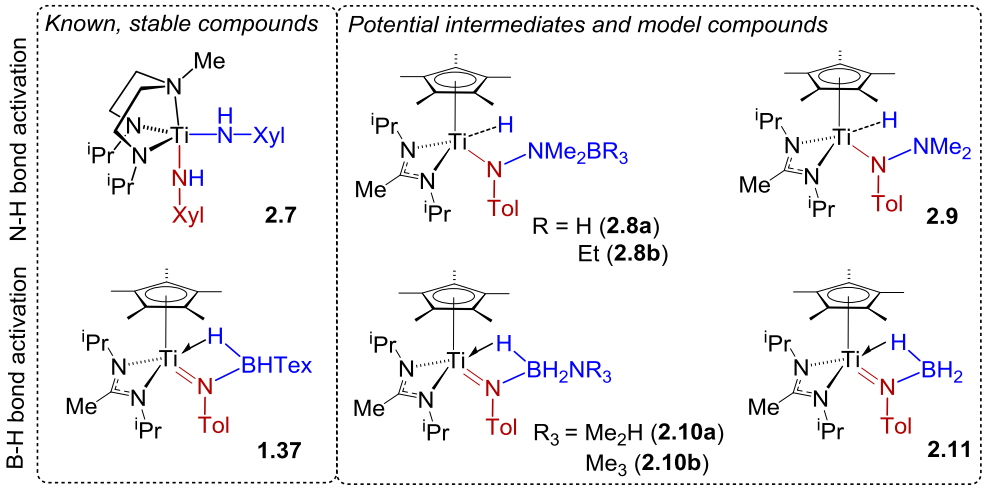
Scheme 2.8 Possible reaction pathways during the first kinetic regime.

Titanium hydride amide **2.6** is proposed to lose dihydrogen by 1,2-elimination, and reform the titanium imide catalyst **1.36a**. Such group 4 hydride amide 1,2-eliminations of dihydrogen are well-known,[5,45–47] and related titanium hydride amide hydrogen loss reactions will also be presented in Chapter Four. Isolated titanium(IV) hydrides are relatively rare, and are known to readily undergo reduction to Ti(III) species *via* dimerisation and loss of dihydrogen.[44,48] Thus, **2.6** might be involved in the catalyst decomposition and formation of Ti(III) species, which was evidenced by EPR spectroscopy of a catalytic reaction mixture.

The second possible pathway for **Ti_adduct** is to undergo BN coupling to eventually release diborazane $Me_2NH{\cdot}BH_2NMe_2{\cdot}BH_3$ (lower part of the cycle in Scheme 2.8). This linear dimer may either be formed by recombination of **Ti_adduct** with $Me_2NH{\cdot}BH_3$, or with previously released $Me_2N{=}BH_2$, and we cannot fully discount either case.

In order to investigate the first activation step and the nature of **Ti_adduct**, we considered various possible reaction pathways. Previous studies showed that amines can undergo N–H bond activation across titanium imide bonds to form stable (bis)amides such as **2.7**

(Scheme 2.9).[49] Similarly, B–H bond activations can occur to form titanium hydride borylamides. As introduced in Chapter One, various boranes were shown to form 1,2-addition products such as Cp*Ti{MeC(N^{i}Pr$_2$)$_2$}{N(Tol)H$_2$BTex} (**1.37**, Tex = 1,1,2-trimethylpropyl) in which the B–H bond is only partially broken. In analogy to these species, we postulate the plausible intermediates summarised in Scheme 2.9, which might lie on the dehydrocoupling reaction coordinate of the Me$_2$NH·BH$_3$ substrate.



Scheme 2.9 Known and postulated N–H and B–H bond activation products of **1.36a**.

In order to detect titanium containing intermediates, a number of reactions were followed using VT NMR spectroscopy. The reaction between stoichiometric amounts of Cp*Ti{MeC(NMe)$_2$}(NTol) (**1.36a**) and Me$_2$NH·BH$_3$ was set up at -78 °C, and followed *via* ^{1}H and ^{11}B NMR spectroscopy while it was gradually warmed in the NMR spectrometer. However, no reaction was observed until *ca* 253 K, at which point the reaction proceeded without observable intermediates. It was reasoned that increased steric bulk might enable the detection of intermediates and ^{i}Pr$_2$NH·BH$_3$ was used as substrate. However, no intermediates could be detected either.

Next, model substrate H$_3$N·BEt$_3$ was investigated. It does not feature B–H bonds, making the system simpler since after initial N–H bond activation there can be no subsequent reactions involving B–H bonds. This makes detection of 1,2-addition products such as

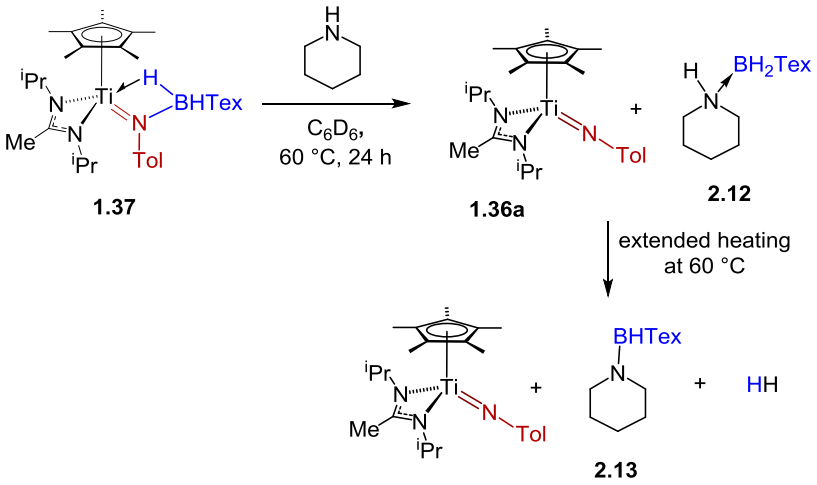
Cp*Ti{MeC(NMe)$_2$}(NHTol)(NMe$_2$BH$_3$) (**2.8a**) or Cp*Ti{MeC(NMe)$_2$}(NHTol)(NMe$_2$) (**2.9**) easier (Scheme 2.9). However, no reaction occurred between this substrate and either Cp*Ti{MeC(NMe)$_2$}(NR), R = ^{t}Bu (**2.1**) or Tol (**1.36a**). This is somewhat expected since previous studies by the Mountford group demonstrated that N–H bond addition of alkylamines across arylimide Ti=NAr multiple bonds are thermodynamically disfavoured.[50] In fact, arylamines such as H$_2$NTol were used to "protonate-off" the alkylamine H$_2$N^{t}Bu from Cp*Ti{MeC(NMe)$_2$}(N^{t}Bu) (**2.1**) to form arylimides such as Cp*Ti{MeC(NMe)$_2$}(NTol) (**1.36a**) in the first place. In agreement with this, control reactions of HNMe$_2$ or piperidine with **1.36a** did not yield any reaction.

By comparison, Manners' [Cp$_2$Ti^{II}] system was proposed to form [Cp$_2$Ti^{IV}(H)NMe$_2$BH$_3$] (**1.89**) *via* oxidative N–H bond addition with Me$_2$NH·BH$_3$.[2] However, since Cp*Ti{MeC(NMe)$_2$}(NTol) (**1.36a**) is already in oxidation state Ti(IV) an analogous oxidative pathway cannot occur.

Analogous reactions were also performed using model substrate Me$_3$N·BH$_3$ with the aim of detecting 1,2-B–H bond addition species such as Cp*Ti{MeC(NMe)$_2$}{N(Tol)BH$_3$NMe$_3$} (**2.10b**) or Cp*Ti{MeC(NMe)$_2$}{N(Tol)BH$_3$} (**2.11**). However, also in this case no reactions were observed with Cp*Ti{MeC(NMe)$_2$}(N^{t}Bu) (**2.1**) or Cp*Ti{MeC(NMe)$_2$}(NTol) (**1.36a**), even under forcing conditions.

Next, Cp*Ti{MeC(N^{i}Pr$_2$)$_2$}{N(Tol)H$_2$BTex} (**1.37**) was investigated since it represents a suitable model for the BH$_3$ analogue **2.11** (Schemes 2.9 and 2.10). It can be conveniently prepared from Cp*Ti{MeC(NMe)$_2$}(NTol) (**1.36a**) with H$_2$BTex, and isolated as stable, crystalline product.[51] It was reasoned that the increased steric bulk at the boron centre may stabilise any titanium-bound intermediates, or slow down certain reaction steps along the

dehydrocoupling reaction such that intermediates might be observed. As a suitable amine counterpart piperidine was chosen, because of the similar steric profile to Me_2NH (which itself is gaseous in free form and thus avoided).



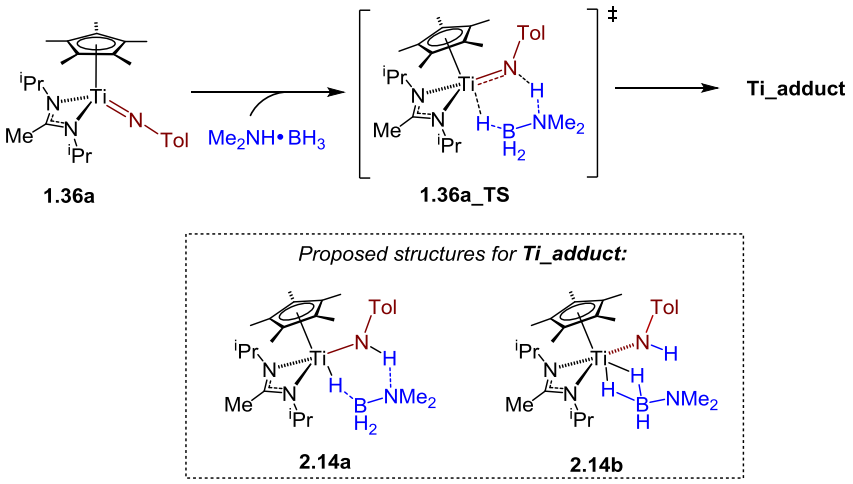
Scheme 2.10 Reaction of piperidine with Cp*Ti{MeC(N^{i}Pr$_2$)$_2$}{N(Tol)H$_2$BTex} (**1.37**).

When 1 equivalent piperidine was added to a solution of Cp*Ti{MeC(N^{i}Pr$_2$)$_2$}{N(Tol)H$_2$BTex} (**1.37**) in C_6D_6 no reaction occurred at RT. When the mixture was heated to 60 °C, the formation of the amine-borane adduct $C_5H_{10}NH{\cdot}BH_2Tex$ (**2.12**) and free **1.36a** were detected. No sign of dehydrocoupling can be observed initially. Only after the starting materials were converted to compounds **2.12** and **1.36a**, H_2 and dehydrocoupled amine-borane $C_5H_{10}N$–BHTex (**2.13**) were detected. This suggests that piperidine attacks the boron centre in **1.37** to form the amine-borane adduct $C_5H_{10}NH{\cdot}BH_2Tex$ (**2.12**) before dehydrocoupling occurs.

Importantly, when isolated amine-borane $C_5H_{10}NH{\cdot}BH_2Tex$ (**2.12**) was dehydrocoupled with Cp*Ti{MeC(NMe)$_2$}(NTol) (**1.36a**) directly, and followed by NMR spectroscopy, there is no sign of the B–H bond activated adduct Cp*Ti{MeC(N^{i}Pr$_2$)$_2$}{N(Tol)H$_2$BTex} (**1.37**) in the reaction mixture. Additionally, a control reaction showed that free piperidine did not react with Cp*Ti{MeC(NMe)$_2$}(NTol) (**1.36a**).

In conclusion, a variety of differently substituted boranes, amines, amine-boranes were tested with Cp*Ti{MeC(NMe)$_2$}(NTol) (**1.36a**). In all cases, no evidence for initial N–H bond or B–H bond activation, or adduct formation to the catalyst was observed. In cases where a B–H bond activated compound was stable (**1.37**), added amines replaced the titanium imide as donor to form free amine-boranes and free catalyst **1.36a**. Formation of amine-boranes was favoured over a dehydrocoupling reaction. These observations suggest that in the reaction between Cp*Ti{MeC(NMe)$_2$}(NTol) (**1.36a**) and Me$_2$NH·BH$_3$ neither N–H, or B–H bond activation occur *individually* in a first step.

Another possibility represents the *concerted* N–H/B–H bond activation as the first reaction step (Scheme 2.11, concerted inner-sphere mechanism). Me$_2$NH·BH$_3$ is proposed to be activated by the cooperative action of the metal and imide functionality as illustrated in **1.36a_TS**, in analogy to the bifunctional Noyori mechanism reported for the asymmetric hydrogenation of ketones.[52] As discussed in Chapter One, Fagnou[53] and Schneider[54] reported analogous, concerted N–H/B–H bond activations. In these cases, a metal-*amide* cooperatively activates amine-boranes, whereas it is a related metal-*imide* ligand system in the present case.



Scheme 2.11 Proposed concerted Noyori-type mechanism as first activation step of Me$_2$NH·BH$_3$.

Subsequent to transition state **1.36a_TS**, **Ti_adduct** is formed and we propose **2.14a** and Cp*Ti{MeC(NMe)$_2$}(NHTol)(η^2-H$_3$B-NMe$_2$) (**2.14b**) as plausible structures. Both of the structures might be stable, and might exist in equilibrium. **2.14a** likely lies on the reaction coordinate and resembles transition state **1.36a_TS**. We favour η^2-bound adduct **2.14b**, which is analogous to a variety of previously reported titanium η^2-bound boranes.[55–58] The 3-centre 2-electron bonds renders the boron less electrophilic, and thus the adjacent nitrogen lonepair is more nucleophilic, which might explain subsequent BN coupling pathways (*vide infra,* Scheme 2.15). η^2-bound amino-boranes as well as amine-boranes were also reported for late transition metals, such as [Ir(PCy$_3$)$_2$(H)$_2$(η^2-H$_3$B·NMe$_2$H)][BAr$^F{}_4$] (**2.15**) and the corresponding [Ir(PCy$_3$)$_2$(H)$_2$(η^2-H$_2$B-NMe$_2$)][BAr$^F{}_4$] (**2.16**) reported by Weller *et al.*[34]

To test the mechanism further, kinetic isotope effects were determined. Thus, the initial rates for Me$_2$NH·BH$_3$ and the corresponding isotopologues were measured and gave the KIE values shown in Table 2.4. In particular, KIE values of 3.3-3.5 for N–H/D, 1.3-1.4 for B–H/D, and 4.0-4.3 for N–H/D and B–H/D were observed, which agree well with corresponding values obtained for Manner's [Cp$_2$Ti] system.[18] These results suggest that N–H bond cleavage is involved in the rate determining step. B–H bond cleavage might also be involved in the rate-determining step, and the relatively low KIE can be explained by an extremely early or late transition state, or small transfer angles.[18,59]

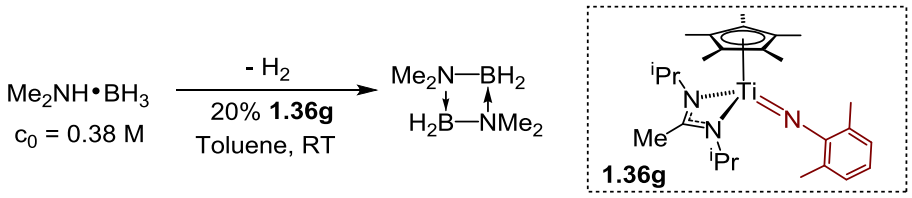
Table 2.4 Kinetic isotope effects for the reaction of substrate (c_0=0.38 M, 273 K, toluene) using 2% catalyst loading (**1.36a**). KIE denotes kinetic isotope effect.

Substrate	**Initial rate (10^{-4} mol dm^{-3} s^{-1})**	**KIE**
Me$_2$NH · BH$_3$	3.5(2)*	-
Me$_2$N<u>D</u> · BH$_3$	1.07(3) and 1.00(3)	3.3-3.5
Me$_2$NH · B<u>D</u>$_3$	2.8(1) and 2.5(1)	1.3-1.4
Me$_2$N<u>D</u> · B<u>D</u>$_3$	0.81(2) and 0.85(3)	4.0-4.3

*Average value of two runs.

Since titanium containing intermediates can neither be detected during catalytic runs, nor during stoichiometric studies at low temperature, the rate determining step might be associated with the first activation step, towards formation of **Ti_adduct**. Thus, transition state **1.36a_TS** could be rate-determining, and the observed KIE are in line with this proposal. In particular, the combined KIE for N–H and B–H bond activation match the product of the two individual KIE (1.3 x 3.3 = 4.29), as would be expected for a concerted mechanism.[60] The difference in size of the KIE of N–H and B–H bond cleavage might arise from an asymmetric, but concerted activation.

Next, the bulkier catalyst Cp*Ti{MeC(NMe)$_2$}(NXyl) (**1.36g**) was investigated. Compared to tolyl congener **1.36a**, the steric demand is increased by the close proximity of two methyl groups next to the imido function in 2,6-positions of the aryl group (Scheme 2.12). Under the "standard conditions" used previously to dehydrocouple $Me_2NH{\cdot}BH_3$ (c_0=0.38 M, toluene, 273 K, 2 mol% catalyst loading), no reaction was observed. The temperature as well as the catalyst loading needed to be increased to 298 K, and 20 mol%, respectively, to drive the reaction to completion.



Scheme 2.12 Catalytic dehydrocoupling of $Me_2NH{\cdot}BH_3$ with Cp*Ti{MeC(NMe)$_2$}(NXyl) (**1.36g**).

The time-concentration profile broadly resembles the one observed for **1.36a** at 273 K, with both $Me_2NH{\cdot}BH_2NMe_2{\cdot}BH_3$ as well as $Me_2N{=}BH_2$ observed as intermediates, before $[Me_2N{=}BH_2]_2$ is formed as final product. However, there is no distinct separation between the two kinetic regimes anymore, and $Me_2NH{\cdot}BH_2NMe_2{\cdot}BH_3$ reaches only a maximum of *ca* 0.13 M instead of 0.18 M (Figure 2.19). This observation is in line with a mechanism

that is more sensitive for the initial conversion of $Me_2NH{\cdot}BH_3$, compared to the subsequent conversion of $Me_2NH{\cdot}BH_2NMe_2{\cdot}BH_3$.

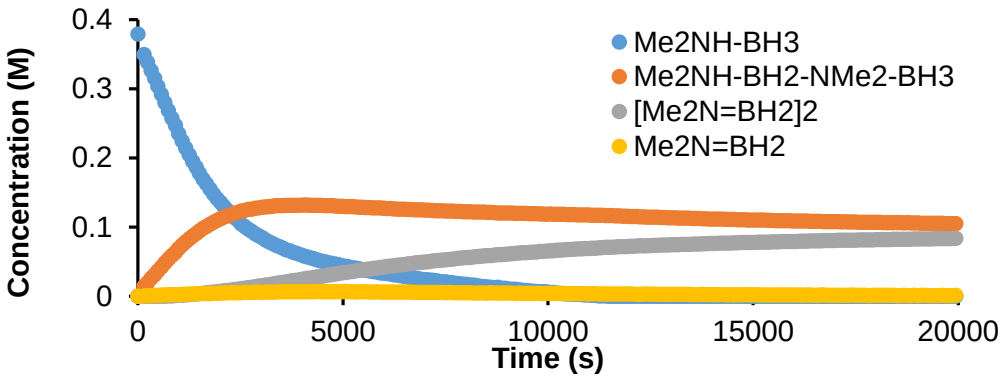


Figure 2.19 Concentration-time profiles for the catalytic dehydrocoupling of $Me_2NH{\cdot}BH_3$ using Cp*Ti{MeC(NMe)$_2$}(NXyl) (**1.36g**).

Hence, we conclude that the catalytic dehydrocoupling of $Me_2NH{\cdot}BH_3$ is very sensitive towards steric bulk in proximity to the Ti=N moiety, highlighting its importance during catalysis.

Next, we investigated the effect of electronic properties on the rate-determining step of linear diborazane formation by varying the aryl group of the catalyst. Initial rates of the reactions between $Me_2NH{\cdot}BH_3$ and Cp*Ti{MeC(NMe)$_2$}(NAr) with Ar = Tol (**1.36a**), Ar^{NMe_2} (**1.36b**), Ar^{OMe} (**1.36c**), Ph (**1.36d**), Ar^{Cl} (**1.36e**), Ar^{Br} (**1.36f**) are given in Table 2.5, along with the corresponding Hammett substituent constants σ_p.[61] The Hammett plot of log(IR/IR_H) *vs* σ_p is shown in Figure 2.20 (IR denotes the initial rate using catalysts **1.36a-1.36f**, and IR_H refers to the initial rate of catalyst **1.36d**).

The reaction rate increases going from the electron-donating NMe_2 group to the phenyl substituent, which featured the largest initial rate of 37 x 10^{-5} mol dm^{-3} s^{-1}. Significantly, the initial rates corresponding to the para substituents NMe_2, OMe, Me and H follow a straight line (R^2 = 0.984). When moving to more electron withdrawing groups such as Cl

and Br, the initial rate is observed to drop, with both substituents featuring comparable Hammett parameters σ_p, as well as comparable initial rates.

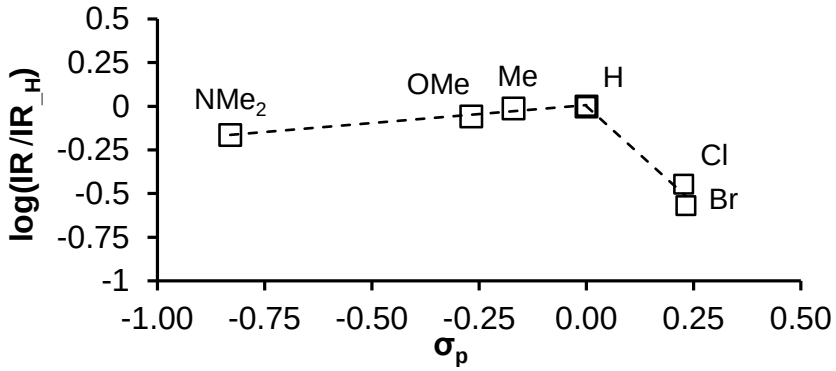


Figure 2.20 Hammett plot log(IR/IR_H) *vs* σ_p in the reaction of $Me_2NH{\cdot}BH_3$ (c_0=0.38 M, toluene, 0 °C) and Cp*Ti{MeC(NMe)$_2$}(NAr) with Ar = Tol (**1.36a**), Ar^{NMe_2} (**1.36b**), Ar^{OMe} (**1.36c**), Ph (**1.36d**), Ar^{Cl} (**1.36e**), Ar^{Br} (**1.36f**). IR = Initial rate, IR_H = Initial rate using **1.36d**.

Table 2.5 Initial rates and Hammett parameters σ_p corresponding to the dehydrocoupling of $Me_2NH{\cdot}BH_3$ (c_0=0.38 M, toluene, 0 °C) with 2% Cp*Ti{MeC(NMe)$_2$}(N-4-C_6H_4X) (**1.36a-1.36f**).

X	**σ_p**	**Initial rate (10^{-5} mol dm^{-3} s^{-1})***
NMe_2	-0.83	25
OMe	-0.27	32
Me	-0.17	35.5
H	0	36.5
Cl	0.227	13.1
Br	0.232	9.9

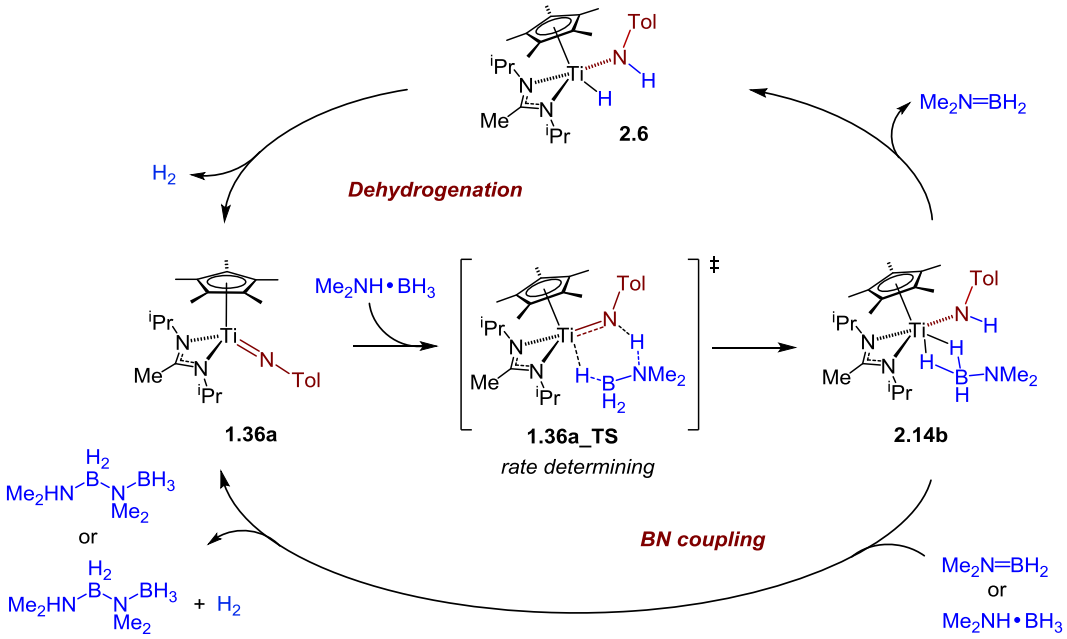
*All runs are duplicates.

It has been reported frequently that reactions with multiple mechanisms or steps may not exhibit linear Hammett relationships.[62–64] These two cases should be clearly distinguished. First, if a reaction occurs by two or more competing mechanisms, the substituent effect will generally differ between different mechanisms. Accordingly, one can expect different reaction constants to apply. In the σ region in which the rates due to two competing mechanisms are comparable, the overall reaction rate will be given as sum of the two individual rates. Thus, the overall dependence of log(IR/IR_H) on σ_p necessarily needs to be concave upward.[62,63] By contrast, a change in the identity of the rate-determining step, induced by changing the substitutents, appears as concave downward line in the Hammett

plot. Such a concave downward line, as is observed in Figure 2.20, cannot result from a change in mechanism.[62]

The shape of the Hammett plot thus suggests that the consumption of $Me_2NH{\cdot}BH_3$ is controlled by one major mechanistic pathway, and the concave downward line reflects a shift in position of the rate determining step rather than a change in mechanism. To confirm this experimentally, we measured the KIE on the extrema of the Hammett plot, using $Me_2ND{\cdot}BD_3$ and catalysts Cp*Ti{MeC(NMe)$_2$}(NAr), Ar = Br and NMe_2, respectively. Initial rates of 2.4 and 11 x 10^{-5} mol dm^{-3} s^{-1} were measured, corresponding to combined KIE values of 4.1 and 2.3, respectively. The values are significant, and comparable to the corresponding one observed for Ar = Tol (4.0-4.3), in line with a change in position of the rate-determining step of the same operating mechanism. These observations are all in line with the proposed concerted N–H/B–H bond activation as rate-determining step. In particular, since we do not expect a charge build-up on the imido moiety in this mechanism, we also would not expect a linear Hammett line.

In summary, a combination of model substrate and low-temperature NMR studies, concentration-time profile analysis, kinetic isotope effects and investigation of steric as well as electronic catalyst effects were used to probe the mechanistic cycle of the dehydrocoupling of $Me_2NH{\cdot}BH_3$ with catalyst Cp*Ti{MeC(NMe)$_2$}(NTol) (**1.36a**). The results are in agreement with a plausible mechanistic cycle shown in Scheme 2.13. A variety of model substrates suggested that *individual* N–H or B–H bond activations are unlikely to be the first step of the reaction between $Me_2NH{\cdot}BH_3$ and titanium imide Cp*Ti{MeC(NMe)$_2$}(NTol) (**1.36a**). Thus, we propose a *concerted* N–H/B–H bond activation with transition state **1.36a_TS**, which is in agreement with measured KIE values.



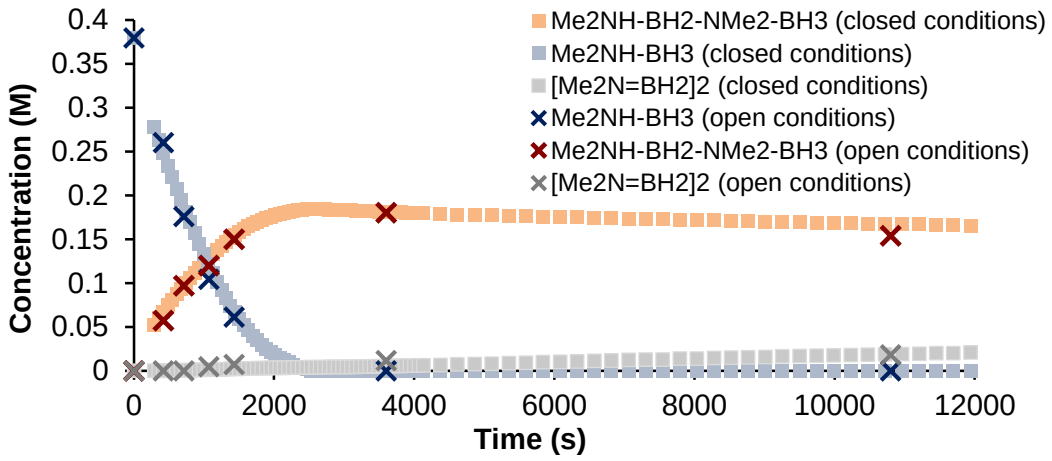
Scheme 2.13 Plausible reaction pathways during the first kinetic regime.

Such concerted N–H/B–H bond activation by the cooperative action of the titanium-imide moiety is further supported by literature precedent for similar concerted N–H/B–H bond activations using transition metal-amide moieties.[53,54] Following the concerted activation step we propose an adduct species Cp*Ti{MeC(NMe)$_2$}(NHTol)(η^2-H$_3$B-NMe$_2$) (**2.14b**), which can account for the observed concentration-time profiles of the organic intermediates (*vide infra*, 2.3.8).

In the following, the effect of dihydrogen accummulation during catalysis will be discussed, and dihydrogen loss of proposed titanium hydride **2.6** (Top, dehydrogenation part of Scheme 2.13), and subsequently the BN coupling pathway (Bottom, Scheme 2.13).

Routinely, the reactions were performed in a sealed NMR tube, under closed conditions. Hence, dihydrogen is built-up during the catalytic runs. To investigate the effect H_2 might have on the overall reaction a large scale protocol was developed to run the reaction under open conditions. Therefore, reactions were set up in a three-necked round bottom Schlenk connected to a T-piece that allowed a continous flow of nitrogen during the catalytic run. The reaction progress was monitored by taking regular aliquots (0.1 mL) which were

quenched with a solution of toluene (0.35 mL) containing water (15 µL). The reaction mixture immediately changed colour from green to yellow, and the yellow precipiate indicated formation of the known [Cp*Ti{MeC(N^{i}Pr)$_2$}(µ-O)]$_2$ (**2.5**).[65] The reaction progress was then immediately quantified *via* ^{11}B NMR spectroscopy (Scheme 2.14).



Scheme 2.14 Overlapped catalytic runs of $Me_2NH{\cdot}BH_3$ (c_0=0.38 M, toluene, 0 °C) with 2% **1.36a**, under closed (NMR scale) conditions and open conditions.

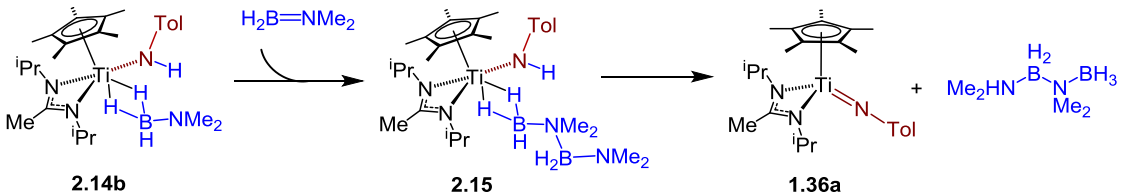
As can can be seen from the concentration-time profiles shown in Scheme 2.14, there is excellent overlap between the catalytic runs using sealed, and open conditions. This contrasts to observations made using late-transition metal dehydrocoupling catalysts, for which dihydrogen can often inhibit catalysis.[37] These results suggest that there are no rate-determining equilibria with H_2, and that hydrogen loss is likely irreversible.

This step was previously proposed to occur *via* 1,2-dihydrogen loss from titanium hydride amide Cp*Ti(H){MeC(NMe)$_2$}(NHTol) (**2.6**, Scheme 2.12). In a control reaction, both Cp*Ti{MeC(NMe)$_2$}(N^{t}Bu) (**2.1**) and Cp*Ti{MeC(NMe)$_2$}(NTol) (**1.36a**) were subjected to an atmosphere of 4 bar of H_2 atmosphere. In line with the previous experiments and an irreversible reaction, no reaction was observed within one week at RT.

Next, the BN coupling pathway is discussed. The previously mentioned $Me_2NH{\cdot}BH_3$ titanium adduct Cp*Ti{MeC(NMe)$_2$}(NHTol)(η^2-H$_3$B-NMe$_2$) (**2.14b**) is proposed to either

enter the dehydrogenation pathway, eventually forming $Me_2N{=}BH_2$ and dihydrogen, or enter the BN coupling pathway to eventually release $Me_2NH{\cdot}BH_2NMe_2{\cdot}BH_3$ (Scheme 2.13). This linear dimer may either be formed by recombination of **2.14b** with $Me_2NH{\cdot}BH_3$, or with previously released $Me_2N{=}BH_2$, and we cannot fully discount either case.

One possibility for the latter is the attack of the nucleophilic NMe_2 moiety in Cp*Ti{MeC(NMe)$_2$}(NHTol)(η^2-H_3B-NMe_2) (**2.14b**) to $Me_2N{=}BH_2$ to form a η^2-bound diborazane complex Cp*Ti{MeC(NMe)$_2$}(NHTol)(η^2-H_3B-$NMe_2BH_2{\cdot}NMe_2$) (**2.14b**, Scheme 2.15). Although there is multiple bond character in $Me_2N{=}BH_2$, previous DFT calculations have shown that the LUMO orbital in the related $H_2N{=}BH_2$ congener features the largest coefficient on the boron atom and is susceptible to nucleophilic attack.[66] Indeed, an entirely analagous mechanism was proposed for the polymerisation of $NH_3{\cdot}BH_3$ using Brookhart's iridium pincer catalyst [Ir(H)$_2$(POCOP)] (**1.104**, POCPOP = [μ_3-1,3-(OP^{t}Bu$_2$)$_2$C$_6$H$_3$]).[66] Initial reaction with $NH_3{\cdot}BH_3$ led to formation of [Ir(H)(η^2-H_3B-NH_2)(POCOP)] (**1.106**), featuring a nucleophilic lonepair on the N-terminus. This is proposed to attack free $H_2N{=}BH_2$ on the boron site, forming [Ir(H)(η^2-H_3B-NH_2BH_2-NH_2)(POCOP)] (**1.105**), followed by subsequent propagation steps in the same manner. The barrier for this process was calculated to be 3.6 kcal mol^{-1}. Although a slightly higher barrier would be expected for the attack on the more bulky $H_2B{=}NMe_2$, the extremely low value illustrates that such a process could be very fast, in accordance to the experimental results presented here.



2.14b **2.15** **1.36a**

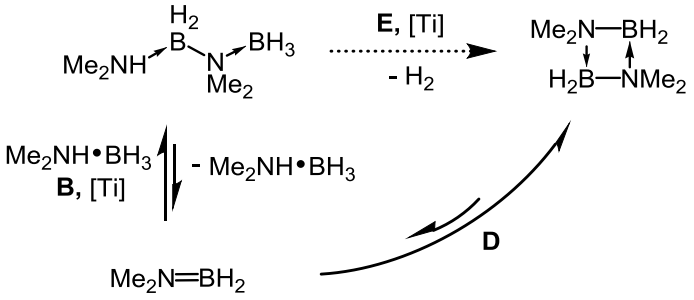
Scheme 2.15 Plausible BN coupling pathway: Terminal NMe_2 attacks previously dehydrogenated and released $Me_2N{=}BH_2$.

Analogous complexes to **2.15** have been invoked previously, such as $Cp_2Ti(\eta^2\text{-}H_3B{\cdot}NMe_2BH_2{\cdot}NHMe_2)$ (**1.91**) by Manners,[2] $Cp_2Zr(OMes)(\eta^2\text{-}H_3B{\cdot}NMe_2BH_2{\cdot}NHMe_2)]^+$ (**1.119**) by Wass,[67] and the crystallographically authenticated late-metal complexes $[Rh(P^iBu_3)_2(\eta^2\text{-}H_3B{\cdot}NMe_2BH_2{\cdot}NHMe_2)][BAr^F{}_4]$ (**1.82**) and $[Ir(H)_2(PCy)_2(\eta^2\text{-}H_3B{\cdot}NHMeBH_2{\cdot}NH_2Me)][BAr^F{}_4]$ (**1.84**) by Weller *et al.*[29,41] The terminal NMe_2 unit of **2.15** can then abstract the TiN<u>H</u> proton in an intramolecular process, reforming the catalyst **1.36a** with concomittant release of free $Me_2NH{\cdot}BH_2NMe_2{\cdot}BH_3$. This latter process is entirely analogous to the chain termination mechanism proposed in the dehydropolymerisation of $H_3N{\cdot}BH_3$ using $[Ir(H)_2(POCOP)]$ (**1.104**).[66]

Similarly, the formation of $Me_2NH{\cdot}BH_2NMe_2{\cdot}BH_3$ was previously suggested to occur *via* initial activation of amine-borane $Me_2NH{\cdot}BH_3$, followed by on-metal recombination with amino-borane $Me_2N{=}BH_2$, using Ru,[32] Rh,[36] and Ir[34] transition metal catalysts. The mechanism shown in Scheme 2.15 differs slightly from the coordination/insertion pathways invoked for the catalysed formation of B–N oligomeric/polymeric species starting from the related primary amine-boranes.[37,68]

2.3.7 Investigation of the second kinetic regime

After investigating the first kinetic regime, the second regime will be discussed in detail, in which $Me_2NH{\cdot}BH_2NMe_2{\cdot}BH_3$ is ultimately converted to $[Me_2N{=}BH_2]_2$ (Scheme 2.16).



Scheme 2.16 Dehydrocoupling reaction pathways starting from diborazane.

Catalytic conversion of $Me_2NH{\cdot}BH_2NMe_2{\cdot}BH_3$ with 0.5 mol% Cp*Ti{MeC(NMe)$_2$}(NTol) (**1.36a**) (toluene, 298 K) showed a maximum conversion of only 80%, corresponding to a TON_{MAX} of 160. The lower TON as compared to catalysis starting with $Me_2NH{\cdot}BH_3$ (measured at 273 K, TON_{MAX} = 800), is ascribed in part due to higher reaction temperatures. To avoid complications from catalyst decomposition, catalyst loadings of 21 mol% are thus employed to evaluate the reaction order in $Me_2NH{\cdot}BH_2NMe_2{\cdot}BH_3$. At this loading, quantitative ^{1}H NMR spectroscopy confirmed that >90% of catalyst is still intact after >85% conversion of $Me_2NH{\cdot}BH_2NMe_2{\cdot}BH_3$.

Both zeroth and second order plots show distinct curved lines (Figure 2.21, top-left, and bottom-left, respectively). By contrast, the first order [$Me_2NH{\cdot}BH_2NMe_2{\cdot}BH_3$] *vs* time plot features an excellent fit to a linear function (top-right), in line with being first order in $Me_2NH{\cdot}BH_2NMe_2{\cdot}BH_3$. This suggests that there is <u>one</u> dominant pathway of $Me_2NH{\cdot}BH_2NMe_2{\cdot}BH_3$ conversion, being pathways B and D (Scheme 2.16).

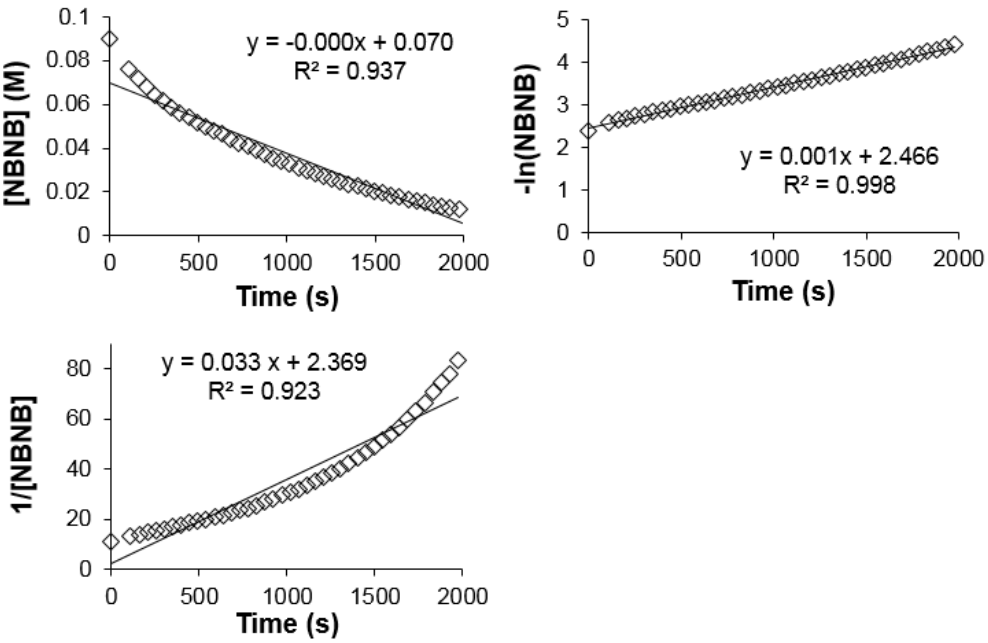


Figure 2.21 Order plots for the dehydrocoupling of $Me_2NH{\cdot}BH_2NMe_2{\cdot}BH_3$ ("NBNB", c_0 = 0.09 M, toluene, 298 K) using 21 mol% **1.36a**, and corresponding least squares fit function.

In analogy to the case using $Me_2NH{\cdot}BH_3$, we varied the catalyst loading of **1.36a** in the catalysis of $Me_2NH{\cdot}BH_2NMe_2{\cdot}BH_3$. The initial rates *vs* catalyst loading plot features an excellent fit to a linear function with a slope of *ca.* 1 (Figure 2.22). Thus, the reaction is apparently first order in **1.36a**, and first order in $Me_2NH{\cdot}BH_2NMe_2{\cdot}BH_3$.

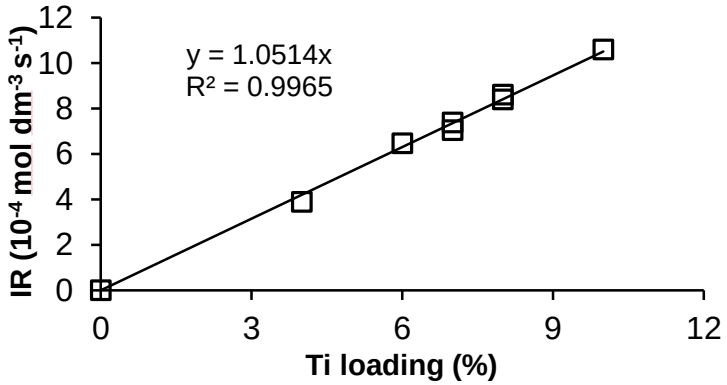


Figure 2.22 Initial rates *vs* **1.36a** catalyst loading plot. Conditions: $c_0(Me_2NH{\cdot}BH_2NMe_2{\cdot}BH_3)$ = 0.19 M, RT, toluene.

The titanium imide catalyst **1.36a** is observed throughout the catalysis using $Me_2NH{\cdot}BH_2NMe_2{\cdot}BH_3$ as substrate, and no titanium containing intermediates were found using ^{1}H NMR spectroscopy. Similarly, no adducts or intermediates were identified when the reaction was set up at -30 °C and slowly warmed in the NMR spectrometer.

Next, we synthesised a related but asymmetric diborazane, $Me_2NH{\cdot}BH_2\underline{NHMe}{\cdot}BH_3$, which was previously reported by Wass (^{11}B NMR (C_6D_6, 128.4 MHz): δ -2.4 (q, ^1J = 108 Hz, BH_2), -18.1 (q, ^1J = 93 Hz, BH_3) ppm).[67] The middle piece features a NHMe rather than a NMe_2 unit, and was used to probe a related redistribution reaction of diborazanes using a zirconium based FLP catalyst. Diffraction-quality crystals were grown from a saturated diethyl ether solution at -80 °C, and the thermal ellipsoid plot is shown in Fig 2.23 confirming the connectivity. The bond lengths and angles are comparable to those in $H_3N{\cdot}BH_2NH_2{\cdot}BH_3$.[40] Notably, $H_3N{\cdot}BH_2NH_2{\cdot}BH_3$ exhibited a *gauche* conformation in contrast to the *anti* conformation found in butane. This was attributed to the stabilisation by a weak dihydrogen bond B(2)–H(7)$\cdots$H(1)–N(1) of 2.5 Å, which is comparable to the

sum of van-der-Waals radii of 2.4 Å.[69] In our case, the "NBNB" unit also adopts a gauche conformation, and the B(2)–H(7)···H(1)–N(1) distance is shorter with 2.212(14) Å, suggesting a dihydrogen bond interaction as well.

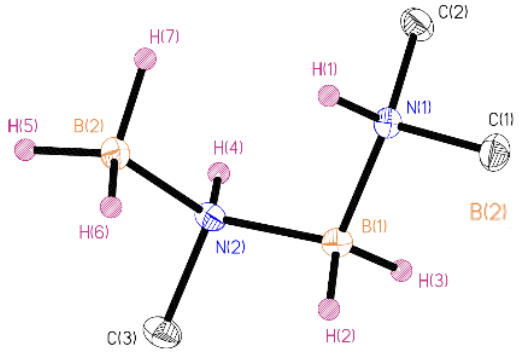


Figure 2.23 Displacement ellipsoid plot (20% probability) of $Me_2NH{\cdot}BH_2NHMe{\cdot}BH_3$. C–bound H atoms are omitted. H atoms are drawn as a sphere of arbitrary radius. Selected bond lengths (Å): N(1)–B(1), 1.5986(9); N(2)–B(1), 1.5709(9); N(2)–B(2), 1.5915(9). Selected bond angles (°): N(1)–B(1)–N(2), 109.98(5); B(1)–N(2)–B(2), 115.31(5); B(2)–H(7)···H(1)–N(1), 2.212(14).

When Cp*Ti{MeC(NMe)$_2$}(NTol) (**1.36a**) was subjected to a solution of $Me_2NH{\cdot}BH_2NHMe{\cdot}BH_3$, we found strong evidence for a redistribution reaction, in analogy to $Me_2NH{\cdot}BH_2NMe_2{\cdot}BH_3$. In particular, $Me_2NH{\cdot}BH_3$ was detected after 3 min (Figure 2.24). Additionally, although direct detection of $MeHN{=}BH_2$ is impossible under the chosen reaction conditions,[70] the detection of $[MeN{-}BH]_3$ ($^{11}B(C_6D_6)$ = 33.6 ppm, $^1J_{B\text{-}H}$ = 138 Hz; Lit: $^{11}B(C_6D_6)$ = 33.2 ppm, $^1J_{B\text{-}H}$ = 132 Hz)[71] provides indirect evidence for the formation of $MeHN{=}BH_2$. $MeHN{=}BH_2$ is thought to trimerise to initially form $[MeHN{-}BH_2]_3$, and subsequently dehydrogenates to ultimately form $[MeN{-}BH]_3$.[37]

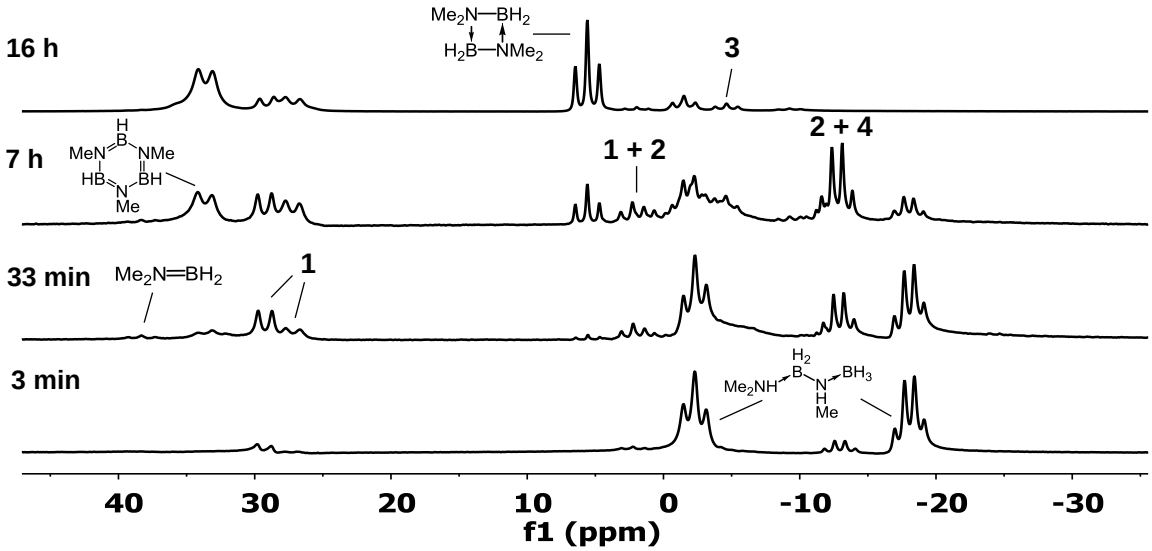
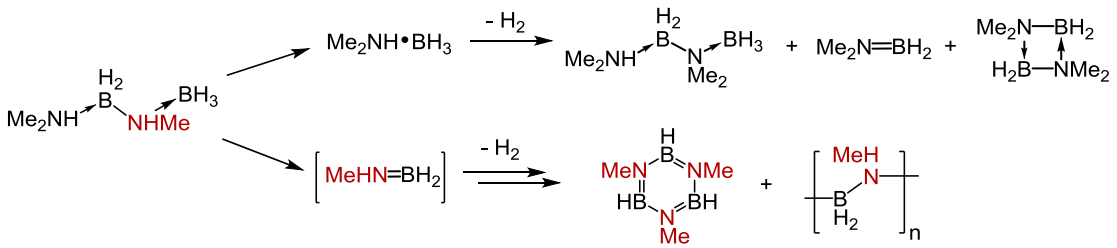


Figure 2.24 Stacked ^{11}B NMR spectra (128 MHz, 298 K, C_6D_6) of the reaction between $Me_2NH{\cdot}BH_2NHMe{\cdot}BH_3$ (c_0 = 0.19 M) with 21 mol% **1.36a**. 1 = asymmetric borazines and/or {HB–NMe–$(H_2BNMe)_2$} and {$(HBNMe)_2$–H_2BNMe}, 2 = $Me_2NH{\cdot}BH_2NMe_2{\cdot}BH_3$, 3 = oligomeric $[MeNH–BH]_n$, 4 = $Me_2NH{\cdot}BH_3$.

Overall, the spectroscopic data suggests that $Me_2NH{\cdot}BH_2NHMe{\cdot}BH_3$ is converted into $Me_2NH{\cdot}BH_3$ as well as $MeHN{=}BH_2$, which react further as outlined in Scheme 2.16. This redistribution gives further support for the reaction using the symmetric $Me_2NH{\cdot}BH_2NMe_2{\cdot}BH_3$ diborazane. As discussed previously, significant amounts of $Me_2NH{\cdot}BH_3$ as well as $Me_2N{=}BH_2$ are detected, giving direct evidence for a redistribution reaction (pathway B, Scheme 2.16), rather than a dehydrocyclisation to form $[Me_2N{=}BH_2]_2$ (pathway E).

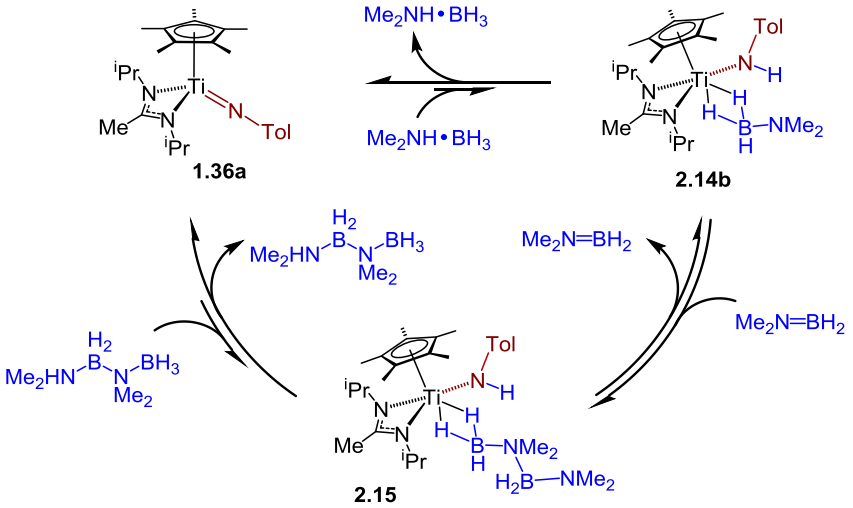


Scheme 2.16 Proposed reaction pathway of the catalytic conversion of $Me_2NH{\cdot}BH_2NHMe{\cdot}BH_3$ using **1.36a**.

As discussed previously, $Me_2NH{\cdot}BH_2NMe_2{\cdot}BH_3$ is most likely formed from a catalysed recombination of $Me_2NH{\cdot}BH_3$ as well as $Me_2N{=}BH_2$ during the first kinetic regime. Subsequently, $Me_2NH{\cdot}BH_2NMe_2{\cdot}BH_3$ is converted into the same two molecules. This

implies the presence of reversible equilibria which are controlled by the relative rates and concentrations of the involved processes and species. Related observations were previously made in a rhodium catalysed dehydrocoupling of $Me_2NH{\cdot}BH_3$.[36]

Importantly, if the mechanism for the forward reaction starting from $Me_2NH{\cdot}BH_3$ and $Me_2N{=}BH_2$ to form $Me_2NH{\cdot}BH_2NMe_2{\cdot}BH_3$ is known, the principle of microreversibility demands that the backward reaction follows the same reaction mechanism to reform the starting materials. Previously, we hypothesised a plausible mechanism for the forward reaction pathway, that is, nucleophilic attack of a metal-bound "$Me_2NH{\cdot}BH_3$" species **2.14b** to a free $Me_2N{=}BH_2$, which subsequent to proton transfer forms free $Me_2NH{\cdot}BH_2NMe_2{\cdot}BH_3$ (Scheme 2.17). If this pathway is indeed taking place in the forward reaction, the principle of microreversibility demands that the reverse reaction must undergo the same reaction mechanism (Scheme 2.17).



Scheme 2.17 Forward and backward BN coupling reaction.

To test this hypothesis, the kinetic isotope effects of the selectively labelled analogues of $Me_2NH{\cdot}BH_2NMe_2{\cdot}BH_3$ were measured, as summarised in Table 2.6. There is no distinct KIE for B–H/D bonds, while a KIE of 2.2-2.4 is measured for N–H bond cleavage, suggesting N–H bond cleavage to be rate determining. These results are fully in line with

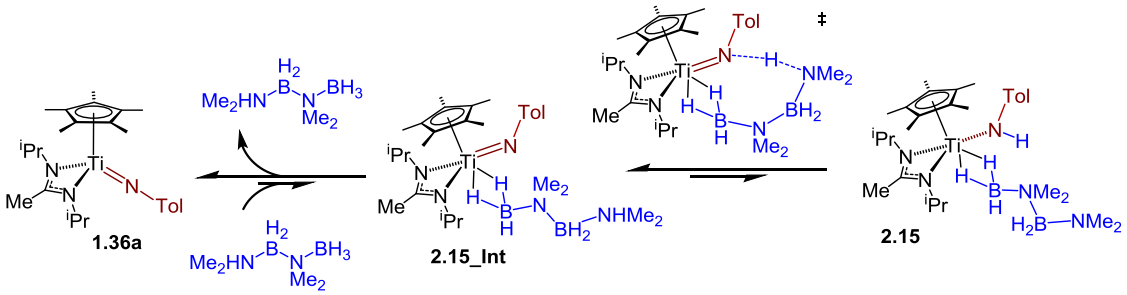
the proposed mechanism shown in Scheme 2.17, in which the reaction of **1.36a** with $Me_2NH{\cdot}BH_2NMe_2{\cdot}BH_3$ forms the titanium amide compound Cp*Ti{MeC(NMe)$_2$}(NHTol)(η^2-H_3B-$NMe_2BH_2{\cdot}NMe_2$) (**2.15**) *via* N–H bond activation. This step is thus likely rate-limiting.

Table 2.6 Kinetic isotope effects for the reaction of substrate (c_0=0.19 M, 298 K, toluene) using 7% catalyst loading (**1.36a**). KIE denotes kinetic isotope effect.

Substrate	**Initial rate (10^{-4} mol dm^{-3} s^{-1})**	**KIE**
$Me_2NH{\cdot}BH_2NMe_2{\cdot}BH_3$	2.4 (1)*	-
$Me_2N\underline{D}{\cdot}BH_2NMe_2{\cdot}BH_3$	1.0 (1) and 1.1 (1)	2.2 – 2.4
$Me_2NH{\cdot}BD_2NMe_2{\cdot}B\underline{D}_3$	2.2 (1) and 2.3 (1)	1.0 – 1.1
$Me_2N\underline{D}{\cdot}B\underline{D}_2NMe_2{\cdot}B\underline{D}_3$	1.1 (1) and 1.3 (1)	1.8 – 2.2

*Average value for two runs.

While there is no distinct B–H/D KIE using $Me_2NH{\cdot}BH_2NMe_2{\cdot}BH_3$, the previously discussed $Me_2NH{\cdot}BH_3$ featured a KIE for B–H/D bonds of 1.3-1.4. This difference is in further support for the latter KIE arising from a rate-determining, concerted N–H/B–H bond activation mechanism. If the latter represented an equilibrium isotope effect, we would expect comparable KIE values for B–H/D bonds for both $Me_2NH{\cdot}BH_2NMe_2{\cdot}BH_3$ and $Me_2NH{\cdot}BH_3$. This is because both substrates form closely related σ-complexes, **2.15** and **2.14b** (Scheme 2.17), featuring Ti–H–B 3-centre 2-electron interactions which are in equilibrium with Cp*Ti{MeC(NMe)$_2$}(NTol) (**1.36a**). In the case of $Me_2NH{\cdot}BH_2NMe_2{\cdot}BH_3$, a concerted N–H/B–H bond activation is less likely since it would require an 8-membered transition state. Instead, we favour a step-wise mechanism in which there is pre-coordination of the BH_3 moiety to the metal centre (**2.15_Int**, Scheme 2.18), followed by rate-determining N–H bond transfer accounting for the observed KIE values (or *vice versa*).



Scheme 2.18 Plausible step-wise mechanism and transition state for the activation of $Me_2NH{\cdot}BH_2NMe_2{\cdot}BH_3$ with Cp*Ti{MeC(NMe)$_2$}(NTol) (**1.36a**).

To investigate the rate-determining step further, the electronic properties of the employed catalysts were varied using titanium imides **1.36a-1.36f**. The corresponding initial rates and Hammett parameters σ_p are summarised in Table 2.6, and the Hammett plot is shown in Figure 2.25.

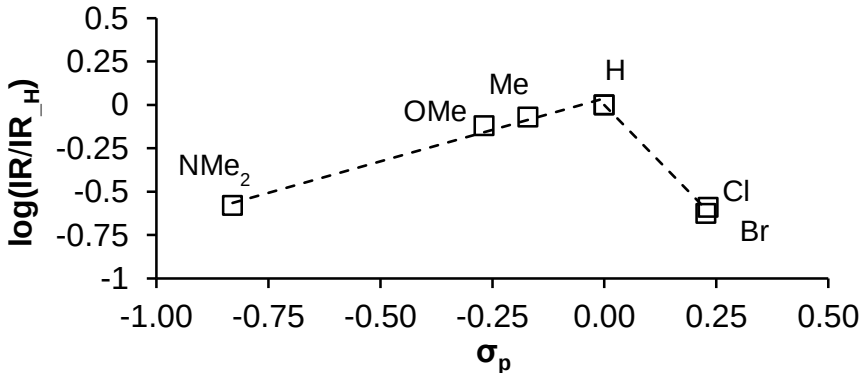


Figure 2.25 Hammett plot log(IR/IR_H) *vs* σ_p in the reaction of $Me_2NH{\cdot}BH_2NMe_2{\cdot}BH_3$ (c_0=0.19 M, toluene, 298 K) and 7% Cp*Ti{MeC(NMe)$_2$}(NAr), Ar = Tol (**1.36a**), Ar^{NMe_2} (**1.36b**), Ar^{OMe} (**1.36c**), Ph (**1.36d**), Ar^{Cl} (**1.36e**), Ar^{Br} (**1.36f**). IR = Initial rate, IR_H = Initial rate using **1.36d**.

Table 2.6 Initial rates and Hammett parameters σ_p corresponding to the dehydrocoupling catalytic with $Me_2NH{\cdot}BH_2NMe_2{\cdot}BH_3$ (c_0 = 0.19 M, toluene, 298 K) and 7% Cp*Ti{MeC(NMe)$_2$}(N–4–C_6H_4X) (**1.36a-1.36f**).

X	σ_p	Initial rate (10^{-5} mol dm^{-3} s^{-1})*
NMe_2	-0.83	7.4
OMe	-0.27	21
Me	-0.17	23
H	0	28
Cl	0.227	12
Br	0.232	8

*All runs are duplicates.

The Hammett plot broadly parallels the one discussed using $Me_2NH{\cdot}BH_3$ as substrate. Moving from the most electron donating aryl group Ar^{NMe_2} to Ph, the initial rates increase from 7.4 to 28 x 10^{-5} mol dm^{-3} s^{-1}. There is a good least squares fit to a linear function (R^2 = 0.984), suggesting the involvement of the titanium imide moiety during catalysis. When the more electron-withdrawing aryl imides Ar^{Cl} and Ar^{Br} the initial rate decreased to 12 and 8 x 10^{-5} mol dm^{-3} s^{-1}, respectively.

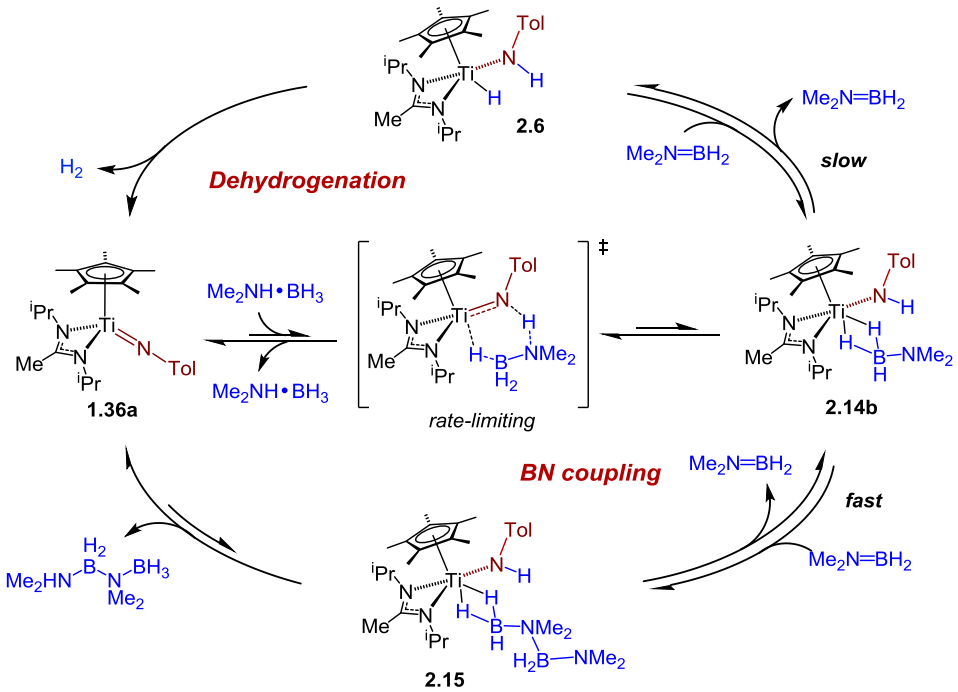
The concave downward shape of the Hammett line is indicative of a single operating reaction mechanism, in which the nature of the rate-determining step is changed. This was further supported by measuring the KIE values on the extrema of the Hammett σ-scale. Catalysts Cp*Ti{MeC(NMe)$_2$}(NAr^{NMe_2}) (**1.36b**), and Cp*Ti{MeC(NMe)$_2$}(NAr^{Br}) (**1.36f**) featured combined N–H/D and B–H/D kinetic isotope effects 2.1(1) and 1.9(1), respectively. These values are comparable to the value obtained for Cp*Ti{MeC(NMe)$_2$}(NTol) (**1.36a**, 1.8-2.2), suggesting only a small change of the rate determining step overall.

Finally, we tested the influence of H_2 build-up during catalysis. When the reaction was scaled up with a strong flow of N_2 gas in an open system with vigorous stirring, no difference was observed to the (closed) NMR tube scale reactions. Thus, there is no evidence for dihydrogen inhibiting the catalysis, the same observation as made previously when catalysis was started from $Me_2NH{\cdot}BH_3$. In fact, since $Me_2NH{\cdot}BH_2NMe_2{\cdot}BH_3$ redistributes to form $Me_2NH{\cdot}BH_3$ and $Me_2N{=}BH_2$, we would expect the same dehydrogenation mechanism to occur converting $Me_2NH{\cdot}BH_3$ to $Me_2N{=}BH_2$ and H_2. The same dependence on H_2 build-up during catalysis would thus be expected and is in line with the proposed mechanism.

2.3.8 Proposed unified mechanistic model

To conclude, we propose the plausible mechanistic cycle shown in Scheme 2.19 which can account for the previous experimental observations. The cycle is bifunctonal: The top half represents the dehydrogenation pathway, and the bottom half represents a BN coupling pathway.

Concerted, rate-determining N–H/B–H bond activation of $Me_2NH{\cdot}BH_3$ is in line with the observed individual KIE values for both NH and BH, as well as the combined KIE which is the product of the individual KIE values. The absence of titanium containing intermediates is in agreement with this initial step being rate-determining, while the following steps are relatively faster. Concerted activation can also explain why no evidence for individual B–H or N–H bond activation was found using model substrates. It is in further agreement with a relatively large sensitivity towards increased steric bulk, and the Hammett behaviour.



Scheme 2.19 Proposed, unified mechanism of the dehydrocoupling of $Me_2NH{\cdot}BH_3$ using titanium imide catalysts.

After concerted N–H/B–H bond activation, $Me_2NH{\cdot}BH_3$ stays bound to the metal, and species Cp*Ti{$MeC(NMe)_2$}(NHTol)(η^2-H_3B-NMe_2) (**2.14b**) is proposed as likely adduct. Such an adduct is required in order to catalytically form $Me_2NH{\cdot}BH_2NMe_2{\cdot}BH_3$ and can explain the presence of two kinetic regimes (*vide infra*). From **2.14b**, there are two possible pathways. First, entering the dehydrogenation pathway, and second, entering the BN coupling cycle. In the former, **2.14b** releases $Me_2N{=}BH_2$ to form titanium hydride amide Cp*Ti(H){$MeC(NMe)_2$}(NHTol) (**2.6**) which irreversibly loses dihydrogen *via* 1,2-elimination. The invoked titanium hydride **2.6** could explain the formation of EPR active decomposition species during catalysis, and why more is observed at higher catalyst concentrations.

Alternatively, Cp*Ti{$MeC(NMe)_2$}(NHTol)(η^2-H_3B-NMe_2) (**2.14b**) reacts with previously generated $Me_2N{=}BH_2$ to form Cp*Ti{$MeC(NMe)_2$}(NHTol)(η^2-H_3B-$NMe_2BH_2{\cdot}NMe_2$) (**2.15**). This step represents the metal catalysed recombination of $Me_2NH{\cdot}BH_3$ with $Me_2N{=}BH_2$, and subsequent proton transfer forms $Me_2NH{\cdot}BH_2NMe_2{\cdot}BH_3$ as well as catalyst **1.36a**. When catalysis is started from $Me_2NH{\cdot}BH_2NMe_2{\cdot}BH_3$, $Me_2N{=}BH_2$ as well as $Me_2NH{\cdot}BH_3$ are reformed again. Thus, the lower half of the mechanism is drawn as equilibrium, in line with the principle of microreversibility. The N–H bond activation of $Me_2NH{\cdot}BH_2NMe_2{\cdot}BH_3$ to form η^2 bound "NBNB" species Cp*Ti{$MeC(NMe)_2$}(NHTol)(η^2-H_3B-$NMe_2BH_2{\cdot}NMe_2$) (**2.15**) can account for the observed KIE values.

Importantly, this model is able to explain the presence two different kinetic regimes. The first few turnovers starting from $Me_2NH{\cdot}BH_3$ as substrate will necessarily go through the dehydrogenation cycle (given the absence of $Me_2N{=}BH_2$). During this process small amounts of free $Me_2N{=}BH_2$ accummulate which can then start to react with species Cp*Ti{$MeC(NMe)_2$}(NHTol)(η^2-H_3B-NMe_2) (**2.14b**), and form $Me_2NH{\cdot}BH_2NMe_2{\cdot}BH_3$

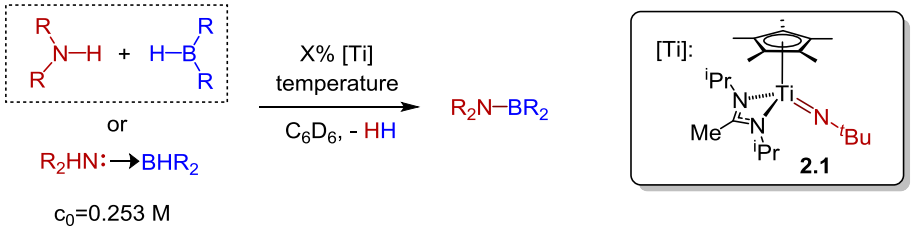
following the BN coupling pathway. This reaction is proposed to be fast since near-quantitative amounts of the linear dimer are formed during the first kinetic regime. When the overall reaction concentration lowered, there is relatively more free $Me_2N{=}BH_2$ detected (compared to $Me_2NH{\cdot}BH_2NMe_2{\cdot}BH_3$). This is in full agreement with the model discussed since loss of $Me_2N{=}BH_2$ from **2.14b** is unimolecular, while the BN coupling reaction between **2.14b** and free $Me_2N{=}BH_2$ is bimolecular, and thus strongly dependent on the overall concentration.

After $Me_2NH{\cdot}BH_3$ is converted to near quantitative amounts of $Me_2NH{\cdot}BH_2NMe_2{\cdot}BH_3$ the second, slower kinetic regime starts. The catalyst **1.36a** is shown to react slower with $Me_2NH{\cdot}BH_2NMe_2{\cdot}BH_3$ than with $Me_2NH{\cdot}BH_3$. Higher concentrations of the diborazane favour its reaction with catalyst **1.36a** to form $Cp^*Ti\{MeC(NMe)_2\}(NHTol)(\eta^2\text{-}H_3B\text{-}NMe_2)$ (**2.14b**) with concomittant release of $Me_2N{=}BH_2$. From compound **2.14b**, the bound $Me_2NH{\cdot}BH_3$ can be dehydrogenated under release of a second equivalent of $Me_2N{=}BH_2$. Alternatively, **2.14b** can react to reform catalyst **1.36a** as well as $Me_2NH{\cdot}BH_3$, explaining its formation starting the catalysis from $Me_2NH{\cdot}BH_2NMe_2{\cdot}BH_3$. As more molecules are irreversibly dehydrogenated to form $Me_2N{=}BH_2$ during the second kinetic regime, this species accummulates to a greater extent, and slowly dimerises in an off-metal process.

In summary, the proposed mechanistic model can explain the various experimental observations, including the presence of two kinetic distinct regimes. The relative concentrations of the involved species, and relative reaction rates of the various processes then explain the observed concentration-time profiles and kinetic regimes.

2.4 Scope: Dehydrocoupling of amines and boranes and amine-boranes

The synthetic value of the dehydrocoupling catalyst Cp*Ti{MeC(NMe)$_2$}(N^{t}Bu) (**2.1**) was explored further. Therefore, a variety of differently substituted amines and boranes were tested in analogy to Table 2.2, including substrate pairs that do not form amine-borane adducts in solution (Scheme 2.20). The reactions were followed by ^{1}H and ^{11}B NMR spectroscopy and Table 2.7 shows the required reaction conditions on the NMR tube scale, along with the results previously obtained in Table 2.2 for reference (entries 12-16).



Scheme 2.20 Dehydrocoupling of different amines (R = H, alkyl, aryl) with boranes (R = H, alkyl, boryl) catalysed by Cp*Ti{MeC(NMe)$_2$}(N^{t}Bu) (**2.1**).

Amines and boranes often form adducts, amine-boranes, by the coordination of the nitrogen based lonepair into the empty boron based p-orbital. Wherever formed, coupling reactions started from the corresponding adducts. In the cases of HBPin (entries 1-5), no such amine-boranes are formed which can be rationalised by the two oxygen atoms donating their lonepairs into the boron based p-orbital, making it less electrophilic. In the case of Ph$_2$NH (entry 6), there was also no formation of an adduct in benzene at RT, presumably due to the conjugation of the nitrogen based lonepair with the neighbouring phenyl systems.[72] Finally, for the substrate pair Cy$_2$NH and 9-BBN an equilibrium between free substrates, and amine-borane adduct was formed (^{11}B NMR, K_{eq} (298 K, C_6D_6) = 1.2 M^{-1}). This is due to steric effects and was studied previously by Brown.[73] While Et$_2$NH·9-BBN was reported to be formed quantitatively in cyclohexane, the slightly bulkier substrate pair ^{i}Pr$_2$NH/9-BBN formed an equilibrium (K_{eq} (298 K, cyclohexane) = 10 M^{-1}) as found for to the Cy$_2$NH/9-BBN pair.[73]

Table 2.7 Amines and boranes tested in the dehydrocoupling catalysed by **2.1**, the corresponding temperature, catalyst loading, and time to conversion of the substrate starting materials.

Entry	Substrates	Temp	[Ti] loading (mol%)	Time (h)	Conversion (%)[d]	Conversion (no [Ti], %)[d]
1	Ph_2NH + HBPin [a]	60 °C	30	48	> 99	30
2	$C_5H_{10}NH$ + HBPin [a]	60 °C	10	12	> 99	40
3	Et_2NH + HBPin [a]	60 °C	20	16	> 99	50
4	$^tBuNH_2$ + HBPin [a]	RT	10	<1	> 99	10
5	Cy_2NH + HBPin [a]	60 °C	10	-	0	0
6	Ph_2NH + 9-BBN [a]	60 °C	30	48	> 99	30
7	$C_5H_{10}NH$·9-BBN [b]	RT	10	12	> 99	0
8	Et_2NH·9-BBN [b]	RT	10	96	> 99	5
9	Cy_2NH + 9-BBN [c]	60 °C	10	-	0	0
10	$^tBuNH_2$·9-BBN [b]	RT	10	<1	> 99	0
11	$C_5H_{10}NH$·H_2BTex [b]	60 °C	10	48	> 99	0
12	NH_3·BH_3 [b]	RT	10	<0.16	> 99	0
13	$^tBuNH_2$·BH_3 [b]	RT	10	2	> 99	0
14	$MeNH_2$·BH_3 [b]	RT	10	<0.16	> 99	0
15	Me_2NH·BH_3 [b]	RT	10	<0.16	> 99	0
16	$^iPr_2NH$·BH_3 [b]	60 °C	10	24	> 99	0

All reactions were carried out in a J-Young NMR tube under nitrogen atmosphere. [a] These amines and boranes were premixed and no adduct formation was observed. [b] Quantitative adduct formation observed. [c] Equilibrium between free substrates, and amine-borane adduct observed [d] Conversion measured by $^{11}B\{^1H\}$ NMR.

In the cases where pinacolborane was the borane (entries 1-5) relatively harsh reaction conditions at 60 °C were needed to drive the reaction (and Cy_2NH + HBPin (entry 5) showed no coupling). The exception is $^tBuNH_2$ + HBPin (entry 4) which coupled readily at RT. However, for entries 1-4 as well as 6, significant dehydrocoupling in the absence of any catalyst was observed under the otherwise same conditions.

Compared to the forcing reaction conditions required for the aromatic amine Ph_2NH, a variety of seconday and primary amines could be catalytically coupled with 9-BBN and texylborane under relatively milder conditions (entries 7-11). An exception is the Cy_2NH/9-BBN pair (entry 9), which resisted dehydrocupling even under forcing conditions. In these cases (entries 7-11), no dehydrocoupling was observed in the absence of titanium catalyst. In principle, the presence of two NH or BH moieties allows for two consecutive

dehydrocoupling events, forming disubstituted aminoborane products for entries 4, 10 and 11. However, exclusive monosubstitution is observed, presumably due to the increased bulk after the first dehydrocoupling event (addition of a second equivalent of borane or amine did not lead to a second dehydrocoupling reaction).

Reactions involving the parent borane BH_3 are the most rapid (entries 12-16), and were discussed previously. In summary, these coupling reactions point to a few general trends. First, steric bulk requires harsher reaction conditions (as can be seen by comparing entry 15 and 16). Secondly, in the cases where there is no quantitative formation of amine-borane adducts, relatively harsher reaction conditions were required and highlights the importance of pre-assembly.

The presented substrate screen highlights that the dehydrocoupling protocol using catalyst **2.1** is not synthetically useful for HBPin since latent thermal reactivity achieved comparably high conversions under the same reaction conditions.[20] However, couplings using alkyl boranes and BH_3 proved to be efficient, and could couple a variety of differently substituted amine-boranes under mild conditions. For reference, primary and secondary amine-borane adduct generally require heating >100 °C to undergo thermally induced dehydrocoupling.[20]

2.5 Summary and outlook

A novel family of titanium imide catalysts for the dehydrocoupling of amine-boranes is presented. We explored the scope and showed that a variety of differently substituted amines and boranes can be coupled efficiently. Titanium *tert*-butyl imide Cp*Ti{MeC(NMe)$_2$}(N^{t}Bu) (**2.1**) featured a TOF$_{90\%}$ of 1600 h^{-1} for the dehydrocoupling of dimethylamineborane, the fastest group 4 catalyst to date.

Subsequently, a detailed mechanistic study in the dehydrocoupling of dimethylamineborane was presented using the related aryl imide catalysts Cp*Ti{MeC(NMe)$_2$}(NAr) (**1.36a-f**). A variety of tests indicated that the catalysis is homogeneous, and involves a constant oxidation state of Ti(IV) which contrasts to previously reported titanium catalysts. During catalysis, Me$_2$NH·BH$_3$ is almost quantitatively converted to Me$_2$NH·BH$_2$NMe$_2$·BH$_3$ in a first, rapid kinetic regime. This allowed the development of a useful, multigram synthetic method for this molecule, as well as the previously unknown, selectively labelled isotopologues Me$_2$N(H/D)·B(H/D)$_2$NMe$_2$·B(H/D)$_3$. Since diborazanes are key intermediates in the dehydrocoupling of primary and secondary amine-boranes, these selectively labelled molecules could provide valuable mechanistic insights for other dehydrocoupling catalysts.

A combination of a variety of kinetic studies including concentration-time plot analysis, kinetic isotope effects, the use of model substrates and of sterically and electronically tuned catalysts led to the proposal of a plausible mechanistic model: A bifunctional mechanism featuring a dehydrogenation cycle and a BN coupling cycle. After initial, concerted N–H/B–H bond activation of Me$_2$NH·BH$_3$ a titanium bound adduct Cp*Ti{MeC(NMe)$_2$}(NHTol)(η^2-H$_3$B-NMe$_2$) (**2.14b**) is formed which can enter either cycle. Release of Me$_2$N=BH$_2$ and H$_2$ reforms the initial catalyst and represents the

dehydrogenation cycle, and was found to be an irreversible process. The BN coupling cycle involves the recombination of this titanium adduct **2.14b** with free $Me_2N{=}BH_2$ to form "NBNB" bound adduct **2.15** which can undergo proton transfer to release $Me_2NH{\cdot}BH_2NMe_2{\cdot}BH_3$. This cycle is proposed to be reversible. Finally, accummulated $Me_2N{=}BH_2$ can dimerise to give the final product $[Me_2N{=}BH_2]_2$ in an off-metal process.

After investigating the dehydrocoupling mechanism of $Me_2NH{\cdot}BH_3$, the next logic step is the application of the insights gained here and explore the mechanism of the closely related primary amine-boranes $RNH_2{\cdot}BH_3$ as well as $NH_3{\cdot}BH_3$. The presented catalyst system was already shown to dehydrocouple both of these substrate classes efficiently. A detailed mechanistic understanding of the dehydropolymerisation might enable rational tuning the properties of the resulting inorganic oligomeric and polymeric materials.

2.6 References

1 T. J. Clark, C. A. Russell and Ian Manners, *J. Am. Chem. Soc.*, 2006, **128**, 9582–9583.

2 M. E. Sloan, A. Staubitz, T. J. Clark, C. A. Russell, G. C. Lloyd-Jones and I. Manners, *J. Am. Chem. Soc.*, 2010, **132**, 3831–3841.

3 H. Helten, B. Dutta, J. R. Vance, M. E. Sloan, M. F. Haddow, S. Sproules, D. Collison, G. R. Whittell, G. C. Lloyd-Jones and I. Manners, *Angew. Chem. Int. Ed.*, 2013, **52**, 437–440.

4 T. Jurca, T. Dellermann, N. E. Stubbs, D. A. Resendiz-Lara, G. R. Whittell and I. Manners, *J. Am. Chem. Soc*, 2018, **9**, 3360–3366.

5 D. Pun, E. Lobkovsky and P. J. Chirik, *Chem. Commun.*, 2007, **0**, 3297–3299.

6 T. Beweries, S. Hansen, M. Kessler, M. Klahn and U. Rosenthal, *Dalton Trans.*, 2011, **40**, 7689–7692.

7 A. M. Chapman, M. F. Haddow and D. F. Wass, *J. Am. Chem. Soc.*, 2011, **133**, 8826–8829.

8 A. M. Chapman and D. F. Wass, *Dalt. Trans.*, 2012, **41**, 9067–9072.

9 M. Klahn, D. Hollmann, A. Spannenberg, A. Brückner and T. Beweries, *Dalt. Trans.*, 2015, **44**, 12103–12111.

10 H. A. Kalviri, F. Artner, G. Ye, I. Korobkov and R. T. Baker, *Chem. Sci.*, 2015, **6**, 618–624.

11 K. A. Erickson, J. P. W. Stelmach, N. T. Mucha and R. Waterman, *Organometallics*, 2015, **34**, 4693–4699.

12 O. J. Metters, S. R. Flynn, C. K. Dowds, H. A. Sparkes, I. Manners and D. F. Wass,

ACS Catal., 2016, **6**, 6601–6611.
13 A. M. Chapman, M. F. Haddow and D. F. Wass, *J. Am. Chem. Soc.*, 2011, **133**, 8826–8829.
14 A. E. Guiducci, C. L. Boyd, E. Clot and P. Mountford, *Dalton Trans.*, 2009, 5960–5979.
15 D. Fletcher, R. McMeeking and D. Parkin, *J Chem Inf Comput Sci*, 1996, **36**, 746–749.
16 C. A. Jaska, K. Temple, A. J. Lough and I. Manners, *J. Am. Chem. Soc.*, 2003, **125**, 9424–9434.
17 M. Roselló-Merino, R. J. Rama, J. Dí Ez and S. Conejero, *Chem. Commun.*, 2016, **52**, 8389–8392.
18 M. E. Sloan, A. Staubitz, T. J. Clark, C. A. Russell, G. C. Lloyd-Jones and I. Manners, *J. Am. Chem. Soc.*, 2010, **132**, 3831–3841.
19 N. T. Coles, M. F. Mahon and R. L. Webster, *Organometallics*, 2017, **36**, 2262–2268.
20 K. Niedenzu and J. W. Dawson, *Boron-Nitrogen Compounds*, Springer Berlin Heidelberg, 1965.
21 J. A. Widegren and R. G. Finke, *J. Mol. Catal. A Chem.*, 2003, **198**, 317–341.
22 Jason A. Widegren, Martin A. Bennett and R. G. Finke, *J. Am. Chem. Soc*, 2003, **125**, 10301–10310.
23 D. J. Wolstenholme, K. T. Traboulsee, A. Decken and G. S. Mcgrady, *Organometallics*, 2010, **29**, 5769–5772.
24 D. R. M. And and D. G. Nocera, *Inorg. Chem.*, 2003, **42**, 4431–4436.
25 B. Cordero, V. Gómez, A. E. Platero-Prats, M. Revés, J. Echeverría, E. Cremades, F. Barragán and S. Alvarez, *Dalt. Trans.*, 2008, **0**, 2832.
26 S. C. W. C. R. Groom, I. J. Bruno, M. P. Lightfoot, *Acta Cryst*, 2016, **B72**, 171–179.
27 J. C. Green, M. L. H. Green and G. Parkin, *Chem. Commun.*, 2012, **48**, 11481.
28 M. S. Hill, M. Hodgson, D. J. Liptrot and M. F. Mahon, *Dalt. Trans.*, 2011, **40**, 7783.
29 T. M. Douglas, A. B. Chaplin, A. S. Weller, X. Yang and M. B. Hall, *J. Am. Chem. Soc.*, 2009, **131**, 15440–15456.
30 P. Bellham, M. S. Hill, G. Kociok-Köhn and D. J. Liptrot, *Chem. Commun.*, 2013, **49**, 1960.
31 A. P. M. Robertson, E. M. Leitao, T. Jurca, M. F. Haddow, H. Helten, G. C. Lloyd-Jones and I. Manners, *J. Am. Chem. Soc.*, 2013, **135**, 12670–12683.
32 A. Friedrich, M. Drees and S. Schneider, *Chem. Eur. J*, 2009, **15**, 10339–10342.
33 P. M. Zimmerman, A. Paul, Z. Zhang and C. B. Musgrave, *Inorg. Chem.*, 2009, **48**, 1069–1081.
34 C. J. Stevens, R. Dallanegra, A. B. Chaplin, A. S. Weller, S. A. Macgregor, B. Ward, D. McKay, G. Alcaraz and S. Sabo-Etienne, *Chem. - A Eur. J.*, 2011, **17**, 3011–3020.
35 H. Nöth and H. Vahrenkamp, *Chem. Ber.*, 1967, **100**, 3353–3362.
36 L. J. Sewell, G. C. Lloyd-Jones and A. S. Weller, *J. Am. Chem. Soc.*, 2012, **134**, 3598–3610.
37 H. C. Johnson, T. N. Hooper and A. S. Weller, 2015, pp. 153–220.
38 A. Antiñolo, F. Carrillo-Hermosilla, R. Fernández-Galán, M. P. Montero-Rama, A. Ramos, E. Villaseñor, R. S. Rojas and A. Rodríguez-Diéguez, *Dalt. Trans.*, 2016, **45**, 15350–15363.
39 G. A. Hahn and R. Schaeffer, *J. Am. Chem. Soc.*, 1964, **86**, 1503–1504.
40 X. Chen, J.-C. Zhao and S. G. Shore, *J. Am. Chem. Soc.*, 2010, **132**, 10658–10659.
41 H. C. Johnson, A. P. M. Robertson, A. B. Chaplin, L. J. Sewell, A. L. Thompson, M. F. Haddow, I. Manners and A. S. Weller, *J. Am. Chem. Soc*, 2011, **133**, 11076–

11079.
42 A. Shamiri, M. Chakrabarti, S. Jahan, M. Hussain, W. Kaminsky, P. Aravind and W. Yehye, *Materials (Basel).*, 2014, **7**, 5069–5108.
43 J. F. Harrod, *Coord. Chem. Rev.*, 2000, 493–531.
44 J. M. Fischer, W. E. Piers, S. D. P. Batchilder and M. J. Zaworotko, .
45 C. C. Cummins, C. P. Schaller, G. D. Van Duyne, P. T. Wolczanski, A. W. E. Chan and R. Hoffmann, *J. Am. Chem. Soc.*, 1991, **113**, 2985–2994.
46 J. L. Bennett and P. T. Wolczanski, *J. Am. Chem. Soc*, 1997, **119**, 10696–10719.
47 J. Robert E. Blake, D. M. Antonelli, L. M. Henling, W. P. Schaefer, K. I. Hardcastle and John E. Bercaw, *Organometallics*, 1998, **17**, 718–725.
48 H. Nöth and S. Thomas, *Eur. J. Inorg. Chem.*, 1999, **1999**, 1373–1379.
49 L. C. Stevenson, DPhil Thesis, University of Oxford, 2015.
50 P. E. Collier, S. C. Dunn, P. Mountford, O. V Shishkin and D. Swallow, *Dalton Trans.*, 1995, **0**, 3743–3745.
51 S. Mellino, L. C. Stevenson, E. Clot and P. Mountford, *Organometallics*, 2017, **36**, 3329–3342.
52 C. A. Sandoval, T. Ohkuma, K. Muñ and R. Noyori, *J. Am. Chem. Soc*, 2003, **125**, 13490–13503.
53 N. Blaquiere, S. Diallo-Garcia, S. I. Gorelsky, D. A. Black and K. Fagnou, *J. Am. Chem. Soc.*, 2008, **130**, 14034–14035.
54 A. N. Marziale, A. Friedrich, I. Klopsch, M. Drees, V. R. Celinski, J. Schmedt auf der Günne and S. Schneider, *J. Am. Chem. Soc.*, 2013, **135**, 13342–13355.
55 J. A. Jensen and G. S. Girolami, *J. Chem. Soc. Chem. Commun.*, 1986, **0**, 1160.
56 J. A. Jensen, S. R. Wilson and G. S. Girolami, *J. Am. Chem. Soc.*, 1988, **110**, 4977–4982.
57 L. Scoles and S. Gambarotta, *Inorganica Chim. Acta*, 1995, **235**, 375–380.
58 D. G. Dick, J. J. H. Edema, R. Duchateau and S. Gambarotta, *Inorg. Chem.*, 1993, **32**, 1959–1962.
59 R. A. M. O'Ferrall, *J. Chem. Soc. B Phys. Org.*, 1970, 785.
60 G. Parkin, *Acc. Chem. Res.*, 2009, **42**, 315–325.
61 C. Hansch, A. Leo and R. W. Taft, *Chem. Rev.*, 1991, **91**, 165–195.
62 H. H. Jaffe, *Chem. Rev.*, 1953, **53**, 191–261.
63 B. M. Anderson and W. P. Jencks, *J. Am. Chem. Soc.*, 1960, **82**, 1773–1777.
64 S. Bajo, G. Laidlaw, A. R. Kennedy, S. Sproules and D. J. Nelson, *Organometallics*, 2017, **36**, 1662–1672.
65 Aldo E. Guiducci, A. Catherine L. Boyd and P. Mountford, *Organometallics*, 2006, **25**, 1167–1187.
66 S. Bhunya, T. Malakar and A. Paul, *Chem. Commun.*, 2014, **50**, 5919.
67 O. J. Metters, S. R. Flynn, C. K. Dowds, H. A. Sparkes, I. Manners and D. F. Wass, *ACS Catal.*, 2016, **6**, 6601–6611.
68 H. C. Johnson, E. M. Leitao, G. R. Whittell, I. Manners, G. C. Lloyd-Jones and A. S. Weller, *J. Am. Chem. Soc.*, 2014, **136**, 9078–9093.
69 S. S. Batsanov, *Inorg. Mater.*, 2001, **37**, 871–885.
70 O. J. Metters, A. M. Chapman, A. P. M. Robertson, C. H. Woodall, P. J. Gates, D. F. Wass and I. Manners, *Chem. Commun.*, 2014, **50**, 12146–12149.
71 C. A. Jaska, K. Temple, A. J. Lough and I. Manners, *Chem. Commun.*, 2001, 962
72 C. Camacho, M. A. Paz-Sandoval and R. Contreras, *Polyhedron*, 1986, **5**, 1723–1732.
73 H. C. Brown and G. G. Pai Richard B, *J. Org. Chem*, 1981, **46**, 4713–4716.

Chapter Three

Reactivity of the titanium borylimide complex Cp*Ti(HPP){NB(NDippCH)$_2$} with alkynes, heterocumulenes and carbonyls

3.1 Overview

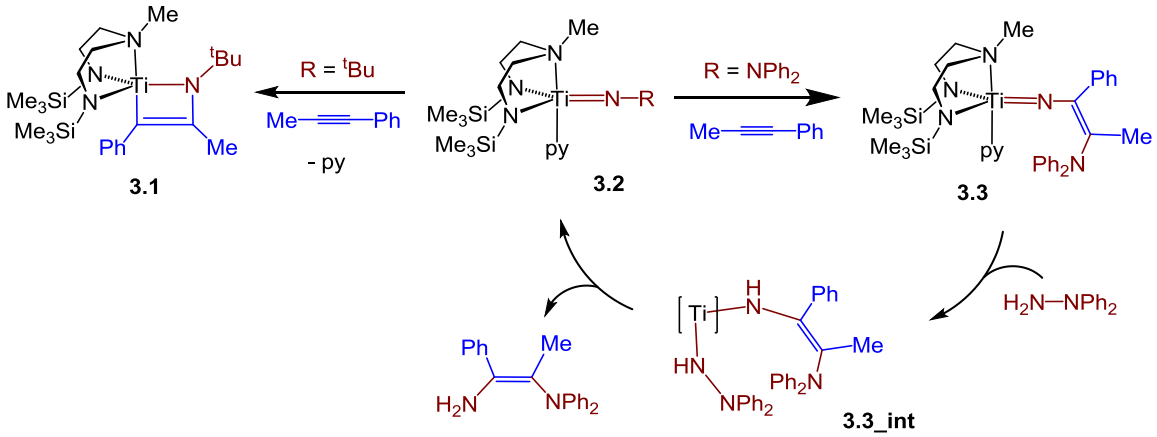
This Chapter describes the reactivity of a representative borylimido complex, namely Cp*Ti(HPP){NB(NDippCH)$_2$} (**1.83**), with a variety of small unsaturated substrates. To begin, the chemistry with a variety of terminal and internal alkynes will be explored. Additionally, the behaviour of borylimide **1.83** will be contrasted with the structurally related alkylimido and arylimido complexes Cp*Ti(HPP)(NR), with R = ^{t}Bu (**1.83b**), and Xyl (**1.83c**), respectively. Next, [2 + 2] cycloadditions followed by cycloreversions with the heterocumulenes CO_2, and isocyanates ArNCO, as well as their heavier thio-congeners CS_2, and ArNCS will be presented. Finally, the reactivity with a variety of small organic carbonyls will be discussed, including aldehydes, ketones, esters, as well as amides.

3.2 Introduction

As introduced in Chapter One, the stoichiometric and catalytic reactions of Group 4 alkyl- and arylimido complexes (L)M=NR (L = ancillary ligand set, M = Group 4 metal, R = alkyl, or aryl group) has been explored in considerable depth in the past few decades. In contrast, the exploration of N heteroatom substituted analogues of the type (L)M=N–E(R) (E = heteroatom) is a relatively underdeveloped field – despite the potential of this substitution to have profound effects on bonding, structural and reactivity aspects compared to their alkyl- and arylimido congeners.

In particular, the incorporation of a NR_2 moiety in the β position to form transition metal hydrazide complexes of type (L)M=N_α–$N_\beta R_2$ led to the discovery of a variety of important transformations. In addition to M–N_α reactivity, it has been shown that group 4 hydrazide complexes undergo reductive N_α–N_β cleavage and insertion reactions, which sets them apart from their imido analogues. As introduced in Chapter One, CO[1] and isonitriles[2,3] were reported to induce the reductive cleavage of N_α–N_β bonds in Ti and Zr based systems.

Similarly, although titanium diamide-amine supported aryl- and alkylimido catalysts are known to react with alkynes *via* [2 + 2] cycloaddition to form metallacycles of type **3.1**,[4] it was shown that the diamide-amine supported titanium hydrazide complex **3.2** reductively inserts alkynes into the N_α–N_β bond instead (Scheme 3.1).[5] This example serves to illustrate the dramatic shift in reactivity the heteroatom substitution on the imido group can have. With the addition of H_2NNPh_2 to **3.3**, a catalytic cycle is set up, in which the vinylimido ligand is cleaved from the metal centre *via* protonolysis, and a hydrazido complex regenerated. This was the first example of this type of coupling of a hydrazine with an alkyne, and can be performed catalytically from either **3.2** or **3.3**, with the overall result being the 1,2-diamination of the alkyne, a previously unknown process.



Scheme 3.1 Reactivity shift for Ti{MeN($CH_2CH_2NSiMe_3$)$_2$}(NR)(py) (**3.2**). For R = ^{t}Bu, MeCCPh undergoes [2 + 2] cycloaddition to form metallacycle **3.1** (left). For R = NPh_2, MeCCPh undergoes reductive alkyne insertion, and with excess MeCCPh and H_2N-NPh_2 a catalytic 1,2-diamination cycle can be set up (right).

Encouraged by profound differences observed between hydrazide (L)M=N_α–$N_\beta R_2$ and imide complexes (L)M=N_α–R (R = alkyl, aryl), our group recently explored the incorporation of boryl groups in β-position, forming borylimide complexes of type (L)MNBR_2. Specifically, borylamine H_2NB(NDippCH)$_2$ was used in imide/amine exchange reactions to furnish useful titanium borylimide synthons. After subsequent ligand exchange and salt-metathesis reactions, borylimide complexes with a variety of different ligand sets, including bis-cyclopentadienyl sandwich (**3.4**) and cyclopentadienyl-

guanidinate HPP (H-HPP = 1,3,4,6,7,8-hexahydro-pyrimido[1,2-*a*]pyrimidine) half-sandwich complexes (**1.83**), were prepared (Figure 3.1).[6]

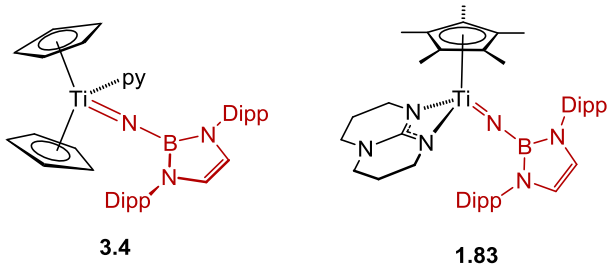


Figure 3.1 Exemplar titanium borylmido complexes formed *via* imide/borylamine exchange.

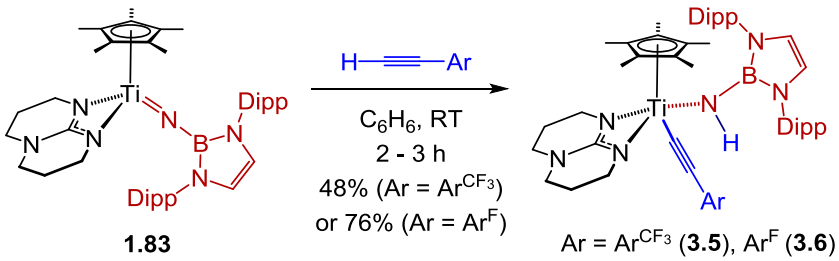
However, examples of these borylimido complexes (L)M=N-BR_2 remain rare, and the reactivity of this motif is virtually unexplored.[4] Thus, this Chapter introduces an exploratory study of the chemistry using the model titanium borylimido complex **1.83** with terminal and internal alkynes, with heterocumulenes, and a variety of small molecules featuring carbonyl groups, as well as alcohols. This ligand platform was chosen, since the cyclopentadienyl-guadinato ligand sets, and the closely related amidinato ligand sets, has proved to be a robust platform for studying and comparing the reactivity of imido, hydrazido, and alkoxyimido compounds.[7–13]

3.3 Reactions of Cp*Ti(HPP){NB(NDippCH)$_2$} with alkynes

3.3.1 Reactions with terminal alkynes

Addition of $HCCAr^F$ (Ar^F = C_6F_5) or $HCCAr^{CF_3}$ (Ar^{CF_3} = 4-$C_6H_4CF_3$) to a C_6D_6 solution of **1.83** gave immediate and quantitative formation of the C–H bond activation products, Cp*Ti(HPP){NH(B(NDippCH)$_2$)}(CCAr), Ar = Ar^{CF_3} (**3.5**), Ar^F (**3.6**), respectively (Equation 3.1). On the preparative scale, the reactions were rapidly finished at RT within less than 3 h, with immediate colour changes from brown to red being observed in both cases. The reactions proceeded cleanly, and thus the products were isolated without need

for further purification and characterised by elemental analysis, NMR and IR spectroscopy, as well as X-ray analysis.



Equation 3.1

The identification of **3.5** and **3.6** as acetylide structures, formed by C–H bond activation across the Ti=N multiple bond, was initially achieved through inspection of the respective ^{1}H, ^{11}B and ^{13}C NMR spectra (^{1}H NMR spectrum shown for **3.6** in Figure 3.2). The ^{1}H NMR spectrum of **3.6** shows a broad 1 H singlet at a high chemical shift of 7.34 ppm (the corresponding signal for **3.5** is coincident with residual protio solvent at 7.16 ppm). This signal reveals no ^{1}H-^{13}C correlations in the HSQC or HMBC spectra, and is thus assigned the NH moiety. The ^{11}B singlet resonances of 23.7 and 23.8 ppm are diagnostic for N(H)B moieties of titanium borylamides.[6] It is noteworthy that no ^{1}H signals were found at diagnostic low field shifts of ca. 11-10 ppm for methine groups, typical for titanium azametallacycles formed *via* [2 + 2] cycloaddition with terminal alkynes.[14]

The two acetylide carbons have ^{13}C resonances observed at 147.9 or 167.4 ppm for the carbon directly bonded to the metal, and 106.2 or 89.4 ppm for the carbons bonded to the aryl group, for species **3.5** or **3.6**, respectively. Noteworthy, the TiC<u>C</u> resonance for Cp*Ti(HPP){NH(B(NDippCH)$_2$)}(CCAr^F) (**3.6**) is broadened, likely arising from ^{13}C–^{19}F couplings with the perfluorinated ring.

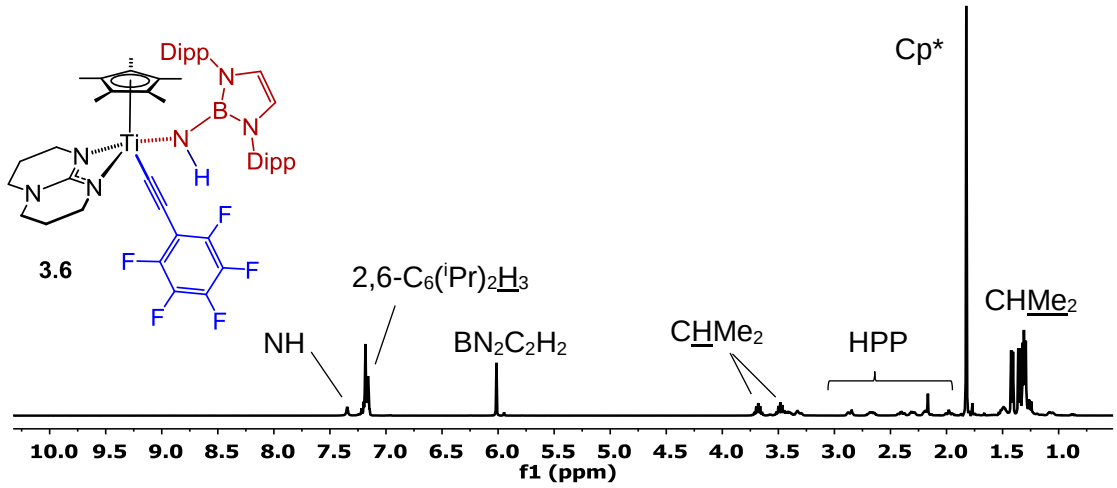


Figure 3.2 ^{1}H NMR spectrum (400.1 MHz) of Cp*Ti(HPP){NH(B(NDippCH)$_2$)}(CCAr^{F}) (**3.6**) in C_6D_6 at 298 K.

These ^{13}C shift values agree well with the corresponding signals of previously isolated titanium acetylide complexes. For example, the closely related cyclopentadienyl-2-aminopyrrolinato supported titanium acetylide complexes Cp*Ti(N^{Xyl}N)(CCAr)(NH^{t}Bu) (Ar = Ph, Tol; N^{Xyl}N = 2-(3,5-dimethylphenylamino)pyrrolinato) featured TiC resonances at 153.2 and 152.5 ppm, and TiC<u>C</u> resonances at 108.8 and 108.6 ppm, respectively.[14] Similarly, the previously isolated borylamido acetylide Ti(N$_2$N^{py}){NHB(NDippCH)$_2$}(CCAr^{F}) (**3.7**, N$_2$N^{py} = (2-C$_5$H$_4$N)CMe(CH$_2$NSiMe$_3$)$_2$) featured corresponding signals at 161.1 and 87.6 ppm, respectively.[6] Additionally, bands at 2081 (**3.5**) or 2096 cm^{-1} (**3.6**) in the IR spectrum (Nujol mull) were attributed to ν(C≡C, st.), which are consistent with Cp-supported titanium and zirconium acetylide ligand frequencies reported previously.[15–17]

Diffraction quality crystals of both **3.5** and **3.6** were successfully grown from saturated hexane solutions at RT and -30 °C, respectively. The solid state structures of **3.5** and **3.6** are shown in Figure **3.3**, and selected bond lengths and angles are given in Table 3.1.

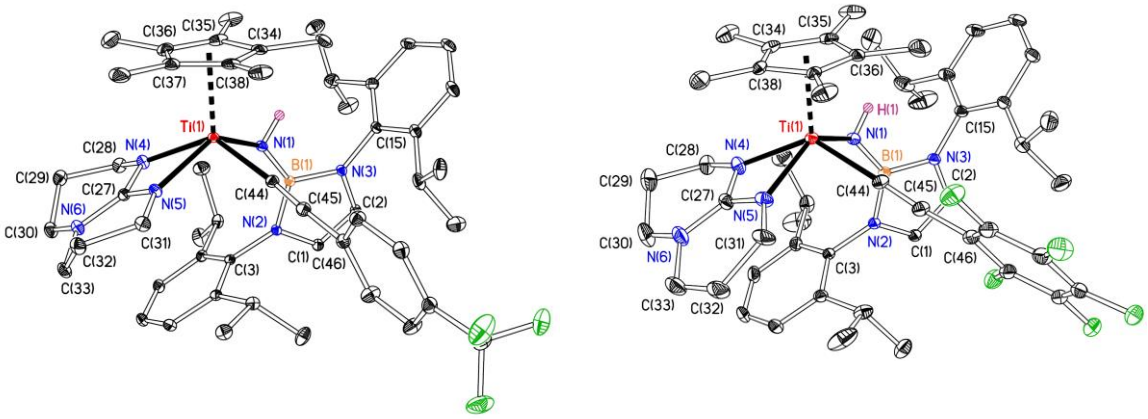


Figure 3.3 Displacement ellipsoid plots (20% probability) of Cp*Ti(HPP)(NH{B(NDippCH)$_2$})(CCAr), with Ar = Ar^{CF_3} (**3.5**), and Ar = Ar^{F} (**3.6**). C–bound H atoms are omitted. H(1) are drawn as a spheres of arbitrary radius, and were located from the fourier difference map.

Table 3.1 Selected bond distances (Å) and angles (°) for Cp*Ti(HPP)(NH{B(NDippCH)$_2$})(CCAr), with Ar = Ar^{CF_3} (**3.5**), and Ar = Ar^{F} (**3.6**). Cp$_{cent}$ refers to the computed η^5-Cp* ring centroid.

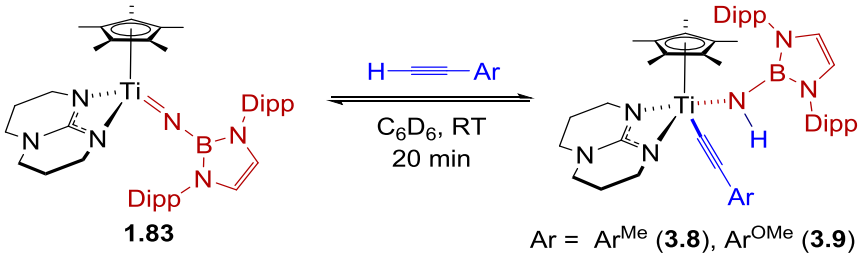
Parameter	**3.5**	**3.6**
Ti(1)–N(1)	1.9670(10)	1.9558(14)
Ti(1)–N(4)	2.0978(11)	2.0938(17)
Ti(1)–N(5)	2.0985(10)	2.0998(16)
Ti(1)–C(44)	2.1288(13)	2.1321(19)
N(1)–B(1)	1.4285(16)	1.434(2)
C(44)–C(45)	1.2147(19)	1.213(3)
Ti(1)–N(1)–B(1)	147.45(8)	141.07(12)

The two complexes are both confirmed to have a four-legged piano stool-type geometry with a η^5-Cp*, bidentate HPP, the acetylido and borylamido ligands. It is the borylimido ligand that was protonated during the reaction, as evidenced by the metric parameters of the Ti–N–B linkage. Firstly, the Ti(1)–N(1) bonds are lengthened significantly from 1.743(2) Å in **1.83** to 1.9670(10) Å (**3.5**) and 1.9558(14) Å (**3.6**). Next, the Ti(1)–N(1)–B(1) angles of 147.45(8)° and 141.07(12)°, as well as the sum of subtended angles at N(1)

of 355.2(1)° and 352.5(1)°, for **3.5** and **3.6**, respectively, are all in agreement with the nitrogen atom being mostly sp^2 rather than sp hybridised.

Non-sandwich Group 4 acetylide complexes are scarce, and the best analogue in terms of meaningful structural comparisons is probably Ti(N_2Npy){NHB(NDippCH)$_2$}(CCAr^F) (**3.7**) isolated recently in our group.[18] The Ti(1)–N(1) distance of **3.7** was found to be 1.9591(8) Å which agrees well with the present findings. The Ti(1)–C(44) bond lengths of 2.1288(13) and 2.1321(19) Å, for **3.5** and **3.6**, respectively, also agree well with **3.7** (2.1552(10) Å). Noteworthy, the N(1)–B(1) distance of 1.4285(16) and 1.434(2) Å is almost unchanged from the corresponding N(1)–B(1) distance of 1.422(3) Å found in **1.83**. They fall within the range (*ca* 1.34 – 1.51 Å) of all N–B single bonds with sp hybridised N and three-coordinate B in the Cambridge Structural Database.[101] The C≡C bond lengths of 1.2147(19) and 1.213(3) Å are in line with a triple bond for both complexes (1.2143(15) Å for **3.7**).

Next, the electronic influence of the alkyne aryl group was studied. The para substituent in terminal alkynes of type HCC-4-C_6H_4X were varied, where X = Me (Tol), and X = OMe (Ar^{OMe}), respectively. When these alkynes were added to a C_6D_6 solution of Cp*Ti(HPP){NB(NDippCH)$_2$} (**1.83**) at RT, a single new reaction product was formed which was found to be in equilibrium with the respective starting materials. The equilibria were established within 20 min, and warming the NMR tube solutions to 60 °C favoured the two starting materials. This is expected for reactions in which entropic contributions are significant. The products **3.8** and **3.9** were assigned the acetylide structures shown in Equation 3.2, based on *in-situ* spectroscopic NMR data (see experimental section). The ^{1}H, ^{13}C and ^{11}B NMR spectra are in agreement with their previously described analogues **3.5** and **3.6** and are not further discussed.

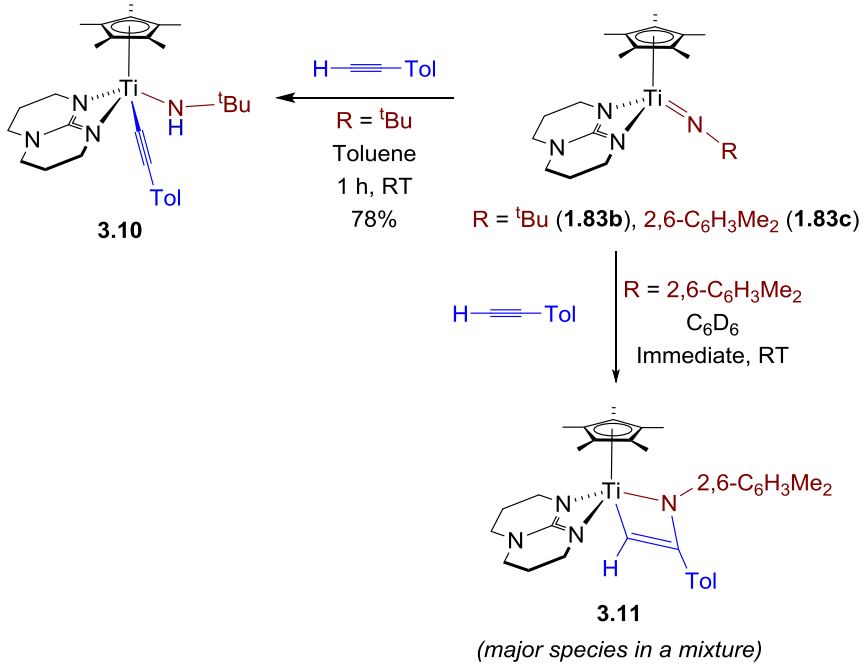


Equation 3.2

Equilibrium constants were determined to be K_{eq}^{298K} = 88 (9) and 39 (4) M^{-1}, corresponding to ΔG_{eq} values of -2.7(3) and -2.2(2) kcal mol^{-1} for Ar^{Me} and Ar^{OMe}, respectively. Interestingly, when Cp*Ti(HPP)(NH{B(NDippCH)$_2$})(CCAr^{CF_3}) 3.5 was heated to 60 °C on the NMR tube scale, free HCCAr^{CF_3} alkyne and borylimide **1.83** could be observed, which reformed 3.5 upon cooling to RT. By contrast, no reaction occurred upon heating Cp*Ti(HPP)(NH{B(NDippCH)$_2$})(CCAr^{F}) (**3.6**) at 60 °C. Taken together, these experiments show that there is a trend by which the more electron poor the alkyne, the further the equilibrium lies in favour of the acetylide complex.

As a comparison to the above reactions using the borylimide **1.83**, we next investigated the reactions of HCCTol with the previously reported *tert*-butylimido and xylylimido analogues of **1.83**.[6] On the NMR tube scale, introduction of HCCTol to C_6D_6 solutions of Cp*Ti(HPP)(NR) (R = ^{t}Bu (**1.83b**), Xyl (**1.83c**)) gave immediate colour changes from red-brown to orange and deep brown, respectively. On the preparative scale, Cp*Ti(HPP)(NH^{t}Bu)(CCTol) (**3.10**) could be isolated as a yellow powder in 78% yield (263 mg, Scheme 3.2). The ^{1}H NMR spectrum of isolated **3.10** has a broad N–H resonance at 7.81 ppm, which correlates to both the $\underline{C}Me_3$ and $C\underline{Me}_3$ ^{13}C nuclei in an HMBC experiment, confirming formation of a *tert*-butylamido compound *via* C–H bond activation of the alkyne. A ^{13}C resonance at 151.3 ppm is diagnostic for the Ti-bound carbon in the acetylido ligand, agreeing well with the corresponding values of 147.9 or 167.4 ppm for

Cp*Ti(HPP){NH(B(NDippCH)$_2$)}(CCAr^{CF_3}) (**3.5**) and Cp*Ti(HPP){NH(B(NDippCH)$_2$)}(CCAr^F) (**3.6**), respectively.



Scheme 3.2 Reactions of Cp*Ti(HPP)(NR) (R = ^{t}Bu (**1.83b**), 2,6-C$_6$H$_3$Me$_2$ (**1.83c**)) with HCCTol.

Unfortunately, it was not possible to isolate a single product cleanly from the reaction of **1.83c** with HCCTol on the preparative scale. Inspection of the NMR tube scale ^{1}H spectrum indicated that the azametallacyclobutene complex Cp*Ti(HPP){N(Xyl)C(Tol)CH} (**3.11**) was formed *via* [2 + 2] cycloaddition (Scheme 3.2) as the major product within a mixture, but multiple overlapping signals precluded full NMR characterisation of this species. Nevertheless, a ^{1}H resonance at 10.36 ppm which shows a HSQC correlation to a ^{13}C resonance at 216.1 ppm, and an HMBC correlation to a ^{13}C resonance at 134.8 ppm, is indicative of an azametallacycle having Markovnikov regiochemistry (so-called because this is the isomer that would give rise to that hydroamination product upon protolysis). Attempts to stabilise an azametallacycle with the more electron-deficient alkyne HCCAr^F were unsuccessful, forming a complex mixture of intractable species.

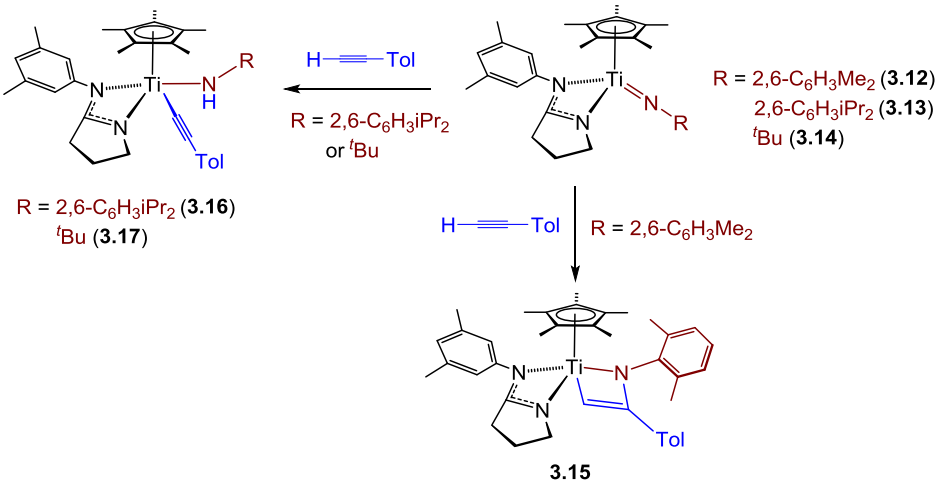
Since complexes **1.83**, **1.83b** and **1.83c** carry the same innocent supporting ligands, namely Cp* and HPP, comparisons can be drawn with the model alkyne HCCTol. Within the series

of these titanium imides the steric demand increases in the order Xyl < *t*Bu < $B(NDippCH)_2$. At the same time, we have shown previously,[6] using bond lengths, MO and QTAIM analysis, that aryl imido compounds are electronically closely related to the borylimido complexes bearing the $B(NDippCH)_2$ moiety (e.g., also representing an aromatic π-system), acting as electronic model compounds for borylimides. Therefore, it is striking to note that the tendency to undergo C–H bond activation to form acetylides follows the trend of steric demand of the imido group. Specifically, the two bulky borolyl and *t*Bu substituted imides form exclusively acetylides whereas the more open (sterically demanding in only 2 dimensions) xylyl-substituted imide undergoes [2+2] cycloaddition, despite being electronically closely related to borylimide **1.83**. Therefore, sterics is likely the major factor in determining the preference between the two observed reaction modes.

The identity of the reaction products of **1.83b** and **1.83c** with HCCTol are entirely analogous to those reported by Gade and co-workers in related *tert*-butylimido and arylimido systems incorporating the 2-aminopyrollinato ligand $N^{3,5\text{-Xyl}}N^{pyr}$ (2-(3,5-dimethylphenylamino)pyrrolinato).[10] While the reaction of HCCTol with $Cp^*Ti(N^{Xyl}N)(N\text{-}2,6\text{-}C_6H_3\underline{Me}_2)$ (**3.12**) gave [2 + 2] cycloaddition, the related but more bulky $Cp^*Ti(N^{Xyl}N)(N\text{-}2,6\text{-}C_6H_3{}^{i}\underline{Pr}_2)$ (**3.13**), as well as the *tert*butylimido analogue $Cp^*Ti(N^{Xyl}N)(N^{t}Bu)$ (**3.14**) gave C–H bond activations instead (Scheme 3.3).

Gade also reported DFT analysis of the differing selectivity of these reactions, with cycloaddition expected to be the favoured pathway, both kinetically and thermodynamically, in all cases. It was surmised that the experimental outcome is dominated by steric effects with the bulkier imides giving C–H bond activation, rather than cycloaddition, due to steric clash in the alternative metallacyclic product. We have also previously reported on competing metallacycle or acetylide formation in reactions between diamide-amine-supported titanium borylimides and terminal alkynes.[18] In some cases,

acetylide-borylamides could be isolated as kinetic products before being converted to metallacyclic thermodynamic products at high temperature. In the case of Cp*Ti(HPP)(NH^{t}Bu)(CCTol) (**3.10**), heating up to 90 °C resulted only in conversion to a complex mixture of products.

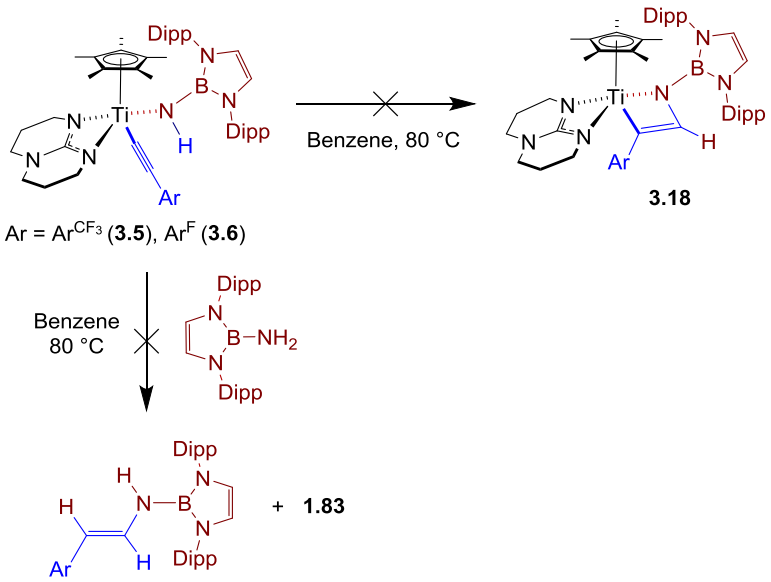


Scheme 3.3 Reactions of Cp*Ti(N^{Xyl}N)(NR) (R = 2,6-$C_6H_3Me_2$ (**3.12**), 2,6-$C_6H_3{}^iPr_2$(**3.13**), ^{t}Bu (**3.14**)) with HCCTol.[14]

It has been reported that the M–X bond enthalpies correlate with H–X bond enthalpies.[19–22] Moreover, it has been observed by experiment that the M–C bond energies increase more rapidly with changes in substituents than the corresponding C–H bonds.[23] This means that M–C bond strengths change to a larger extent than the corresponding C–H bonds. Thus, there is an overall thermodynamic preference to break the stronger C–H bond.[23] Similarly, DFT studies validated these trends by predicting changes in relative bond enthalpies with varying substitutents.[24]

C–H stretching frequencies of terminal alkynes can be a useful guide for the strength of C–H bonds and thus for the corresponding M–C bonds. Thin film IR spectra of HCCAr (Ar = Ar^F, Ar^{CF_3}, Tol, Ar^{OMe}) were obtained to give C–H bond stretches of 3310, 3306, 3291, and 3286 cm^{-1}, respectively. Hence, the more electron poor the alkyne, the stronger the resulting C–H bond. To clarify, the observed trend of C–H bond strengths is the reverse trend observed in acidity of the alkynes.

In conclusion, the more electron withdrawing the alkyne HCCAr, the stronger the corresponding M–C bond (which outweighs the stronger C–H bond). Thus, there is a thermodynamic preference to form titanium acetylide complexes using more electron withdrawing alkynes, following the trend Ar^{F} > Ar^{CF_3} > Tol > Ar^{OMe}, in full agreement with the experimental results presented.



Scheme 3.4 Reaction of Cp*Ti(HPP){NH(B(NDippCH)$_2$)}($CCAr^{CF_3}$) (**3.5**) and Cp*Ti(HPP){NH(B(NDippCH)$_2$)}($CCAr^{F}$) (**3.6**) with heat and free borylamine $H_2NB(NDippCH)_2$.

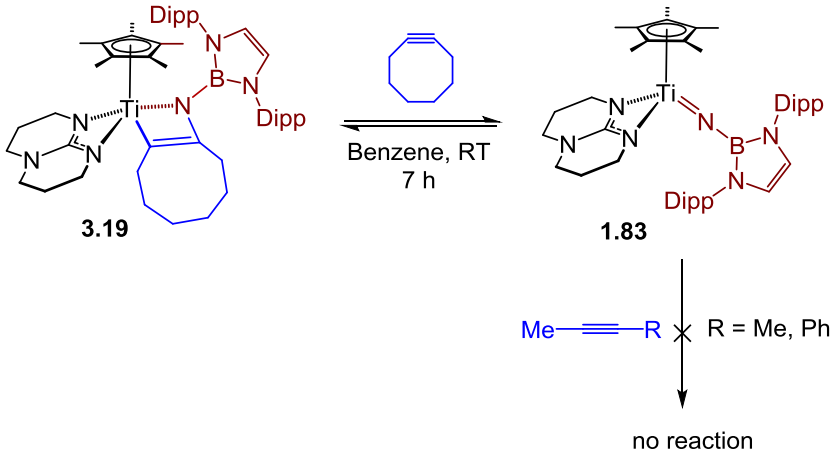
Given our previous success in the development of catalytic cycles for the hydroamination and hydrohydrazination of alkynes, we were interested in the chemistry of isolated acetylides Cp*Ti(HPP)(NH{B(NDippCH)$_2$})(CCAr), with Ar = Ar^{CF_3} (**3.5**), and Ar = Ar^{F} (**3.6**). In particular, whether the corresponding metallacycles could be accessed, which were identified as key intermediates in hydroamination chemistry.[10] Titanium amido acetylide complexes were previously shown to be converted to the corresponding metallacycle complexes upon heating. For example, the related titanium borylamido acetylide Ti(N_2iPrNMe){NHB(DippCH)$_2$}($CCAr^{F}$) could be converted into the corresponding metallacycle upon heating at 60 °C. [18]

Both **3.5** and **3.6** are stable in solution over days at 298 K and no reaction is observed under forcing conditions of extended heating at 60 °C for **3.6**, while traces of free alkyne and

borylimide are observed for **3.5** (Scheme 3.4). Elevating the reaction temperature to 80 °C lead to slow decomposition to a complex mixture of unidentifiable compounds in both cases, along with free borylamine. No sign of metallacycles of type **3.12** were observed. Similarly, no reaction was observed when 1 equiv. of free borylamine was added to solutions of **3.5** or **3.6**, respectively, even under extended heating at 80 °C. No aminolysis of transient metallacycle could be detected, however.

3.3.2 Reactions with internal alkynes

Addition of the internal alkynes dimethylacetylene or methylphenylacetylene to a solution of borylimide **1.83** in C_6D_6 yielded no reaction, even under extended heating at 70 °C (Scheme 3.5). This could be rationalized by steric clashes that would arise in the formation of potential [2 + 2] cycloaddition products.



Scheme 3.5 Reaction of titanium borylimide **1.83** with cyclooctyne formed cycloaddition product Cp*Ti(HPP){N(B(NDippCH)$_2$}C(=C)(CH$_2$)$_6$ (**3.19**) in equilibrium (K_{eq}^{298K}= 19 M^{-1}, left). No reaction is observed with PhCCMe and MeCCMe (bottom).

Therefore, we were interested to see whether [2 + 2] cycloaddition with a more reactive alkyne was feasible. When the strained, and sterically tied back cyclooctyne was added to a solution of **1.83** in C_6D_6, an equilibrium to a single new species was established after 7 h at room temperature. Warming the NMR tube solution to 60 °C favoured the two starting materials, as expected on the basis of entropic considerations. Upon cooling to 298 K the

equilibrium shifted back to the initial position. Product **3.19** was assigned the metallacycle structure shown in Scheme 3.5, based on *in-situ* spectroscopic NMR data. For example, the quarternary metallacycle ^{13}C signals feature diagnostic shifts of 218.4 and 136.7 ppm, for the carbon directly bound to the metal center (TiC) and the neighbouring one (TiC=C), respectively. This is in good agreement with the analogous metallacycle structures Cp*Ti(N^{Xyl}N){N(2,6-$C_6H_3Me_2$)C(Tol)=CH} (**3.15**), featuring ^{13}C shifts of 228.9 (TiC) and 147.5 (TiC=C),[14] as well as Cp*Ti(HPP){N(2,6-$C_6H_3Me_2$)C(Tol)CH} (**3.11**) that showed a shift of 216.1 ppm for the Ti–C carbon. The equilibrium constant at room temperature was determined to be K_{eq}^{298K}= 19 M^{-1} (**1.83**:**3.19** ratio of ~ 7:3). Addition of one equivalent of borylamine H_2NB(NDippCH)$_2$ did not lead to a reaction at RT or upon extended periods of heating.

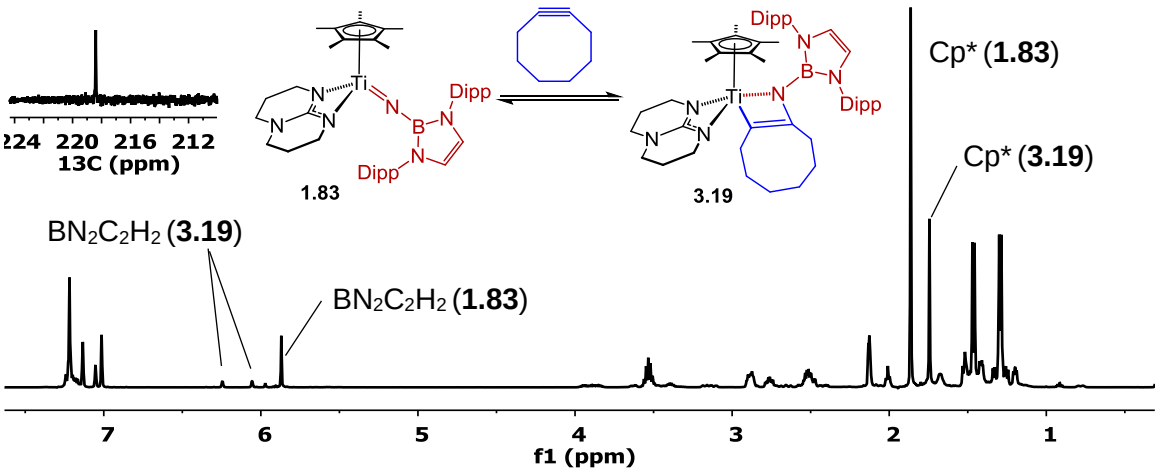
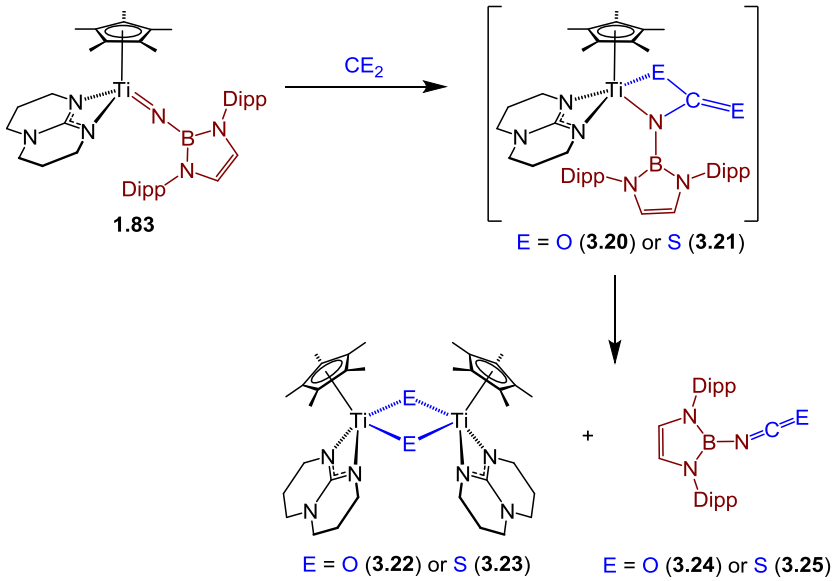


Figure 3.4 ^{1}H NMR spectrum (400 MHz) of an equilibrated mixture of equimolar amounts of **1.83** and cyclooctyne to form Cp*Ti(HPP){N(B(NDippCH)$_2$}C(=C)(CH$_2$)$_6$ (**3.19**) in C_6D_6 at 298 K. Inset: ^{13}C NMR spectrum (500 MHz) featuring the Ti–C carbon of **3.19**.

3.4 Reactions of Cp*Ti(HPP){NB(NDippCH)$_2$} (1.83) with heterocumulenes

As mentioned previously, Group 4 imido, hydrazido and alkoxyimido complexes typically undergo [2 + 2] cycloaddition reactions with heterocumulenes such as CO_2, isocyanates and their heavier congeners. The formed metallacycle products can be isolated in some cases, and are observed to react further to engage in retro-cyclisation and extrusion of a new organic species, or insertion of a second molecule of substrate into the first-formed metallacycles.[25–28]

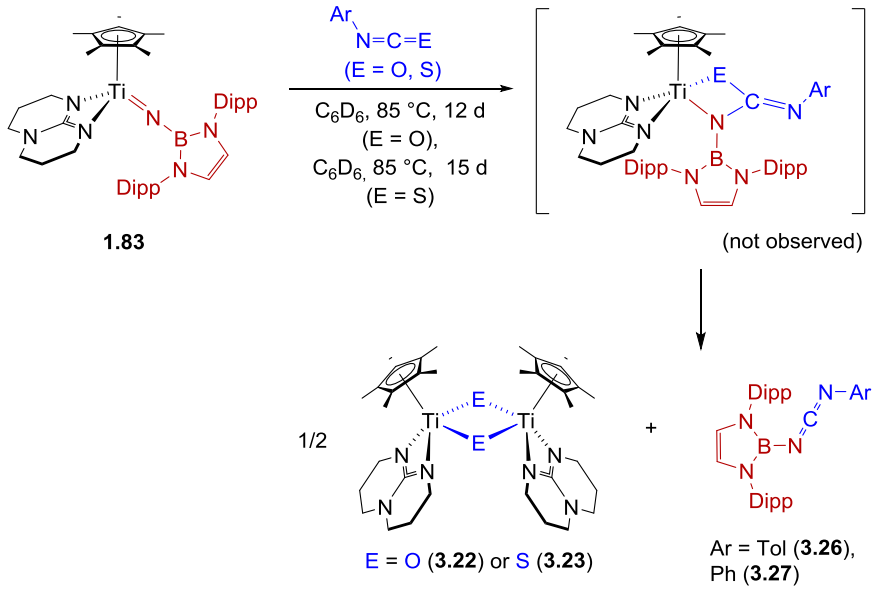
Initial studies by Dr Ben Clough, a previous D.Phil student in the Mountford group have established the reactions with Cp*Ti(HPP){NB(NDippCH)$_2$} (**1.83**) with CO_2 and CS_2.[18] It was found that initial [2 + 2] cycloaddition is followed by rapid extrusion of a boryliso(thio)cyanate ECNB(NDippCH)$_2$ (E = O (**3.20**), S (**3.21**)), with concomittant formation of oxo- or sulfido-bridged titanium dimers [Cp*Ti(HPP)(μ-E)]$_2$ (E = O (**3.22**), S (**3.23**); Scheme 3.5), respectively. The reaction with CO_2 proceeded smoothly at RT and was fully converted within 2.5 days at this temperature, while heating to 80 °C for 3.5 days was required to drive the reaction using CS_2.



Scheme 3.6 Reactions of Cp*Ti(HPP){NB(NDippCH)$_2$} (**1.83**) with CO_2 and CS_2. Reaction conditions: E = O: Benzene, RT, 2.5 days; E = S: Toluene, 80 °C, 3.5 days.

Prompted by this initial success with these heterocumulenes, we set out to investigate the

reactions with the related, but bulkier, iso(thio)cyanates ArNCE (E = S, O; Ar = Ph, Tol) summarized in Scheme 3.7. When Cp*Ti(HPP){NB(NDippCH)$_2$} (**1.83**) was treated with TolNCO on the NMR tube scale, no conversion was observed until the sample was heated to 85 °C, reflecting the increased steric bulk as compared to reaction with CO_2. After 12 d at 85 °C the starting materials were consumed and one major species **3.26** was observed, along with a few known decomposition products such as free borylamine (which is typical at elevated temperatures for the title compound **1.83**). This major species was identified as the organic extrusion product TolNCNB(NDippCH)$_2$ (**3.26**) based on spectroscopic data discussed later.



Scheme 3.7 Reactions of Cp*Ti(HPP){NB(NDippCH)$_2$} (**1.83**) with iso(thio)cyanates.

A colour change from dark red to orange was accompanied with the formation of a yellow precipitate and gradual loss of the ^{1}H NMR signals corresponding to the Cp* and HPP ligand. The latter observation can be explained by the formation of the previously isolated [Cp*Ti(HPP)(μ-O)]$_2$ (**3.22**).[18] This species was found to be insoluble in apolar solvents such as benzene, but was identified by comparison of the ^{1}H NMR shifts in CD_2Cl_2 in which it showed improved solubility. The heavier congener TolNCS required an even longer reaction time of 15 d at 85 °C to go to completion on the NMR tube scale, and

formed more unidentified side products. In this case, one set of HPP signals in the range between 3.6-1.7 ppm as well as a Cp* signal at 2.36 ppm were still observed. The corresponding compound was identified as the known $[Cp^*Ti(HPP)(\mu\text{-}S)]_2$ (**3.23**), which displays a higher solubility in apolar solvents compared to the oxo analogue **3.22**.[18] Additionally, the same organic species **3.26** was observed as in the previous case.

Scaling up the reaction with TolNCO proved difficult given the high temperatures and long reaction times required to drive the reactions (and the resulting formation of side products). Nevertheless, successful scale up on the preparative scale was achieved using TolNCS. The reaction was complete after 7 d at 90 °C in toluene. The volatiles were removed *in vacuo*, and the organic $TolNCNB(NDippCH)_2$ (**3.26**) could be extracted into cold hexanes and subsequently purified by recrystallisation to give 64 mg yield (30%). By contrast, the relatively insoluble dimeric $[Cp^*Ti(HPP)(\mu\text{-}S)]_2$ (**3.23**) remained left behind.

In line with the described mechanism in Scheme 3.6, $\underline{Ph}NCNB(NDippCH)_2$ (**3.27**) and $[Cp^*Ti(HPP)(\mu\text{-}E)]_2$ (E = O (**3.22**), S (**3.23**)) were formed when the aryl groups wer varied and $\underline{Ph}NCO$ and $\underline{Ph}NCS$ were used as substrates, respectively. However, in none of the cases could we find evidence for the putative metallacycle intermediates.

These reactions can be described as overall functional group transfers of the borylimido unit "R_2BN" onto small organic molecules, forming $ECNB(NDippCH)_2$ (E = O (**3.20**), E = S (**3.21**)) or $ArNCNB(NDippCH)_2$ (Ar = Tol (**3.26**), Ph (**3.27**)). The E atom of EC=E, and ArNCE goes to form one half of the respective oxo- or sulfido-bridged titanium dimer $[Cp^*Ti(HPP)(\mu\text{-}E)]_2$ (E = O (**3.22**), S (**3.23**); Scheme 3.7). Direct methodologies to incorporate "R_2BN" units into organic molecules are rather limited, and none go directly *via* amines (*vide infra*), or metal-bound "R_2BN". Bettinger *et al.* reported the only alternative route, incorporating "R_2BN" *via* the *in-situ* formation of borylnitrenes formed by photolyzing the parent borylazides.[29–36] For example, C–H bond activation of methane

was observed, forming MeN(H)BCat (Cat = $C_6H_4O_2$), from the reaction of transient borylnitrene [NBCat] with methane under UV irradiation.[29] Similarly, the corresponding isocyanate OCNBCat could be formed starting from CO.[31] Generally, these borylisocyanates can be accessed through salt metathesis reactions, for example, reacting $ClB(N^tBuCH)_2$ with AgNCO gives $OCNB(N^tBuCH)_2$.[37] Other compounds, such as iminoboranes, have also been obtained *via* salt metathesis.[38,39]

Our group has shown previously that steric bulk played an important role in reactions of related titanium imido complexes and CE_2 as well as RCNE (E = O, or S).[26,40] Of particular relevance is the observation that the transition from the metallacyle intermediate to organic extrusion is stabilised by increased steric bulk. Thus, the large steric bulk of the borolyl unit could explain why the putative metallacycles are difficult to observe. Compared to the case of CO_2 and CS_2, in which there was NMR evidence of a short-lived metallacycle species, iso(thio)cyanates display an increased steric bulk. Hence, these increased sterics along with the necessary harsher reaction conditions likely account for the fact that no evidence for any intermediates was found.

The spectroscopic signature of both mono-borylated carbodiimides **3.26** and **3.27** are very similar. The ^{1}H-NMR spectra display a septet (4 H) and two doublets (12 H each) attributed to the four isopropyl groups, and a singlet (2 H) of the alkene backbone protons of the borolyl unit. Very low intensity ^{13}C signals at 128.7 and 129.4 ppm were observed corresponding to the central carbon in the carbodiimide moiety. This value agrees very well with that of the analogous mono-borylated ^{t}BuNCNB$(NMeCH_2)_2$ at 127.8 ppm, and those of the two bis-borylated carbodiimides $(RNMe)_2BNCNB(NMeR)_2$ (R = CH_2, or C_6H_4) at 123.0 and 123.2 ppm, respectively, which were all prepared by Haubald *via* a salt metathesis route using R'NCNSiMe$_3$ with $XB(NMeR)_2$ (R' = SiMe$_3$ or ^{t}Bu, X = Cl or Br).[41] These values are also similar to that of R'NCNSiMe$_3$ (R' = SiMe$_3$ or ^{t}Bu) of 130.7 and 123.9

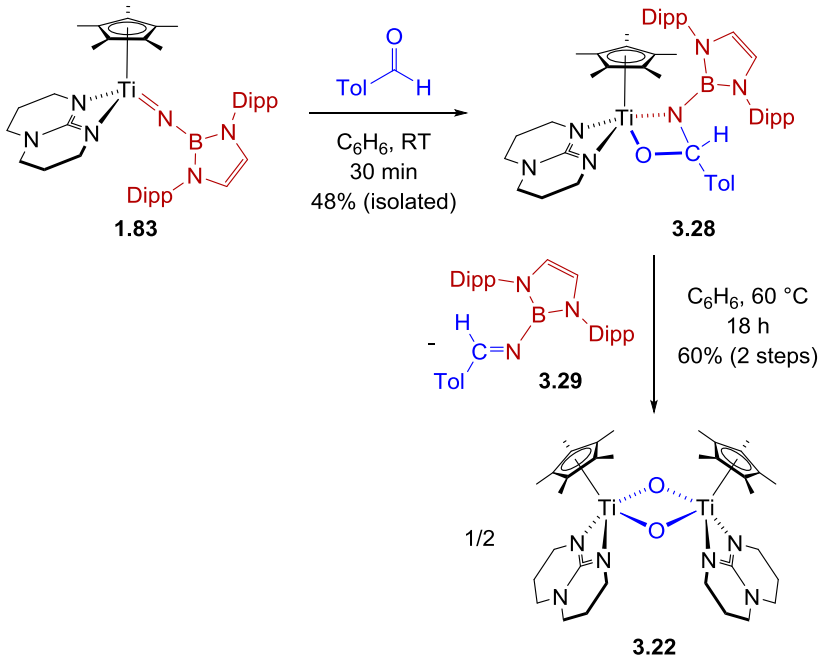
ppm, respectively.[42] The IR spectra of **3.26** and **3.27** display a very intense band at 2182 and 2185 cm^{-1}, respectively, which can be assigned to the antisymmetric stretches of the N=C=N units. Again, these values agree well with the previously discussed $^{t}BuNCNB(NMeCH_2)_2$, and $(RNMe)_2BNCNB(NMeR)_2$ (R = CH_2, or C_6H_4) at 2170, 2220 and 2250 cm^{-1}, respectively.[41]

3.5 Reactions of Cp*Ti(HPP){NB(NDippCH)$_2$} (1.83) with organic small molecules featuring carbonyl groups

3.5.1 Reactions with aldehydes

When Cp*Ti(HPP){NB(NDippCH)$_2$} (**1.83**) was treated with TolCHO on the NMR tube scale at 298 K, an immediate color change from brown to light-orange was observed. Following the reaction *via* ^{1}H NMR spectroscopy revealed that the starting materials are rapidly converted into a single new species **3.28**, which subsequently slowly converted to the known [Cp*Ti(HPP)(μ-O)]$_2$ (**3.22**) along with an organic species **3.29**. No further reaction was observed.

The intermediate compound **3.28** was found to be a relatively rare example of a [2 + 2] cycloaddition product Cp*Ti(HPP){N(B(NDippCH)$_2$)C(H)(Tol)O} (Scheme 3.8) derived from a titanium imido complex and an aldehyde. As would be expected (*vide infra*) by virtue of ligands with increased steric bulk this species is found to be a relatively stable compound and can be isolated in 48% yield (168 mg) on the preparative scale. It can be stored for weeks at RT as powder without appreciable decomposition. However, higher yields and crystal growth were hampered by slow conversion of Cp*Ti(HPP){N(B(NDippCH)$_2$)CH(Tol)O} **3.28** into final products N(CHTol){B(NDippCH)$_2$} **3.29** and titanium dioxo complex **3.22** in solution phase.



Scheme 3.8 Reaction of borylimide **1.83** with tolylaldehyde.

Cp*Ti(HPP){N(B(NDippCH)$_2$)C(H)(Tol)O} (**3.28**) was analysed using elemental analysis, NMR and IR spectroscopy which are in line with the assigned structure shown in Scheme 3.8. The presence of four inequivalent CHMe$_2$ groups of the borolyl ligand confirm the expected C_1 symmetry of the compound. There is a lack of any signals in the region typical for C=O stretches in the IR spectrum. The singlet for the metallacyclic TolC<u>H</u> is found at the diagnostic region of 7.35 ppm, which features an HSQC correlation to the metallacyclic ^{13}C resonance of Tol<u>C</u>H (88.0 ppm), and an HMBC correlation to the *i*-*C*$_6$H$_4$-Me carbon (137.4 ppm). The ^{13}C signal for the metallacyclic Tol<u>C</u>H is diagnostic and in line with chemical shifts of related literature complexes (84.1 ppm for Cp*Ti{N(Tol)C(Ph)(Me)O}{MeC(N^{i}Pr)$_2$},[43] 82.8-83.4 ppm for Cp*Ti{PhC(N^{i}Pr)$_2$}{N(C(Ar^F)NOtBu)CH(Ar^X)O}, X = Me, ^{t}Bu, OMe, NMe$_2$ or CF$_3$).[25]

Only one set of signals were observed in the NMR spectra, consistent with the formation of a single diastereomer (both the metal and the Tol<u>C</u>H being stereogenic centres). A nuclear Overhauser effect (NOE) experiment revealed through-space interactions between the Cp* ligand and the Tol<u>C</u>H of the metallacycle. This is consistent with the assigned

structure shown in Scheme 3.8 with the tolyl group pointing away from the Cp* ligand, representing the least sterically congested conformation.

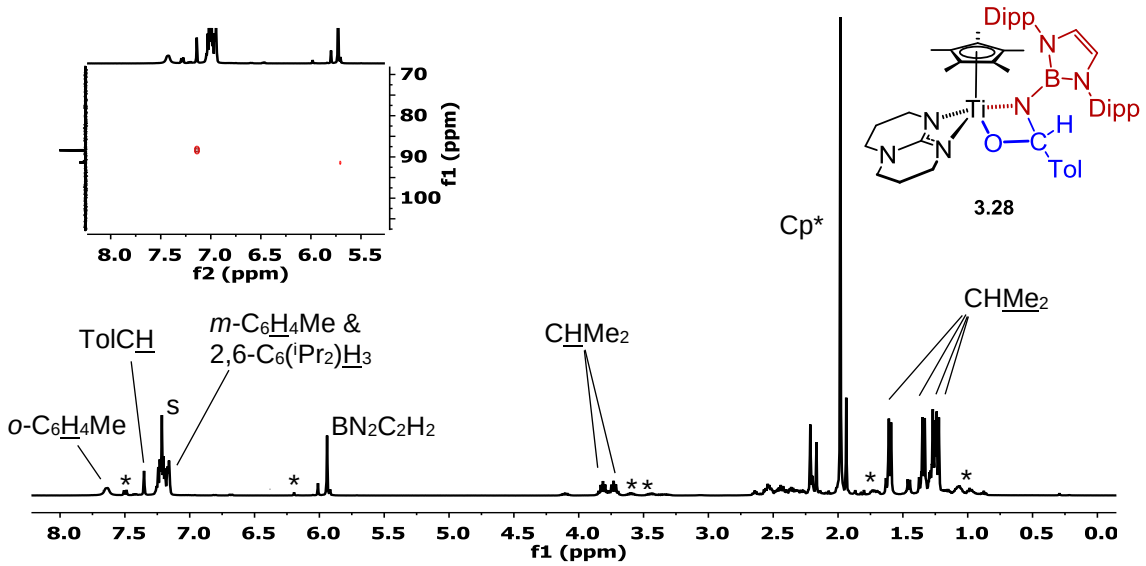
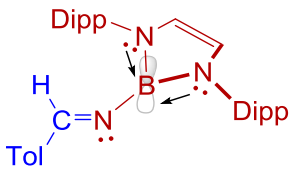


Figure 3.4 ^{1}H NMR spectrum (400.1 MHz) of Cp*Ti(HPP){N(B(NDippCH)$_2$}C(H)(Tol)O)} (**3.28**) in C_6D_6 at 298 K. Inset shows the HSQC spectrum revealing the correlation between the ^{1}H NMR signal at 7.35 ppm (TolC<u>H</u>), and the ^{13}C signal at 88 ppm (Tol<u>C</u>H). "s" denotes residual protio solvent, "*" denotes organic extrusion product N(CHTol){B(NDippCH)$_2$} (**3.29**).

The formation of the metallacycle Cp*Ti(HPP){N(B(NDippCH)$_2$}C(H)(Tol)O)} (**3.28**) is followed by slow extrusion to form titanium dioxo complex [Cp*Ti(HPP)(μ-O)]$_2$ (**3.22**) and the organic iminoborane N(CHTol){B(NDippCH)$_2$} (**3.29**) which can be isolated as an orange powder in 85% yield. Compound **3.29** was assigned the structure shown in Scheme 3.8. High resolution ESI mass spectrometry, NMR and IR spectroscopy and DFT calculations are all in line with the proposed structure. A sharp singlet corresponding to the N=C<u>H</u> imine proton is observed at a diagnostic upfield shift of 8.66 ppm, featuring an HSQC correlation to the imine carbon N=C and an HMBC correlation to the *i*-C$_6$H$_4$-Me. In particular, we tentatively assigned iminoborane **3.29** the thermodynamically more stable *E* configuration, in which the steric interactions between the bulky borolyl moiety and the tolyl group are minimised. The diagnostic stretch at 1661 cm^{-1} in the IR spectrum confirms the presence of a C=N imine moiety, and is suggestive of a bent C=N–B structure with only

little imine N–B dative bond character.[44] Electronically, this can be rationalised by the fact that the boron atom is flanked by two additional nitrogen atoms. These compete to donate their lone pairs into the empty boron based p-orbital, formally forming an aromatic borolyl ring (Figure 3.5). Thus, there is likely only limited interaction of the C=N based lone pair into the boron atom.



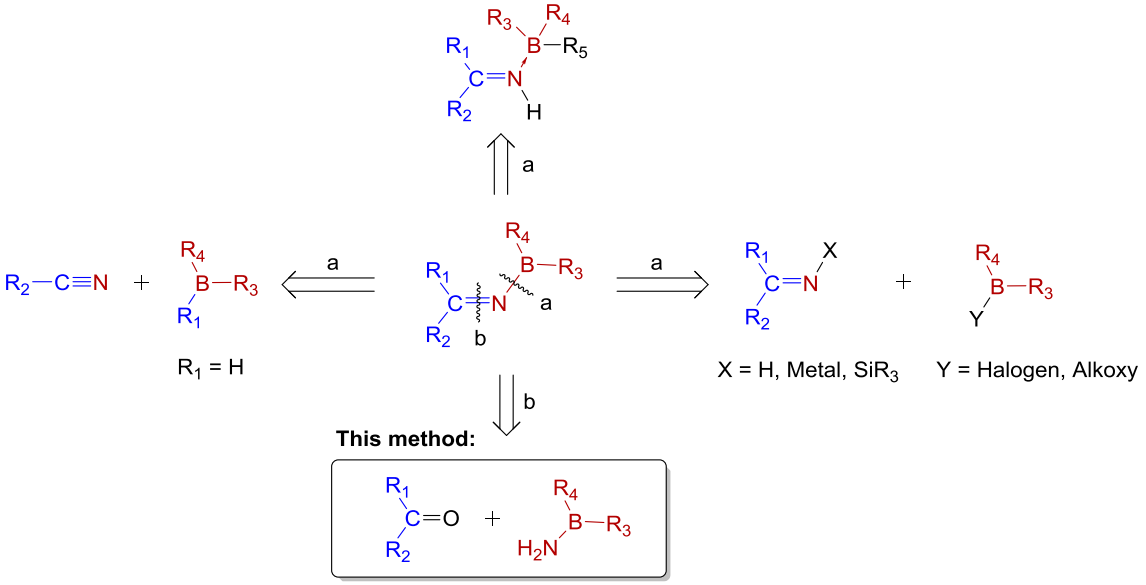
3.29

Figure 3.5 *E*-conformation of N(CHTol){B(NDippCH)$_2$} (**3.29**).

Subsequent to the presented experimental studies, Philip Mountford analysed this compound by DFT calculations.[45] Specifically, the experimentally observed ^{11}B NMR shift of 24.3 ppm is closest to the computed value of 24.2 ppm for the *E* isomer, compared the value of 25.6 ppm for the *Z* isomer, as well as for 20.7 ppm for a linear conformation. Analogously, the experimentally observed ν(C=N) stretch at 1661 cm^{-1} is closest to the DFT computed value for the *E* isomer (1632 cm^{-1}), compared to the *Z* (1701 cm^{-1}) or linear isomers (1836 cm^{-1}).

Compound N(CHTol){B(NDippCH)$_2$} (**3.29**) represents the first example of an iminoborane with a bent N=C–B moiety. Previously reported examples of organic iminoborane compounds, include the dimeric [Ph$_2$CNBCat]$_2$, monomeric Ph$_2$CNBCat and PhC(H)NB(Mes)$_2$.[46] Instead of a bent N=C–B moiety, Ph$_2$CNBCat and PhC(H)NB(Mes)$_2$ display a linear B=C=N arrangement which is reflected by intense ν(N=C=B) IR stretches between 1765 – 1820 cm^{-1}. This difference can be rationalised by the two nitrogen atoms flanking the boron atom in N(CHTol){B(NDippCH)$_2$} (**3.29**). The nitrogen lone pairs donate into the boron based p-orbital, thus reducing the N=C–B bond order. Analogous observations were made with iminoketones Ph$_2$CNBPh$_2$, (PhCN)$_2$BPh, and (Ph$_2$C=N)$_3$B.

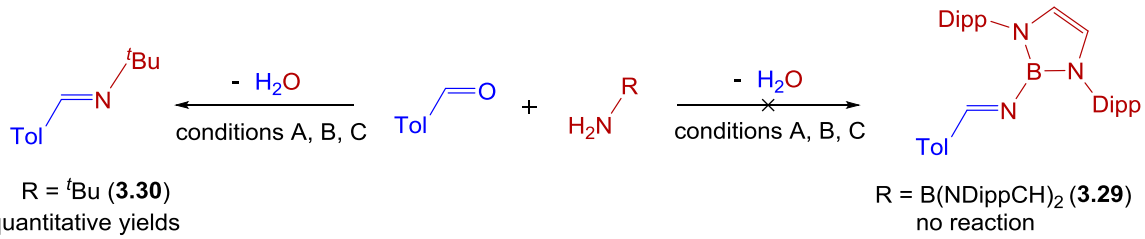
The N–B bond order decreased as the number of nitrogen atoms bound to boron increased. In the order of decreasing N–B bond order Ph_2CNBPh_2 > $(PhCN)_2BPh$ > $(Ph_2C{=}N)_3B$, the corresponding IR stretches decreased from 1790, 1672 to 1667 cm^{-1}, with the lowest value being very close to the imine stretch of 1661 cm^{-1} observed in **3.29**.



Scheme 3.9 Retrosynthetic disconnections of iminoboranes.

N(CHTol){B(NdippCH)$_2$} (**3.29**) represents a relatively rare example of an iminoborane. Previously reported syntheses focused on the retrosynthetic disconnection of the N–B linkage, starting from precursors featuring C-N bonds already (disconnection a, Scheme 3.9). Synthetic strategies include hydroboration of nitriles,[47–50] thermal treatment of amineborane adducts,[38,51] nucleophilic attack of imines to borane moieties carrying a leaving group and salt metathesis.[38,39,52,53] Our method represents a novel, complementary synthetic strategy to access iminoboranes, where it is the C=N bond which is formed ultimately, starting from aldehydes and borylamines (disconnection b).

To demonstrate the importance of the presented methodology, we explored the possibility for a more direct way to form iminoboranes: the condensation of aldehydes with primary borylamines.

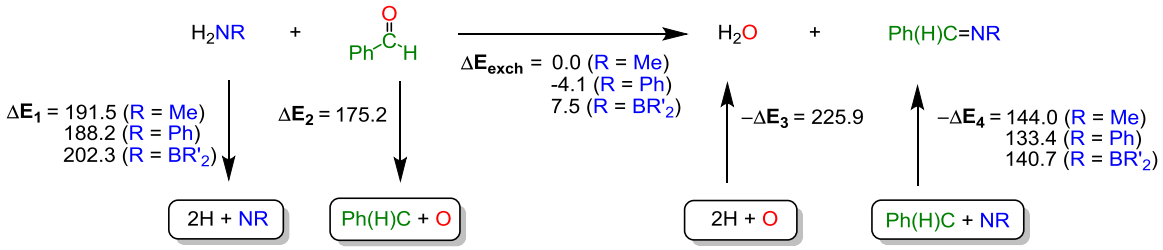


Scheme 3.10 Condensation reactions of tolylaldehyde with *tert*-butylamine (left), and borylamine $H_2NB(NDippCH)_2$ (right) using three different reaction conditions: A) CH_2Cl_2, NEt_3, $MgSO_4$, 1 h reflux; B) Et_2O, mol. sieves (4 Å), 16 h, RT; C) Tol, $MgSO_4$, 16 h, 100 °C.

We employed three common literature procedures for the condensation of tolylaldehyde with our model borylamine $H_2NB(NDippCH)_2$ to form iminoborane **3.29**, and with *tert*-butylamine to form **3.30** for comparison (Scheme 3.10).[54,55] Using *tert*-butylamine, all three reaction conditions afforded the desired imine **3.30** quantitatively. Surprisingly, no traces of iminoborane **3.29** could be detected by ^{1}H NMR spectroscopy when borylamine $H_2NB(NDippCH)_2$ was used with any of the three reaction conditions, even under forcing conditions (high temperature or longer reaction times).

Next, DFT calculations (using the B3PW91 functional and def2-svp basis set) are discussed which shed light on the underlying factors of the two imine forming methods presented above. First, the condensation reactions between amines with aldehydes are presented, and then contrasted with the corresponding titanium imide / aldehyde metathesis reactions. These calculations were performed by Dr Simona Mellino.[56]

For the condensation reactions, the model thermodynamic cycle shown in Scheme 3.11 is analysed. The model substrate PhCHO reacts with H_2NR, with R = Me, Ph, and $B(NMeCH)_2$ to form water and the corresponding imines Ph(H)C=NR, respectively. The overall energy of this exchange (ΔE_{exch}) can be expressed as the sum of the four stepwise bond dissociation energies (BDEs): ΔE_1 (homolytic N–H bond cleavages), ΔE_2 (C=O homolysis), $-\Delta E_3$ (O–H bond formations), $-\Delta E_4$ (Ph(H)N=NR imine bond formation) ($\Delta E_{exch} = \Delta E_1 + \Delta E_2 - \Delta E_3 - \Delta E_4$).



Scheme 3.11 Energy decomposition scheme for selected isodesmic multiple bond exchanges and computed bond dissociation energies for reactions between amines H_2NR (R = Me, Ph, and BR'$_2$ = $B(NMeCH)_2$) and PhCHO (ΔE, kcal mol^{-1}). All species are spin state singlets except for the fragments O, and NR which are spin triplets, and H which is a spin doublet. $\Delta E_{exch} = \Delta E_1 + \Delta E_2 - \Delta E_3 - \Delta E_4$.

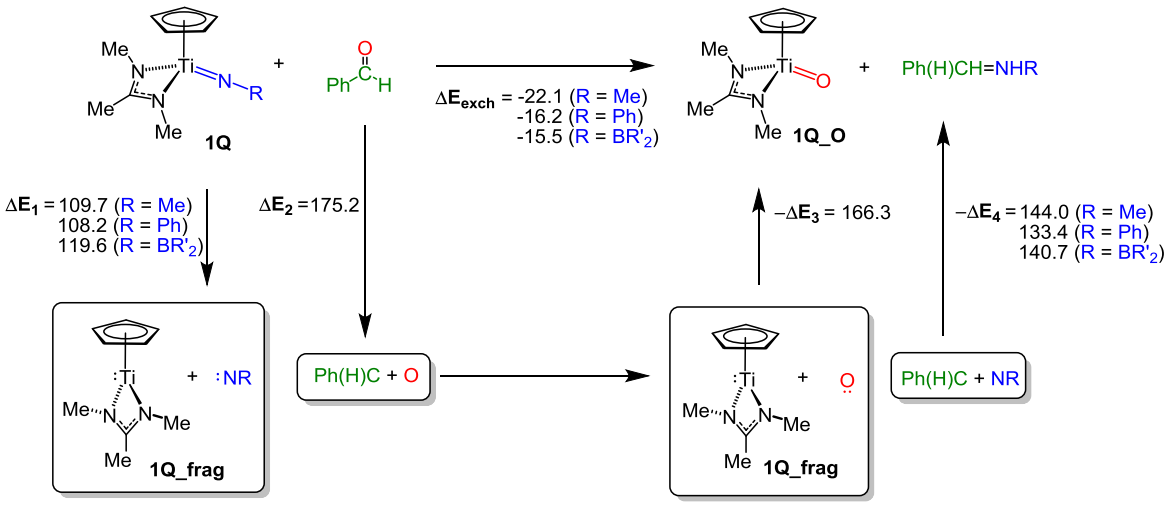
As can be seen in Scheme 3.11, the C=O multiple bond in the starting aldehyde is stronger than the C=N bond of the imines Ph(H)C=NR (175.2 kcal mol^{-1} vs 144.0, 133.4 and 140.7 kcal mol^{-1} for R = Me, Ph, $B(NMeCH)_2$, respectively). The key driving force of the reaction favouring the right hand side is the formation of water (225.9 kcal mol^{-1}). However, it is evident that the formation of water is not enough to compensate for breaking both the Ph(H)C=O and the N–H bonds in the case of $H_2NB(NMeCH)_2$. The homolytic N–H bond cleavage for $H_2NB(NMeCH)_2$ amounts to 202.3 kcal mol^{-1}, which is significantly higher than the corresponding values for H_2NMe (191.5 kcal mol^{-1}) and H_2NPh (188.2 kcal mol^{-1}).

Since both the borolyl and phenyl systems are electronically related, these differences cannot be explained by conjugation effects between the nitrogen and the π systems of the borolyl and phenyl group, respectively. It is postulated that the high value for $H_2NB(NMeCH)_2$ arises from the σ-effect present in the $NB(NMeCH)_2$ fragment, originating from the electropositive nature of the boron atom. DFT calculations have shown that the borolyl group raises the σ-donor orbital on the nitrogen, thus making it a stronger σ-donor itself.[6,18] As a consequence, it was shown that the nitrogen in the $NB(NDippCH)_2$ group forms relatively stronger σ-bonds compared to the alkyl and aryl substituted

congeners.[6] This observation can rationalise the relatively stronger N–H bonds in the $H_2NB(NDippCH)_2$ amine as well.

Overall, the condensation reaction using $H_2NB(NDippCH)_2$ was calculated to be endothermic, featuring a ΔE_{exch} value of +7.5 kcal mol^{-1}. By contrast, imine formation using H_2NMe (ΔE_{exch} = 0.0 kcal mol^{-1}) and H_2NPh (ΔE_{exch} = -4.1 kcal mol^{-1}) were found to be more exothermic, agreeing with the experimental observations.

Next, the titanium imide mediated imine formation is studied to better understand the overall impact of both the Ti=N and the organic framework bond dissociation energies. The model thermodynamic cycle in Scheme 3.12 shows the reaction between model substrates $CpTi\{MeC(NMe)_2\}(NR)$ (R = Me (**1Q_Me**), Ph (**1Q_Ph**), BR'$_2$ = $B(NMeCH)_2$) (**1Q_B(NMeCH)$_2$**) and PhC(H)O to form Cp*Ti(HPP)(μ-O) (**1Q_O**) and Ph(H)C=NR with R = Me, Ph, and $B(NMeCH)_2$, and the corresponding BDEs, respectively.



Scheme 3.12 Energy decomposition scheme for selected isodesmic multiple bond exchanges and computed bond dissociation energies for the teaction of $CpTi\{MeC(NMe)_2\}(NR)$ (R = Me, Ph, BR'$_2$ = $B(NMeCH)_2$) with PhCHO (ΔE, kcal mol^{-1}). All species are spin state singlets except for the fragments $CpTi\{MeC(NMe)_2\}$, O, and NR which are spin triplets and H which is a spin doublet. $\Delta E_{exch} = \Delta E_1 + \Delta E_2 - \Delta E_3 - \Delta E_4$.

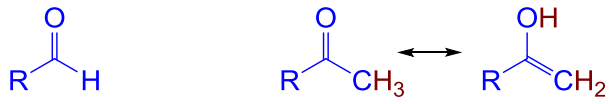
The BDE values for Ti=NR were found to be lower in the cases of R = Me (109.7 kcal mol^{-1}) and R = Ph (108.2 kcal mol^{-1}), compared to R = $B(NMeCH)_2$ (119.6 kcal mol^{-1}). This trend parallels the one previously described for the corresponding N–H bond dissociation

energies, and can be explained by the tendency of the $NB(NMeCH)_2$ fragment to form stronger nitrogen based σ-bonds.[6,18] Although the Ph(H)C=O BDE is higher than the Ph(H)C=NMe, Ph(H)C=NPh and Ph(H)C=$NB(NMeCH)_2$ BDEs (175.2 *vs*. 144.0, 133.4 and 140.7 kcal mol^{-1} respectively), the Ti=O BDE (166.3 kcal mol^{-1}) more than compensates for this contribution. Overall, the reactions are all found to be exothermic, with ΔE_{exch} values of -22.1, -16.2 and -15.5 kcal mol^{-1} for **1Q_NMe, 1Q_Ph** and **1Q_B(NMeCH)2**, respectively, in line with experimental results. It is important to note that these calculations do not consider the dimerisation reaction that follows the formation of monomeric CpTi(HPP)(μ-O). The dimerisation process using the full system Cp*Ti(HPP)(μ-O) was calculated to be -39.4 kcal mol^{-1}, thus represents an additional thermodynamic driving force to form the imines.

In conclusion, although alkyl- and arylamines could be condensated using tolylaldehyde to form the corresponding imines arylimines Tol(H)C=NR (R = alkyl, aryl), the relatively stronger N–H bonds in borylamines H_2NBR_2 render this transformation thermodynamically unfavourable in this case. By contrast, Ti=NR/C=O metathesis reactions between titanium alkyl, aryl and borylimides with aldehydes were found to be exothermic in all cases. The formation of strong titanium oxygen bonds, as well as the following dimerisation of the titanium oxo compounds represent large thermodynamic driving forces for the reactions. Thus, this reaction is shown to be a more general route towards imines of type $R(H)C=NR'_2$, and particularly useful to furnish iminoboranes of type $R(H)C=NBR'_2$.

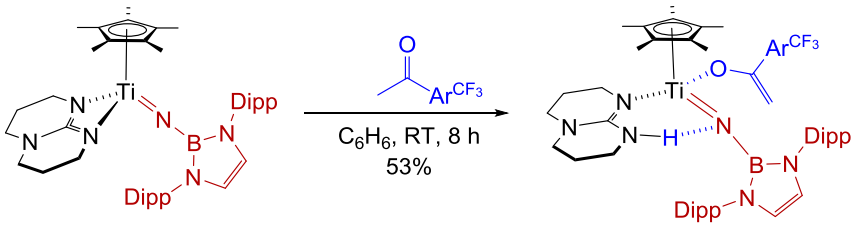
3.5.2 Reactions with ketones

There was no reaction when Cp*Ti(HPP){NB(NDippCH)$_2$} (**1.83**) was treated with benzophenone, even under extended periods of heating. Presumably, compared to the case of TolCHO in which metallacycle formation was observed, substitution of H to Ph at carbon C_1 renders the analogous metallacycle sterically too encumbered to be formed. Furthermore, the formation of a titanium enolate was impossible due to the absence of α-H atoms (Scheme 3.13).



Scheme 3.13 Left: Aldehyde lacking protons in alpha position to the carbonyl group. Right: A related ketone featuring three α-protons marked in red, and the corresponding enolate form.

In the case of enolisable ketones, different chemistry was observed. Treating **1.83** with MeC(O)Ar^{CF_3} in C_6D_6 at RT led to an immediate colour change from brown to red. Inspection of the ^{1}H NMR revealed quantitative formation of a single product which was isolated in 53% yield on the preparative scale. The analytic signature of this species speaks against a structure of a [2 + 2] cycloaddition in favour of titanium enolate formation, depicted in Equation 3.3.



1.83 **3.31**

Equation 3.3

The ^{13}C-NMR spectrum shows no diagnostic resonances in the region 80-90 ppm, expected for a metallacycle by analogy with Cp*Ti(HPP){N(B(NDippCH)$_2$)C(H)(Tol)O} (**3.28**). The ^{1}H NMR spectrum features two singlets at 5.09 and 5.00 ppm integrating to 1 H, respectively, both bound to the same carbon shifted to 92.1 ppm, a value typical for olefins. Noteworthy, one of these singlets is broadened while the other one is sharp and will be

discussed later. At 3.7-3.5 ppm, there are two overlapping septets corresponding to the C<u>H</u>Me$_2$ moieties of the Dipp groups, in line with a C1 symmetric molecule. The CH<u>Me</u>$_2$ groups are located at 1.39, 1.32, and 1.29 ppm, with corresponding integrals of 6, 6 and 12, respectively. Additionally, the infrared (NaCl plates, Nujol mull) spectrum shows no signal in the range typical for carbonyls (1800-1650 cm^{-1}). However, a strong signal at 1608 cm^{-1} is observed, typical for C=C stretches adjacent to oxygen atoms.[57] The ^{1}H NMR spectrum reveals a broad singlet at 6.08 ppm which does not feature cross-correlations with any ^{13}C resonances in the HSQC or HMBC spectra, and which we thus assign to a NH moiety. The infrared (NaCl plates, Nujol mull) spectrum shows a signal at 3229 cm^{-1}, in line with a N–H stretch whose broadened feature indicates hydrogen bonding. These observations are all in line with an O-bound enolate Cp*Ti(HPP-H){NB(NDippCH)$_2$}{OC(CH$_2$)Ar^{CF_3}} (**3.31**) shown in Equation 3.3.

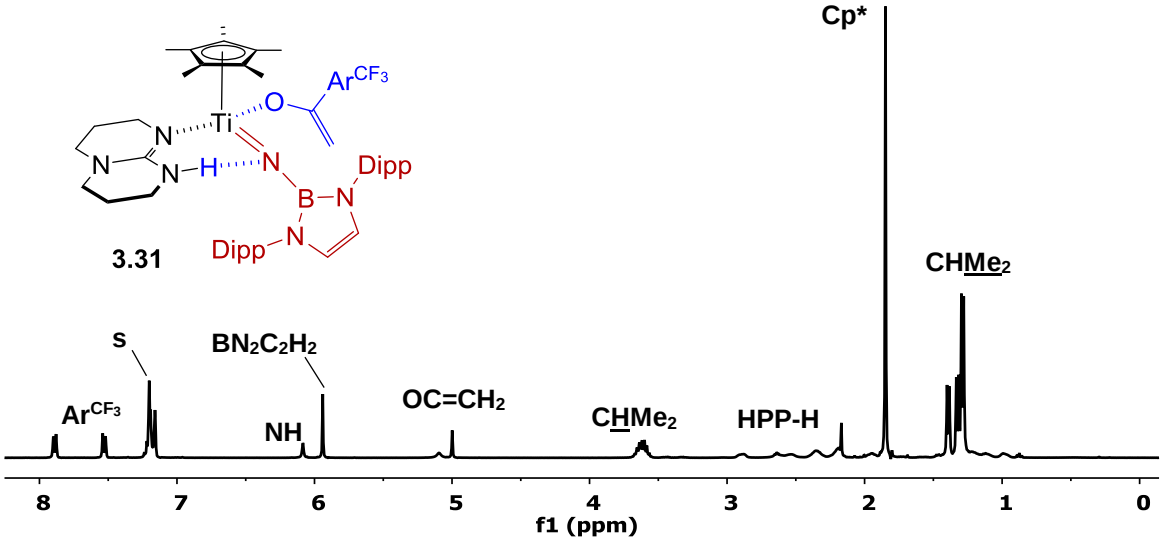
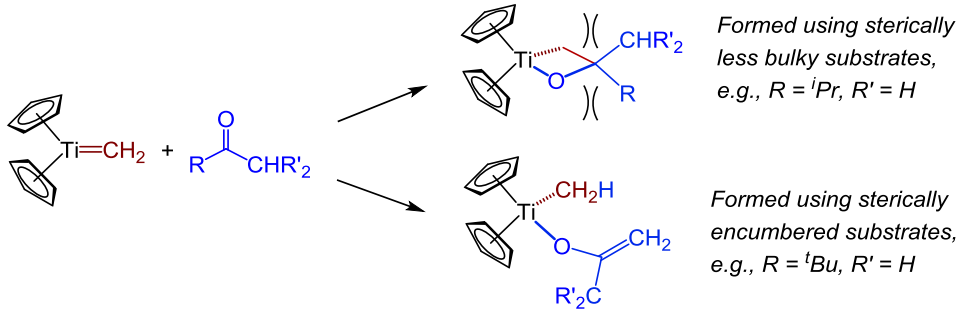


Figure 3.5 ^{1}H NMR spectrum (400.1 MHz) of Cp*Ti(HPP-H){NB(NDippCH)$_2$}{OC(CH$_2$)Ar^{CF_3}} (**3.31**) in C$_6$D$_6$ at 298 K. "s" denotes residual protio solvent.

The observed reaction outcome can be rationalised by the large steric demand of the borolyl ligand in **1.83**. Metallacycles that would be formed *via* [2 + 2] cycloaddition are sterically crowded, and thus the competing enolate formation pathway is favoured. Analogous observations were previously made by Grubbs *et al.*, who reported reactions between the

titanium methylidene $Cp_2Ti{=}CH_2$ and enolisable ketones (Scheme 3.14).[58] In the case of ^{i}PrC(O)Me, [2 + 2] cycloaddition occurred to form a titanacene metallacycle, followed by cycloreversion. By contrast, the slightly more bulky ^{t}BuC(O)Me gave exclusive *O*-bound enolate formation instead, and was surmised due to steric reasons.



Scheme 3.14 Reaction of $Cp_2Ti{=}CH_2$ with RCOMe. Top: [2 + 2] cycloaddition to form metallacycles. For bulky ketones this product features unfavourable steric clashes. Bottom: Enolate formation observed for bulky ketones.

It is noted that enolates generally bind with the oxygen to the metal center for early transition metals, while the (softer) late transition metal enolates are often carbon-bound.[59–63] Similar reactions were also reported by Bergman *et al.* using a zirconium imide system with a variety of ketones, affording analogous *O*-bound Group 4 amide enolate species.[64]

Diffraction quality crystals of Cp*Ti(HPP-H){NB(NDippCH)$_2$}{OC(CH$_2$)Ar^{CF_3}} (**3.31**) were grown from a saturated hexane solution at -30 °C, and solid state structure is shown in Figure 3.7. Compound **3.31** has a three-legged piano stool geometry with a η^5-Cp*, η^1-borylimido, a κ^1-*N*-bound HPP and an κ^1-*O*-bound enolate ligand. The Ti–N–B linkage is of particular interest.

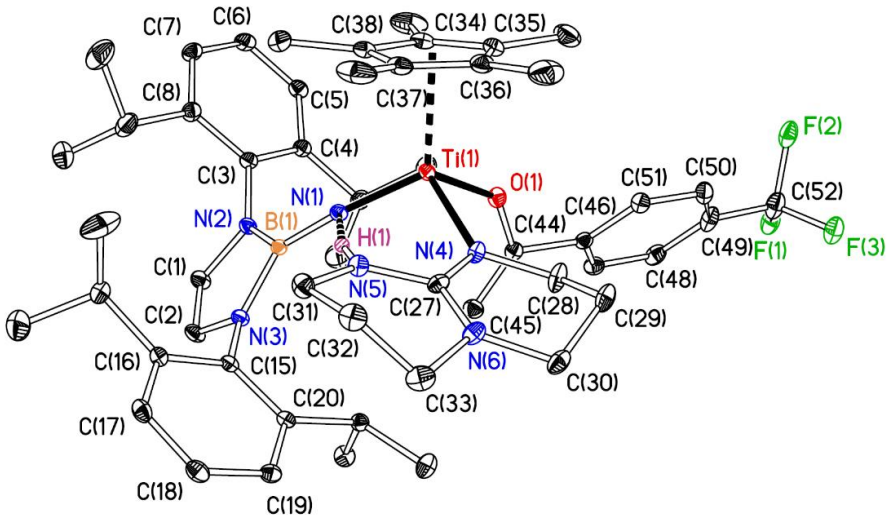


Figure 3.7 Displacement ellipsoid plot (20% probability) of Cp*Ti(HPP-H){NB(NDippCH)$_2$}{OC(CH$_2$)Ar^{CF_3}} (**3.31**). C-bound H atoms are omitted for clarity. H(1) is drawn as a sphere of arbitrary radius.

Table 3.2 Selected bond distances (Å) and angles (°) for Cp*Ti(HPP-H){NB(NDippCH)$_2$}{OC(CH$_2$)Ar^{CF_3}} (**3.31**). Cp$_{cent}$ refers to the computed η^5-Cp* ring centroid.

Ti(1)–N(1)	1.7603(17)	Ti(1)–O(1)–C(44)	141.3(1)
Ti(1)–N(4)	2.1193(17)	Ti(1)–N(1)–B(1)	164.3(1)
Ti(1)–O(1)	1.9194(15)	O(1)–C(44)–C(45)	124.9(2)
N(1)···B(1)	1.420(3)	C(45)–C(44)–C(46)	121.5(2)
N(1)–H(1)	2.23(3)		
N(5)–H(1)	0.86(3)		
B(1)–N(2)	1.466(3)		
B(1)–N(3)	1.466(3)		
O(1)–C(44)	1.331(3)		
C(44)–C(45)	1.336(3)		

Inspection of the Ti–N bond suggests significant multiple bond character, but somewhat reduced as compared to the formal triple bond of the parent borylimide Cp*Ti(HPP){NB(NDippCH)$_2$} (**1.83**): Ti(1)–N(1) of 1.7603(17) Å in **3.31** is slightly elongated compared to the corresponding value for the borylimide **1.83** at 1.7433(19) Å, but significantly shorter than expected for a Ti–N borylamide single bond, e.g., 1.9670(10) and 1.9558(14) Å for titanium amide acetylides Cp*Ti(HPP){NH(B(NDippCH)$_2$)}(CCAr)

with Ar = Ar^{CF_3} (**3.5**), and Ar = Ar^{F} (**3.6**), respectively. The Ti(1)–N(1)–B(1) bond angle is 164.33(14)°, and lies between that of the starting material **1.83** at 176.00(17)°, and the borylamides **3.5**, and **3.6** featuring values of 147.45(8) and 141.07(12)°, respectively.

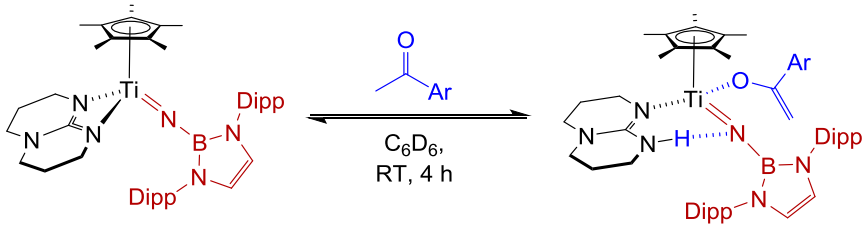
The H(1) atom was found on the Fourier difference map, and featured a N(5)–H(1) bond length of 0.86(3) Å. Interestingly, the N(1)···H(1) distance of 2.23(3) Å is significantly shorter than the sum of the van-der-Waals radii of nitrogen and hydrogen (2.65 Å), giving evidence for the presence of hydrogen bonding.[65] Furthermore, the ^{11}B spectrum features a singlet signal at 20.8 ppm, a value close to those observed for related borylamides, which reflects that the H(1) is being shared between N(1) and N(5) in solution, *via* hydrogen bonding.

Previously, the ^{1}H NMR spectrum was discussed to feature one sharp and one broadened C=C(45)H_2 resonance. In the solid state structure, the C(45)H_2···N(1) distance between the closest hydrogen atom and N(1) is 2.973(1) Å, which is larger than the sum of the van-der-waals radii of N and H (2.7 Å).[66] Although there is no evidence for a hydrogen bond in the solid state, the distance is relatively small and there might be interactions in the solution phase which could explain the broadening observed in the ^{1}H NMR spectrum.

The previously bidentate κ^2-*N*,*N'*-bound HPP ligand has been protonated to afford a κ^1-*N*-bound HPP-H ligand. In the starting material **1.83**, the N(5)–C(27)–N(4) unit showed very similar bond lenghts (1.348(3) Å for N(4)–C(27), and 1.332(3) for N(5)–C(27)), suggesting a uniform delocalization of the negative charge of the HPP(-1) ligand. By contrast, compound **3.31** now features a more asymmetric N(5)–C(27)–N(4) unit, indicative of a localized imine double bond. The N(5)–C(27) bond is lengthened to 1.355(3) Å, typical for N–C single bonds with sp^3 hybridized N and sp^2 hybridized C, and the N(4)–C(27) bond is shortened to 1.318(3) Å, typical for an imine C=N bond. N(5) is oriented towards the

borylimido moiety to form a hydrogen bond, while it is the imine nitrogen N(4) that is bound to the metal centre, forming a Ti–N(4) bond of 2.1193(17) Å.

There is a κ^1-*O*-bound enolate group featuring a Ti–O(1) bond of 1.9194(15) Å. This value lies at the higher end of the range observed for previously reported half-sandwich titanium enolate species (1.826-1.966 Å), which reflects somewhat limited $2p_\pi$-$3d_\pi$ interactions of the oxygen lone pairs with the titanium centre.[67–69] This can be due to several factors. First, there is π-bonding competition between Ti(1)–O(1), Ti(1)–N(1) as well as Ti(1)–N(4) ($2p_\pi$-$3d_\pi$). Additionally, the oxygen atom is bound to the sp^2 hybridized carbon C(44), and conjugated to an extended π-system comprised of the alkene and aryl moiety. The sum of angles subtended at C(44) are 360(2)° confirm the sp^2-hydridised nature of the atom. Finally, the borolyl unit is sterically demanding and might contribute to an elongated Ti(1)–O(1) bond.



1.83

Ar = Ph (**3.32**), Ar^{OMe} (**3.33**)

Scheme 3.15 Reversible reactions of **1.83** with MeC(=O)Ar to form titanium enolates Cp*Ti(HPP-H){NB(NDippCH)$_2$}{OC(CH$_2$)Ar}, with Ar = Ph (**3.32**), and Ar = Ar^{OMe} (**3.33**), respectively. K_{eq}^{298K} = 86 M^{-1} for Ar = Ph, and 21 M^{-1} for Ar = Ar^{OMe}.

To study the electronic effect of the aryl group on the chemical behaviour we have varied the *para* substituent X in the MeC(O)-4-C$_6$H$_4$X ketone starting materials. When more electron rich congeners (X = H, OMe) were tested, both ketones reacted cleanly to give analogous titanium enolate species Cp*Ti(HPP-H){NB(NDippCH)$_2$}{OC(CH$_2$)Ar}, with Ar = Ph (**3.32**), and Ar = Ar^{OMe} (**3.33**), respectively. The ^{1}H, ^{11}B, and ^{13}C spectra were completely analogous to those obtained for **3.31**, excluding the possibility for [2 + 2] cycloaddition. Additionally, the spectroscopic signature suggests an analogous isomeric

structure for both molecules. In particular, the ^{11}B shifts of 20.1 and 20.3 ppm and the ^{1}H shifts of NH at 6.08 and 6.07 ppm agree well with the ones observed for **3.31** (20.8 ppm and 6.08 ppm) so that we assign an analogous chemical structure to that depicted in Scheme 3.15 for **3.32** and **3.33**.

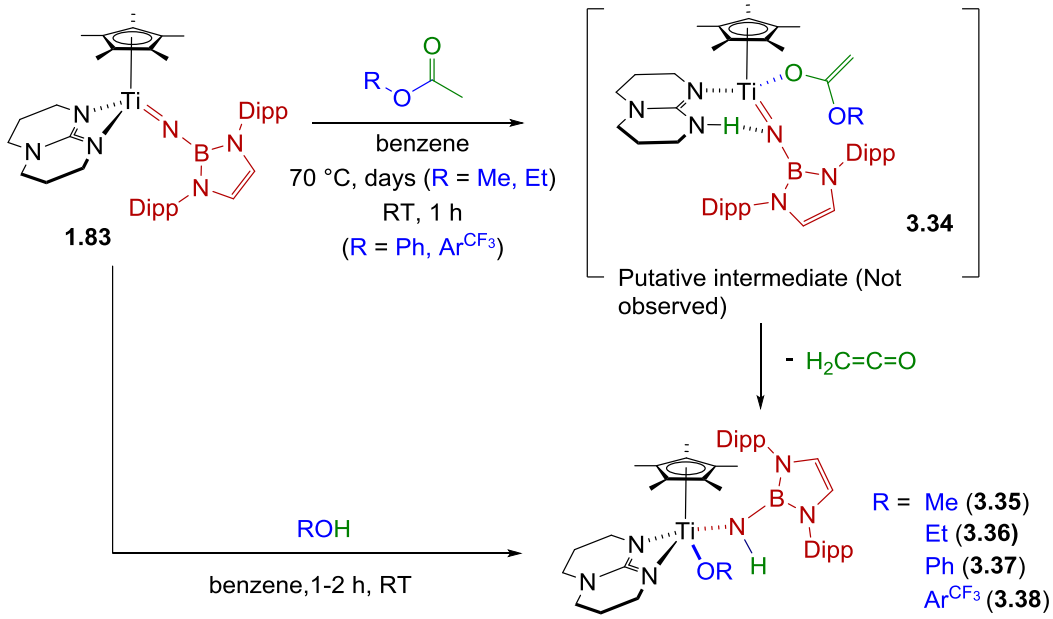
In contrast to Ar = Ar^{CF_3}, the reactions using Ar = Ph, Ar^{OMe} were observed to be in equilibrium with the starting materials, paralleling the results observed for the previously described alkynes. The equilibrium constants were determined by quantitative ^{1}H NMR integration to be K_{eq}^{298K} = 86 (9) M^{-1} and 21 (2) M^{-1}, the corresponding Gibbs free energies to be $\Delta_r G°$= -2.6(3) and -1.8(2) kcal mol^{-1}, for X = H, and X = OMe, respectively. Complexes **3.31-3.33** are stable in solution for weeks without appreciable decomposition, and upon heating the equilibrium is driven to the side of the starting materials, without further reactions.

The more electron deficient, and thus more acidic the aryl ketone starting material, the further the equilibrium is shifted towards metal enolate formation. It is interesting to note in this context that the formed titanium oxygen bonds are relatively weak in nature. Comparisons can be made to the related titanium alkoxy complexes Cp*Ti(HPP)(NH{B(NDippCH)$_2$})(OR) with R = Me (**3.35**) and (**3.36**), which will be discussed in depth later in this Chapter. The Ti(1)–O(1) bonds of 1.8069(8) and 1.8096(13) Å for **3.35** and **3.36**, respectively, are much shorter than the corresponding value of 1.9194(15) Å observed in Cp*)Ti(HPP-H){NB(NDippCH)$_2$}{OC(CH$_2$)Ar^{CF_3}} (**3.31**). This elongation indicates a lower bond order (weaker $2p_\pi$-$3d_\pi$ interactions) between the metal and the oxygen atom in **3.31**. This could be explained by C(44) being sp^3-hybridised in **3.35** and **3.36**, and thus there can be no competing π-interactions between O(1) and C(44).

3.5.3 Reactions with esters

Differing reaction outcomes were observed when borylimide **1.83** was reacted with tolylaldehyde, benzophenone, and acetophenone, depending on the accessibility of α-protons and steric bulk. Since no reactions of metal-nitrogen multiple bonded complexes with esters of type MeC(O)OR have been reported, it was of interest to extend this type of chemistry using a variety of esters as well.

When the dried and pre-distilled esters MeC(O)OR (R = Me, Et) were subjected to Cp*Ti(HPP){NB(NDippCH)$_2$} (**1.83**) on the NMR tube scale, no reaction was observed below 70 °C, when monitored *via* ^{1}H NMR spectroscopy. At this temperature, the starting materials were slowly converted to a single major species, and the color of the reaction mixture changed from brown to light red in both cases (Scheme 3.16.). Higher temperatures led to decomposition - a complex mixture of intractable compounds was observed along with gradual formation of yellow precipitate, which was identified as [Cp*Ti(HPP)(μ-O)]$_2$ (**3.22**).



Scheme 3.16 Reactions of Cp*Ti(HPP){NB(NDippCH)$_2$} (**1.83**) with esters MeOC(O)R and the corresponding free alcohols to form alkoxy/aryloxylates with R = Me (**3.35**), Et (**3.36**), Ph (**3.37**), and Ar^{CF_3} (**3.38**), respectively. The reactions are proposed to proceed *via* enolate intermediate **3.34** for the case of the esters.

In the case of MeC(O)OMe, we were able to successfully isolate the major species after 2 days at 60 °C on the preparative scale in 20% crystalline yield, and identify it as the titanium methoxy complex Cp*Ti(HPP){NH(B(NDippCH)$_2$)](OMe) (**3.35**). In the case of MeC(O)OEt, the reaction could not be scaled-up cleanly. Nevertheless, we were able to independently synthesise the major product *via* an alternative route (*vide infra*), and confirm the identitiy to be the corresponding titanium ethoxy complex Cp*Ti(HPP){NH(B(NDippCH)$_2$)}(OEt) (**3.36**), as judged by NMR spectroscopy.

Surprisingly, we did neither find any evidence for the expected [2 + 2] cycloaddition nor enolate type pathways observed for aldehydes and ketones, respectively. In particular, there were no ^{13}C resonances in the diagnostic region for titanium azametallacycles in analogy to Cp*Ti(HPP){N(B(NDippCH)$_2$}C(H)(Tol)O)} (**3.28**), or alkene protons as expected for titanium enolates in analogy to species **3.31**-**3.33**, observed with enolizable ketones.

The ^{11}B NMR spectrum reveals single resonances at 24.0 and 24.4 ppm, for R = Me, Et, respectively, indicating titanium borylamido species. The IR spectra confirm the presence of NH moieties with observed ν(N–H) stretching signals at 3329 and 3336 cm^{-1}, respectively. Surprisingly, no signals were observed in the region diagnostic for C=O and C=C stretch frequencies of 1765-1645 and 1600-1690 cm^{-1}, respectively.[57] Additionally, the ^{1}H NMR signals reveal only the presence of a Me or Et moiety, for the case of R = Me or Et, respectively, besides the signals for the supporting ligands Cp*, HPP and the borylamide. This leaves a total of 2 protons missing by atom mass balance (starting from the two reactants). These results are all in line for the formation of titanium alkoxy species Cp*Ti(HPP)(NH{B(NDippCH)$_2$})(OR) (R = Me (**3.35**), Et (**3.36**), Scheme 3.16). Analogous titanium aryloxy compounds Cp*Ti(HPP){NH(B(NDippCH)$_2$)}(OR) (R = Ph (**3.37**), R = Ar^{CF_3} (**3.38**)) are observed when MeC(O)OR, with R = Ph and Ar^{CF_3} were used as esters, but will be discussed later.

To confirm the proposed identities of species **3.35**-**3.38**, we synthesized these compounds independently *via* protonolysis using the corresponding free alcohols and Cp*Ti(HPP){NB(NDippCH)$_2$} (**1.83**) (Scheme 3.16). The ^{1}H NMR spectra obtained from the independently synthesised compounds and the ones obtained using the corresponding esters matched.

These protonolysis reactions proved to be rapid, and an instant color change to red was observed upon addition of the respective alcohol to C_6D_6 solutions of **1.83**, respectively. For MeOH and EtOH, the reactions were quantitative on the NMR tube scale, and when the reaction using EtOH was scaled up, the titanium ethoxy complex Cp*Ti(HPP){NH(B(NDippCH)$_2$)}(OEt) was obtained in 90% yield after removal of the volatiles, without further purification. By contrast, the more acidic PhOH and Ar^{CF_3}OH showed some degree of "overprotonation", forming ca. 33-45% of free borylamine H$_2$NB(NDippCH)$_2$ as side product.

Diffraction quality crystals were grown from saturated hexane solutions at 0 °C for Cp*Ti(HPP){NH(B(NDippCH)$_2$)}(OR) (R = Me (**3.35**) and R = Et (**3.36**), Figure **3.7** and Table **3.3**), confirming the identity of these species. The two complexes both feature a four-legged piano stool-type geometry with a η^5-Cp*, HPP, the alkoxy and borylamido ligands. In this case, it is the borylimido ligand that was protonated during the reactions, in analogy to the reactions using alkynes, but in contrast to the chemistry observed with ketones as evidenced by the parameters of the Ti(1)–N(1)–B(1) linkage. The Ti–N bond lengths are elongated to 2.0068(9) and 2.0121(14) Å for **3.35** and **3.36**, respectively, which are slightly longer than the corresponding bonds in Cp*Ti(HPP){NH(B(NDippCH)$_2$)}(CCAr), Ar = Ar^{CF_3} (**3.5**) and Ar = Ar^F (**3.6**) at 1.9670(10) Å and 1.9558(14) Å, respectively. This elongation may be attributed to the additonal π-bonding competition between Ti(1)–N(1) as well as Ti(1)–O(1) ($2p_\pi$-$3d_\pi$). Additionally, the Ti(1)–N(1)–B(1) angles of 138.65(8) and

141.19(11)° (compared to 176.00(17)° in **1.83**) are consistent with sp^2 hybridisation at the N(1) site.

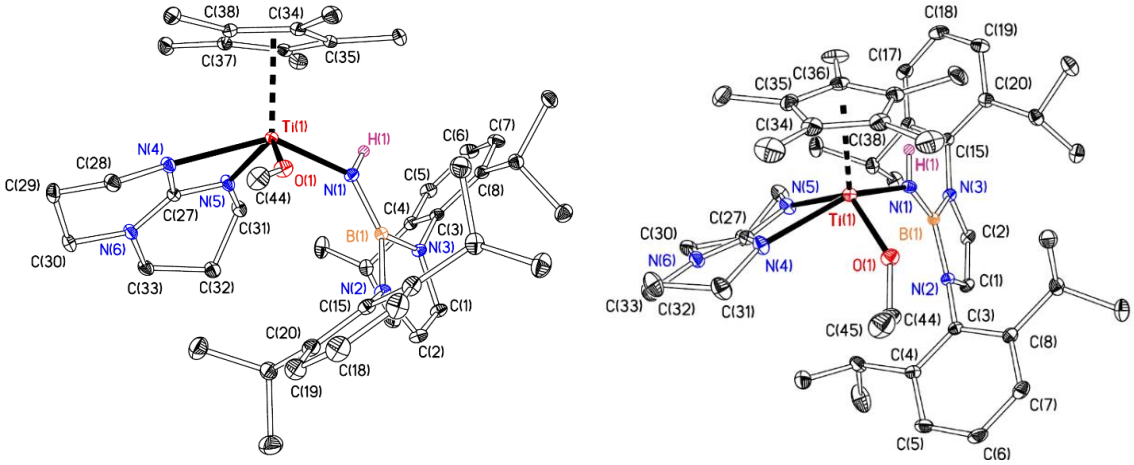


Figure 3.7 Displacement ellipsoid plots (20% probability) of Cp*Ti(HPP){NH(B(NDippCH)$_2$)}(OR) with R = Me (**3.35**), and Et (**3.36**). C-bound H atoms are omitted for clarity.

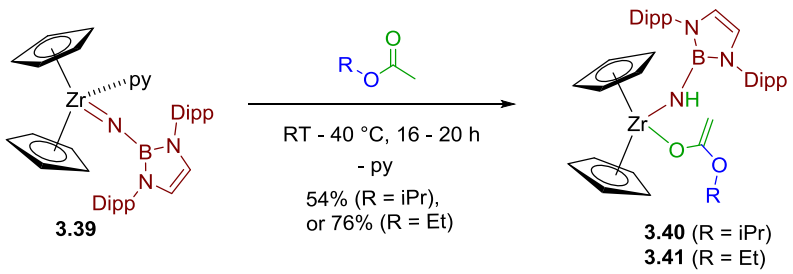
Table 3.3 Selected bond lengths (Å) and angles (°) for Cp*Ti(HPP){NH(B(NDippCH)$_2$)}(OMe) with R = Me (**3.35**), and Et (**3.36**).

Parameter	**3.35**	**3.36**
Ti(1)–N(1)	2.0068(9)	2.0121(14)
Ti(1)–N(4)	2.2277(9)	2.2294(16)
Ti(1)–N(5)	2.0800(10)	2.0791(15)
Ti(1)–O(1)	1.8069(8)	1.8096(13)
N(1)–H(1)	0.917(19)	0.88(3)
N(1)–B(1)	1.4246(14)	1.415(2)
O(1)–C(44)	1.3913(15)	1.370(3)
Ti(1)–N(1)–B(1)	138.65(8)	141.19(11)

In full analogy to the crystallographically observed titanium ketone enolate species Cp*Ti(HPP-H){NB(NDippCH)$_2$}{OC(CH$_2$)Ar^{CF_3}} (**3.31**) obtained from treating the title compound **1.83** with enolizable ketone MeC(O)Ar^{CF_3}, we propose ester enolates of the type Cp*Ti(HPP-H){NB(NDippCH)$_2$}{OC(CH$_2$)OR} (**3.34**, R = Me, Et, Ph, Ar^{CF_3}) as possible intermediates in our reactions. These are proposed to be transient due to the possibility of

the ester enolate Ti–OC(CH_2)OR moiety to rearrange to form a Ti–OR bond with concomitant release of ketene H_2CCO. Unfortunately, the observation of complicated mixtures of products and harsh reaction temperatures of 70 °C hampered any attempts to detect or trap the extremely sensitive, putative, ketene H_2CCO.

This work represents the first examples of reactions between methyl esters with transition metal nitrogen multiple bonded complexes. Inspired by this novelty, Dr Bowen Xie, another previous D.Phil student in the Mountford group, subsequently started analogous reactions between methyl esters and zirconocene borylimido complex **3.39** (Equation 3.5).[45] **3.39** reacted with MeC(O)OR (R = Et, ^{i}Pr) to form the expected ester enolate species $Cp_2Zr\{NHB(NDippCH)_2\}\{OC(CH_2)CH_2CO_2R\}$ (R = ^{i}Pr (**3.40**), Et (**3.41**)). Importantly, for R = ^{i}Pr the compound was isolated and structurally authenticated *via* X-ray crystallography. Importantly, when zirconocene enolate ester **3.40** was heated to 60 °C for 16 h, it was demonstrated that ketene H_2CCO was eliminated to undergo a self-trapping reaction with the starting material, and this self-trapped product has been structurally authenticated *via* X-ray crystallography as well. However, in analogy to our system, ketenes were never directly observed *via* ^{1}H NMR spectroscopy, presumably due to their high reactivity.

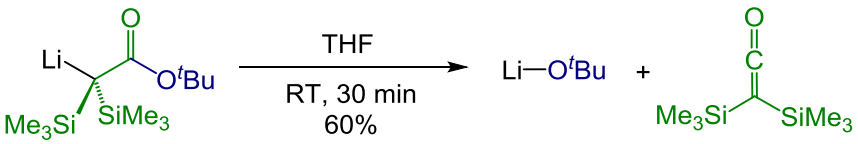


Equation 3.5

Since the zirconium borylimide compound $Cp_2Zr\{NB(NDippCH)_2\}$ (**3.39**) is analogous to the studied titanium borylimide $Cp^*Ti(HPP)\{NB(NDippCH)_2\}$ (**1.83**), these reactions give

further support for the proposed titanium ester enolate intermediate proposed above, followed by ketene elimination.

In fact, enolate cleavage reactions forming alcoholates and ketenes have been previously invoked too. For example, in 1965, Vaughan suggested a ketene intermediate for the self-condensation of the reagent prepared from ethyl α-bromoisobutyrate and zinc metal,[70] and later Trost reported the first isolation of a ketene from the decomposition of an ester enolate in 1977.[71] The lithiated ester enolate $(SiMe_3)_2CLiC(=O)O\textit{t}Bu$ decomposed upon warming into $(SiMe_3)_2CCO$ and $LiO\textit{t}Bu$, and further examples of lithiated ester enolates to form ketenes followed (see Eq. 3.6).[9,72–75]



Equation 3.6

In contrast to the previously discussed reactions using alkyl esters with **1.83**, the reaction conditions were found to be milder for the related aryl esters MeC(O)OR with R = Ph and Ar^{CF_3}. The reactions occurred at room temperature over 1 hour, by which time two main organometallic species were observed in each case: titanium aryloxy species Cp*Ti(HPP){NH(B(NDippCH)$_2$)}(OR) with R = Ph (**3.37**), or Ar^{CF_3} (**3.38**), respectively, as well as an additional compound Cp*Ti(HPP){OC(=CH$_2$)N(B(NDippCH)$_2$}) (**3.42**), which was found to be universally formed, independent which arylester was used (see Figure 3.8).

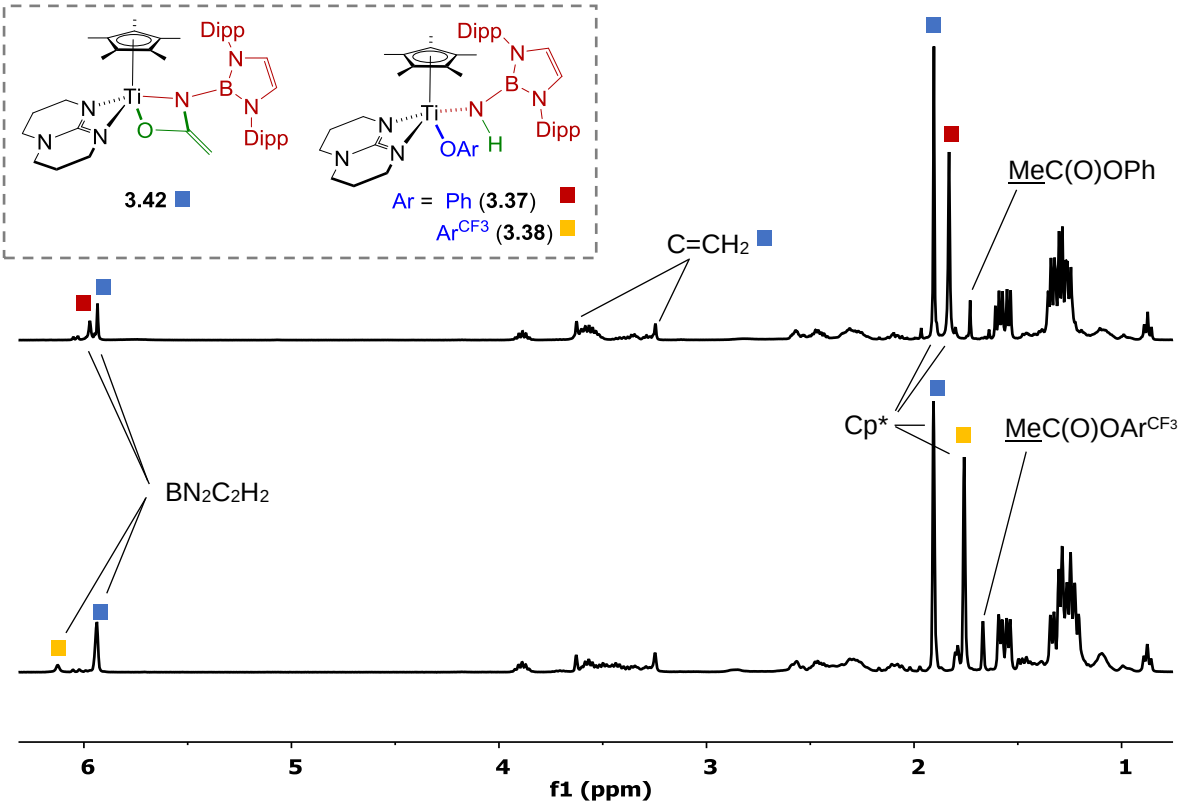
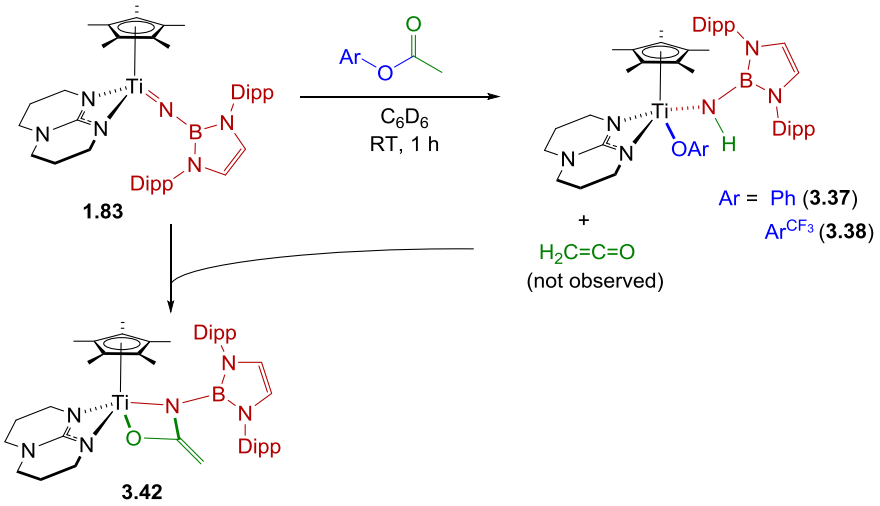


Figure 3.8 Partial ^{1}H NMR spectra (400 MHz) of reactions of **1.83** with aryl esters after 1 h in C_6D_6 at 298 K. Top: Reaction using MeC(O)OPh. Bottom: Reaction using MeC(O)OAr^{CF_3}. The squares denote species **3.37**-**3.42** and are depicted in the inset.

Importantly, arylester starting materials MeC(O)OAr were still found to be present in both reactions, and only when a slight excess of borylimide **1.83** to aryl ester ratio was used, there was full conversion of the aryl ester. Titanium aryloxy compounds **3.37** and **3.38** show analogous spectroscopic features as their alkoxy congeners **3.35** and **3.36** and are thus not further discussed. The second main organometallic species Cp*Ti(HPP){OC(=CH$_2$)N(B{NDippCH}$_2$}) (**3.42**) features the typical spectroscopic signature for intact HPP and borolyl moieties, as well as a strong Cp* resonance. Additionally, the ^{1}H NMR spectrum shows two sharp singlets in the alkene region at 3.50 and 3.15 ppm, both of which integrate to 1 proton each. These protons both show HSQC correlations to the same carbon shifted at 63.9 ppm (OC=CH_2), as well as HMBC correlations to a carbon at 159 ppm (OC=CH$_2$). The ^{11}B spectrum features a signal at 14.5

ppm, indicative of a borylamide in which the nitrogen formed a bond to an additional substituent.



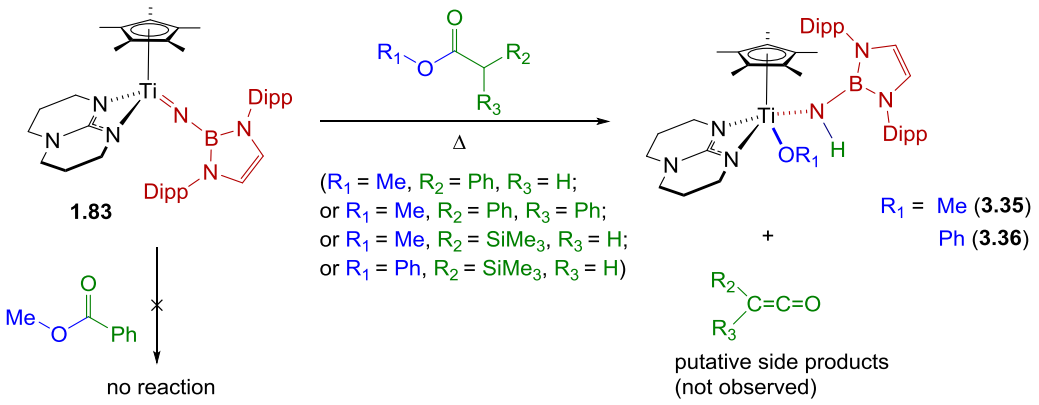
Scheme 3.17 Reactions of Cp*Ti(HPP){NB(NDippCH)$_2$} (**1.83**) with aryl esters MeOC(O)R to form titanium aryloxy Cp*Ti(HPP){NH(B(NDippCH)$_2$)}(OR) with R = Ph (**3.37**), or Ar^{CF_3} (**3.38**), and concomitant release of ketene that is self-trapped with **1.83** to form metallacycle Cp*Ti(HPP){OC(=CH$_2$)N(B(NDippCH)$_2$)} (**3.42**).

These observations all agree with a self-trapping scenario summarised in Scheme 3.17. Borylimide Cp*Ti(HPP){NB(NDippCH)$_2$} (**1.83**) react with aryl esters MeC(O)OAr to form the corresponding aryloxy titanium complexes Cp*Ti(HPP){NH(B(NDippCH)$_2$)}(OR) with R = Ph (**3.37**), or Ar^{CF_3} (**3.38**), with concomittant release of ketene H$_2$CCO. As the reaction proceeds, the formed ketene reacts with starting material **1.83** to form metallacycle Cp*Ti(HPP){OC(=CH$_2$)N(B(NDippCH)$_2$)} (**3.42**). This "self-trapping" can explain the observation that an excess of 1.5-2 equivalents of borylimide **1.83** compared to arylester is necessary to fully consume the aryl ester.

Unfortunately, however, the reaction compounds **3.37-3.42** are found to be unstable, forming a complex mixture of multiple organometallic products preventing the preparative isolation of **3.42**. Furthermore, attempts to synthesize ketene-type metallacycles in analogy to **3.42** failed. For example, when freshly prepared Me$_3$Si(H)CCO was added to **1.83** at -

35 °C, an instant, violent reaction occured resulting in immediate precipitation. The ^{1}H NMR spectrum showed only weak signals of **1.83** and was otherwise featureless, while the precipitate was found to be insoluble in any common NMR solvents and may represent ketene-related polymers.

To further probe the mechanism and complement our evidence for ketene formation during the reaction, we also varied the substituents in $R^{1}OC(O)CR$ (Scheme 3.18). Notably, there is no reaction when non-enolisable ester MeOC(O)Ph is used, highlighting the importance of α-protons to form an enolate for the reaction to occur.



Scheme 3.18 Reactions of Cp*Ti(HPP){NB(NDippCH)$_2$} (**1.83**) with various esters.

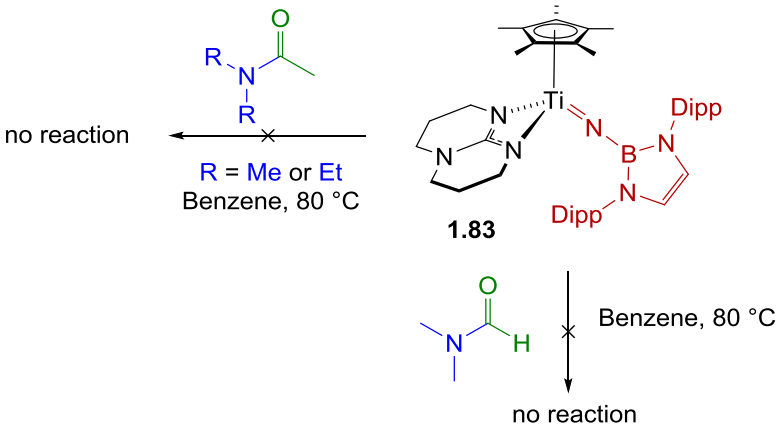
We reasoned that additional steric bulk at the site of enolization R = CHR^2R^3 would potentially stabilize the corresponding ketenes R^1R^2CCO sufficiently to allow for detection. In further agreement with the proposed reaction mechanism (outlined in Scheme 3.14), we form titanium alkoxy/aryloxy species of type Cp*Ti(HPP)(NH{B(NDippCH)$_2$})(OR^1) in all cases (R^1=Me, R^2=Ph, R^3=H; R^1=Me, R^2=$SiMe_3$, R^3=H; R^1=Ph, R^2=$SiMe_3$, R^3=H). However, the reaction was found to be extremely sensitive to steric bulk at this α-position: In all mono-substituted cases extended periods of heating at 60-80 °C is required to drive the reaction, and for disubstituted $MeOC(O)C(H)Ph_2$ the reaction is essentially shut down (the starting complex **1.83** decomposes before product formation is detected). Thus, as we vary the substituents at the

site of enolization to produce more stable ketenes, we require increasingly harsh reaction conditions hampering detection of these putative side products.

3.5.4 Reactions with amides

Next, the reactivity with amides is discussed. *N*,*N*-dimethylformamide Me_2NCHO is sterically open, yet sufficiently stable, and was thus studied first. Given the lack of α-protons required to form an enolate, and the amine moiety being protected by two methyl groups, the most reactive functional group is the carbonyl C=O bond, which, in principle, is amenable to [2 + 2] cycloaddition.

When *N*,*N*-dimethylformamide was subjected to borylimide **1.83** no reaction occurred, even under forcing conditions of extended periods of heating at 80 °C (Scheme 3.19). This observation could be rationalised by the neighbouring nitrogen lone pair donating electron density into the carbonyl moiety, thereby lowering the double bound character required to undergo [2 + 2] cycloaddition with the Ti=N bond of **1.83**.



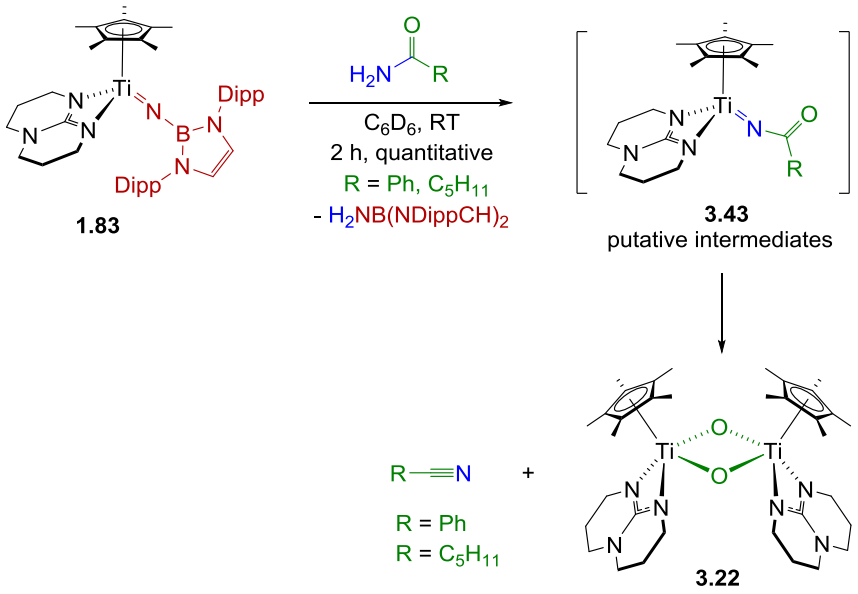
Scheme 3.19 Reactions of *N*,*N*-dimethylformamide, and *N*,*N*-dialkylacetamide, where R = Me or Et, with Cp*Ti(HPP){NB(NDippCH)$_2$} (**1.83**), respectively.

When the carbonyl proton Me_2NCHO is replaced for a methyl group this would allow, in principle, for the formation of an enolate species and thus an analogous chemistry as observed for esters. However, when *N*,*N*-dialkylacetamides Me_2NCOR with R = Me, Et

were subjected to **1.83** no reaction was observed, even under forcing conditions of extended periods of heating at 80 °C (Scheme 3.19). This could again be rationalised by the conjugation effect of the neighbouring nitrogen moiety.

So far, we focused on amides where the nitrogen group is protected *via* alkyl groups. We thus turned our attention to amides featuring protons on the nitrogen (Scheme 3.20). When benzamide H_2NCOPh was subjected to a solution of Cp*Ti(HPP){NB(NDippCH)$_2$} (**1.83**) in C_6D_6 an immediate colour change from brown to red occurred, with a considerable amount of yellow precipitate typical for [Cp*Ti(HPP)(μ-O)]$_2$ (**3.22**) being formed on the bottom of the NMR tube. Inspection of the ^{1}H NMR revealed quantitative formation of benzonitrile along with free borylamine $H_2NB(NDippCH)_2$ (while the μ-dioxo species **3.22** is insoluble in benzene). Since the benzamide H_2NCOPh formally lost an equivalent of H_2O in forming the corresponding nitrile NCPh, this type of reaction is also referred to as dehydration reaction.[76]

For example, Bergman reported a related dehydration of primary amides using Group 4 metals. The reaction was shown to proceed *via* an *N*-acylimidozirconocene intermediate, which then rearranges to form the corresponding zirconium oxo species and organonitrile, in full analogy to Scheme 3.20.[76] Based on this mechanistic work, we propose our reaction to proceed *via* the analogous intermediate **3.43**, formed *via* proton transfers and release of the borylamine (which was detected in its free form in solution), which then rearranges to extrude the organonitrile along with the formation of the μ-dioxo dimer **3.22**. Unfortunately, this overall process is very fast and attempts to observe intermediates **3.43** *via* low temperature NMR failed.



Scheme 3.20 Dehydration reaction of benzamide (R = Ph), and hexanamide (R = C_5H_{11}) with Cp*Ti(HPP){NB(NDippCH)$_2$} (**1.83**) to go *via* proposed intermediates **3.43** to form [Cp*Ti(HPP)(μ-O)]$_2$ (**3.22**) and extrusion of corresponding nitriles.

Additionally, an intramolecular competition experiment was conducted using hexanamide $H_2NC(O)C_6H_{13}$ to probe the relative reaction rates of enolate-type chemistry and dehydration pathways. This amide features α-protons and can thus form enolates. Additionally, the amine moiety is unprotected and could thus also react in a dehydration pathway in analogy to benzamide. When hexanamide was subjected to a benzene solution containing **1.83** in a Young's NMR tube, again the brown colour instantly changed to red. The spectroscopic signature in the NMR spectra revealed a fully analogous picture to the case using benzamide: the reaction proceeded quantitatively to form free borylamine, the organic nitrile, along with μ-dioxo dimer [Cp*Ti(HPP)(μ-O)]$_2$ (**3.22**, Scheme 3.20). The overall dehydration process is thus shown to be more feasible than either of the two alternatives: [2 + 2] cycloaddition or enolate type chemistry observed in the case of ketones.

3.7 Miscellaneous substrates

Borylimide **1.83** was also tested with a variety of different substrate classes, but was found not to react. Tested substrated include alkenes (norbornene, cyclohexene), isonitriles (ethyl, phenyl, and pentafluorophenylisonitrile), epoxides (isobutyleneoxide, cyclohexene oxide, styrene oxide), and halogen containing molecules (methyl iodide, benzyl bromide).

3.8 Conclusions and outlook

This Chapter has described the first comprehensive reactivity study of a Group 4 borylimido compound, namely Cp*Ti(HPP)(NB(NDippCH)$_2$}) (**1.83**), with a variety of unsaturated small molecules. Firstly, the reactions of **1.83** with terminal alkynes afforded titanium acetylide complexes in excellent selectivities *via* terminal C–H bond activation. By varying the electronic properties of the alkynes equilibria were established in some cases, and it was shown experimentally that the more electron poor the alkyne, the more favoured is acetylide formation. By contrast, the thermodynamically generally more stable [2 + 2] cycloaddition products could not be observed, which contrasts to previous reports of Group 4 imido and hydrazido complexes. Benchmarking using analogous Cp*Ti(HPP)(NR) with R = *t*Bu and Xyl systems revealed that the high selectivity for C–H bond activation is likely due to the large steric bulk of the used borolyl unit. However, by use of the highly strained (internal) cyclooctyne we were able to furnish a [2 + 2] cycloaddition product in equilibrium with the starting materials.

Next, heterocumulenes CE_2 and ArNCE (E = O, S; Ar = Tol or Ph), lead to [2 + 2] cycloaddition, followed by extrusion of ECNB(NDippCH)$_2$ and ArNCNB(NDippCH)$_2$, respectively, with concomittant formation of [Cp*Ti(HPP)(μ-E)]$_2$ (E = O (**3.34**), S (**3.35**)).

This reaction formally represents the transfer of the $NB(NDippCH)_2$ unit to organic fragments.

Finally, carbonyl compounds showed a remarkable chemistry with borylimide **1.83**. The model aldehyde tolylaldehyde underwent [2 + 2] cycloaddition followed by slow extrusion to form a relatively rare example of a iminoborane **3.29** and $[Cp^*Ti(HPP)(\mu\text{-}O)]_2$ **3.34**, representing another example of a NBR_2 group transfer reaction to a small organic fragment. Alternative condensation methodologies to form this iminoborane, starting from the corresponding borylamine and tolylaldehyde, failed (in contrast to analogous reactions using *tert*-butylamine).

DFT calculations showed that the N–H bonds are significantly stronger for borylamines H_2NBR_2 than for alkyl- and arylamines, and render this condensation reaction thermodynamically unfeasible. By contrast, Ti=NR/C=O metathesis reactions between titanium alkyl, aryl and borylimides with aldehydes were found to be highly exothermic in all cases. The formation of strong titanium oxygen bonds, as well as the following dimerisation of the titanium oxo compounds represent large thermodynamic driving forces for the reactions. Thus, this reaction is shown to be a more general route towards imines of type $R(H)C{=}NR'_2$, and particularly useful to furnish iminoboranes of type $R(H)C{=}NBR'_2$

By contrast, when enolisable substrates were used, titanium enolate chemistry was observed rather than [2 + 2] cycloadditions. Ketones MeC(O)Ar (Ar = Ar^{CF_3}, Ph or Ar^{OMe}) reacted with the borylimide **1.83** to form equilibrium mixtures of titanium enolate complexes $Cp^*Ti(HPP\text{-}H)\{NB(NDippCH)_2\}\{OC(CH_2)Ar\}$ (Ar = Ar^{CF_3} (**3.31**), Ph (**3.32**) or Ar^{OMe} (**3.33**)), and **3.31** was structurally authenticated. Evaluation of the formed equilibria showed that there is a thermodynamic trend in which the more acidic, less electron rich aryl ketones form the corresponding titanium enolates more favourably. Reaction of enolizable esters with **1.83** formed the corresponding alkoxy or aryloxy

titanium amides which could be independently synthesized from the corresponding free alcohols. The reaction presumably proceeds *via* ketene elimination from titanium enolate ester intermediates, formed in analogy to the described ketone chemistry. Terminal amides engaged in an overall dehydration reaction with borylimide **1.83**, where the corresponding nitriles along with [Cp*Ti(HPP)(μ-O)]$_2$ (**3.34**) and free borylamine $H_2NB(NDippCH)_2$ were formed.

3.9 References

1 P. J. Walsh, M. J. Carney and R. G. Bergman, *J. Am. Chem. Soc.*, 1991, **113**, 6343–6345.
2 A. D. Schofield, A. Nova, J. D. Selby, A. D. Schwarz, E. Clot and P. Mountford, *Chem. – A Eur. J.*, 2011, **17**, 265–285.
3 T. Gehrmann, J. Lloret Fillol, H. Wadepohl and L. H. Gade, *Angew. Chem. Int. Ed.*, 2009, **48**, 2152–2156.
4 B. D. Ward, A. Maisse-Francois, P. Mountford and L. H. Gade, *Chem. Commun. (Camb).*, 2004, 704–705.
5 J. D. Selby, C. D. Manley, M. Feliz, A. D. Schwarz, E. Clot and P. Mountford, *Chem. Commun.*, 2007, 4937–4939.
6 B. A. Clough, S. Mellino, A. V. Protchenko, M. Slusarczyk, L. C. Stevenson, M. P. Blake, B. Xie, E. Clot and P. Mountford, *Inorg. Chem.*, 2017, **56**, 10794–10814.
7 K. Weitershaus, J. Lloret Fillol, H. Wadepohl and L. H. Gade, *Organometallics*, 2009, **28**, 4747–4757.
8 K. Weitershaus, H. Wadepohl and L. H. Gade, *Organometallics*, 2009, **28**, 3381–3389.
9 D. Seebach, R. Amstutz, T. Laube, W. B. Schweizer and J. D. Dunitz, *J. Am. Chem. Soc.*, 1985, **107**, 5403–5409.
10 K. Weitershaus, B. D. Ward, R. Kubiak, C. Müller, H. Wadepohl, S. Doye and L. H. Gade, *Dalton Trans.*, 2009, 4586–602.
11 L. R. Groom, A. D. Schwarz, A. Nova, E. Clot and P. Mountford, *Organometallics*, 2013, **32**, 7520–7539.
12 M. P. Coles and P. B. Hitchcock, *Organometallics*, 2003, **22**, 5201–5211.
13 M. P. Coles, *Chem. Commun.*, 2009, 3659.
14 K. Weitershaus, B. D. Ward, R. Kubiak, C. Müller, H. Wadepohl, S. Doye and L. H. Gade, *Dalt. Trans.*, 2009, 4586.
15 J. L. Polse, R. A. Andersen and R. G. Bergman, *J. Am. Chem. Soc.*, 1998, **120**, 13405–13414.
16 L. C. Stevenson, DPhil Thesis, University of Oxford, 2015.
17 J. L. Polse, R. A. Andersen and R. G. Bergman, *J. Am. Chem. Soc.*, 1995, **117**, 5393–5394.
18 B. Clough, DPhil Thesis, University of Oxford, 2016.
19 H. E. Bryndza, L. K. Fong, R. A. Paciello, W. Tam and J. E. Bercaw, *J. Am. Chem. Soc.*, 1987, **109**, 1444–1456.

20 P. L. Holland, R. A. Andersen, R. G. Bergman, J. Huang and S. P. Nolan, *J. Am. Chem. Soc.*, 1997, **119**, 12800–12814.
21 P. L. Holland, R. A. Andersen and R. G. Bergman, *Comments Inorg. Chem.*, 1999, **21**, 115–129.
22 L. E. Schock and T. J. Marks, *J. Am. Chem. Soc.*, 1988, **110**, 7701–7715.
23 D. D. Wick and W. D. Jones, *Organometallics*, 1999, **18**, 495–505.
24 E. Clot, C. Mégret, O. Eisenstein and R. N. Perutz, *J. Am. Chem. Soc.*, 2006, **128**, 8350–8357.
25 L. R. Groom, A. F. Russell, A. D. Schwarz and P. Mountford, *Organometallics*, 2014, **33**, 1002–1019.
26 L. R. Groom, A. D. Schwarz, A. Nova, E. Clot and P. Mountford, *Organometallics*, 2013, **32**, 7520–7539.
27 P. J. Tiong, L. R. Groom, E. Clot and P. Mountford, *Chem. - A Eur. J.*, 2013, **19**, 4198–4216.
28 P. J. Tiong, A. Nova, L. R. Groom, A. D. Schwarz, J. D. Selby, A. D. Schofield, E. Clot and P. Mountford, *Organometallics*, 2011, **30**, 1182–1201.
29 H. F. Bettinger and H. Bornemann, *J. Am. Chem. Soc.*, 2006, **128**, 11128–11134.
30 H. F. Bettinger, *Inorg. Chem.*, 2007, **46**, 5188–5195.
31 H. F. Bettinger, M. Filthaus, H. Bornemann and I. M. Oppel, *Angew. Chem. Int. Ed.*, 2008, **47**, 4744–4747.
32 H. F. Bettinger, M. Filthaus and P. Neuhaus, *Chem. Commun.*, 2009, 2186–2188.
33 S. Biswas, I. M. Oppel and H. F. Bettinger, *Inorg. Chem.*, 2010, **49**, 4499–4506.
34 H. F. Bettinger and H. Bornemann, *ZAAC*, 2011, **637**, 2169–2174.
35 M. Filthaus, L. Schwertmann, P. Neuhaus, R. W. Seidel, I. M. Oppel and H. F. Bettinger, *Organometallics*, 2012, **31**, 3894–3903.
36 M. Müller, C. Maichle-Mössmer and H. F. Bettinger, *Chem. Commun.*, 2013, **49**, 11773.
37 L. Weber, E. Dobbert, R. Boese, M. T. Kirchner and D. Bläser, *Eur. J. Inorg. Chem.*, 1998, 1145–1152.
38 C. Summerford and K. Wade, *J. Chem. Soc. A*, 1970, 2010–2016.
39 C. Summerford and K. Wade, *J. Chem. Soc. A*, 1969, 1487–1491.
40 A. E. Guiducci, C. L. Boyd, E. Clot and P. Mountford, *Dalton Trans.*, 2009, 5960–5979.
41 W. Einholz and W. Haubold, *Zeitschrift fuer Naturforschung, Tl. B Anorg. Chemie, Org. Chem*, 1986, **41B**, 1367–1372.
42 I. Ruppert, *Angew. Chem. Int. Ed.*, 1977, **89**, 336–338.
43 Aldo E. Guiducci, A. Catherine L. Boyd and P. Mountford, *Organometallics*, 2006, **25**, 1167–1187.
44 G. J. Bullen, *J. Chem. Soc., Dalt. Trans.*, 1973, **0**, 858–863.
45 B. Xie, DPhil Thesis, Oxford University, 2017.
46 C. Summerford and K. Wade, *J. Chem. Soc. A*, 1970, 2010.
47 M. F. Hawthorne, *Tetrahedron*, 1962, **17**, 117–122.
48 V. A. Dorokhov and M. F. Lappert, *Chem. Commun.*, 1968, 250.
49 J. E. Lloyd and K. Wade, *J. Chem. Soc.*, 1964, 1649.
50 S. Itsuno, C. Hachisuka, K. Kitano and K. Ito, *Tehahedron Lelters*, 1992, **33**, 627–630.
51 I. Pattison and K. Wade, *J. Chem. Soc. A Inorganic, Phys. Theor.*, 1967, 1098.
52 C. E. Bacon, L. Mansour, J. J. Hayward and J. M. Rawson, *Dalt. Trans.*, 2015, **44**, 5284–5287.
53 N. Weis, H. Pritzkow and W. Siebert, *Eur. J. Inorg. Chem.*, 1999, **1999**, 7–9.

54 M. D'hooghe, S. Dekeukeleire, K. Mollet, C. Lategan, P. J. Smith, K. Chibale and N. De Kimpe, *J. Med. Chem.*, 2009, **52**, 4058–4062.
55 F. Marilena, L. Ronzini and T. Luigino, *Tetrahedron*, 2008, **64**, 4979–4984.
56 S. Mellino, .
57 E. Pretsch, P. Bühlmann and M. Badertscher, in *Spektroskopische Daten zur Strukturaufklärung organischer Verbindungen*, Springer Berlin Heidelberg, Berlin, Heidelberg, 2010, pp. 273–339.
58 L. Clawson, S. L. Buchwald and R. H. Grubbs, *Tetrahedron Lett.*, 1984, **25**, 5733–5736.
59 F. Balegroune, D. Grandjean, D. Lakkis and D. Matt, *Chem. Commun.*, 1992, **0**, 1084.
60 J. R. Stille and R. H. Grubbs, *J. Am. Chem. Soc.*, 1983, **105**, 1664–1665.
61 M. D. Curtis, S. Thanedar and W. M. Butler, *Organometallics*, 1984, **3**, 1855–1859.
62 W. A. Howard and G. Parkin, *J. Am. Chem. Soc.*, 1994, **116**, 606–615.
63 J. Zabicky, *The chemistry of metal enolates*, John Wiley, 2009.
64 S. Y. L. and and R. G. Bergman, *J. Am. Chem. Soc*, 1996, **118**, 6396–6406.
65 S. S. Batsanov, *Inorg. Mater.*, **37**, 871–885.
66 S. S. Batsanov, *Inorg. Mater.*, 2001, **37**, 871–885.
67 R. Beckhaus, T. Wagner, C. Zimmermann and E. Herdtweck, *J. Organomet. Chem.*, 1993, **460**, 181–189.
68 A. Rodriguez-Delgado, W. R. Mariott and E. Y.-X. Chen, *Macromolecules*, 2004, **37**, 3092–3100.
69 R. Beckhaus, I. Strauss and T. Wagner, *ZAAC*, 1997, **623**, 654–658.
70 W. R. Vaughan, S. C. Bernstein and M. E. Lorber, *J. Organomet. Chem.*, 1967, **30**, 1790–1795.
71 B. M. Trost and Y. Matsumura, *J. Org. Chem.*, 1977, **42**, 2038–2039.
72 R. Haener, T. Laube and D. Seebach, *J. Am. Chem. Soc.*, 1985, **107**, 5396–5403.
73 D. F. Sullivan, R. P. Woodbury and M. W. Rathke, *J. Org. Chem.*, 1977, **42**, 2038–2039.
74 W. You, Y. Li and M. K. Brown, *Org. Lett.*, 2013, **15**, 1610–1613.
75 U. Schöllkopf and J. Hoppe, *Angew. Chem. Int. Ed.*, 1975, **87**, 814–815.
76 R. T. Ruck and R. G. Bergman, *Angew. Chem. Int. Ed.*, 2004, **43**, 5375–5377.

Chapter Four

Synthesis and reactivity of base-free titanium sandwich complexes *via* an oxidative addition route

4.1 Overview

This Chapter describes the synthesis, characterisation and reactivity of novel titanium borylimido complexes. First, the synthesis of new borylazides and titanium borylimide complexes is presented. The base-free titanocene borylimide Cp"$_2$Ti=NBMes$_2$ (**4.1**, Cp" = η^5-C_5H_3-1,3-(SiMe$_3$)$_2$) will be described in depth, and compared to alkyl, aryl, and silyl congeners. Finally, preliminary reactivity studies with **4.1** will be described.

4.2 Introduction

As mentioned in Chapter One, the Mountford group extended the amine exchange methodology to establish the first rational synthetic protocols for titanium borylimido complexes of type (L)Ti=N–BR$_2$. Titanium borylimides featuring a variety of different supporting ligand sets were synthesised, including guanidinato-cyclopentadienyl as well as several tridentate diamide-amine supported complexes (Figure 4.1).[1]

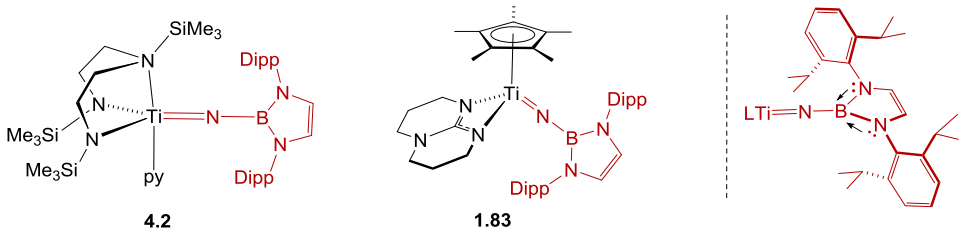
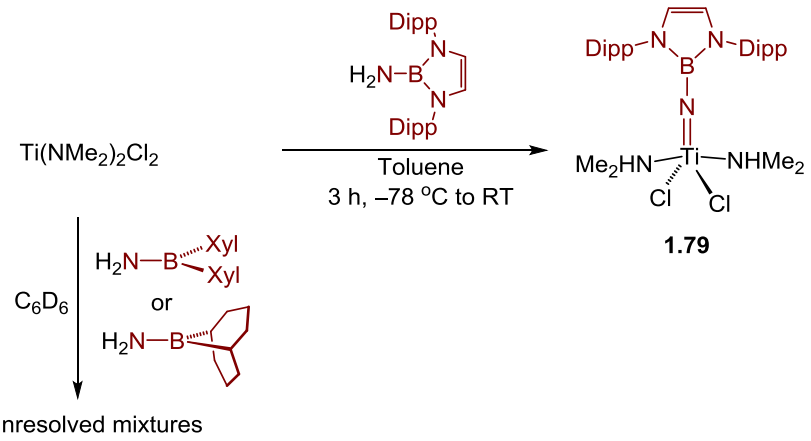


Figure 4.1 Examples of borylimide complexes synthesised in our research group. Dipp = 2,6-diisopropylphenyl (right).

However, one major drawback is that all of these compounds incorporate the same 1,3,2-diazaborolyl, B(NDippCH)$_2$, unit (Dipp = 2,6-diisopropylphenyl). This borolyl unit is sterically very demanding and has limited the chemistry observed with these complexes, as discussed in Chapter Three. Moreover, the electronic structure of the borolyl unit is a rather special case. The boron atom bonded to the imido nitrogen atom, was introduced to study the effect of the empty boron based p-orbital on the resulting chemistry of the borylimido (L)Ti=N–BR$_2$ complexes. However, the borolyl unit features two additional nitrogen atoms adjacent to the boron atom, and the nitrogen based lonepairs compete with the imide

lonepair to donate into the empty boron based p-orbital (Figure 4.1, right). The five membered borolyl ring thus represents a conjugated, 6π electron aromatic system. The result is that there is only limited π-interaction between the Ti=N moiety and the boron atom, and thus comparable to the electronic situation of alkyl imides Ti=N–R (R = alkyl).[1]

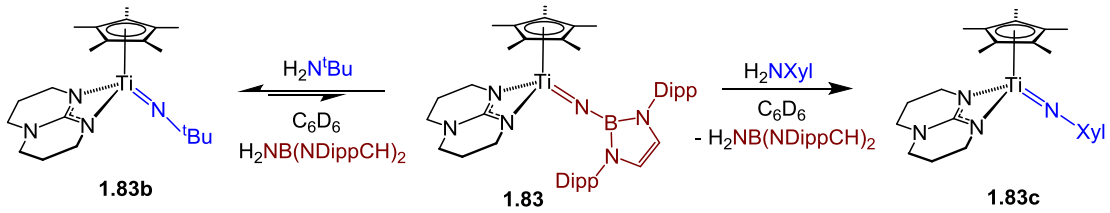
Attempts to synthesise imido complexes with differing borylimido units using the borylamine exchange methodology failed. For example, when $Ti(NMe_2)_2Cl_2$ was treated with borylamines H_2NBXyl_2 (Xyl = 2,6-$C_6H_3Me_2$) or $H_2NBC_8H_{14}$, complex mixtures of unidentified products were formed (Scheme 4.1). Only the known amino-borane[2] $Me_2NBC_8H_{14}$ could be identified from the ^1H and ^{11}B NMR data as side product using $H_2NBC_8H_{14}$, presumably formed *via* an unproductive transamination reaction between a Ti-bound NMe_2 ligand and the NH_2 group of the borylamine.[3] By contrast, when $Ti(NMe_2)_2Cl_2$ was treated with H_2N^tBu, H_2NAr or $H_2NB(NDippCH)_2$, the corresponding titanium imide complexes were formed successfully.



Scheme 4.1 Reactions of $Ti(NMe_2)_2Cl_2$ using $H_2NB(NDippCH)_2$, H_2NBXyl_2, and $H_2NBC_8H_{14}$ (exists in dimeric form but, for clarity, is represented as the monomer).

Similarly, when other titanium *tert*butylimide complexes were treated with either H_2NBXyl_2 or $H_2NBC_8H_{14}$, no imide/borylamine exchange could be effected.[4] In fact, when borylimide **1.83** was treated with H_2NXyl, the borylimide is "protonated off" as the free borylamine, and the corresponding arylimide Cp*Ti(HPP)(NXyl) (**1.83c**) is formed

quantitatively (Scheme 4.2). Similarly, with H_2N^tBu an equilibrium between Cp*Ti(HPP)(N^{t}Bu) (**1.83b**, 70%) and Cp*Ti(HPP)(NB(NDippCH)$_2$) (**1.83**, 30%) is established.



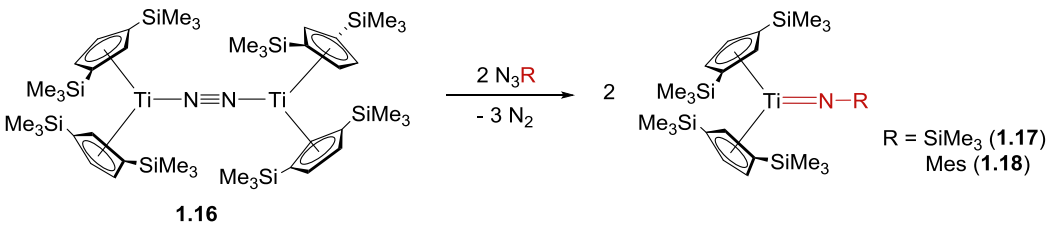
Scheme 4.2 Imide/amine exchange reactions of Cp*Ti(HPP)(NB(NDippCH)$_2$) (**1.83**).

These observations can be rationalised by the electropositive nature of the boron atom, and the resulting insufficient Brønsted acidity of borylamines H_2NBR_2 to protonate alkylimide moieties. Thus, the synthesis of titanium borylimide complexes of type (L)Ti=N–BR_2 starting from the corresponding borylamines was found to be of limited success.

Consequently, the Author aimed to develop an alternative, more general route to access titanium borylimide complexes, and to study sterically and electronically different borylimido scaffolds.

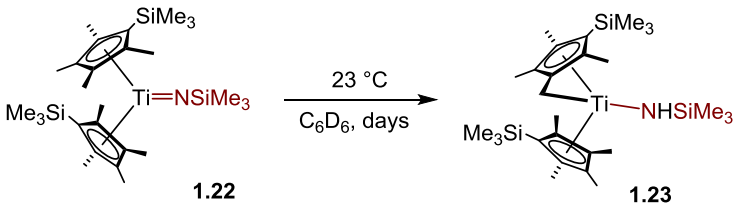
4.3 Choice of suitable synthetic route towards titanium borylimide complexes

Bergman and Andersen have previously shown[5] that the base-free imide Cp*$_2$Ti=NPh (**1.28**) could be prepared from Cp*$_2$Ti(η-C_2H_4) and PhN_3 *via* oxidative addition. Chirik subsequently found that the dinitrogen compound (Cp"$_2$Ti)$_2$(μ_2:η^1,η^1-N_2) (**1.16**) reacts with certain azides to form Cp"$_2$Ti=NR (R = $SiMe_3$ (**1.17**, X-ray structure known) or Mes (**1.18**), Equation 4.1).



Equation 4.1

Notably, the bulky Cp" ligand imparts large thermal stability to Cp"$_2$Ti=NSiMe$_3$ (**1.17**) and Cp"$_2$Ti=NMes (**1.18**), which are stable up to 110 °C in C_6D_6 solutions for several days. This is in marked contrast to (^{t}Bu$_3$SiNH)$_2$Ti=NSi^{t}Bu$_3$ (**1.19**),[6] (^{t}Bu$_3$SiO)$_2$Ti=NSi^{t}Bu$_3$ (**1.20**),[7] and (C$_5$Me$_4$R)$_2$Ti=NSiMe$_3$ (R = ^{i}Pr, **1.21**; SiMe$_3$, **1.22**),[8] that activate C–H bonds more readily. For example, **1.22** gradually undergoes intramolecular cyclometallation at ambient conditions (Equation 4.2).[8] This stability, and lack of C–H bond activation behaviour of **1.17** and **1.18,** is reminiscent of titanocene imido base adducts such as Cp*$_2$Ti=N^{t}Bu(py) (**4.3**).[9]



1.22 **1.23**

Equation 4.2

As discussed in Chapter One, the oxidative addition of a borylazide, specifically N$_3$BMes$_2$, to low oxidation state Group 5 and 6 metals has also been reported.[10,11]

Oxidative addition of alkyl and silylazides to Group 4 metals is known. Additionally, the oxidative addition of borylazides to Group 5 and 6 metals was demonstrated by the addition of Mes$_2$BN$_3$ to W(NMes)$_2$(PMe$_3$)$_3$ and V(Mes)$_3$(THF) forming W{NB(Mes)$_2$}$_2$Cl$_2$(PMe$_3$)$_2$ (**1.73**),[10] and V{NB(Mes)$_2$}(Mes)$_3$ (**1.75**),[11] respectively. Therefore, the use of borylazides to furnish Group 4 borylimide complexes appeared feasible as well. Such a route would circumvent the previously discussed limitation of insufficient Brønsted acidities of borylamines H$_2$NBR$_2$ and potentially allow the installation of borylimides with various steric and electronic properties. Specifically, the Author targeted (Cp"$_2$Ti)$_2$(μ_2:η^1,η^1-N$_2$) (**1.16**) as suitable starting material to furnish potential borylimides of type Cp"$_2$Ti=NBR$_2$. This is due to the enhanced thermal stability the Cp" ligand imparts on the resulting imide complexes (*c.f.* Equation 4.2).

4.4 Synthesis of borylazides

In order to synthesise Ti(IV) borylimido complexes *via* an oxidative route starting from the Ti(II) precursor **1.16** and a borylazide, borylazides **4.4-4.8** were targeted (Figure 4.2). Compounds N_3BMes_2 (**4.4**)[12] and $N_3B(py)C_8H_{14}$ (**4.5**)[13] are known in the literature, and feature two carbon atoms directly bonded to the boron atom. Notably, the base-free analogue of **4.5**, $N_3BC_8H_{14}$, is not stable in solution and slowly reacts with itself, therefore stabilisation with pyridine is required.[13] Borylazide N_3BCat (**4.6**, Cat = 1,2-benzenediol)[13] has also been reported in the literature, and features two π-donating oxygen atoms adjacent to the boron centre. The novel borylazides $N_3\{B(NMe)_2C_6H_4\}$ (**4.7**) and $N_3\{B(NDippCH)_2\}$ (**4.8**) were also targeted. Both feature two additional nitrogen atoms adjacent to the boron atom, along with an unsaturated backbone. While the two structures are electronically closely related, a key difference is that the sterically demanding Dipp moieties in **4.8** are replaced by smaller methyl groups in **4.7**.

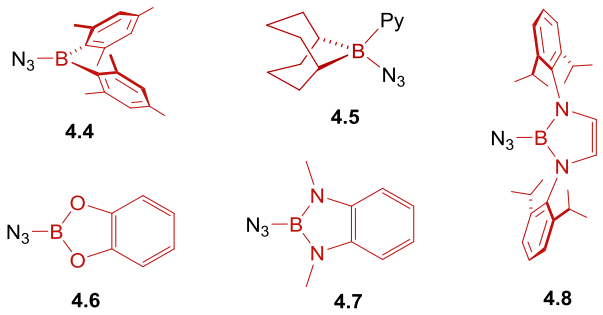
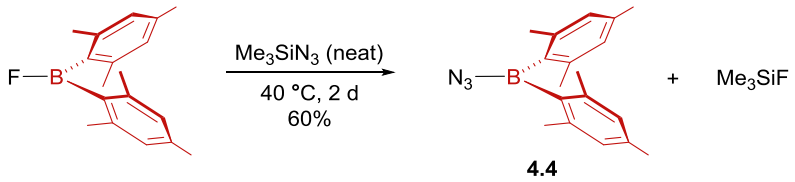


Figure 4.2 Targeted borylazides as precursors to titanium borylimido complexes.

In the following the synthesis of these structures is described. Since azides are known to be explosive,[14] reactions were handled with care and an explosion blast-screen was generally used as a precaution for scales requiring >50 mg of azide. Mes_2BN_3 (**4.4**) was reported by Paetzold[12] to be synthesised upon addition of Me_3SiN_3 to a solution of Mes_2BF in hexanes at 0 °C, followed by stirring two days at room temperature. In our hands, however, no reaction was observed under these conditions, as judged by ^1H and ^{11}B NMR spectroscopy.

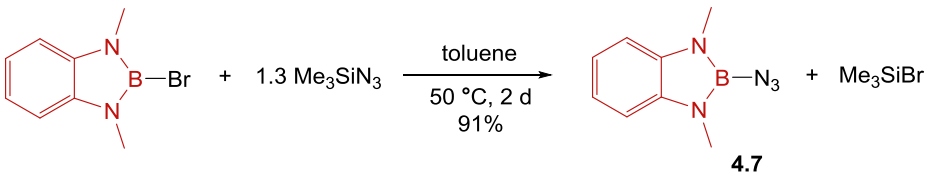
Thus, the reaction was set up by dissolving **4.4** (2 g) in neat Me_3SiN_3 (10 mL) at RT (Equation 4.3). The yellow solution was heated to 40 °C for 2 d before the excess Me_3SiN_3 and Me_3SiF byproduct were removed *in vacuo*. After washing with cold hexanes, the product was isolated as off-white powder in 1.3 g (60%) yield and the spectral properties matched literature values.[12] Notably, Mes_2BN_3 (**4.4**) is reported to be thermally unstable, decomposing at 80 °C, thus higher reaction temperatures are avoided.[12]



Equation 4.3

Borylazides **4.5** and **4.6** were synthesised according to literature procedures, using a similar halide substitution methodology starting from the corresponding boronchlorides as well as Me_3SiN_3.[13]

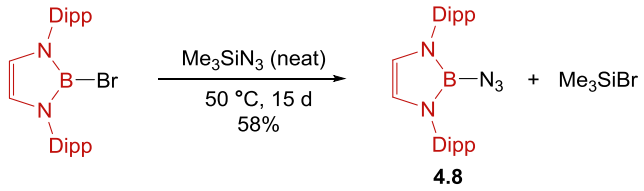
Next, the synthesis of the new borylazide compounds $N_3\{B(NMe)_2C_6H_4\}$ (**4.7**) and $N_3\{B(NDippCH)_2\}$ (**4.8**) is described. $Br\{B(NMe)_2C_6H_4\}$ was dissolved in toluene and 1.3 equivalents of Me_3SiN_3 were added at RT (Equation 4.4). After 2 days at 50 °C, a single peak in the ^{11}B NMR (C_6D_6) could be observed at 21.0 ppm, while the signal of the starting material at 24.5 ppm was absent, indicating full conversion to a single new species.



Equation 4.4

By contrast, the sterically more demanding $Br\{B(NDippCH)_2\}$ required more forcing conditions (Equation 4.5). $Br\{B(NDippCH)_2\}$ was dissolved and stirred in neat Me_3SiN_3 at 50 °C for 15 days, until there was full conversion as judged by ^{11}B NMR spectroscopy.

As in the case for **4.7**, a single peak at a comparable chemical shift of 20.0 ppm was observed in the ^{11}B NMR (C_6D_6).



Equation 4.5

The ^{1}H NMR spectra of compounds **4.7** and **4.8** are shown in Figure 4.3, and match with the assigned structures. In particular, **4.7** features a single methyl peak (6 H) at 2.75 ppm, and two aryl multiplets centred at 7.06 (2 H) and 6.70 (2 H) ppm, consistent with C_{2v} symmetry. For **4.8**, there is a singlet at 5.98 ppm (2 H), a single septet at 3.24 ppm ($CHMe_2$, 4 H, ^3J = 6.9 Hz), and two doublets centered at 1.33 and 1.23 ppm (12 H, d, ^3J = 6.9 Hz, $CH\underline{Me}_2$, respectively).

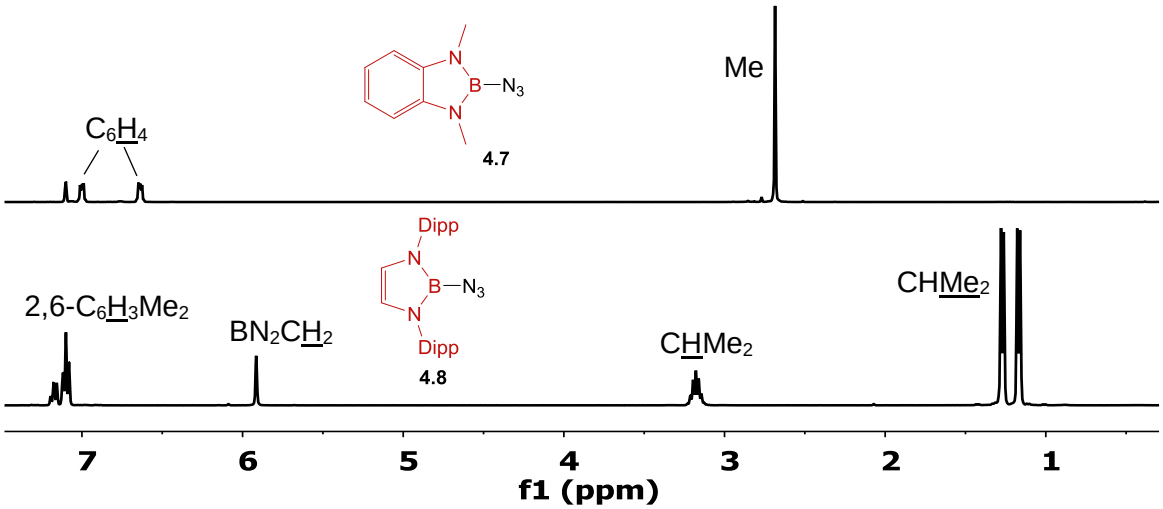


Figure 4.3 ^{1}H NMR spectra (400 MHz) of $N_3\{B(NMe)_2C_6H_4\}$ (**4.7**, top) and $N_3\{B(NDippCH)_2\}$ (**4.8**, bottom) in C_6D_6 at 298 K.

Importantly, the infrared spectra (NaCl plates, nujol mull.) of **4.7** and **4.8** reveal strong bands 2142 and 2143 cm^{-1}, respectively, diagnostic for υ(N=N=N) stretches.[15] These values match well with the corresponding ones for N_3BMes_2 (**4.4**, 2100 cm^{-1})[12], $N_3B(py)C_8H_{14}$ (**4.5**, 2093 cm^{-1})[13], and N_3BCat (**4.6**, 2169 cm^{-1})[13].

Diffraction-quality crystals of **4.8** were grown from a saturated hexane solution at 5 °C, and the solid state structure is shown in Figure 4.5, confirming the assigned connectivity.

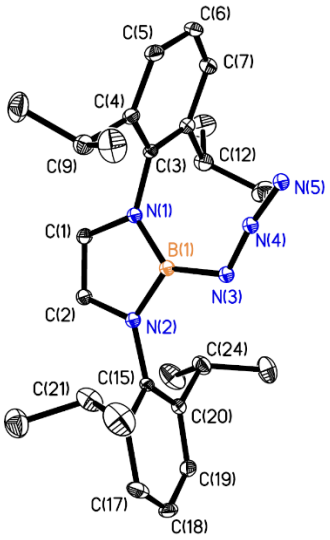


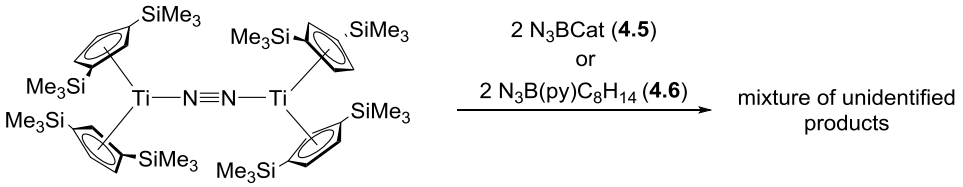
Figure 4.4 Displacement ellipsoid plot (20% probability) of $N_3\{B(NDippCH)_2\}$ (**4.8**). H atoms are omitted. Selected bond lengths (Å): N(4)–N(5), 1.144(3); N(4)–N(3), 1.187(4); B(1)–N(3), 1.475(3); B(1)–N(2), 1.4220(17); B(1)–N(1), 1.4231(17). Selected bond angles (°): B(1)–N(3)–N(4), 120.1(3); N(1)–N(2)–N(3) = 172.6(3).

The near-linear azide group (N(1)–N(2)–N(3) = 172.6(3)°) is directly bonded to the boron atom. The B(1)–N(3)–N(4) angle is 120.1(3) °, a value expected for sp^2 hybridisation on N(3). This suggests that there is only limited interaction between N(3) and B(1). Nevertheless, the N_3 unit is almost coplanar with the boryl ring, and the associated dihedral angle N(1)–B(1)···N(3)–N(4) is 6.5 or 3.4 ° (the two values arise from positional disorder in the N_3 unit in the solid state structure). The B(1)–N(3) bond length is 1.475(3) Å, and is slightly elongated compared to B(1)–N(1) and B(1)–N(2) (1.4231(17) and 1.4220(17) Å, respectively).

4.5 Synthesis and characterisation of novel titanium borylimide complexes

In the following section, the reactions of $(Cp''_2Ti)_2(\mu_2{:}\eta^1,\eta^1\text{-}N_2)$ (**1.16**) with borylazides N_3BR_2 (**4.4-4.8**) are described. When either N_3BCat (**4.5**) or $N_3B(py)C_6H_{14}$ (**4.6**) was subjected, in a 2:1 ratio, to a blue solution of **1.16** in toluene-d8 at room temperature, the

colour turned brown after 2 minutes in both cases. In each case, the ^{11}B NMR spectra were featureless. The ^{1}H NMR spectra revealed complete consumption of the azides, showed >10 very low intensity peaks between 1.5-0 ppm, and were otherwise featureless. No gas evolution was observed, which would have indicated dinitrogen formation (expected after oxidative addition).



1.16

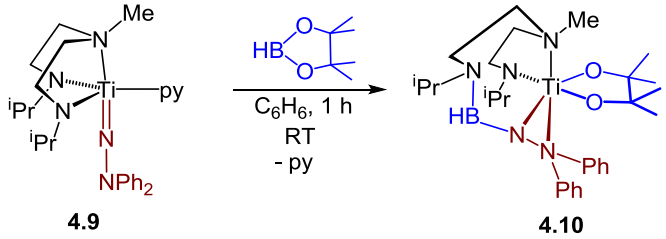
Equation 4.6

Although **1.16** is paramagnetic, the large number of equivalent protons of the $SiMe_3$ moieties (36 H) gives rise to a broadened peak at *ca.* 2.65 ppm (C_6D_6, FWHM = 260 Hz),[16] which serves as a useful NMR handle. The colour change as well as the absence of this peak indicates full consumption of **1.16** in both cases. When the reaction mixtures were heated (60 °C, 2 days), no change was observed.

When the reactions were either set up at -78 °C outside the glovebox using Schlenkline techniques, or at -35 °C in an inert atmosphere within the glovebox, and slowly warmed to room temperature, similar observations were made. Both **1.16**, and the azides were consumed, and the reactions produced almost featureless NMR spectra. The use of different solvent systems, such as hexane, DCM, pyridine, or THF were trialed, however did not lead to improved results. Reactions using these solvent systems were also set up at low temperatures (-35 °C) in an inert atmosphere in the glovebox, and warmed slowly to RT yet did not lead to a different outcome.

The consumption of both $(Cp''_2Ti)_2(\mu_2{:}\eta^1,\eta^1\text{-}N_2)$ (**1.16**) as well as the employed borylazides, together with the observation of almost featureless NMR spectra, suggests that

formation of paramagnetic species is kinetically, at least, more favourable than oxidative addition. Attempts to crystallise these NMR silent species on large scale failed in both cases. No diamagnetic Ti(IV) species could be identified in the NMR spectra. It is speculated that in N_3BCat (**4.5**), as well as in $N_3B(py)C_6H_{14}$ (**4.6**), the boron moiety is insufficiently protected by steric bulk and so side reactions are favoured. For example, the B–O bonds in N_3BCat might be cleaved to form thermodynamically strong Ti–O bonds, as has been observed with other oxygen substituted boranes. Treating titanium imide complex **4.9** with HBPin (Pin = 2,3-dimethylbutane-2,3-diol) lead to compound **4.10** *via* B–O bond cleavage (Equation 4.7).[17]

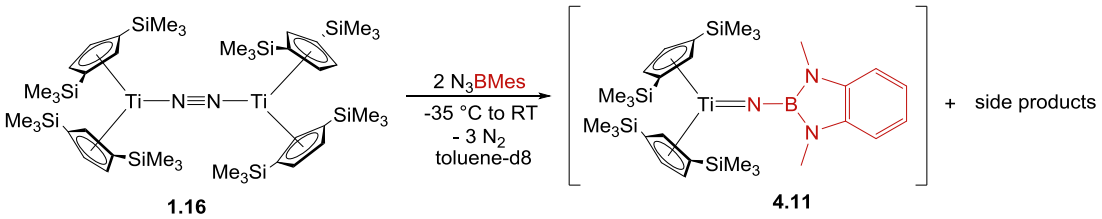


4.9 **4.10**

Equation 4.7

Thus, N_3BCat (**4.5**) and $N_3B(py)C_6H_{14}$ (**4.6**) were abandoned as substrates, and attention was turned to $N_3\{B(NMe)_2C_6H_4\}$ (**4.7**).

When 2 equivalents of **4.7** were added to a solution of **1.16** in toluene-d8 on the NMR tube scale, immediate gas evolution was observed, and the colour changed from blue to brown. The ^1H and ^{11}B NMR spectra indicated full consumption of the starting materials within 5 minutes. In contrast to the previous two tested azides, NMR active species were formed. When the reaction was conducted at room temperature, a large number of different signals in the ^1H and ^{11}B NMR spectra indicated formation of an intractable mixture of species, precluding further analysis. However, the reaction was more controlled when set up at -35 °C and slowly warmed to room temperature (Equation 4.8).



1.16 **4.11**

Equation 4.8

The resulting ^{1}H NMR spectrum (298 K, toluene-d8) indicates the formation of one main species with C_{2v} symmetry, and can be assigned as the desired target complex Cp"$_2$Ti=NB{N(Me)$_2$C$_6$H$_4$} (**4.11**, Figure 4.5).

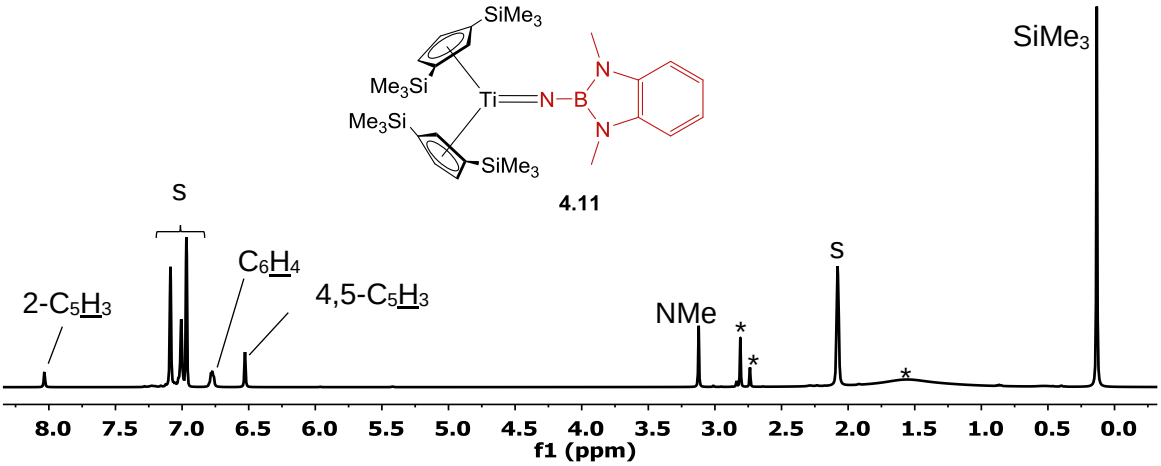


Figure 4.5 Crude ^{1}H NMR spectrum (400 MHz) of the reaction between 2 equivalents of N$_3${B(NMe)$_2$C$_6$H$_4$} (**4.7**) with (Cp"$_2$Ti)$_2$(μ_2:η^1,η^1-N$_2$) (**1.16**) to form Cp"$_2$Ti=NB{N(Me)$_2$C$_6$H$_4$} (**4.11**) in toluene-d8. "s" denotes residual protio-solvent, "*" denote impurities.

There is one singlet resonance at 0.13 ppm integrating to 36 protons corresponding to the SiMe$_3$ groups of the Cp" ring, comparable to the value obtained for Cp"$_2$Ti=NSiMe$_3$ (**1.17**, 0.38 ppm).[16] Another singlet resonance is observed at 3.12 ppm integrating to 6 protons (NMe). Additionally, there is an apparent singlet at 8.02 ppm (2 H), as well as at 6.54 ppm (4 H), which can be assigned to the 2-C$_5$H$_3$ and 4,5-C$_5$H$_3$ protons of the Cp" ring, respectively. The values again agree well with the corresponding ones found in Cp"$_2$Ti=NSiMe$_3$ (**1.17**), namely 8.17 and 6.65 ppm (C$_6$D$_6$), respectively.[16] These proton signals feature HSQC correlations to carbon resonances at 134.9 (2-C$_5$H$_3$), and 127.3 (4,5-C$_5$H$_3$) ppm, respectively, in agreement with the corresponding carbon signals in **1.17** (136.7

and 126.1 ppm, C_6D_6).[16] Additionally, two overlapping multiplets centered at 6.77 (4 H) can be assigned to the aromatic protons of the borolyl backbone in **4.11**. Finally, there is one main species in the ^{11}B NMR spectrum at 17.5 ppm, which is comparable to the ^{11}B NMR resonance of 16 ppm (toluene-d8) for the titanium borylimide Cp*Ti(HPP){NB(NDippCH)$_2$} (**1.83**). Notably, there are two unidentified singlet peaks at 2.81 and 2.74 ppm, as well as broadened peak at 1.56 ppm which might arise from a side reaction forming a paramagnetic species. It was found that Cp"$_2$Ti=NB{N(Me)$_2$C$_6$H$_4$} (**4.11**) is unstable to vacuum, and so could not be isolated on the preparative scale. **4.11** was therefore fully characterised *in-situ*, using ^1H, ^{13}C and ^{11}B NMR spectroscopy.

Species **4.11** represents a base-free sandwich complex and it was reasoned that the addition of coordinating ligands such as DMAP, pyridine or THF might stabilise the species. However, when Lewis bases were added stoichiometrically, to a solution of **4.11** in toluene-d8, slow decomposition to an intractable mixture of unknown products occurred. Similarly, when Cp"$_2$Ti=NB{N(Me)$_2$C$_6$H$_4$} (**4.11**) was attempted to be synthesised in either THF or pyridine at -35 °C directly, an intractable mixture of products was observed in both cases as well.

It was speculated that the additional bulk of the Dipp groups in N$_3${B(NDippCH)$_2$} (**4.8**) might stabilise the resulting titanium borylimide complex to allow for its isolation. Thus, using the same reaction conditions as for N$_3${B(NMe)$_2$C$_6$H$_4$} (**4.7**), two equivalents of **4.8** were added to a solution of (Cp"$_2$Ti)$_2$(μ_2:η^1,η^1-N$_2$) (**1.16**) in toluene-d8 at -35°C. In contrast to the less bulky **4.7**, no gas evolution was observed initially. Only after warming to room temperature the blue color changed to brown, with concomittant gas evolution. After *ca.* 15 min full conversion of both the azide as well as the Ti(II) precursor was observed. The NMR spectra revealed the formation of one major species which can be assigned the target borylimide Cp"$_2$Ti=NB(NDippCH)$_2$ (**4.12**, Figure 4.6).

The ^{11}B NMR spectrum features one major resonance at 17.5 ppm, as was seen in the case of Cp"$_2$Ti=NB{N(Me)$_2$C$_6$H$_4$} (**4.11**). The ^{1}H NMR spectrum reaveals a singlet resonance for SiMe$_3$ integrating to 36 protons at 0.08 ppm (Figure 4.6).

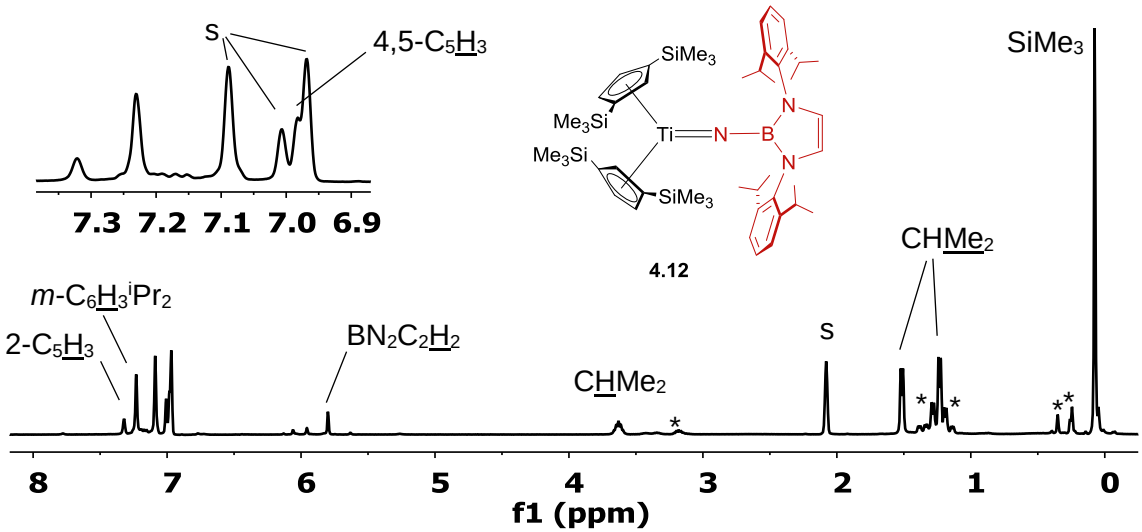
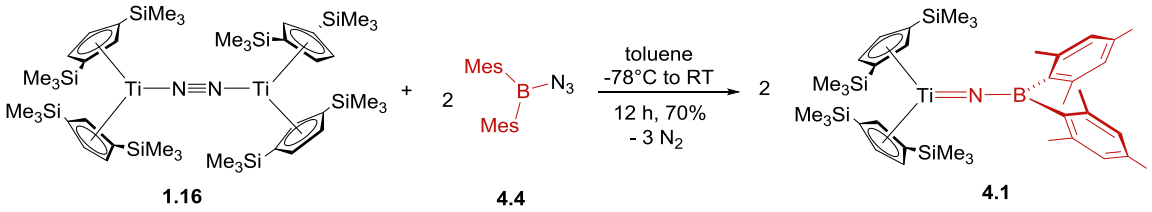


Figure 4.6 Crude ^{1}H NMR spectrum (400 MHz) of the reaction between 2 equivalents of N$_3${B(NDippCH)$_2$} (**4.8**) with (Cp"$_2$Ti)$_2$(μ_2:η^1,η^1-N$_2$) (**1.16**) to form Cp"$_2$Ti=N{B(NDippCH)$_2$} (**4.12**) in toluene-d8. "s" denotes residual protio-solvent. "*" denote impurities. Inset: Overlapping resonances of 4,5-C$_5$H$_3$ and toluene solvent.

Additionally, there are two doublets centred at 1.51 and 1.23 ppm (^3J = 6.8 Hz) integrating to 12 protons each, as well as a septet centred at 3.63 ppm (4 H, ^3J = 6.8 Hz), which corresponds to the CHMe$_2$ moieties of the borolyl ligand. The protons of the unsaturated backbone BN$_2$C$_2$H$_2$ unit can be found at 5.80 ppm, which compares to a value of 5.83 ppm in Cp*Ti(HPP){NB(NDippCH)$_2$} (**1.83**).

However, compound **4.12** was found to be unstable in solution ($t_{1/2} \approx$ 2 days) and forms an intractable mixture of unidentified products. This observation explains the presence of small amounts of side-products in the ^{1}H NMR spectrum (Figure 4.7). Attempted stabilisation of the complex by addition of coordinating solvents such as pyridine or THF failed, as observed for Cp"$_2$Ti=NB{N(Me)$_2$C$_6$H$_4$} (**4.11**). The instability in solution as well as under vacuum prevented clean isolation of Cp"$_2$Ti=N{B(NDippCH)$_2$} (**4.12**) on the preparative scale. Thus, it was fully charaterised *in-situ*.

Next, attention is turned to N_3BMes_2 (**4.4**). The corresponding titanium borylimide complex $Cp''_2Ti{=}NBMes_2$ (**4.1**) was found to be stable towards vacuum, as well as in solution, showing no appreciable decomposition after one week at room temperature in toluene-d8. It was therefore possible to isolate the complex on the preparative scale.



1.16 **4.4** **4.1**

Equation 4.9

The reaction was set up by transferring a solution of two equivalents of **4.4** slowly to a blue solution of $(Cp''_2Ti)_2(\mu_2{:}\eta^1,\eta^1\text{-}N_2)$ (**1.16**) in toluene at -78 °C. The reaction mixture was allowed to warm to room temperature, and vigorous gas evolution was observed along with a colour change to green. The mixture was stirred overnight, and the desired titanium borylimide product $Cp''_2Ti{=}NBMes_2$ (**4.1**) was isolated as green powder (208 mg, 70% yield) after removal of the volatiles and washing with hexanes (Equation 4.9).

The complex was characterised by NMR and infrared spectroscopy, as well as X-ray diffraction (Diffraction quality crystals of $Cp''_2Ti{=}NBMes_2$ (**4.1**) were grown from a saturated hexane solution at 5 °C). Both elemental analysis and mass spectrometry failed, despite using diffraction quality single crystals as samples, presumably due to the high sensitivity of **4.1** outside inert atmosphere.

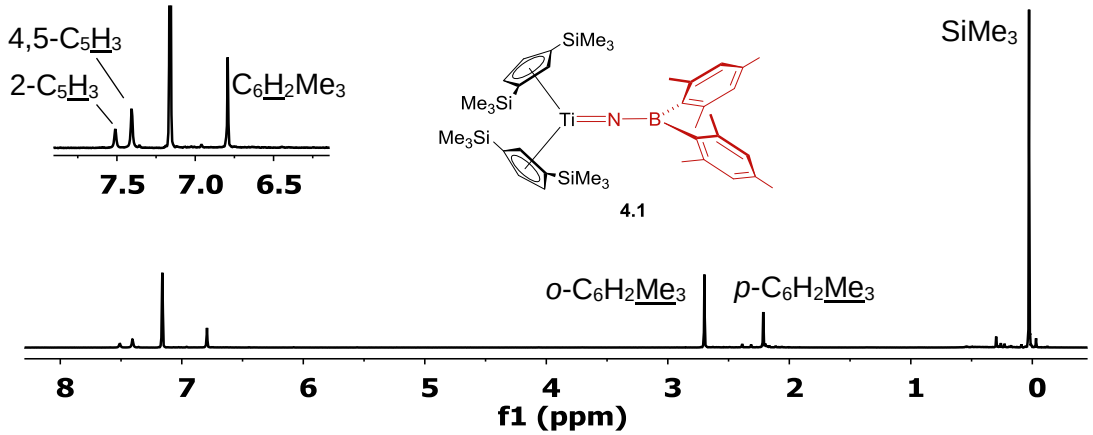


Figure 4.7 ^{1}H NMR spectrum (400 MHz) of Cp"$_2$Ti=NBMes$_2$ (**4.1**) in C_6D_6 at 298 K. Inset: Aromatic region.

The ^{1}H NMR and ^{13}C NMR spectra are in agreement with the assigned structure of **4.1** in C_{2v} symmetry (Fig 4.7). In particular, there is one singlet resonance for the SiMe$_3$ moieties (36 H, 0.01 ppm), one for the methyl groups in *para* position of the mesityl ring (6 H, 2.18 ppm), and *ortho* position (12 H, 2.62 ppm). The ^{11}B NMR spectrum features one singlet resonance at 44.2 ppm. This signal is at significantly higher frequency compared to Cp"$_2$Ti=NB{N(Me)$_2$C$_6$H$_4$} (**4.11**, 17.5 ppm, toluene-d8), or all previously reported titanium borylimido complexes that contain the NB(NDippCH)$_2$ ligand (14-18 ppm, C_6D_6).[1,18] These differences can be explained by the additional two nitrogen atoms that are bonded directly to the boron atom, acting as stronger π-donors compared to the mesityl groups, shielding the boron centre. Analogously, the only known alkyl subsituted borylimido complex Cp*Ti{MeC(N^{i}Pr)$_2$}(NBC$_8$H$_{14}$) (**1.83**) features a ^{11}B NMR shift of 52.8 ppm,[19] suggesting an even more deshielded boron centre.

The solid state structure will be discussed in the following (shown in Figure 4.8, with selected bond distances and angles in Table 4.1), and compared to related structures.

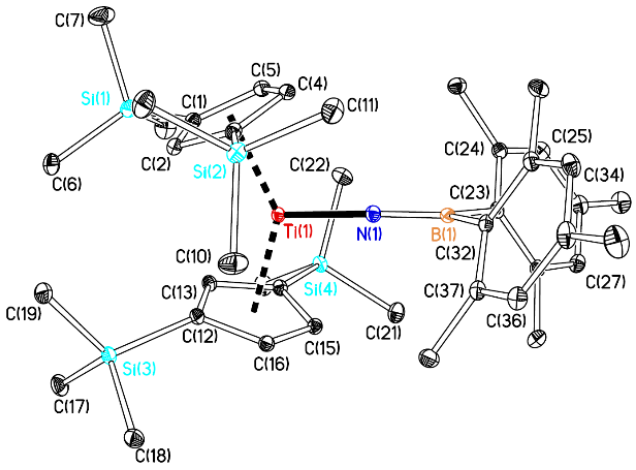


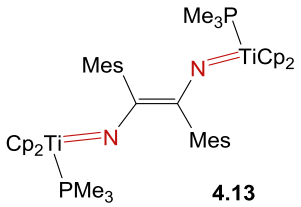
Figure 4.8 Displacement ellipsoid plots (20% probability) of Cp"$_2$Ti=NBMes$_2$ (**4.1**). H atoms are omitted.

Table 4.1 Selected bond distances (Å) and angles (°) for Cp"$_2$Ti=NBMes$_2$ (**4.1**). Cp$_{cent(1)}$ and Cp$_{cent(2)}$ refer to the centroids for Cp″ ring carbons C(1)−C(5) and C(12)−C(16), respectively.

Parameter	**4.1**
Ti(1)–N(1)	1.8069(7)
Ti(1)–Cp$_{cent(1)}$	2.08
Ti(1)–Cp$_{cent(2)}$	2.08
N(1)–B(1)	1.3782(12)
Cp$_{cent(1)}$–Ti(1)–N(1)	109.7
Cp$_{cent(2)}$–Ti(1)–N(1)	109.9
Cp$_{cent(1)}$–Ti(1)–Cp$_{cent(2)}$	140.5
Ti(1)−N(1)−B(1)	175.7(1)

Cp"$_2$Ti=NBMes$_2$ (**4.1**) is a monomeric, base-free species featuring a bent Cp"$_2$Ti moiety bonded to a NBMes$_2$ ligand. The boron atom adopts a trigonal planar conformation, and the sum of the subtended angles being 360(1) °. The two mesityl rings are rotated *ca*. 65° out of the {N(1),B(1),C(23,32)} least-squares plane, indicating little conjugation of the aromatic rings with the Ti(1)−N(1)−B(1) linkage. The Ti(1)−N(1) distance of 1.8069(7) Å is very similar to the Ti−N$_{im}$ distance of 1.810(1) Å in Doxsee's[20] very delocalised {Cp$_2$Ti(PMe$_3$)}$_2${μ-NC(Mes)C(Mes)N}(**4.13**), which features the longest Ti−N$_{im}$ bond reported to date (Figure 4.9). By comparison, the previously discussed titanium borylimide

complexes Cp*Ti(HPP){NB(NDippCH)$_2$} (**1.83**)[1] and Cp*Ti{MeC(N^{i}Pr)$_2$}(NBC$_8$H$_{14}$) (**1.83**)[19] feature Ti−N$_{im}$ bond distances of 1.7433(19) and 1.731(3) Å, respectively. In fact, all crystallographically characterised examples of titanium borylimide complexes found in the Cambridge Structural Database show significantly shorter Ti−N$_{im}$ bond distances as compared to **4.1** (avg. Ti–N$_{im}$ = 1.73 Å, range 1.703(4) – 1.755(2) Å for 9 examples).[21]



4.13

Figure 4.9 Doxsee's {Cp$_2$Ti(PMe$_3$)}$_2${μ-NC(Mes)C(Mes)N} (**4.13**).[20]

The N(1)−B(1) distance of 1.3782(12) Å is significantly shorter than in any previously reported transition metal borylimide (avg. N$_{im}$−B = 1.42 Å, range 1.390(1) – 1.437(2) Å for 13 examples in the Cambridge Structural Database),[21] and is comparable to the crystallographic B−NH$_2$ distance of 1.375(8) Å in H$_2$NBMes$_2$ (monomeric with a trigonal planar boron atom).[22] These observations can be explained by significant 2p$_\pi$−2p$_\pi$ interactions of the nitrogen based lone pair with the empty boron based p-orbital, formally forming a cumulated Ti=N=B system, as illustrated in Figure 4.10.

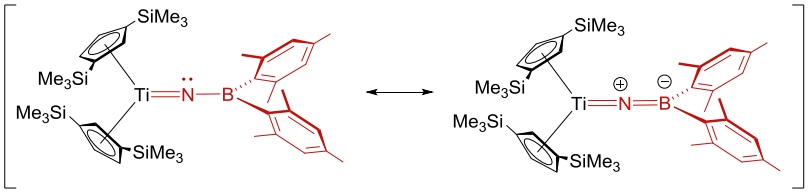
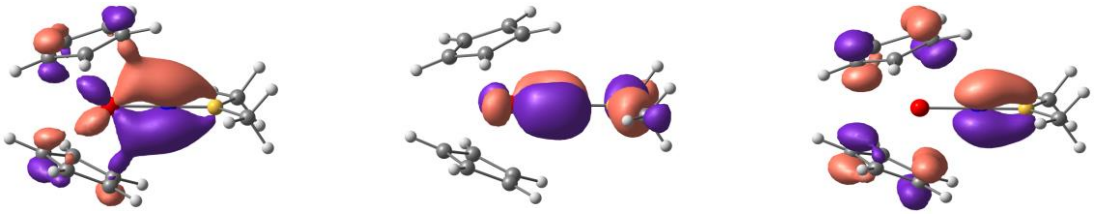


Figure 4.10 Resonance forms of Cp"$_2$Ti=NBMes$_2$ (**4.1**).

The N−BMes$_2$ bond distances in the two previously structurally characterised examples of this type of borylimido ligand (namely, W{NB(Mes)$_2$}$_2$Cl$_2$(PMe$_3$)$_2$ (**1.73**) and W{NB(Mes)$_2$}(NMes)$_2$(PMe$_3$)$_2$ (**1.74**), were very similar, at 1.390(1) and 1.43(1) Å, respectively.

The bonding in metallocenes Cp_2ML_n is usually analysed by considering the frontier molecular orbitals (FMOs) of $[Cp_2M]^{2+}$ and NR^{2-}.[23,24] $[Cp_2Ti]^{2+}$ has three nonbonding, vacant FMOs, that can be used to bind further ligands: $1a_1$, $2b_1$ and $2a_1$ (shown in Figure A1 in the Appendix). The energetically higher lying $2a_1$ is most suitable to form σ-bonds with $[NR]^{2-}$ fragments, and the $1b_2$ FMO lies in the horizontal mirror plane and forms a π_h-bond. However, the $[Cp_2Ti]^{2+}$ has no vacant orbital with suitable symmetry to interact with the second π-orbital (π_v) of the $[NR]^{2-}$ fragment. Nevertheless, it is known that an out-of-plane π-interaction with the $2b_2$ orbital of d^0 Cp_2M (also referred to as "fourth FMO" of bent metallocenes, see Figure A1 in the Appendix) can take place.[24] The principal bonding and non-bonding π-type $Ti–N_{im}$ MOs of $Cp_2TiNBMe_2$ (**4.13**), as a model for $Cp''_2Ti{=}NBMes_2$ (**4.1**), were calculated by Prof. Philip Mountford and are shown in Figure 4.11.



HOMO-5 (π_v) **HOMO-1 (π_h)** **HOMO (π_{nb})**

Figure 4.11 Selected molecular orbitals of $Cp_2TiNBMe_2$ (**4.14**). Isosurfaces are drawn at the 0.063 au contour level.

The $[Cp_2Ti]^{2+}$ $2b_1$ FMO contributes to the HOMO-1 orbital, corresponding to the $Ti–N_{im}$ π_h interaction. The π_v interaction is found in HOMO-5, which also contains significant Cp-Ti bonding character. Notably, there is significant contribution from the empty boron based atomic p-orbital as well. Therefore, the ability of the boron atom to act as π–acceptor delocalises electron-density away from the $Ti–N_{im}$ as well as Ti-Cp bonds, lengthening these bonds as a result. The HOMO (π_{nb}) is entirely ligand-based, and is best represented

as the nitrogen based lone pair, which features significant interactions with the boron atom, in agreement with the structural data discussed above.

$Cp''_2Ti{=}NBMes_2$ (**4.1**) can also be compared to related base-free titanium imide complexes. The previously discussed $Cp''_2Ti{=}NSiMe_3$ (**1.17**) and $Cp''_2Ti{=}NMes$ (**1.18**) feature the same Cp'' ligand set and only differ in their imido substituent $Ti{=}N_{im}{-}\underline{R}$.[16] However, structural data was only reported for **1.17**, and repeated attempts to crystallise **1.18** failed. Similarly, for the base-free arylimido complex $Cp^*_2Ti{=}NPh$ (**1.28**) there is only limited structural information.[16,25] For the purpose of a wider structural comparison, the related alkyl analogue $Cp''_2Ti{=}N^tBu$ (**4.15**) was synthesised using the same methodology, starting from 2 equivalents of $N_3{}^tBu$ and $(Cp''_2Ti)_2(\mu_2{:}\eta^1,\eta^1\text{-}N_2)$ (**1.16**). After workup, $Cp''_2Ti{=}N^tBu$ (**4.15**) was isolated as a red powder in 79% yield on the preparative scale (443 mg), and also crystallographically characterised (Fig 4.12). Selected bond lengths and angles are given in Table 4.2, along with the corresponding values of $Cp^*_2Ti{=}NPh$ (**1.28**), $Cp''_2Ti{=}NBMes_2$ (**4.1**), $Cp''_2Ti{=}NSiMe_3$ (**1.17**).

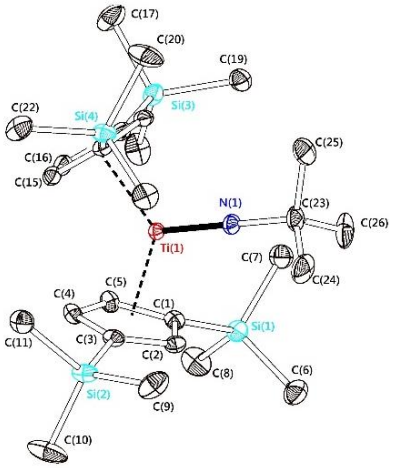


Figure 4.12 Displacement ellipsoid plots (20% probability) of Cp"$_2$Ti=N^{t}Bu (**4.15**). H atoms are omitted for clarity.

Table 4.2 Selected bond distances (Å) and angles (°) for Cp"$_2$Ti=NSiMe$_3$ (**1.17**), Cp*$_2$Ti=NPh (**1.28**), Cp"$_2$Ti=NBMes$_2$ (**4.1**) and Cp"$_2$Ti=N^{t}Bu (**4.15**). Cp$_{cent(1)}$ and Cp$_{cent(2)}$ refer to the centroids for Cp″ ring carbons C(1)−C(5) and C(12)−C(16), respectively.

Parameter	Cp"$_2$Ti=N^{t}Bu (**4.15**)	Cp"$_2$Ti=NSiMe$_3$ (**1.17**)[16]	Cp*$_2$Ti=NPh (**1.28**)[16,25]	Cp"$_2$Ti=NBMes$_2$ (**4.1**)
Ti(1)–N(1)	1.7113(13)	1.722(4)	1.765(3)	1.8069(7)
Ti(1)–Cp$_{cent(1)}$	2.16	2.16	-	2.08
Ti(1)–Cp$_{cent(2)}$	2.16	2.15	-	2.08
Cp$_{cent(1)}$–Ti(1)–Cp$_{cent(2)}$	117.4	128.3	-	140.5
Ti(1)−N(1)−R*	179.62(13)	175.8(2)	176.8(3)	175.7(1)

*R = B(1) for **4.1**; C(23) for **4.15** and **1.28**, Si(5) for **1.17**.

All four species feature sp hybridised N(1) atoms, as suggested by the short Ti−N(1) bond lengths (1.71-1.81 Å) and the near-linear Ti−N(1)−R units (175-180 °). The Ti−N(1) imide bond lengths increase in the order: Cp"$_2$Ti=N^{t}Bu (**4.15**) ≤ Cp"$_2$Ti=NSiMe$_3$ (**1.17**) < Cp*$_2$Ti=NPh (**1.28**) < Cp"$_2$Ti=NBMes$_2$ (**4.1**). As the Ti−N bonds lengthen, the interactions between the titanium and the cyclopentadienyl ligands increases, as is suggested by decreasing Ti(1)–Cp$_{cent}$ bond lengths, and increasing Cp$_{cent(1)}$–Ti(1)–Cp$_{cent(2)}$ angles (Table 4.2).

These structural changes can be rationalised by considering the π-accepting ability of the R groups in the Ti−N−R units, anticipated to be ^{t}Bu ≈ SiMe$_3$ < Ph < BMes$_2$. The better the

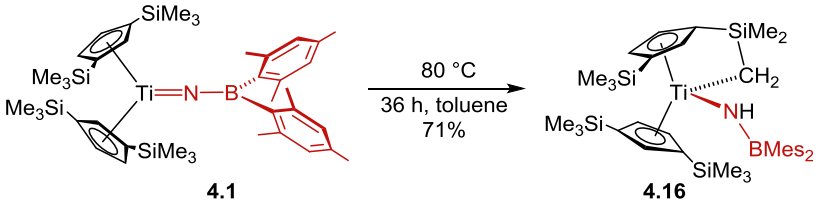
π–accepting ability of the R moieties, the weaker the Ti−N π_v–interactions (*c.f.* Figure 4.11). As the titanium imido π interactions decrease one would expect that the relatively electron deficient titanium centre would compensate for this by increasing interactions with the two cyclopentadienyl ligands.

This is in agreement with theoretical work by Hoffmann and Green.[23,24] Hoffmann showed that bending of a metallocene (decrease Cp-M-Cp angle) leads to a stabilisation of the $2b_2$ orbital involved in the π_v bond. Thus, stronger π_v donors should favour small Cp-M-Cp angles (*c.f.* the relatively large $Cp_{cent(1)}$–Ti(1)–$Cp_{cent(2)}$ angle of 140.5° for the weak π_v donor $Cp''_2Ti{=}NBMes_2$ (**4.1**), and the corresponding angle of 117.4° for $Cp''_2Ti{=}N^tBu$ (**4.15**)). Additionally, it was found that filling the $2b_2$ orbital by the π_v nitrogen lonepair should lead to a lengthening of the Cp–M bonds.

4.6 Preliminary reactivity studies using $Cp''_2Ti{=}NBMes_2$ (4.1)

4.6.1 Reactivity of $Cp''_2Ti{=}NBMes_2$ (4.1) with heat and Lewis bases

As mentioned earlier, Chirik reported that both $Cp''_2Ti{=}NSiMe_3$ (**1.17**) and $Cp''_2Ti{=}NMes$ (**1.18**) are stable up to 110 °C in C_6D_6 solutions for several days. By contrast, when $Cp''_2Ti{=}NBMes_2$ (**4.1**) was dissolved in C_6D_6 and heated to 80 °C complete conversion was observed within 36 h, as judged by ^{1}H NMR spectroscopy. When the reaction was set up on the preparative scale, 100 mg of **4.1** was dissolved in 10 mL of toluene and heated for 36 h at 80 °C at which time the colour changed from green to grey. The cyclometallation product **4.16** could be isolated, *via* removal of the volatiles and subsequent trituration in pentanes in 71% yield (Equation 4.10).



Equation 4.10

The compound was characterised *via* NMR and infrared spectroscopy as well as EI-HRMS, and all data agree with the assigned cyclometallation structure **4.16**. The ^{1}H NMR spectrum features several broadened aromatic and aliphatic peaks at 298 K, presumably due to hindered rotation of the Cp" ring. However, cooling the sample to 263 K led to sharp signals and is indicative for a species with expected C_1 symmetry (Figure 4.13). In particular, there are two different ^{1}H resonances for the *p*-$C_6H_2\underline{Me}_3$ moieties (2.55 and 2.32 ppm, respectively), and four signals for the *o*-$C_6H_2\underline{Me}_3$ moieties (2.25, 2.23 and two overlapping signals at 2.09-2.05 ppm, respectively).

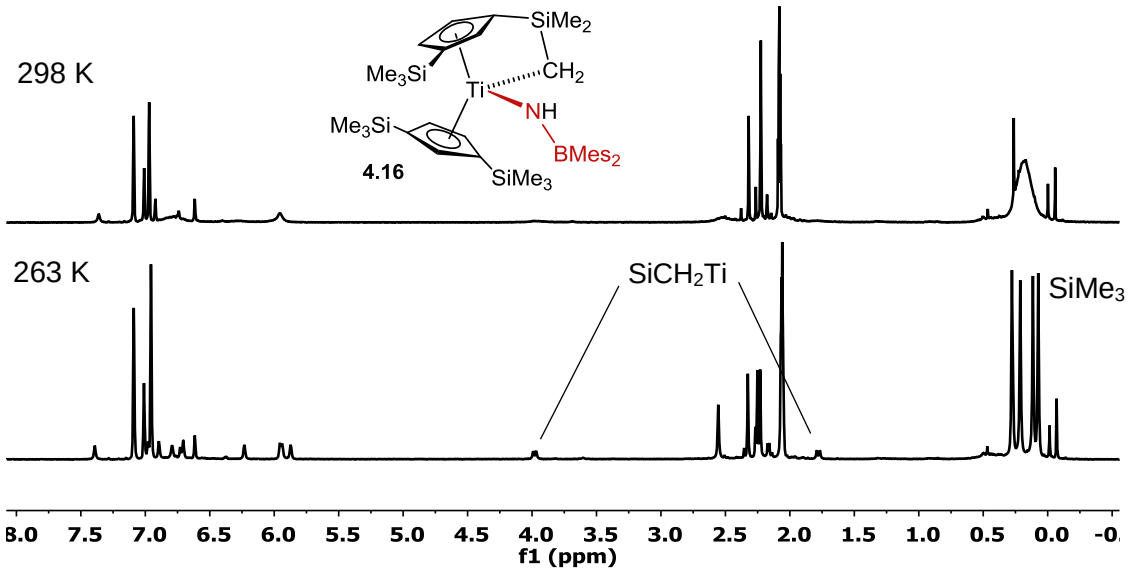


Figure 4.13 ^{1}H NMR spectrum (400 MHz) of **4.16** in toluene-d8 at 298 K (top), and 263 K (bottom).

Additionally, there are four different Si$\underline{C}H_3$ environments at 263 K. Three of these singlet resonances integrate to 9 protons (0.21, 0.12 and 0.07 ppm), and one integrates to 6 protons (0.28 ppm). The latter can be assigned to the $\underline{Me}_2SiCH_2Ti$ unit. Notably, the protons corresponding to the $Me_2Si\underline{C}H_2Ti$ can be assigned to the two doublet resonances at 3.97 (1

H, ^{2}J = 9.6 Hz) and **1.83** (1 H, ^{2}J = 9.6 Hz) ppm, respectively. These show HSQC correlations to the same carbon atom located at a chemical shift of 70.8 ppm in the ^{13}C NMR spectrum. Although the NH peak could not be located in the ^{1}H NMR spectrum, the infrared spectrum featured a peak at 3385 cm^{-1}, diagnostic for N–H stretch frequencies.[15] The decreased thermal stability of Cp"$_2$Ti=NBMes$_2$ (**4.1**) compared to Cp"$_2$Ti=NSiMe$_3$ (**1.17**) and Cp"$_2$Ti=NMes (**1.18**) may reflect the fact that **4.1** is relatively more electron-deficient. The valence electron count of **4.1** is 16 if one considers the [NBMes$_2$]$^{2-}$ fragment as 4 electron donor. As discussed above, the imide lonepair features significant interaction with the boron atom and thus the formal bond order between titanium and nitrogen is less than three, and less than in complexes Cp"$_2$Ti=NSiMe$_3$ (**1.17**) and Cp"$_2$Ti=NMes (**1.18**).

In fact, the overwhelming majority of isolated Group 4 imido sandwich complexes are stabilised by Lewis bases such as THF, pyridine or DMAP.[26] The corresponding base-free species are very reactive and so are often transient, as discussed in Chapter One. As such, Lewis bases were added to Cp"$_2$Ti=NBMes$_2$ (**4.1**) in an attempt to form base-stabilised complexes. Upon addition of a stoichiometric amount of THF or pyridine to a solution of **4.1** in toluene-d8 slow decomposition of **4.1** was observed ($t_{1/2} \approx 1$ day). An intractable mixture of unidentified products was formed, and no base-adducts could be identified.

By contrast, when one equivalent of DMAP was added to a solution of **4.1** in toluene-d8 an immediate colour change from blue to red was observed. Both starting materials are fully consumed within 10 minutes at room temperature, as judged by ^{1}H NMR analysis. Both ^{1}H and ^{13}C NMR spectra are consistent with the formation of base-adduct Cp"$_2$Ti=NBMes$_2$(DMAP) (**4.17**) featuring C_s symmetry in solution. For example, there are two singlet resonances at 0.18 and 0.28 ppm integrating to 18 protons each (SiMe$_3$ moieties, Figure 4.14). In the HSQC spectrum, these feature correlations to resonances in the ^{13}C NMR at 1.1 and 1.0 ppm, respectively, and can be assigned to the SiMe$_3$ moieties. The

aromatic *ortho* and *para* protons of the DMAP molecule can be identified at 8.22 (2 H, d, ^{3}J = 6.4 Hz) and 5.88 ppm (2 H, d, ^{3}J = 6.3 Hz), respectively. These resonances are significantly shifted downfield compared to free DMAP (8.45, and 6.10 ppm; toluene-d8), and indicate that DMAP is coordinated to the metal centre. The ^{11}B NMR spectrum features one singlet at 43.9 ppm, comparable to the chemical shift of the base-free compound (44.2 ppm).

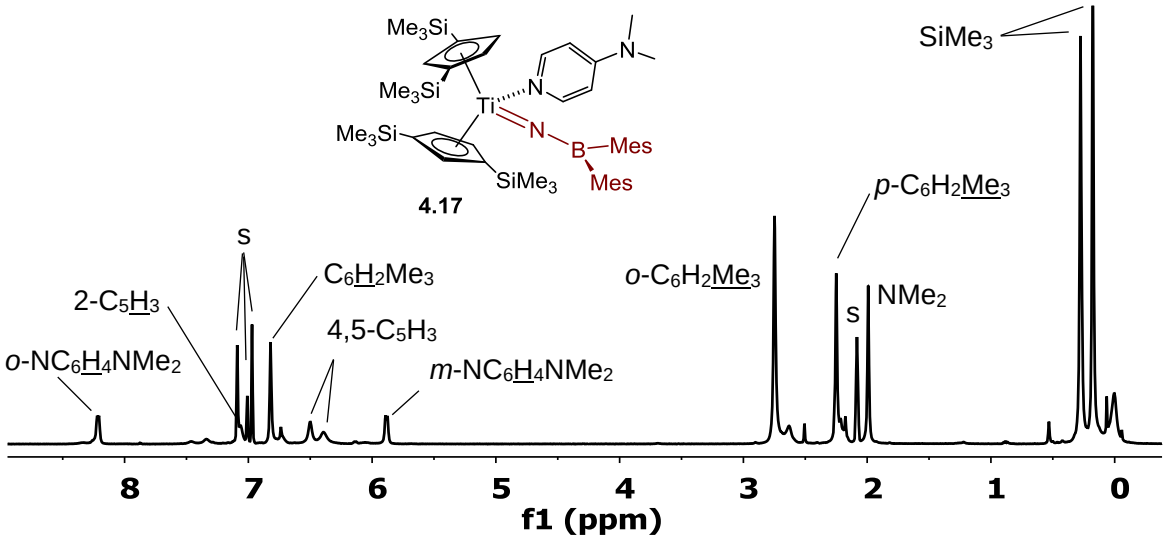


Figure 4.14 ^{1}H NMR spectrum (400 MHz) of Cp"$_2$Ti=NBMes$_2$(DMAP) (**4.17**) in toluene-d8 at 298 K. "s" denotes residual protio-solvent.

However, Cp"$_2$Ti=NBMes$_2$(DMAP) (**4.17**) slowly decomposes in solution ($t_{1/2} \approx 3$ days) at room temperature, explaining the presence of small impurities in Figure 4.14. An intractable mixture of unidentified products was formed, precluding further analysis. Attempts to isolate the complex on the preparative scale failed, since **4.17** was found to be unstable towards vacuum as well as hexane washes.

In summary, Cp"$_2$Ti=NBMes$_2$ (**4.1**) was observed to be unstable in the presence of Lewis bases. Intractable mixtures of a variety of unknown products were formed in all cases. When using either THF or pyridine, no base-adduct could be identified by ^{1}H and ^{11}B NMR spectroscopy. By contrast, the DMAP base adduct Cp"$_2$Ti=NBMes$_2$(DMAP) (**4.17**) was formed near-quantitatively in solution and decomposed relatively slower. This difference

among the three tested Lewis bases could be explained by the fact that DMAP binds more strongly to Lewis acids, such as electron deficient metal centres. The improved binding to $Cp''_2Ti{=}NBMes_2$ (**4.1**) can account for the fact that the corresponding base adduct $Cp''_2Ti{=}NBMes_2(DMAP)$ (**4.17**) is sufficiently stable in solution to be characterised *in-situ*.

The observation that $Cp''_2Ti{=}NBMes_2$ (**4.1**) is unstable in the presence of Lewis bases parallels the previously described attempts to furnish other titanium borylimide base-adducts. It can help rationalise the experimental observations that the *in-situ* generated and transient titanium borylimide complexes $Cp''_2Ti{=}NB\{N(Me)_2C_6H_4\}$ (**4.11**) and $Cp''_2Ti{=}N\{B(NDippCH)_2\}$ (**4.12**) could not be stabilised and trapped as their corresponding Lewis base adducts.

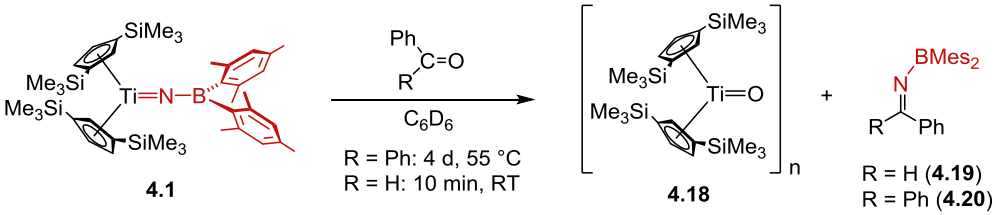
4.6.2 Reactivity of $Cp''_2Ti{=}NBMes_2$ (4.1) with carbonyl groups and dihydrogen

One objective of this project was to synthesise titanium borylimide complexes that are more reactive to small molecule activation, overcoming the steric limitations that were imposed by the $N\{B(NDippCH)_2\}$ moiety. For this reason, preliminary reactivity tests of $Cp''_2Ti{=}NBMes_2$ (**4.1**) were performed with small molecules and compared to the reactivity with $Cp^*Ti(HPP)\{NB(NDippCH)_2\}$ (**1.83**).

As discussed in Chapter Three, **1.83** reacted with arylaldehyde TolCHO to undergo [2 + 2] cycloaddition, followed by cycloreversion, requiring 18 h at 60 °C to go to completion. The sterically more demanding benzophenone Ph_2CO was not observed to react, even under forcing conditions of extended periods of heating.

In contrast to this, when arylaldehydes and arylketones were reacted with $Cp''_2Ti{=}NBMes_2$ (**4.1**) [2 + 2] cycloaddition/reversion was also observed, but under milder conditions compared to $Cp^*Ti(HPP)\{NB(NDippCH)_2\}$ (**1.83**). For example, when one equivalent of arylaldehyde PhCHO was added to a solution of $Cp''_2Ti{=}NBMes_2$ (**4.1**) in C_6D_6 on the

NMR tube scale, an immediate colour change to yellow was observed at room temperature. ^{1}H NMR analysis confirmed full conversion of the starting materials within less than 10 minutes. Comparison with literature values confirmed the quantitative formation of the previously reported borylimine $Mes_2BN{=}C(H)Ph$ (**4.19**),[27] as well as the known titanium oxo complex **4.18**[8] (Equation 4.11). No [2 + 2] cycloaddition products were observed as intermediates.



Equation 4.11

Similarly, mild heating of 55 °C for four days was required to drive the reaction between $Cp''_2Ti{=}NBMes_2$ (**4.1**) and Ph_2CO to completion. The anticipated cycloaddition/cycloreversion reaction occurred; the corresponding titanium oxo complex **4.18** as well as the previously reported borylketimine $Ph_2C{=}NBMes_2$ (**4.20**),[28] were formed, as judged by comparison with reported spectral data.

Next, the H–H bond activation with dihydrogen was investigated. As discussed in Chapter Three, no reaction was observed when H_2 (4 bar) was subjected to a (degassed) solution of $Cp^*Ti(HPP)\{NB(NDippCH)_2\}$ (**1.83**) in C_6D_6. By contrast, $Cp''_2Ti{=}NBMes_2$ (**4.1**) was shown to activate H_2 under ambient conditions. When a (degassed) solution of **4.1** in C_6D_6 was subjected to an atmosphere of H_2 (1 bar) an immediate colour change from green to yellow was observed at room temperature. The ^{1}H NMR confirmed the full consumption of **4.1**, and the appearance of a variety of new, broadened resonances (Figure 4.17). Cooling of the solution to 213 K lead to a sharpening of the resonances. The resulting spectrum is indicative of a species in C_1 symmetry, and, is consistent with titanium hydride amide $Cp''_2Ti(H)N(H)BMes_2$ (**4.21**, Figure 4.15).

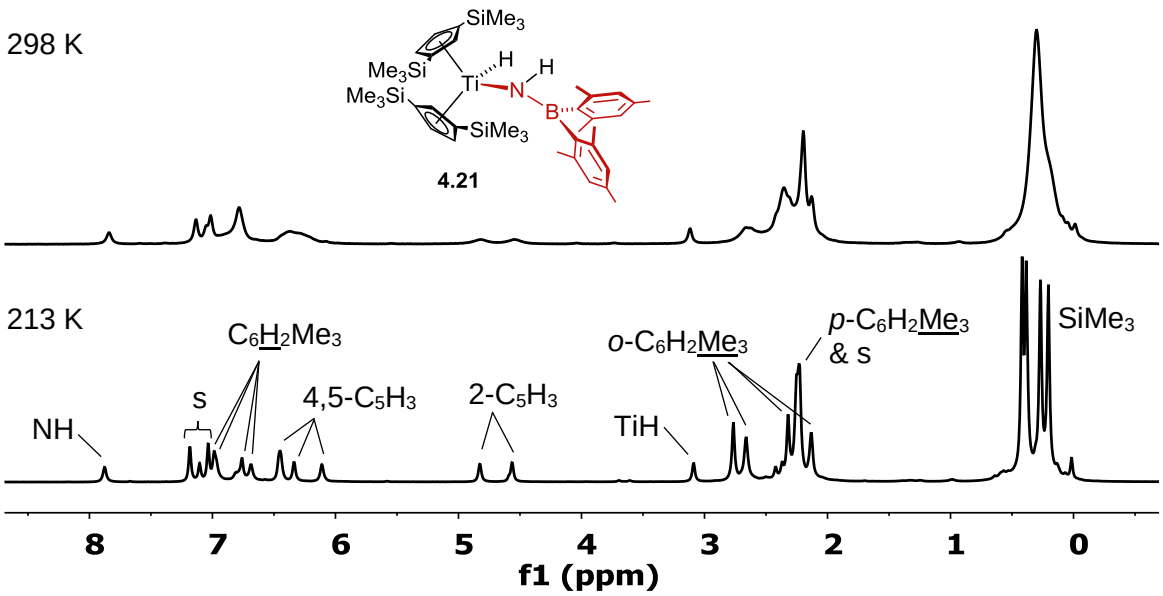


Figure 4.15 Top: ^{1}H NMR spectrum (400 MHz, toluene-d8) of Cp"$_2$Ti(H)N(H)BMes$_2$ (**4.21**) at 298 K. Bottom: ^{1}H NMR spectrum (400 MHz, toluene-d8) of **4.18** at 213 K.

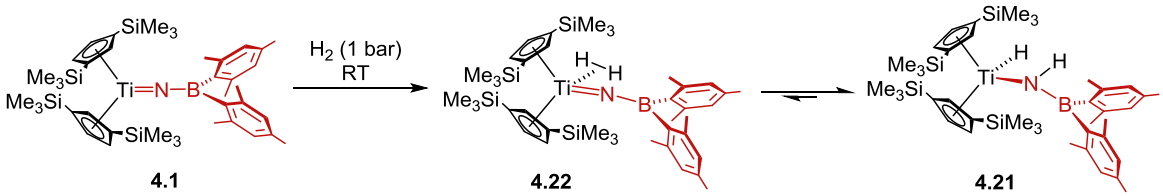
There are four different singlet resonances at 0.32, 0.29, 0.18, and 0.11 ppm, which all integrate to 9 protons and can be assigned to the SiMe$_3$ moieties. Additionally, there is a broadened singlet resonance at 7.78 ppm which does not feature any correlations in the HSCQ or HMBQ spectra, and was hence assigned to the NH moiety. The second singlet resonance that does not feature any correlations in the HSQC or HMBQ spectra is located at 3.00 ppm and was assigned to the TiH moiety.

To confirm this assignment, the reaction was repeated using D$_2$ gas in a solution of protio toluene. Besides the expected signal for D$_2$ at 4.5 ppm, the ^{2}H NMR spectrum revealed the presence of two resonances: a broadened ND resonances at 7.94 ppm, and a sharp singlet resonance at 3.08 ppm for the TiD moiety.

Additionally, the infrared resonances at 3354 and 1646 cm^{-1} attributable to the ν(N–H) and ν(Ti–H) stretches, respectively, are consistent with the ^{1}H NMR data, suggesting formation of a titanium hydride borylamide species. After deuteration, these two resonances are absent, and instead the presence of the two signals at 2409 and 1151 cm^{-1}, attributable to ν(N–D) and ν(Ti–D) stretches, respectively. The experimentally found ratios of ν(Ti–H)/

ν(Ti–D) = 1.43 and ν(N–H)/ν(N–D) = 1.39, are close to the theoretical values of 1.40 and 1.37 obtained using the harmonic oscillator approximation.

Interestingly, all resonances in the ^{1}H NMR spectrum are broadened at 298 K (Figure 4.15). Rather than a single hindered rotation this is more likely due to a dynamic process in solution such as reversible formation of a dihydrogen species **4.22** (Scheme 4.3). The equilibrium would lie on the side of the titanium hydride amide **4.21**, since it is the only species observed when the sample is cooled to 213 K.



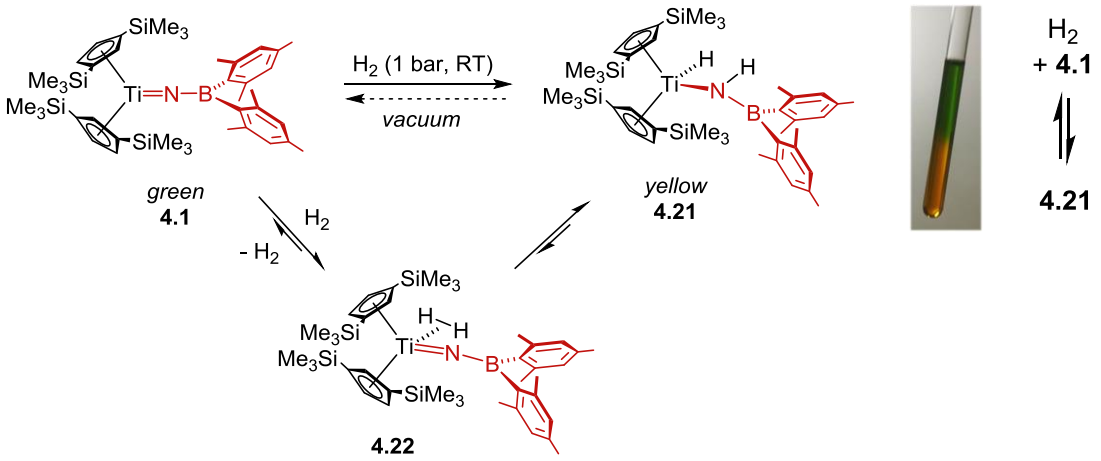
4.1 **4.22** **4.21**

Scheme 4.3 Reaction of dihydrogen with Cp"$_2$Ti=NBMes$_2$ (**4.1**).

Analogous dihydrogen complexes were previously invoked as intermediates in the heterolytic H–H activation.[29–32] For example, Andersen and Bergman showed that Cp*$_2$Ti=S(py) (**4.23**)[32] also activates dihydrogen at room temperature to form titanium hydride sulfide Cp*$_2$Ti(H)S(H) (**4.25**). It was proposed that initial pyridine loss is followed by the formation of a dihydrogen complex Cp*$_2$Ti=S(H$_2$) (**4.24**), which is in equilibrium with the resulting titanium hydride sulfide Cp*$_2$Ti(H)S(H) (**4.25**), in analogy to Scheme 4.3.

Complex Cp"$_2$Ti(H)N(H)BMes$_2$ (**4.21**) was shown to be remarkably stable towards application of vacuum. When the volatiles of a solution of Cp"$_2$Ti(H)N(H)BMes$_2$ (**4.21**) in C_6D_6 were removed, and the resulting yellow precipitate was redissolved in C_6D_6 again, no discernible amounts of Cp"$_2$Ti=NBMes$_2$ (**4.1**) were detected. The application of vaccuum followed by redissolving in C_6D_6 was repeated three times, and no Cp"$_2$Ti=NBMes$_2$ (**4.1**) could be detected in the ^{1}H NMR spectrum. Similarly, the application of continous vacuum for 1 h (1x10^{-1} mbar), and subsequent redissolving in C_6D_6 did not lead to detectable

amounts of Cp"$_2$Ti=NBMes$_2$ (**4.1**). However, when this solution was let to stand one week at room temperature, *ca.* 10% of Cp"$_2$Ti=NBMes$_2$ (**4.1**) was formed. This suggests that 1,2-addition of dihydrogen across the titanium imide bond is reversible, and that dihydrogen loss is slow. Remarkably, this process can be followed by the colour change of the solution (Scheme 4.4).



Scheme 4.4 Reversible reaction of Cp"$_2$Ti=NBMes$_2$ (**4.1**, green) with dihydrogen to form Cp"$_2$Ti(H)N(H)BMes$_2$ (**4.21,** yellow). Right: Picture of a C_6D_6 solution of **4.21** after the dihydrogen was removed from the headspace of the NMR tube, after two weeks at room temperature.

While the lower part of the NMR tube was observed to remain yellow (the colour of **4.21**), the colour of the upper part of the solution changed to green (**4.1**). This can be explained by reversible 1,2-elimination and loss of dihydrogen. Once Cp"$_2$Ti(H)N(H)BMes$_2$ (**4.21**) undergoes 1,2-elimination, presumably *via* dihydrogen adduct Cp"$_2$Ti=NBMes$_2$(H$_2$) (**4.22**), dihydrogen can decoordinate to reform Cp"$_2$Ti=NBMes$_2$ (**4.1**) as well as free H$_2$. This free dihydrogen can either react with **4.1** to reform Cp"$_2$Ti=NBMes$_2$(H$_2$) (**4.22**) and Cp"$_2$Ti(H)N(H)BMes$_2$ (**4.21**), or escape into the headspace of the NMR tube.

As discussed in Chapter One, reversible 1,2-additions of dihydrogen across titanium element muliple bonds have been reported previously, especially in metallocene based systems. The first Group 4 imido complexes undergoing 1,2-addition with H$_2$ forming amido-hydride zirconium and titanium complexes were reported by Wolczanski and co-

workers.[6,33–36] The facile activation of dihydrogen using Cp"$_2$Ti=NBMes$_2$ (**4.1**) parallels the hydrogenation chemistry of Cp*$_2$Ti=NPh (**1.28**)[25] and Cp*$_2$Ti=S(py) (**4.23**),[32] which both reversibly activate dihydrogen at room temperature. However, in contrast to Cp"$_2$Ti(H)N(H)BMes$_2$ (**4.21)**, these systems lose dihydrogen relatively more easily and hamper their isolation on the preparative scale. For example, application of vacuum to a solution of C_6D_6 containing Cp*Ti(H)SH(py) (**4.23**), lead to rapid dihydrogen loss from **4.23** and Cp*Ti=S(py) (**4.23**) is reformed before the solvent could be removed. Chirik also reported the addition of dihydrogen using the previously mentioned titanium imide complexes Cp"$_2$Ti=NSiMe$_3$ (**1.17**) and Cp"$_2$Ti=NMes (**1.18**), to form Cp"$_2$Ti(H)N(H)SiMe$_3$ (**1.32**) and Cp"$_2$Ti(H)N(H)Mes (**1.33**) under ambient conditions (1 bar H_2, room temperature).[16] However, these compounds were only characterised *in-situ*, and no attempts to isolate these compounds on the preparative scale were reported. In fact, there are no monomeric crystallographically authenticated examples of titanium hydride amide complexes reported to date.

In the present case, it was possible to isolate and crystallographically characterise Cp"$_2$Ti(H)N(H)BMes$_2$ (**4.21**), owing its relative stability against dihydrogen loss. After pressurising a degassed solution of Cp"$_2$Ti=NBMes$_2$ (**4.1**, 250 mg) in benzene in a Schlenk tube with 1.2 bar of H_2, the solution turned yellow instantly. The reaction mixture was continued to stir for 2 h under positive hydrogen pressure at room temperature, after which time the mixture was filtered and the volatiles were removed *in vacuo*. The product was isolated as orange powder in good yield (210 mg, 83%), and was found to be stable under a N_2 atmosphere over several weeks when stored at -35 °C. No decomposition was observed as judged by ^{1}H NMR analysis. However, when stored at RT, the powder slowly turns green (3-4 days), indicating dihydrogen loss to form **4.1**. The previously reported complexes Cp"$_2$Ti(H)N(H)SiMe$_3$ (**1.32**), and Cp"$_2$Ti(H)N(H)Mes (**1.33**) were also found to

be sufficiently stable towards vacuum, and were isolated on the preparative scale using an analogous procedure.

Diffraction quality crystals of Cp"$_2$Ti(H)N(H)BMes$_2$ (**4.21**) were grown from a saturated hexane solution under 1 bar pressure of H_2 at -35 °C. The solid state structure is shown in Figure 4.16, and selected bond distances and angles are listed in Table 4.3. Molecules of **4.21** feature a pseudo tetrahedral environment, with staggered Cp" rings, presumably to avoid unfavourable steric interactions.

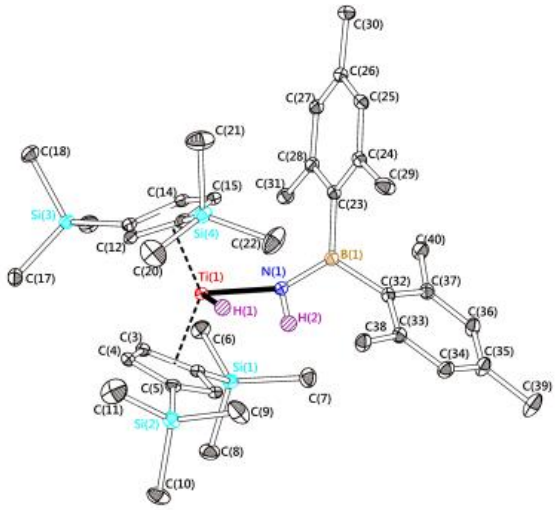


Figure 4.16 Displacement ellipsoid plots (20% probability) of Cp"$_2$Ti(H)N(H)BMes$_2$ (**4.21**). C-bound H atoms are omitted for clarity, H(1) and H(2) drawn as spheres of arbitrary radius.

Table 4.3 Selected bond distances (Å) and angles (°) for Cp"$_2$Ti(H)N(H)BMes$_2$ (**4.21**). $Cp_{cent(1)}$ and $Cp_{cent(2)}$ refer to the centroids for Cp″ ring carbons C(1)−C(5) and C(12)−C(16), respectively.

Parameter	**4.21**
Ti(1)–N(1)	2.0237(16)
Ti(1)–$Cp_{cent(1)}$	2.06
Ti(1)–$Cp_{cent(2)}$	2.08
Ti(1)–H(1)	1.64(4)
N(1)–B(1)	1.418(3)
N(1)–H(2)	0.87(3)
Ti(1)−N(1)−B(1)	150.94(14)
H(1)–Ti(1)···N(1)–Ti(1)	80.0
$Cp_{cent(1)}$–Ti(1)–$Cp_{cent(2)}$	136.5

The Ti(1)−N(1) distance is 2.0237(16) Å, significantly elongated from the corresponding value of 1.8069(7) Å in $Cp''_2Ti{=}NBMes_2$ (**4.1**). Additionally, the Ti(1)−N(1)−B(1) angle decreased from 175.7(1) in **4.1** to 150.94(14)°, which is also in agreement with a reduced titanium imide bond order. The hydrogen atoms H(1) and H(2) were found in the Fourier difference map, and feature Ti(1)–H(1) and N(1)–H(2) bond distances of 1.64(4) and 0.87(3) Å, respectively. The Ti(1)–H(1) bond distance is comparable to the ones found in $Cp^*_2Ti(H)_2$ (**4.26**), namely 1.63(3) and 1.68(3) Å.[37] The hydridic H(1) and protic H(2) moieties are turned away from each other, as indicated by the dihedral H(1)–Ti(1)···N(1)–Ti(1) angle of 80.0°. Notably, $Cp''_2Ti(H)N(H)BMes_2$ (**4.21**) represents the first structurally authenticated example of a titanium hydride amide.

4.7 Conclusions and outlook

This Chapter described a novel synthetic approach towards titanium borylimide complexes, namely the oxidative addition of borylazides N_3BR_2 to Ti(II) precursors. Importantly, this circumvents the limitation of previous protonolysis methodologies, in which the majority of borylamines H_2NBR_2 were insufficiently acidic to be installed on metal centres. Three different examples of highly reactive titanium borylimide complexes of type $Cp''_2Ti{=}NBR_2$ could be prepared this way, namely $Cp''_2Ti{=}NB\{N(Me)_2C_6H_4\}$ (**4.11**), $Cp''_2Ti{=}NB(NDippCH)_2$ (**4.12**) and $Cp''_2Ti{=}NBMes_2$ (**4.1**).

Complex **4.1** is a rare example of a base-free sandwich imide complex which could be isolated and structurally characterised. In contrast to the vast majority of borylimide complexes that feature two nitrogen atoms adjacent to the boron centre, $Cp''_2Ti{=}NBMes_2$ (**4.1**) features two aryl groups. The solid state structure shows there is negligible π-donation of these aryl groups into the boron based p-orbital. Additionally, the solid state structure, as well as MO DFT calculations, suggest significant "Ti=N=B" cumulene character, and

thus the titanium nitrogen bond length of 1.8069(7) Å is one of the longest titanium imide bonds reported to date. Preliminary reactivity studies suggest $Cp''_2Ti{=}NBMes_2$ (**4.1**) to be more reactive towards small molecule activation than the previously studied $Cp^*Ti(HPP)(NB(NDippCH)_2)$ (**1.83**).

Currently, another D.Phil student in the group is exploring the reactivity borylimide complex $Cp''_2Ti{=}NBMes_2$ (**4.1**) with a variety of small molecules, with the aim of understanding the subtle electronic differences the electropositive boron atom has on the reactivity compared to titanium alkyl- and arylimides.

4.8 References

1 B. A. Clough, S. Mellino, A. V. Protchenko, M. Slusarczyk, L. C. Stevenson, M. P. Blake, B. Xie, E. Clot and P. Mountford, *Inorg. Chem.*, 2017, **56**, 10794–10814.

2 K. Niedenzu and J. W. Dawson, *Boron-Nitrogen Compounds*, Springer Berlin Heidelberg, 1965.

3 L. C. Stevenson, S. Mellino, E. Clot and P. Mountford, *J. Am. Chem. Soc.*, 2015, **137**, 10140–10143.

4 B. A. Clough and P. Mountford, *Organometallics*, 2018, ASAP.

5 J. L. Polse, R. A. Andersen and R. G. Bergman, *J. Am. Chem. Soc.*, 1998, **120**, 13405–13414.

6 C. C. Cummins, C. P. Schaller, G. D. Van Duyne, P. T. Wolczanski, A. W. E. Chan and R. Hoffmann, *J. Am. Chem. Soc.*, 1991, **113**, 2985–2994.

7 J. L. Bennett and P. T. Wolczanski, *J. Am. Chem. Soc*, 1997, **119**, 10696–10719.

8 T. E. Hanna, E. Lobkovsky and P. J. Chirik, *Eur. J. Inorg. Chem.*, 2007, **2007**, 2677–2685.

9 S. C. Dunn, P. Mountford and D. A. Robson, *Dalton Trans.*, 1997, **2**, 293–304.

10 A. A. Danopoulos, C. Redshaw, A. Vaniche, G. Wilkinson, B. Hussain-Bates and M. B. Hursthouse, *Polyhedron*, 1993, **12**, 1061–1071.

11 K. Weber, K. Korn, A. Schorm, J. Kipke, M. Lemke, A. Khvorost, K. Harms and J. Sundermeyer, *ZAAC*, 2003, **629**, 744–754.

12 P. Paetzold and R. Truppat, *Chem. Ber.*, 1983, **116**, 1531–1539.

13 W. Fraenk, T. Habereder, T. M. Klapötke, H. Nöth and K. Polborn, *Dalt. Trans.*, 1999, **0**, 4283–4286.

14 S. Bräse, C. Gil, K. Knepper and V. Zimmermann, , DOI:10.1002/anie.200400657.

15 E. Pretsch, P. Bühlmann and M. Badertscher, in *Spektroskopische Daten zur Strukturaufklärung organischer Verbindungen*, Springer Berlin Heidelberg, Berlin, Heidelberg, 2010, pp. 273–339.

16 T. E. Hanna, I. Keresztes, E. Lobkovsky, W. H. Bernskoetter and P. J. Chirik, *Organometallics*, 2004, **23**, 3448–3458.

17 L. C. Stevenson, DPhil Thesis, University of Oxford, 2015.

18 B. Clough, DPhil Thesis, University of Oxford, 2016.

19 L. C. Stevenson, S. Mellino, E. Clot and P. Mountford, *J. Am. Chem. Soc.*, 2015, **137**, 10140–10143.
20 K. M. Doxsee, L. C. Garner, J. Juliette, J. K. . Mouser, T. Weakley and H. Hope, *Tetrahedron*, 1995, **51**, 4321–4332.
21 S. C. W. C. R. Groom, I. J. Bruno, M. P. Lightfoot, *Ward*, *Acta Cryst*, 2016, **B72**, 171–179.
22 R. A. Bartlett, H. Chen, H. V. R. Dias, M. M. Olmstead and P. P. Power, *J. Am. Chem. Soc.*, 1988, **110**, 446–449.
23 J. W. Lauher and R. Hoffmann, *J. Am. Chem. Soc.*, 1976, **98**, 1729–1742.
24 J. C. Green, *Chem. Soc. Rev.*, 1998, **27**, 263.
25 J. L. Polse, R. A. Andersen and R. G. Bergman, *J. Am. Chem. Soc.*, 1998, **120**, 13405–13414.
26 A. P. Duncan and R. G. Bergman, *Chem. Rec.*, 2002, **2**, 431–445.
27 C. Summerford and K. Wade, *J. Chem. Soc. A*, 1970, 2010.
28 D. P. Emerick, F. C. Nahm, K. Niedenzu, L. Komorowski and J. Lipinski, *ZAAC*, 1980, **468**, 44–54.
29 K. I. Gell, B. Posin, J. Schwartz and G. M. Williams, *J. Am. Chem. Soc.*, 1982, **104**, 1846–1855.
30 Marcel Schlaf, A. Alan J. Lough and R. H. Morris, *Organometallics*, 1996, **15**, 4423–4436.
31 D. Sellmann, G. H. Rackelmann and F. W. Heinemann, *Chem. - A Eur. J.*, 1997, **3**, 2071–2080.
32 Z. K. Sweeney, J. L. Polse, R. G. Bergman and R. A. Andersen, *Organometallics*, 1999, **18**, 5502–5510.
33 J. L. Bennett and P. T. Wolczanski, *J. Am. Chem. Soc.*, 1994, **116**, 2179–2180.
34 J. L. Bennett and P. T. Wolczanski, *J. Am. Chem. Soc.*, 1997, **119**, 10696–10719.
35 C. P. Schaller, C. C. Cummins, P. T. Wolczanski and N. York, *J. Am. Chem. Soc.*, 1996, **118**, 591–611.
36 T. R. Cundari, T. R. Klinckman and P. T. Wolczanski, *J. Am. Chem. Soc.*, 2002, **124**, 1481–1487.
37 J. Pinkas, R. Gyepes, I. Císařová, J. Kubišta, M. Horáček and K. Mach, *Dalt. Trans.*, 2017, **46**, 8229–8244.

Chapter Five

Experimental details and characterising data

5.1 General methods and implementation

All manipulations were carried out using standard Schlenk line or dry-box techniques under an atmosphere of argon or dinitrogen. Solvents were either degassed by sparging with dinitrogen and dried by passing through a column of the appropriate drying agent[1] or refluxed over sodium (toluene), potassium (THF), Na/K alloy (Et_2O) or CaH_2 (pyridine) and distilled. Deuterated solvents were dried over potassium (C_6D_6) or CaH_2 (pyridine-d_5), distilled under reduced pressure and stored under argon in Teflon valve ampoules. Unless otherwise stated NMR samples were prepared under dinitrogen in 5 mm Wilmad 507-PP tubes fitted with J. Young Teflon valves. ^{1}H, $^{13}C\{^{1}H\}$, $^{11}B\{^{1}H\}$ and ^{2}H spectra were recorded on a Bruker Ascend 400 NMR spectrometer, a Bruker Avance III 500 NMR spectrometer or on a Bruker AVC 500 spectrometer fitted with a ^{13}C cryoprobe. Unless otherwise stated, all NMR spectra were recorded at 298 K. ^{1}H and $^{13}C\{^{1}H\}$ and spectra were referenced internally to residual protio-solvent (^{1}H) or solvent (^{13}C) resonances, and are reported relative to tetramethylsilane ($\delta = 0$ ppm). ^{2}H NMR spectra were referenced to the natural abundance deuterium resonance of the protio solvent. ^{11}B NMR spectra were referenced externally to $Et_2O{\cdot}BF_3$ respectively. Assignments were confirmed as necessary with the use of two dimensional ^{1}H–^{1}H and ^{13}C–^{1}H correlation experiments. Chemical shifts are quoted in δ (ppm) and coupling constants in Hz. Unless otherwise stated, IR spectra were recorded on a Thermo Scientific Nicolet iS5 FTIR spectrometer and samples prepared in a dry-box using NaCl plates as a Nujol mull. The data are quoted in wavenumbers (cm^{-1}). Mass spectra were recorded by the mass spectrometry service of Oxford University's Department of Chemistry. Elemental analyses were carried out by the Elemental Analysis Service at the London Metropolitan University. $H_3B{\cdot}NMe_2H$ and $H_3B{\cdot}NMe_3$ were purchased from Aldrich and sublimed twice and once prior to use (5×10^{-2} Torr, 298 K), respectively. $TiCl_3{\cdot}AlCl_3$ was purchased from Aldrich and used as received. Distilled water was obtained from a Millipore-Q distillation apparatus in house. HCCAr,

TolC(=O)H, ArC(=O)Me, ArC(=O)OMe and H_2N*t*Bu were dried over CaH_2 and distilled before use. Cyclohexene was purchased from Aldrich, dried over sodium, vacuum distilled and stored over 3 Å molecular sieves. Quantitative ^{11}B NMR measurements were conducted using a 1D sequence for suppression of background signals using composite pulsewith inverse gated decoupling.[2] All other reagents were purchased from commercial suppliers, and (for liquid reagents) degassed before use.

5.2 Literature preparations

$H_2NB(NDippCH)_2$,[3] Cp*Ti(HPP){$NB(NDippCH)_2$} (**1.83**),[4] TMS(H)C=C=O,[5] $Me_2NH{\cdot}BD_3$,[6] $Me_2ND{\cdot}BH_3$,[6] $Me_2ND{\cdot}BD_3$,[6] $^iPr_2NH{\cdot}BH_3$,[7] $Et_2NH{\cdot}$9-BBN, $^tBuNH_2{\cdot}$9-BBN,[7] $^tBuNH_2{\cdot}BH_3$,[8] $MeNH_2{\cdot}BH_3$,[7] $Et_3B{\cdot}NMe_2H$,[9] $[H_2B(\mu\text{-}H)(\mu\text{-}NHMe)BH_2]$,[10] $Me_2NH{\cdot}BH_2NHMe{\cdot}BH_3$,[11] $TiCl_3{\cdot}(THF)_3$,[12] CpLi,[13] $MesN_3$,[14] $(Cp''_2Ti)_2(\mu_2,\eta^1,\eta^1\text{-}N_2)$ (Cp'' = $\eta^5\text{-}C_5H_3\text{-}1,3\text{-}(SiMe_3)_2$), **1.16**),[15] $Cp''_2Ti{=}NSiMe_3$ (**1.17**),[15] $Cp''_2Ti{=}NMes$ (**1.18**),[15] $Cp''_2Ti(H)N(H)SiMe_3$ (**1.32**),[15] $Cp''_2Ti(D)N(D)SiMe_3$ (**1.32-d$_2$**),[15] $Cp''_2Ti(H)N(H)Mes$ (**1.33**),[15] $Cp''_2Ti(D)N(D)Mes$ (**1.33-d$_2$**),[15] $(1,2\text{-}C_6H_4O_2)B(N_3)$,[16] Cp*Ti($N^tBu$){$MeC(N^iPr)_2$} (**2.5**),[17] Cp*Ti(NAr){$MeC(N^iPr)_2$} (**2.6**),[17] were synthesised according to literature procedures.

5.3 X-ray data collection and processing parameters

Crystals were mounted on glass fibres using perfluoropolyether oil and cooled rapidly in a stream of cold N_2 using an Oxford Cryosystems Cryostream unit. Diffraction data were measured using either an Enraf-Nonius KappaCCD or Agilent Technologies Supernova diffractometer using Mo-K_a or Cu-K_a radiation, respectively. As appropriate, absorption and decay corrections were applied to the data and equivalent reflections merged.[18] The structures were solved with SIR92[19] or Superflip,[20] and further refinements and all other crystallographic calculations were performed using the CRYSTALS program suite.[21] Other details of the

structure solutions and refinements are given in the individual CIFs contained in the CD Appendix.

5.4 Computational details

DFT calculations described in this Thesis were performed by Philip Mountford and Simona Mellino at The University of Oxford in collaboration with Dr Eric Clot at Université Montpellier 2, and have been published.[4,22] Geometry optimisations were performed with the Gaussian09 package[23] at the B3PW91 level of hybrid density functional theory,[24,25] with inclusion of Grimme's D3(bj) correction[26,27] in the optimisation process. For geometry optimisations in the gas phase all atoms were represented by the Def2-SVP basis set.[28] Single-point calculations took into account both solvent and dispersion effects. The solvent (benzene) influence was taken into consideration through single point calculations on the gas-phase optimized geometry with SCRF calculations within the SMD model.[29] For the SCRF calculations all the atoms were treated with a Def2-TZVP basis set.[30] Influence of the dispersion forces was also considered by computing the D3(bj) corrections.[26,27] SCF energies reported in this work are for gas-phase model systems using the Def2-TZVP basis set.

5.5 Experimental details and characterising data for Chapter Two

Synthesis of Cp*Ti(NAr){MeC(N^{i}Pr)$_2$}, with Ar = Xylil (1.36g), C$_6$H$_4$X, X=Me (1.36a), NMe$_2$ (1.36b), OMe (1.36c), H (1.36d), Cl (1.36e), Br (1.36f), CF$_3$ (1.36h). These compounds were synthesized in adaption to a known literature procedure.[17] A schlenk was charged with Cp*Ti(N^{t}Bu){MeC(N^{i}Pr)$_2$} (**2.1**, 1 g, 0.415 mmol) and aniline (1 equiv., 0.415 mmol). The compounds were dissolved in 15 mL of benzene and the red solution was stirred for 2 h at RT upon which time the color changed to dark green. The volatiles were removed under reduced pressure and the product was washed using hexanes (0 °C, 1 x 15 mL) and then dried *in vacuo* to yield Cp*Ti(NAr){MeC(N^{i}Pr)$_2$} as green powder. Yield: 60-80%.

Data for Cp*Ti(NAr){MeC(N^{i}Pr)$_2$}, Ar = C$_6$H$_4$OMe (1.36c). **^{1}H NMR (Tol-d8, 400MHz):** δ 6.61 (2 H, app. s, o-C_6H_4OMe), 6.61 (2 H, app. s, m-C_6H_4OMe), 3.59 (2 H, sept., ^3J = 6.3 Hz, C<u>H</u>Me$_2$), 3.35 (3 H, s, OMe), 2.08 (15 H, s, C_5Me_5), 1.64 (3 H, s, Me), 1.12 (6 H, d, ^3J = 6.3 Hz, CH<u>Me</u>$_2$), 1.03 (6 H, d, ^3J = 6.3 Hz, CH<u>Me</u>$_2$) ppm. **^{13}C{^{1}H} NMR (Tol-d8, 100.6 MHz):** δ 163.3 (N_2CN), 155.5 (*i*-C_6<u>H</u>$_4$OMe), 153.3 (*p*-C_6<u>H</u>$_4$OMe), 124.0 (*o*-C_6<u>H</u>$_4$OMe), 120.4 (<u>C</u>$_5$Me$_5$), 113.0 (*m*-C_6<u>H</u>$_4$OMe), 54.9 (OMe), 49.4 (<u>C</u>HMe$_2$), 26.3 (CH<u>Me</u>$_2$), 25.4 (CH<u>Me</u>$_2$), 12.3 (C_5<u>Me</u>$_5$), 11.5 (N_2C<u>Me</u>) ppm. **IR (NaCl plates, Nujol mull, cm^{-1}):** 2724 (w), 1596 (w), 1489 (s), 1463 (s), 1377 (s), 1321 (s), 1291 (m), 1268 (s), 1233 (s), 1214 (s), 1177 (m), 1093 (m), 1039 (m), 966 (m), 825 (s), 787 (m), 754 (w), 723 (w). Repeated elemental analysis yielded in consistently too low numbers indicating incomplete combustion or product sensitivity.

Data for Cp*Ti(NAr){MeC(N^{i}Pr)$_2$}, Ar = Ph (1.36d). **^{1}H NMR (C$_6$D$_6$, 400 MHz):** δ 7.14-7.10 (2 H, m, o-C_6H_5), 6.79-6.77 (2 H, m, m-C_6H_5), 6.76-6.73 (1 H, m, p-C_6H_5), 3.56 (2 H, sept, ^3J = 6.9 Hz, C<u>H</u>Me$_2$), 2.89 (15 H, s, C_5Me_5), 1.57 (3 H, s, Me), 1.11 (6 H, d, ^3J = 6.4 Hz, CH<u>Me</u>$_2$), 1.01 (6 H, d, ^3J = 6.4 Hz, CH<u>Me</u>$_2$) ppm. **^{13}C{^{1}H} NMR (C$_6$D$_6$, 100.6 MHz):** δ 163.8 (N_2CN), 160.9 (*i*-C_6H_5), 128.5 (*o*-C_6H_5), 123.4 (*m*-C_6H_5), 120.9 (<u>C</u>$_5$Me$_5$), 119.3 (p-C_6H_5), 49.4 (<u>C</u>HMe$_2$), 26.3 (CH<u>Me</u>$_2$), 25.3 (CH<u>Me</u>$_2$), 12.4 (C_5<u>Me</u>$_5$), 11.7 (N_2C<u>Me</u>) ppm. **IR (NaCl plates, Nujol mull, cm^{-1}):** 2725 (w), 1653 (w), 1626 (w), 1592 (w), 1580 (s), 1456 (s), 1377 (s), 1318 (s), 1261 (s), 1214 (s), 1172 (m), 1122 (m), 1062 (m), 1019 (m), 994 (m), 958 (m), 879 (w), 850 (w), 812 (m), 754 (s), 722 (m), 689 (m), 621 (w). **Anal. found (calcd. for C$_{25}$H$_{38}$N$_3$Ti):** C, 69.8 (70.08); H, 8.73 (8.94); N, 9.29 (9.31)%.

Data for Cp*Ti(NAr){MeC(N^{i}Pr)$_2$}, Ar = C$_6$H$_4$Cl (1.36e). **^{1}H NMR (C$_6$D$_6$, 400MHz):** δ 7.07 (2 H, d, ^3J = 8.4 Hz, *m*-C_6<u>H</u>$_4$Cl), 6.54 (2 H, d, ^3J = 8.4 Hz, *o*-C_6<u>H</u>$_4$Cl), 3.51 (2 H, sept, ^3J = 6.4 Hz, C<u>H</u>Me$_2$), 2.04 (15 H, s, C_5Me_5), 1.54 (3 H, s, N_2CCH_3), 1.04 (6 H, d, ^3J = 6.4 Hz, CH<u>Me</u>$_2$), 0.98 (6 H, d, ^3J = 6.4 Hz, CH<u>Me</u>$_2$) ppm. **^{13}C{^{1}H} NMR (C$_6$D$_6$, 100.6 MHz):** δ 163.9 (N_2CN), 159.1 (*p*-<u>C</u>$_6$H$_4$Cl), 129.4 (*m*-<u>C</u>$_6$H$_4$Cl), 124.4 (*o*-<u>C</u>$_6$H$_4$Cl), 123.5 (*i*-<u>C</u>$_6$H$_4$Cl), 121.2 (<u>C</u>$_5$Me$_5$), 49.4

($\underline{C}HMe_2$), 26.2 ($\underline{C}HMe_2$), 25.2 ($\underline{C}HMe_2$), 12.4 ($C_5\underline{Me}_5$), 11.7 ($N_2C\underline{Me}$) ppm. **IR (NaCl plates, Nujol mull, cm^{-1}):** 2725 (w), 2670 (w), 1654 (w), 1622 (w), 1572 (w), 1463 (s), 1377 (s), 1323 (s), 1261 (s), 1213 (m), 1170 (m), 1158 (m), 1088 (m), 1017 (m), 962 (m), 890 (w), 824 (m), 801 (m), 723 (m), 668 (m). **EI-MS:** *m*/*z* = 449.21 $[M]^+$ (5%).

Data for Cp*Ti(NAr){MeC(N^{i}Pr)$_2$}, Ar = C$_6$H$_4$Br (1.36f). **^{1}H NMR (C$_6$D$_6$, 400MHz):** δ 7.21 (2 H, d, ^3J = 8.6 Hz, *m*-$C_6\underline{H}_4Br$), 6.48 (2 H, d, ^3J = 8.6 Hz, *o*-$C_6\underline{H}_4Br$), 3.51 (2 H, sept, ^3J = 6.4 Hz, $C\underline{H}Me_2$), 2.04 (15 H, s, C_5Me_5), 1.53 (3 H, s, N_2CCH_3), 1.03 (6 H, d, ^3J = 6.4 Hz, $CH\underline{Me}_2$), 0.98 (6 H, d, ^3J = 6.4 Hz, $CH\underline{Me}_2$) ppm. **^{13}C{^{1}H} NMR (C$_6$D$_6$, 100.6 MHz):** δ 163.9 (N_2CN), 159.4 (*p*-$\underline{C}_6H_4Br$), 131.4 (*m*-$\underline{C}_6H_4Br$), 124.9 (*o*-$\underline{C}_6H_4Br$), 121.3 ($\underline{C}_5Me_5$), 111.0 (*i*-$\underline{C}_6H_4Br$), 49.4 ($\underline{C}HMe_2$), 26.2 ($\underline{C}HMe_2$), 25.2 ($\underline{C}HMe_2$), 12.4 ($C_5\underline{Me}_5$), 11.7 ($N_2C\underline{Me}$) ppm. **IR (NaCl plates, Nujol mull, cm^{-1}):** 2723 (w), 1859 (w), 1582 (w), 1566 (m), 1463 (s), 1377 (s), 1320 (s), 1262 (s), 1212 (s), 1171 (s), 1088 (m), 1068 (m), 961 (m), 822 (s), 723 (m), 704 (m). **Anal. found (calcd. for C$_{24}$H$_{36}$BrN$_3$Ti):** C, 58.31 (58.12); H, 7.17 (7.34); N, 8.39 (8.5)%. Compounds Ar = Xylil, and C_6H_4X, X = Me (**1.36a**), CF_3 (**1.36h**), NMe_2 (**1.36b**) were reported previously in the literature.[17]

General procedure for NMR tube scale dehydrocoupling reactions at 0 °C. In the glovebox, 0.1 mL of the appropriate titanium catalyst stock solution, dissolved in toluene, was introduced into a first NMR tube fitted with a J. Youngs valve. A second NMR tube fitted with a J. Youngs valve was charged with amine-borane dissolved in 0.7 mL of toluene. The total amount of solvent in both NMR tubes was always kept at 0.8 mL. The NMR tubes were sealed and cycled out of the glovebox. The NMR tubes were then fitted with a glass adapter which was connected to a high vacuum line and first cycled 3 times, and subsequently purged under a constant flow of argon for 10 minutes. The NMR tubes were opened under a strong counter flow of argon and the glass adapters were fitted with a subaseal. Subsequently, the adapters were purged for 10 min. Additionally, both NMR tubes were cooled in an ice/water bath at 0

°C and equilibrated for 20 min at this temperature. Then, the solution containing the amineborane substrate was transferred into the solution containing the titanium catalyst using a short canula. The NMR tube was sealed with a J. Youngs valve and NMR spectra were recorded immediately using a pre-cooled and pre-shimmed NMR spectrometer.

General procedure for NMR tube scale dehydrocoupling reactions at room temperature. In the glovebox, 0.1 mL of appropriate titanium catalyst stock solution, dissolved in toluene, was introduced into a first NMR tube. To this solution was added a solution (0.7 mL of toluene) of appropriate amount of amine-borane. The total amount of solvent in the NMR tubes was always kept at 0.8 mL. The NMR tube was sealed with a J. Youngs valve. After transferring out of the glovebox, the reaction was immediately followed by NMR spectroscopy using a pre-shimed NMR spectrometer.

Readdition experiment. In the glovebox, 0.1 mL of a stock solution of Cp*Ti(NTol){MeC(N^{i}Pr)$_2$} (**1.36a**, 0.00606 mmol) dissolved in toluene was introduced into a first NMR tube. To this solution was added a solution (0.7 mL of toluene) with 50 equivalents of $Me_2NH{\cdot}BH_3$ (0.302 mmol). The NMR tube was immediately sealed with a J. Youngs valve. After transferring out of the glovebox, the reaction was followed by $^{11}B\{^1H\}$ NMR spectroscopy using a pre-shimed NMR spectrometer (298 K). After full conversion was reached (*ca.* 30 min) the NMR tube was reintroduced into the glovebox. The solution was transferred into a glass vial containing additional 50 equivalents of $Me_2NH{\cdot}BH_3$ (0.302 mmol). After dissolving all amine-borane the solution was reintroduced into the NMR tube, sealed, transferred out of the glovebox, and the reaction process was continued to be monitored using $^{11}B\{^1H\}$ NMR spectroscopy.

Mercury poisoning. In the glovebox, 0.1 mL of a stock solution of Cp*Ti(NTol){MeC(N^{i}Pr)$_2$} (**1.36a**, 0.00302 mmol) dissolved in toluene was introduced into a NMR tube. To this solution

was added *ca.* 100 equiv. of elementar Hg (60.1 mg), and subsequently a solution of 0.7 mL of toluene containing 100 equivalents of $Me_2NH{\cdot}BH_3$ (0.302 mmol). The NMR tube was immediately sealed with a J. Youngs valve. After transferring out of the glovebox, the NMR tube was fixed onto a Fisher lab shaker to ensure vigorous shaking. After *ca.* 17 min a $^{11}B\{^1H\}$ NMR was recorded and showed 50% conversion of the amine-borane.

Alternative synthesis for $(^iPr)_2N{=}BH_2$. $(^iPr)_2NH{\cdot}BH_3$ (2 g, 174 mmol) was placed in a two-necked Schlenk equipped with a reflux condensor, and heated to 190 °C for 20 h. The resulting terpid liquid was distilled (bp = 88 °C/1 atm) to give a clear, colorless oil in good yield (1.7 g, 86%). **^{1}H NMR (C_6D_6, 400MHz)**: δ.4.76 (s, 2 H, BH_2), 3.29-3.02 (m, 2 H, CH), 1.04 (d, ^3J = 6.6 Hz, 12 H, CH_3). ^{11}B NMR (C_6D_6, 128.4 MHz): δ 34.8 (t, ^1J = 127 Hz) ppm. These values match those of previously reported literature values.[31]

General procedure for table entries 1-14 (Table 2.2 and Table 2.9). Cp*Ti(N^tBu){$MeC(N^iPr)_2$} (**2.1**, 5 mg, 12.6 mmol) was weighed into a small glass vial in the dry-box, and more in cases higher catalyst loadings were required. Amine-boranes were weighed into a second glass vial (126 mmol) and dissolved in benzene (C_6D_6, 0.5 mL). In cases where no isolable amine-boranes were formed, an approproate amount of amine and borane were weighed out and premixed in benzene (C_6D_6, 0.5 mL). The solution was transferred into the first vial and mixed using a glass pipette until all catalyst was dissolved. The solution was transferred into a NMR tube fitted with a J. Youngs valve and the reaction progress was monitored *via* ^{1}H and ^{11}B NMR spectroscopy.

NMR tube scale synthesis of $Cy_2NH{\cdot}HBC_8H_{14}$. HBC_8H_{14} (13.9 mg, 113 mmol) and Cy_2NH (22.6 µL, 113 mmol) were dissolved in a total of 1 mL of C_6D_6 at RT. The equilibrium between borane, amine and $Cy_2NH{\cdot}HBC_8H_{14}$ was established within 3 h, and the ^{11}B NMR showed a ratio of ca. 1:1.4 between 9-BBN dimer and the amineborane adduct (note, HBC_8H_{14} exists

almost exclusively in dimeric form in solution).[32] The equilibrium constant was determined *via* quantitative ^{11}B NMR spectroscopy, K_{eq} (298 K, C_6D_6) = 1.2 M^{-1}. **^{1}H NMR (C_6D_6, 400MHz):** δ 2.87-2.8 (2 H, m, NCH), 2.52-2.4 (4 H, m, NCC$\underline{H}_2$), 2.32-2.23 (4 H, m, NCC$\underline{H}_2$), 1.85-1.76 (2 H, m, BCC$\underline{H}_2$ overlapping with free Cy_2NH), 1.71-1.64 (4 H, m, NCCC$\underline{H}_2$ overlapping with free Cy_2NH and 9-BBN dimer), 1.64-1.58 (2 H, m, BCC$\underline{H}_2$ overlapping with free Cy_2NH and 9-BBN dimer), 1.56-1.45 (2 H, m, BCCC$\underline{H}_2$ overlapping with free Cy_2NH and 9-BBN dimer), 1.52-1.45 (2 H, m, BCC$\underline{H}_2$ overlapping with free Cy_2NH and 9-BBN dimer), 1.4-1.33 (2 H, m, NCCCC$\underline{H}_2$), 1.29-1.17 (4 H, m, NCCC$\underline{H}_2$ overlapping with free Cy_2NH), 1.27-1.19 (2 H, m, BCC$\underline{H}_2$ overlapping with free Cy_2NH), 1.15 (2 H, s, BCH overlapping with free Cy_2NH), 1.0-0.9 (2 H, m, BCCC$\underline{H}_2$ overlapping with free Cy_2NH), 0.8-0.75 (2 H, m, NCCCC$\underline{H}_2$), 0.39 (1 H, s, NH) ppm. *The BH signal could not be located.* **^{13}C{^{1}H} NMR (C_6D_6, 100.6 MHz):** δ 57.6 (NCH), 35.8 (NC$\underline{C}H_2$), 31.3 (BC$\underline{C}H_2$), 30.8 (BC$\underline{C}H_2$), 26.4 (BCC$\underline{C}H_2$), 26.3 (NCC$\underline{C}H_2$), 26.0 (NCCC$\underline{C}H_2$), 25.7 (BCC$\underline{C}H_2$), 24.0 (broad, BCH) ppm. **^{11}B NMR (C_6D_6, 128.4 MHz):** δ -5.6 (broad) ppm.

$C_5H_{12}N$-BC_8H_{14}. To a mixture of 9-BBN (1.5 g, 12.3 mmol) in toluene (10 mL) was added piperidine (1.2 mL, 12.3 mmol) at RT. The reaction mixture was heated to 60 °C for 50 h, and subsequently all volatiles were removed *in vacuo*. The product was distilled to yield a colorless oil. Yield: 2.2 g (87 %). **^{1}H NMR (C_6D_6, 400MHz):** δ 3.24-3.00 (4 H, m, NCH_2), 1.96-1.88 (4 H, m, BCHC$\underline{H}_2$), 1.85-1.76 (4 H, m, BCHC$\underline{H}_2$), 1.59-1.55 (2 H, m, BCH), 1.52-1.42 (4 H, m, overlapping $BCHCH_2C\underline{H}_2$ and $NCHCH_2C\underline{H}_2$), 1.33-1.27 (4 H, m, $NCH_2C\underline{H}_2$) ppm. **^{13}C{^{1}H} NMR (C_6D_6, 125.8 MHz):** δ 48.4 (NCH_2), 33.4 (BCH$\underline{C}H_2$), 29.2 ($NCH_2\underline{C}H_2$), 26.0 ($NCH_2CH_2\underline{C}H_2$), 24.1 ($BCHCH_2\underline{C}H_2$), 23.3 (broad, BCH) ppm. ^{11}B NMR (C_6D_6, 128.4 MHz): δ 46.4 (s) ppm. **IR (NaCl plates, Nujol mull, cm^{-1}):** 2663 (w), 2363 (m), 2314 (m), 1738 (w), 1475 (s), 1377 (m), 1348 (w), 1306 (w), 1284 (w), 1260 (m), 1221 (w), 1196 (w), 1064 (s), 957

(w), 826 (m), 799 (m), 722 (w). **EI-MS:** *m*/*z* = 205.201 $[M]^+$. **Anal. found (calcd. for $C_{13}H_{24}BN$):** C, 76.41 (76.11); H, 11.60 (11.79); N, 6.80 (6.83)%.

[Cp*Ti{N(Tol)BN(Tol)}]$_2$ (2.3). To a mixture of $Me_2NH{\cdot}BH_3$ (2 g, 34 mmol) in benzene (10 mL) was added Cp*Ti{MeC(N^iPr)$_2$}NTol (120 mg, 0.280 mmol) at RT. Immediate bubbling indicates release of hydrogen. The mixture was stirred at RT for 48 h. The volatiles were removed in vacuo to give a brown solid. Recrystallisation in hexanes afforded orange crystals. Yield: 20 mg (18 %). The compound was found to be not sufficiently soluble in a variety of solvents, precluding full characterisation.

Alternative synthesis for $BD_3{\cdot}THF$. $NaBD_4$ (5 g, 119 mmol) and I_2 (15.1 g, 59.7 mmol) were placed in two different Schlenk tubes and THF was added to give a slurry in the Schlenk containing $NaBD_4$ (ca. 30 mL), and a brown solution for the Schlenk containing I_2 (70 mL). Both mixtures were cooled to 0 °C, and the brown iodine solution was added slowly to the sodium borodeuteride slurry. Heat and gas (D_2 gas) evolution is observed and the reaction is complete after the color changed from brown to white (*ca.* 1 h). The mixture is distilled (trap-to-trap) to give a colorless solution of BD_3 in THF. The absence of signals in the ^{1}H NMR, and a single peak at -1 ppm in the ^{11}B NMR show the clean formation of the target compound.[33] The solution was used without concentration determination in order to synthesize amine-borane $Me_2NH{\cdot}BD_3$. This protocol was developed in collaboration with Dr Andrey Protchenko.

$Me_2NH{\cdot}BH_2$<u>NHMe</u>$\cdot BH_3$. The title compound was synthesized according to an adaption of a literature synthesis of $H_3N{\cdot}BH_2NH_2{\cdot}BH_3$.[34] This compound was first reported by Wass et al., however, characterising data were missing in their initial report.[11] $MeNH_2{\cdot}BH_3$ (1.6 g, 35.9 mmol) was dissolved in THF (10 mL) and $BH_3{\cdot}SMe_2$ (3.4 mL, 37 mmol) was added at RT. The solution was heated to 60 °C and stirred for 24 h at this temperature. ^{11}B NMR was used to estimate how much $BH_3{\cdot}SMe_2$ was left and an equimolar amount of PPh_3 was added, and stirred

for 10 min at RT subsequently (an adduct is formed that allows for an easier purification by distillation). The reaction mixture was subsequently vacuum transferred to yield a pure solution of [$H_2B(\mu\text{-}H)(\mu\text{-}NHMe)BH_2$]. To this colorless solution was added $Me_2NH{\cdot}THF$ (17.5 mL, 35 mmol) at -78 °C. The mixture was stirred for 10 min at this temperature and then allowed to warm to RT and stirred overnight. The resulting solution was dried *in vacuo*, and purified by recrystallisation on diethyl ether at -30 °C. Yield: 900 mg (49% overall). **$^1H\{^{11}B\}$ NMR (Tol-d8, 400MHz):** δ 4.71 (1 H, s, br., N<u>H</u>Me_2), 2.21 (3 H, d, ^3J = 5.9 Hz, NH<u>Me</u>), 1.83-1.8 (3 H, s, br., BH_3), 1.77-1.74 (2 H, s, br., BH_2), 1.72-1.65 (6 H, m, NH<u>Me</u>$_2$), 1.48 (1 H, s, br., N<u>H</u>Me) ppm. **$^{13}C\{^1H\}$ NMR (C_6D_6, 125.8 MHz):** 40.4 (NHMe), 40.0 ($NHMe_2$), 39.7 ($NHMe_2$) ppm. **^{11}B NMR (C_6D_6, 128.4 MHz):** δ -2.4 (q, ^1J = 108 Hz, BH_2), -18.1 (q, ^1J = 93 Hz, BH_3) ppm. **IR (NaCl plates, Nujol mull, cm^{-1}):** 3242 (s, υ(N-H) st.), 3182 (s, υ(N-H) st.), 2413 (m, υ(B-H) st.), 2382 (m, υ(B-H) st.), 2307 (m, υ(B-H) st.), 2254 (m, υ(B-H) st.), 1460 (s), 1377 (s), 1315 (m), 1260 (w), 1245 (w), 1209 (w), 1170 (w), 1152 (w), 1051 (m), 1023 (m), 1022 (m), 1005 (m), 932 (w), 914 (w), 876 (w), 841 (w), 800 (w), 722 (m). **Anal. found (calcd. for $C_3H_{16}B_2N_2$):** C, 35.26 (35.40); H, 15.77 (15.84); N, 37.39 (27.52)%.

Catalytic synthesis of $Me_2NH{\cdot}BH_2NMe_2{\cdot}BH_3$. $Me_2NH{\cdot}BH_3$ (2 g, 33.9 mmol) was dissolved in 60 mL of toluene, and Cp*Ti{$MeC(N^iPr)_2$}NTol (**1.36a**, 146 mg, 0.34 mmol, 1% loading) was dissolved in 29 mL of toluene. After stirring both solutions 0 °C for 20 minutes the solution containing $Me_2NH{\cdot}BH_3$ was added to the catalyst containing solution *via* canula transfer. After 100 min an aliquot was taken and analysed *via* ^{11}B NMR, indicating the presence of *ca.* 90% $Me_2NH{\cdot}BH_2NMe_2{\cdot}BH_3$. The reaction was quenched with 1 drop of distilled water (ca. 20 uL) upon which the green solution turned light yellow after *ca.* 5 minutes. The solution was filtered and the volatiles removed *in vacuo.* The resulting off-white solid recrystallized in diethyl ether (ca. 25 mL) at -80 °C to produce long, white needles of the product. The off-white

supernatant was removed *via* canula transfer, and the product was isolated in good yield (1.59 g, 81%). ^{1}H and ^{11}B NMR analysis agreed with literature values.[35]

$Me_2NH{\cdot}BD_2NMe_2{\cdot}BD_3$. $Me_2NH{\cdot}BD_3$ (0.9 g, 14.5 mmol) was dissolved in 28 mL of toluene, and Cp*Ti{MeC(NiPr)2}NTol (**1.36a**, 62.4 mg, 0.145 mmol, 1% loading) was dissolved in 10 mL of toluene. After stirring both solutions 0 °C for 20 minutes the solution containing $Me_2NH{\cdot}BD_3$ was added to the catalyst containing solution *via* canula transfer. After 2.5 h an aliquot was taken and analysed *via* ^{11}B NMR, indicating the presence of *ca.* 90% $Me_2NH{\cdot}BD_2NMe_2{\cdot}BD_3$. The reaction was quenched with 1 drop of distilled water (ca. 20 uL) upon which the green solution turned light yellow after *ca.* 5 minutes. The solution was filtered and the volatiles removed *in vacuo*. The resulting off-white solid recrystallized in diethyl ether (ca. 25 mL) twice subsequently at -80 °C to produce long, white needles of the product. The off-white supernatant was removed *via* canula transfer, and the product was isolated in good yield (568 mg, 63%). ^{1}H-NMR analysis indicates >95% deuteration. **^{1}H NMR (C_6D_6, 400MHz):** δ 4.95 (1 H, broad, s, NH), 2.33 (6 H, s, NMe_2BD_3), 1.81 (6 H, d, ^{3}J = 5.8 Hz, $HNMe_2$) ppm. ^{13}C{^{1}H} NMR (C_6D_6, 125.8 MHz): δ 52.4 (NMe_2BD_3), 42.7 ($HNMe_2$) ppm. **^{11}B NMR (C_6D_6, 128.4 MHz):** δ **1.83** (1 B, app. s, BD_2), -13.4 (1 B, app. s, BD_3) ppm. **^{2}D NMR (C_6H_6, 61.4 MHz):** δ 2.28 (2 D, br, s, BD_2), 1.95 (3 D, br, s, BD_3) ppm. **IR (NaCl plates, Nujol mull, cm^{-1}):** 3198 (s, υ(N-H) st), 2726 (w), 2670 (w), 2599 (w), 2418 (w), 2374 (w), 2312 (m), 1811 (s, υ(B-H) st), 1749 (s, υ(B-H) st), 1709 (s, υ(B-H) st), 1636 (s, υ(B-H) st), 1456 (s), 1404 (m), 1377 (s), 1307 (s), 1261 (m), 1225 (m), 1203 (m), 1157 (s), 1129 (s), 1023 (s), 970 (s), 894 (s), 827 (m), 722 (w).

$Me_2ND{\cdot}BH_2NMe_2{\cdot}BH_3$. $Me_2ND{\cdot}BH_3$ (1.5 g, 25 mmol) was dissolved in 56 mL of toluene, and Cp*Ti{MeC($N^{i}Pr)_2$}NTol (**1.36a**, 107 mg, 0.25 mmol, 1% loading) was dissolved in 10 mL of toluene. After stirring both solutions 0 °C for 20 minutes the solution containing $Me_2ND{\cdot}BH_3$ was added to the catalyst containing solution *via* canula transfer. After 3 h 10 min

an aliquot was taken and analysed *via* ^{11}B NMR, indicating the presence of *ca.* 80% $Me_2ND{\cdot}BH_2NMe_2{\cdot}BH_3$. The reaction was quenched with 1 drop of $\underline{D_2O}$ (ca. 20 uL) upon which the green solution turned light yellow after *ca.* 5 minutes. The solution was filtered and the volatiles removed *in vacuo.* The resulting off-white solid recrystallized in diethyl ether (ca. 50 mL) twice subsequently at -80 °C to produce long, white needles of the product. The supernatant was removed *via* canula transfer, and the product was isolated in good yield (700 mg, 47%). ^{1}H-NMR analysis indicates >95% deuteration. **^{1}H NMR (C_6D_6, 400 MHz):** δ 2.34 (6 H, s, NMe_2, overlapping with BH_2 and BH_3), 2.27 (3 H, q, ^1J = 94 Hz, BH_3 overlapping with NMe_2, BH_2), 2.06 (2 H, q, ^1J = 110 Hz, BH_2 overlapping with NMe_2 and BH_3), 1.75 (6 H, s, $NDMe_2$ overlapping with BH_3 and BH_2) ppm. **^{13}C{^{1}H} NMR (C_6D_6, 125.8 MHz):** δ 52.5 (NMe_2), 42.5 ($DNMe_2$) ppm. **^{11}B NMR (C_6D_6, 128.4 MHz):** δ 2.08 (1 B, t, ^1J = 110 Hz, BH_2), -12.8 (1 B, q, ^1J = 94 Hz, BH_3) ppm. **^{2}D NMR (C_6H_6, 61.4 MHz):** δ 4.79 (br., s, ND) ppm. **IR (NaCl plates, Nujol mull, cm^{-1}):** 2715 (w), 2456 (m, υ(B-H) st), 2383 (s, υ(B-H) st), 2358 (s, υ(N-H) st), 2284 (s, υ(B-H) st), 2252 (s, υ(B-H) st), 2108 (w), 1456 (s), 1421 (m), 1401 (w), 1377 (s), 1307 (w), 1224 (w), 1196 (m), 1152 (m), 1104 (m), 1060 (m), 1028 (m), 1003 (m), 947 (s), 898 (s), 833 (m), 813 (m), 723 (m).

$Me_2ND{\cdot}BD_2NMe_2{\cdot}BD_3$. $Me_2ND{\cdot}BD_3$ (1.4 g, 22 mmol) was dissolved in 46 mL of toluene, and Cp*Ti{MeC(N^{i}Pr)$_2$}NTol (**1.36a**, 95.5 mg, 0.22 mmol, 1% loading) was dissolved in 10 mL of toluene. After stirring both solutions 0 °C for 20 minutes the solution containing $Me_2ND{\cdot}BD_3$ was added to the catalyst containing solution *via* canula transfer. After 6 h an aliquot was taken and analysed *via* ^{11}B NMR, indicating the presence of *ca.* 80% $Me_2ND{\cdot}BH_2NMe_2{\cdot}BD_3$. The reaction was quenched with 1 drop of $\underline{D_2O}$ (ca. 20 uL) upon which the green solution turned light yellow after *ca.* 5 minutes. The solution was filtered and the volatiles removed *in vacuo.* The resulting off-white solid recrystallized in diethyl ether (ca. 40 mL) twice subsequently at -80 °C to produce long, white needles of the product. The

supernatant was removed *via* canula transfer, and the product was isolated in good yield (870 mg, 64%). ^{1}H NMR analysis indicates >95% deuteration. **^{1}H NMR (C_6D_6, 400MHz):** δ 2.34 (6 H, s, NMe_2), 1.77 (6 H, s, $DNMe_2$) ppm. **$^{13}C\{^{1}H\}$ NMR (C_6D_6, 125.8 MHz):** δ 52.4 (NMe_2), 42.5 ($DNMe_2$) ppm. **^{11}B NMR (C_6D_6, 128.4 MHz):** δ 1.77 (1 B, s, BD_2), -13.4 (1 B, s, BD_3) ppm. **^{2}H NMR (C_6H_6, 61.4 MHz):** δ 4.8 (1 D, s, ND), 2.29 (2 B, br., s, BD_2), 1.99 (3 B, br., s, BD_3) ppm. **IR (NaCl plates, Nujol mull, cm^{-1}):** 2725 (w), 2411 (w), 2362 (m, υ(N-D) st), 1812 (m, υ(B-D) st), 1750 (m, υ(B-D) st), 1704 (m, υ(B-D) st), 1636 (m, υ(B-D) st), 1459 (s), 1403 (w), 1377 (s), 1304 (w), 1227 (w), 1203 (m), 1155 (m), 1080 (w), 1025 (m), 974 (s), 921 (m), 899 (s), 856 (m), 824 (m), 755 (w), 722 (m).

$C_8H_{10}NH{\cdot}H_2BTex$. H_2BTex (0.5 g, 5.16 mmol) was dissolved in 10 mL of toluene, cooled to 0 °C, and piperidine (0.51 mL, 5.16 mmol) was added dropwise. The colorless solution was stirred 1 h at RT, and subsequently dried *in vacuo* to afford a colorless oil. Yield: 790 mg (84 %). **^{1}H NMR (C_6D_6, 400 MHz):** δ 2.79 (2 H, app. d, ^{3}J = 13.1 Hz, NCH_2), 2.22-2.14 (2 H, m, NCH_2 overlapping with BH_2), 2.07 (2 H, q, ^{1}J = 82 Hz, BH_2 overlapping with NCH_2), 1.65 (1 H, ^{3}J = 6.8 Hz, $BCMe_2C\underline{H}Me_2$), 1.26 (6 H, d, ^{3}J = 6.8 Hz, $BCMe_2CH\underline{Me}_2$), 1.07 (6 H, s, $BC\underline{Me}_2CHMe_2$), 1.02 - 0.95 (2 H, m, $NCCC\underline{H}_2$), 0.71-0.56 (4 H, m, $NCC\underline{H}_2$) ppm. *The NH signal could not be located*. $^{13}C\{^{1}H\}$ NMR (C_6D_6, 100.6 MHz): δ 53.7 (NCH_2), 38.6 ($BCMe_2\underline{C}HMe_2$), 26.4 ($BC\underline{Me}_2CHMe_2$), 25.6 ($B\underline{C}Me_2CHMe_2$), 25.4 ($NC\underline{C}H_2$), 22.5 ($NCC\underline{C}H_2$), 19.2 ($BCMe_2CH\underline{Me}_2$) ppm. **^{11}B NMR (C_6D_6, 128.4 MHz):** δ -2.34 (t, ^{1}J = 98.4 Hz) ppm. **IR (NaCl plates, thin film, cm^{-1}):** 3252 (s, υ(N-H) st), 2950 (s), 2863 (s), 2702 (w), 2594 (w), 2335 (s, terminal υ(B-H)), 2028 (w, bridging υ(B-H)), 1978 (w, bridging υ(B-H)), 1454 (s), 1402 (s), 1383 (s), 1370 (s), 1277 (s), 1219 (s), 1146 (s), 1131 (s), 1088 (s), 1032 (s), 942 (m), 881 (m), 862 (m), 820 (m), 799 (w), 742(w), 679 (w). **Anal. found (calcd. for $C_{24}H_{36}BrN_3Ti$):** C, 72.04 (72.14); H, 14.16 (14.31); N, 7.80 (7.65)%.

C_8H_{10}N-BHTex. $C_8H_{10}NH{\cdot}H_2BTex$ (430 mg, 2.35 mmol) and Cp*Ti(NTol){MeC(N^iPr)$_2$} (**1.36a**, 21.5 mg, 0.054 mmol, 2.3%) were dissolved in 5 mL of benzene. The red reaction mixture was heated to 70 °C and stirred for 4 days at this temperature. The volatiles were removed *in vacuo*. Yield: 430 (95 %). **^{1}H NMR (C_6D_6, 400MHz):** δ 4.54 (1 H, br. q, ^1J = 125 Hz, BH), 3.17-3.11 (4 H, m, NCH_2), 1.75 (1 H, hept, ^3J = 6.9 Hz, C<u>H</u>Me_2), 1.37-1.27 (6 H, m, overlapping NCC<u>H</u>$_2$CH$_2$ and NCCH$_2$C<u>H</u>$_2$), 1.03 (6 H, s, BC<u>Me</u>$_2$), 0.99 (6 H, d, ^3J = 6.9 Hz, BCC<u>Me</u>$_2$) ppm. ^{13}C{^{1}H} NMR (C_6D_6, 100.6 MHz): δ 57.2 (NCH_2), 48.2 (NCH_2), 36.8 (BC<u>C</u>HMe_2), 29.1 (NC<u>C</u>H$_2$), 28.2 (NC<u>C</u>H$_2$), 27.5 (br., BC), 25.3 (NCC<u>C</u>H$_2$), 23.4 (BC<u>Me</u>$_2$), 18.7 (BCC<u>Me</u>$_2$) ppm. **^{11}B NMR (C_6D_6, 128.4 MHz):** δ 43.4 (d, ^1J = 125 Hz) ppm. **IR (NaCl plates, thin film, cm^{-1}):** 2120 (w), 2662 (w), 2450 (s, terminal υ(B-H)), 2369 (m), 1654 (w, bridging υ(B-H)), 1479 (s), 1375 (s), 1325 (s), 1258 (s), 1231 (s), 1213 (m), 1163 (m), 1146 (m), 1126 (s), 1093 (s), 1031 (s), 958 (m), 914 (w), 893 (w), 855 (m), 806 (m). **EI-MS:** *m*/*z* = 182.2 $[M]^+$ (40%).

Reaction of Cp*Ti{MeC(N^iPr_2)$_2$}{N(Tol)H_2BTex} (1.37) with piperidine. In the glovebox, a red solution of Cp*Ti{MeC(N^iPr_2)$_2$}{N(Tol)H_2BTex} (**1.37**, 0.035 mmol) dissolved in C_6D_6 (0.5 mL) in a NMR tube was prepared. Subsequently, an equimolar amount of piperidine (3.5 μL, 0.035 mmol) was added *via* microsyringe at room temperature and the NMR tube was immediately sealed using a J. Youngs valve. The NMR tube was introduced into a NMR spectrometer equilibrated at 60 °C, and the reaction was monitored by ^{1}H and ^{11}B NMR spectroscopy.

Large scale procedure for dehydrogenations under open conditions. A flame-dried two necked round bottom flask equipped with a stir bar was charged with Cp*Ti(NTol){MeC(N^iPr)$_2$} (**1.36a**, 32.6 mg, 75.9 mmol, 2%), dissolved in toluene (2 mL), and cooled to 0 °C. A second schlenk was charged with dimethylamineborane (223.5 mg, 3.79 mol), dissolved in toluene (8 mL) and cooled to 0 °C. The round bottom flask containing the

catalyst is fitted with a T-piece that allows a continous flow of nitrogen on top, and with a rubber subaseal on the side. The solution containing dimethylamineborane was transferred into the two necked round bottom flask and the time was recorded. The reaction progress was monitored by taking regular aliquots (0.1 mL) which were quenched into a solution of toluene (3.5 mL) with water (15 µL). The quenched reaction mixture immediately changed color and showed yellow precipitation indicating the formation of titanium dimer $[Cp^*Ti\{MeC(N^iPr)_2\}(\mu\text{-}O)]_2$. The reaction progress was then quantified *via* ^{11}B NMR spectroscopy.

Alternative synthesis for $[Me_2N{=}BH_2]_2$. To a mixture of $Me_2NH{\cdot}BH_3$ (1 g, 17 mmol) in benzene (10 mL) was added $Cp^*Ti\{MeC(N^iPr)_2\}NTol$ (**1.36a**, 120 mg, 0.280 mmol) at RT. Immediate bubbling indicates release of hydrogen. The mixture was stirred at RT for 24 h and then vacuum transferred to a second Schlenk tube. The resulting colorless solution was carefully subjected to vacuum to afford the product as pure white powder (*Note*: $[Me_2N{=}BH_2]_2$ is volatile and can be lost in the vacuum). The spectral properties matched literature values.[36] Yield: 453 mg (47%).

5.6 Experimental details and characterising data for Chapter Three

$Cp^*Ti(HPP)\{NH(B(NDippCH)_2))(CCAr^{CF_3})\}$ (3.5). To a brown solution of $Cp^*Ti(HPP)\{NB(NDippCH)_2\}$ (**1.83**, 200 mg, 0.277 mmol) dissolved in benzene (5 mL), was added $HCCAr^{CF_3}$ (45.1 µL, 0.277 mmol) at RT. The solution turned deep red within minutes. The volatiles were removed under reduced pressure after 3 h to afford a red powder. The product was isolated by crystallization from a saturated hexane solution at RT. Yield: 0.086 g (48 %). Diffraction-quality crystals were grown from a saturated hexane solution at RT. **^1H NMR (C_6D_6, 400MHz):** δ 7.32 (2 H, d, ^3J = 8.1 Hz, o-$C_6H_4CF_3$), 7.27 (2 H, d, ^3J = 8.1 Hz, m-$C_6H_4CF_3$) 7.08-7.02 (7 H, m, overlapping *p*-, *m*-$C_6\underline{H}_3{}^iPr_2$ and NH), 5.89 (2 H, s, NCH), 3.60 (2

H, sept, ^{3}J = 6.8 Hz, C<u>H</u>Me$_2$), 3.32 (2 H, sept, ^{3}J = 6.8 Hz, C<u>H</u>Me$_2$), 3.25 (1 H, dt, ^{2}J = 13.6, ^{3}J = 4.5 Hz, TiNC<u>H</u>$_2$), 3.11 (1 H, dt, ^{2}J = 13.6, ^{3}J = 4.5 Hz, TiNC<u>H</u>$_2$), 2.70 (1 H, dt, ^{2}J = 12.6, ^{3}J = 4.0 Hz, TiNC<u>H</u>$_2$), 2.55 (1 H, m, N$_2$CNC<u>H</u>$_2$), 2.25 (1 H, m, N$_2$CNC<u>H</u>$_2$), 2.17 (1 H, m, N$_2$CNC<u>H</u>$_2$), 2.05 (1 H, m, N$_2$CNC<u>H</u>$_2$), 1.81 (1 H, dt, ^{2}J = 12.6, ^{3}J = 4.0 Hz, TiNC<u>H</u>$_2$), 1.68 (15 H, s, Cp*), 1.34 (3 H, m, CH$_2$C<u>H</u>$_2$CH$_2$), 1.25 (6 H, d, ^{3}J = 6.8 Hz, CH<u>Me</u>$_2$), 1.16 (6 H, d, ^{3}J = 6.8 Hz, CH<u>Me</u>$_2$), 1.15 (6 H, d, ^{3}J = 6.8 Hz, CH<u>Me</u>$_2$), 1.13 (6 H, d, ^{3}J = 6.8 Hz, CH<u>Me</u>$_2$), 0.91 (1 H, m, CH$_2$C<u>H</u>$_2$CH$_2$) ppm. **^{13}C{^{1}H} NMR (C$_6$D$_6$, 125.8 MHz):** δ 156.6 (N$_2$CN), 150.4 (Ti-C), 147.9 (*o*-<u>C</u>$_6$H$_3$^{i}Pr$_2$), 147.5 (*o*-<u>C</u>$_6$H$_3$^{i}Pr$_2$), 141.6 (*i*-<u>C</u>$_6$H$_3$^{i}Pr$_2$), 132.6 (*i*-<u>C</u>$_6$H$_4$CF$_3$), 131.4 (*o*-<u>C</u>$_6$H$_4$CF$_3$), 127.1 (*p*-<u>C</u>$_6$H$_3$^{i}Pr$_2$), 127.0 (1 C, $^{2}J_{C\text{-}F}$ = 32.5 Hz, *p*-<u>C</u>$_6$H$_4$CF$_3$), 125.2 (2 C, $^{2}J_{C\text{-}F}$ = 3.6 Hz, *m*-<u>C</u>$_6$H$_4$CF$_3$), 123.8 (*m*-<u>C</u>$_6$H$_3$^{i}Pr$_2$), 123.5 (*m*-<u>C</u>$_6$H$_3$^{i}Pr$_2$), 122.8 (<u>Cp*</u>), 118.3 (NCH), 106.2 (TiC<u>C</u>), 46.1(N$_2$CN<u>C</u>H$_2$), 45.5 (N$_2$CN<u>C</u>H$_2$), 44.1 (TiNCH$_2$), 43.8 (TiNCH$_2$), 28.8 (<u>C</u>HMe$_2$), 28.5 (<u>C</u>HMe$_2$), 26.0 (CH<u>Me</u>$_2$), 25.9 (CH<u>Me</u>$_2$), 24.2 (CH$_2$<u>C</u>H$_2$CH$_2$), 23.8 (CH<u>Me</u>$_2$), 23.7 (CH<u>Me</u>$_2$), 23.1 (CH$_2$<u>C</u>H$_2$CH$_2$), 12.4 (Cp*) ppm. **^{11}B{^{1}H} NMR (C$_6$D$_6$, 128.4 MHz):** δ 23.8 ppm. **^{19}F{^{1}H} NMR (C$_6$D$_6$, 282.1 MHz):** δ -61.8 ppm. **IR (NaCl plates, Nujol mull, cm^{-1})**: 3292 (w), 3168 (w), 2725 (w), 2670 (w), 2081 (w), 1607 (w), 1566 (m), 1525 (m), 1460 (s), 1377 (s), 1342 (s), 1320 (s), 1299 (s), 1261 (m), 1206 (m), 1164 (m), 1125 (m), 1101 (m), 1065 (m), 1021 (m), 967 (w), 882 (w), 840 (m), 804 (m), 749 (m), 722 (m). **Anal. found (calcd. for C$_{52}$H$_{70}$BF$_3$N$_6$OTi):** C, 69.77 (69.95); H, 7.81 (7.68); N, 9.30 (9.41)%.

Cp*Ti(HPP){NH(B(NDippCH)$_2$))CCAr^{F}} (3.6). To a brown solution of Cp*Ti(HPP){NB(NDippCH)$_2$} (**1.83**, 300 mg, 0.415 mmol) dissolved in benzene (10 mL), was added HCCAr$_{F5}$ (56.9 µL, 0.415 mmol) at RT. The solution turned deep red within minutes. The volatiles were removed under reduced pressure after 2 h, and the product was obtained as red powder without further purification. Yield: 0.280 g (74 %). Diffraction-quality crystals were grown from a saturated hexane solution at -30 °C. **^{1}H NMR (C$_6$D$_6$, 400MHz):** δ 7.34 (1 H, s, NH), 7.22-7.16 (6 H, m, overlapping *p*-, *m*-C$_6$<u>H</u>$_3$^{i}Pr$_2$), 6.01 (2 H, s, NCH), 3.68 (2 H, sept,

^{3}J = 6.9 Hz, C<u>H</u>Me$_2$), 3.48 (2 H, sept, ^{3}J = 6.9 Hz, C<u>H</u>Me$_2$), 3.41 (1 H, m, TiNCH$_2$), 3.33 (1 H, m, TiNCH$_2$), 2.84 (1 H, m, TiNCH$_2$), 2.66 (1 H, m, N$_2$CNCH$_2$), 2.41 (1 H, m, N$_2$CNCH$_2$), 2.30 (1 H, m, N$_2$CNCH$_2$), 2.20 (1 H, m, N$_2$CNCH$_2$), 1.98 (1 H, m, TiNCH$_2$), 1.82 (15 H, s, Cp*), 1.49 (3 H, m, CH$_2$C<u>H</u>$_2$CH$_2$), 1.41 (6 H, d, ^{3}J = 6.8 Hz, CH<u>Me</u>$_2$), 1.35 (6 H, d, ^{3}J = 6.8 Hz, CH<u>Me</u>$_2$), 1.31 (6 H, d, ^{3}J = 6.7 Hz, CH<u>Me</u>$_2$), 1.29 (6 H, d, ^{3}J = 6.7 Hz, CH<u>Me</u>$_2$), 1.06 (1 H, m, CH$_2$C<u>H</u>$_2$CH$_2$) ppm. **^{13}C{^{1}H} NMR (C$_6$D$_6$, 125.8 MHz):** δ 167.4 (Ti-C), 157.0 (N$_2$CN), 147.8 (*o*-<u>C</u>$_6$H$_3$^{i}Pr$_2$), 147.7 (*o*-<u>C</u>$_6$H$_3$^{i}Pr$_2$), 141.3 (*i*-<u>C</u>$_6$H$_3$^{i}Pr$_2$), 140.2 (1 C, m, *o*-C$_6$F$_5$), 139.1 (1 C, m, *p*-C$_6$F$_5$) , 138.2 (1 C, m, *o*-C$_6$F$_5$), 127.1 (*p*-<u>C</u>$_6$H$_3$^{i}Pr$_2$), 123.8 (*m*-<u>C</u>$_6$H$_3$^{i}Pr$_2$), 123.4 (*m*-<u>C</u>$_6$H$_3$^{i}Pr$_2$), 123.2 (Cp*), 118.3 (NCH), 104.6 (1 C, td, *i*-C$_6$F$_5$, $^{2}J_{C\text{-}F}$ = 19.1, $^{3}J_{C\text{-}F}$ = 3.7 Hz), 89.4 (1 C, app. d, TiC<u>C</u>, $^{3}J_{C\text{-}F}$ = 3.2 Hz), 46.1 (N$_2$CN<u>C</u>H$_2$), 45.5 (N$_2$CN<u>C</u>H$_2$), 44.0 (TiNCH$_2$), 43.8 (TiNCH$_2$), 28.8 (<u>C</u>HMe$_2$), 28.5 (<u>C</u>HMe$_2$), 25.9 (CH<u>Me</u>$_2$), 25.7 (CH<u>Me</u>$_2$), 24.2 (CH$_2$<u>C</u>H$_2$CH$_2$), 23.9 (CH<u>Me</u>$_2$), 23.8 (CH<u>Me</u>$_2$), 23.6 (CH$_2$<u>C</u>H$_2$CH$_2$), 12.4 (Cp*) ppm. **^{11}B{^{1}H} NMR (C$_6$D$_6$, 128.4 MHz):** 23.7 ppm. **^{19}F{^{1}H} NMR (C$_6$D$_6$, 282.1 MHz):** -139.1 (2 F, dd, ^{3}J = 23.5, ^{4}J = 7.5 Hz, *o*-C$_6$F$_5$), -160.4 (1 F, t, ^{3}J = 16.9 Hz, *p*-C$_6$F$_5$), -164.67 (2 F, m, *m*-C$_6$F$_5$) ppm. **IR (NaCl plates, Nujol mull, cm^{-1}):** 3318 (w), 2725 (w), 2096 (m), 2079 (w), 1570 (s), 1511 (s), 1491 (s), 1460(s), 1378 (s), 1340 (s), 1297 (s), 1262 (m), 1205 (m), 1183 (m), 1149 (m), 1111 (m), 1165 (m), 1025 (m), 981 (m), 959 (s), 883 (w), 805 (m), 748 (m), 722 (m), 654 (m). **Anal. found (calcd. for C$_{51}$H$_{64}$BF$_5$N$_6$Ti):** C, 66.81 (66.96); H, 6.87 (7.05); N, 9.11 (9.19)%.

Determination of equilibria constants on the NMR tube scale. A total of 0.5 mL of C$_6$D$_6$ was used in each experiment. The general procedure was as follows. To a solution of Cp*Ti(HPP){NB(NDippCH)$_2$} (**1.83**, 20 mg, 0.0277 mmol) in C$_6$D$_6$ in a NMR tube equipped with a J. Young Teflon valve was added substrate (0.0277 mmol) at RT. The reaction was monitored *via* ^{1}H NMR spectroscopy (relaxation delay 100 s). The equilibrium constant was calculated by measuring the integrals of the NCH resonances of protons, respectively, and

using hexamethyldisiloxane as internal standard for the determination of the absolute concentrations. The relaxation delay was set to D1 = 100 s.

Characterisation data for Cp*Ti(HPP){NH(B(NDippCH)$_2$)}(CCTol) (3.8), in the equilibrium with Cp*Ti(HPP){NB(NDippCH)$_2$} (1.83) and HCCTol. ^{1}H NMR (C$_6$D$_6$, 400MHz): δ 7.54 (2 H, d, ^3J = 7.8 Hz, *o*-C$_6$H$_4$Me), 7.24-7.16 (7 H, m, overlapping *p*-, *m*-C$_6$H$_3$^{i}Pr$_2$, NH), 7.04 (2 H, d, ^3J = 7.8 Hz, *m*-C$_6$H$_4$Me), 6.06 (2 H, s, NCH), 3.83 (2 H, sept, ^3J = 6.8 Hz, CHMe$_2$), 3.56 (2 H, sept, ^3J = 6.8 Hz, CHMe$_2$), 3.50 (1 H, m, TiNCH$_2$), 3.32 (1 H, m, TiNCH$_2$), 2.86 (1 H, m, TiNCH$_2$), 2.73 (1 H, m, N$_2$CNCH$_2$), 2.39 (1 H, m, N$_2$CNCH$_2$), 2.32 (1 H, m, N$_2$CNCH$_2$), 2.19 (1 H, m, N$_2$CNCH$_2$), 2.12 (3 H, s, C$_6$H$_4$Me), 1.96 (1 H, m, TiNCH$_2$), 1.87 (15 H, s, Cp*), 1.51 (3 H, m, CH$_2$CH$_2$CH$_2$), 1.45 (6 H, d, ^3J = 6.8 Hz, CHMe$_2$), 1.38 (6 H, d, ^3J = 6.8 Hz, CHMe$_2$), 1.33 (12 H, app. t., app. ^3J = 7.2 Hz, CHMe$_2$), 1.05 (1 H, m, CH$_2$CH$_2$CH$_2$) ppm. **^{13}C{^{1}H} NMR (C$_6$D$_6$, 100.6 MHz):** δ 156.4 (N$_2$CN), 152.8 (Ti-C), 148.0 (*o*-C$_6$H$_3$^{i}Pr$_2$), 148.7 (*o*-C$_6$H$_3$^{i}Pr$_2$), 141.7 (*i*-C$_6$H$_3$^{i}Pr$_2$), 134.8 (*p*-C$_6$H$_4$Me), 131.4 (*o*-C$_6$H$_4$Me), 129.0 (*m*-C$_6$H$_4$Me), 127.0 (*p*-C$_6$H$_3$^{i}Pr$_2$), 125.9 (*i*-C$_6$H$_4$Me), 123.8 (*m*-C$_6$H$_3$^{i}Pr$_2$), 123.5 (*m*-C$_6$H$_3$^{i}Pr$_2$), 122.7 (Cp*), 118.3 (NCH), 106.5 (Ti-CC), 46.1 N$_2$CNCH$_2$), 45.6 N$_2$CNCH$_2$), 44.1 (TiNCH$_2$), 44.0 (TiNCH$_2$), 28.8 (CHMe$_2$), 28.6 (CHMe$_2$), 26.0 (CHMe$_2$), 26.0 (CHMe$_2$), 24.3 (CH$_2$CH$_2$CH$_2$), 23.8 (CHMe$_2$), 23.8 (CH$_2$CH$_2$CH$_2$), 23.7 (CHMe$_2$), 21.4 (C$_6$H$_4$Me), 12.5 (Cp*) ppm. **^{11}B{^{1}H} NMR (C$_6$D$_6$, 128.4 MHz):** 23.8 ppm. $K_{eq}^{298K} = 88$ L mol^{-1}.

Characterisation data for Cp*Ti(HPP){NH(B(NDippCH)$_2$)}(CCAr^{OMe}) (3.9), in the equilibrium with Cp*Ti(HPP){NB(NDippCH)$_2$} (1.83) and HCCAr^{OMe}. ^{1}H NMR (C$_6$D$_6$, 400MHz): δ 7.54 (2 H, d, ^3J = 8.5 Hz, *o*-C$_6$H$_4$OMe), 7.24-7.18 (7 H, m, overlapping *p*-, *m*-C$_6$H$_3$^{i}Pr$_2$, NH, starting material), 6.84 (2 H, d, ^3J = 8.4 Hz, *m*-C$_6$H$_4$OMe), 6.06 (2 H, s, NCH), 3.83 (2 H, sept, ^3J = 6.8 Hz, CHMe$_2$), 3.56 (2 H, m, overlapping CHMe$_2$ and starting material),

3.49 (1 H, m, overlapping TiNCH$_2$ and starting material), 3.33 (1 H, m, TiNCH$_2$), 3.30 (3 H, s, OMe), 2.71 (1 H, m, TiNCH$_2$), 2.41 (1 H, m, N$_2$CNCH$_2$), 2.34 (2 H, m, N$_2$CNCH$_2$), 2.21 (1 H, m, N$_2$CNCH$_2$), 1.97 (1 H, m, TiNCH$_2$), 1.87 (15 H, s, overlapping Cp* and starting material), 1.52 (2 H, m, CH$_2$CH$_2$CH$_2$), 1.41-1.26 (25 H, m, overlapping CHMe$_2$, CH$_2$CH$_2$CH$_2$ and starting material), 1.06 (1 H, m, CH$_2$CH$_2$CH$_2$) ppm. **^{13}C{^{1}H} NMR (C$_6$D$_6$, 100.6 MHz):** δ 158.2 (*p*-C$_6$H$_4$OMe), 156.4 (N$_2$CN), 152.0 (Ti-C), 148.1 (*o*-C$_6$H$_3$^{i}Pr$_2$), 147.1 (*o*-C$_6$H$_3$^{i}Pr$_2$), 141.7 (*i*-C$_6$H$_3$^{i}Pr$_2$), 132.6 (*o*-C$_6$H$_4$OMe), 127.0 (*p*-C$_6$H$_3$^{i}Pr$_2$), 123.8 (*m*-C$_6$H$_3$^{i}Pr$_2$), 123.5 (*m*-C$_6$H$_3$^{i}Pr$_2$), 122.6 (Cp*), 121.3 (*i*-C$_6$H$_4$OMe), 118.3 (NCH), 114.0 (*m*-C$_6$H$_4$OMe), 106.0 (Ti-CC), 54.8 (OMe), 46.2 (N$_2$CNCH$_2$), 45.6 (N$_2$CNCH$_2$), 44.1 (TiNCH$_2$), 44.0 (TiNCH$_2$), 28.8 (CHMe$_2$), 28.6 (CHMe$_2$), 26.0 (CHMe$_2$), 26.0 (CHMe$_2$), 24.3 (CHMe$_2$), 24.3 (CH$_2$CH$_2$CH$_2$), 23.8 (CHMe$_2$), 23.8 (CHMe$_2$), 23.8 (CH$_2$CH$_2$CH$_2$), 23.7 (CHMe$_2$), 12.5 (Cp*) ppm. **^{11}B{^{1}H} NMR (C$_6$D$_6$, 128.4 MHz):** 23.6 ppm. $K_{eq}^{298K} = 39$ L mol^{-1}.

Characterisation data for Cp*Ti(HPP)N(B(NDippCH)$_2$)C(=C)(CH$_2$)$_6$ (3.19), in the equilibrium with Cp*Ti(HPP){NB(NDippCH)$_2$} (1.83) and cyclooctyne. ^{1}H NMR (C$_6$D$_6$, 400MHz): δ 7.26-7.18 (6 H, m, overlapping *p*-, *m*-C$_6$H$_3$^{i}Pr$_2$ and starting material), 6.26 (1 H, d, ^3J = 2.6 Hz, NCH), 6.08 (1 H, d, ^3J = 2.6 Hz, NCH), 3.99-3.83 (3 H, m, CHMe$_2$), 3.66-3.58 (1 H, m, TiNCH$_2$), 3.52-3.32 (2 H, m, overlapping CHMe$_2$ and TiNCH$_2$), 3.18-3.11 (1 H, m, TiNCH$_2$), 2.90-2.82 (2 H, m, overlapping CH$_2$(CH$_2$)$_2$CH$_2$ and starting material), 2.84-2.78 (3 H, m, overlapping N$_2$CNCH$_2$, TiNCH$_2$ and starting material), 2.70-2.62 (3 H, m, overlapping N$_2$CNCH$_2$ and TiC=CCH$_2$), 2.38 (1 H, m, TiC=CCH$_2$), 2.14-2.04 (2 H, m, CH$_2${CH$_2$}$_2$CH$_2$), 1.75 (15 H, s, Cp*), 1.73-1.69 (2 H, m, TiCCH$_2$), 1.64-1.59 (2 H, m, CH$_2${CH$_2$}$_2$CH$_2$), 1.51 (3 H, d, ^3J = 6.5 Hz, CHMe$_2$), 1.44-1.38 (6 H, m, overlapping CHMe$_2$ and starting material), 1.39-1.35 (2 H, m, NCH$_2$CH$_2$CH$_2$), 1.33 (3 H, d, ^3J = 6.5 Hz, CHMe$_2$), 1.28-1.26 (3 H, m, overlapping CHMe$_2$ and starting material), 1.27-1.25 (3 H, m, overlapping CHMe$_2$ and starting

material), 1.21 (3 H, d, ^3J = 6.5 Hz, CHMe$_2$), 1.20 (3 H, d, ^3J = 6.5 Hz, CHMe$_2$), 1.19-1.11 (2 H, m, CH$_2${CH$_2$}$_2$CH$_2$), 0.85-0.80 (1 H, m, NCH$_2$CH$_2$CH$_2$), 0.26-0.21 (1 H, m, NCH$_2$CH$_2$CH$_2$) ppm. **^{13}C{^{1}H} NMR (C$_6$D$_6$, 125.8 MHz):** 218.4 (Ti-C), 157.2 (NCN$_2$), 146.8 (*o*-C$_6$H$_3$^{i}Pr$_2$), 146.7 (*o*-C$_6$H$_3$^{i}Pr$_2$), 146.2 (*o*-C$_6$H$_3$^{i}Pr$_2$), 143.4 (*i*-C$_6$H$_3$^{i}Pr$_2$), 143.0 (*i*-C$_6$H$_3$^{i}Pr$_2$), 136.7 (TiC=C), 127.1 (*p*-C$_6$H$_3$^{i}Pr$_2$), 126.7 (*p*-C$_6$H$_3$^{i}Pr$_2$), 123.3 (*m*-C$_6$H$_3$^{i}Pr$_2$), 123.2 (*m*-C$_6$H$_3$^{i}Pr$_2$), 120.0 (NCH), 119.8 (Cp*), 119.2 (NCH), 46.8 (N$_2$CNCH$_2$), 46.6 (N$_2$CNCH$_2$), 43.2 (TiNCH$_2$), 42.1 (TiNCH$_2$), 35.1 (TiC=CCH$_2$), 32.0 (TiCCH$_2$), 30.2 (CHMe$_2$), 28.5 (CHMe$_2$), 28.4 (CH$_2${CH$_2$}$_2$CH$_2$), 28.3 (CHMe$_2$), 28.2 (CH$_2${CH$_2$}$_2$CH$_2$), 28.1 (CHMe$_2$), 27.5 (CHMe$_2$), 26.9 (CHMe$_2$), 26.5 (CHMe$_2$), 25.3 (CH$_2${CH$_2$}$_2$CH$_2$), 24.5 (CH$_2${CH$_2$}$_2$CH$_2$), 23.7 (CHMe$_2$), 22.8 (NCH$_2$CH$_2$CH$_2$), 22.3 (NCH$_2$CH$_2$CH$_2$), 21.6 (CHMe$_2$), 12.1 (Cp*) ppm. **^{11}B{^{1}H} NMR (C$_6$D$_6$, 128.4 MHz):** 24.5 ppm.

Cp*Ti(HPP)(NH^{t}Bu)(CCTol) (3.10). To a toluene solution (20 mL) of Cp*Ti(HPP)(N^{t}Bu) (**1.83b**, 0.260 g, 0.663 mmol) was added HCCTol (84 μL, 0.663 mmol) at RT. The mixture was allowed to stir for 1 h, then the volatiles removed under reduced pressure. The crude product was triturated in hexane (10 mL), then dried *in vacuo*, giving **3.10** as a yellow powder. Yield: 0.263 g (78%). **^{1}H NMR (C$_6$D$_6$, 400MHz, 298 K):** δ 7.81 (1 H, s, NH), 7.60 (2 H, d, ^3J = 7.9 Hz, *o*-C$_6$H$_4$Me), 7.00 (2 H, d, ^3J = 6.9 Hz, *m*-C$_6$H$_4$Me), 4.11 (1 H, m, TiNCH$_2$), 3.41 (1 H, m, TiNCH$_2$), 3.30 (1 H, m, TiNCH$_2$), 3.14 (1 H, m, TiNCH$_2$), 2.49 (4 H, m, CH$_2$CH$_2$CH$_2$), 2.15 (15 H, s, Cp*), 2.10 (3 H, s, C$_6$H$_4$Me), 1.54 (4 H, m, N$_2$CNCH$_2$), 1.46 (9 H, s, CMe$_3$) ppm. **^{13}C{^{1}H} NMR (C$_6$D$_6$, 100.6 MHz, 298 K):** δ 155.8 (N$_2$CN), 151.4 (TiCCTol), 134.5 (*i*-C$_6$H$_4$Me), 131.1 (*o*-C$_6$H$_4$Me), 129.1 (*p*-C$_6$H$_4$Me), 128.6 (*m*-C$_6$H$_4$Me), 120.9 (Cp*), 108.7 (TiCCTol), 59.0 (CMe$_3$), 46.6 (N$_2$CNCH$_2$), 46.2 (N$_2$CNCH$_2$), 45.6 (TiNCH$_2$), 45.5 (TiNCH$_2$), 32.1 (CMe$_3$), 24.3 (CH$_2$CH$_2$CH$_2$), 24.2 (CH$_2$CH$_2$CH$_2$), 21.3 (C$_6$H$_4$Me), 12.8 (Cp*) ppm. **IR (NaCl plates, Nujol mull, cm^{-1}):** 3340 (w, N–H), 1647 (br., m), 1559 (s), 1523 (s), 1504 (s),

1318 (w), 1296 (m), 1203 (s), 1145 (w), 1100 (m), 1068 (m), 966 (w), 873 (w), 815 (m), 801 (m), 723 (m). EI-MS: *m*/*z* = 417 $[M - \text{Tol}]^+$ (75%). **Anal. found (calcd. for $C_{30}H_{44}N_4Ti$):** C, 70.81 (70.85); H, 8.88 (8.72); N, 10.95 (11.02)%.

TolNCNB(NDippCH)$_2$ (3.26). To a Schlenk tube containing Cp*Ti(HPP){NB(NDippCH)$_2$} (**1.83**, 0.3 g, 0.415 mmol) dissolved in toluene (10 mL) was added *p*-tolyl isothiocyanate (60.7 µL, 0.415 mmol) at RT. The mixture was heated to 90 °C and stirred for 7 days at that temperature. Subsequently, the volatiles were removed *in vacuo* and the organic extrusion compound was extracted into cold hexanes (1 x 10 mL). The remaining orange solid phase was dried *in vacuo* to afford the known [Cp*Ti(HPP)(µ-S)]$_2$ (**3.22**) (95 mg, 65%). The organic phase was filtered, and extrusion compound **(3.26)** was purified *via* recrystallisation at -30 °C (64 mg, 30%). **^{1}H NMR (C_6D_6, 400MHz):** 7.20-7.17 (6 H, overlapping 2 × m, *m*- and *p*-$C_6\underline{H}_3{}^i\text{Pr}_2$), 6.70 (2 H, d, ^3J = 8.0 Hz, *o*-$C_6\underline{H}_4$-Me), 6.28 (2 H, d, ^3J = 8.1 Hz, *m*-$C_6\underline{H}_4$-Me), 6.02 (2 H, s, NCH), 3.23 (4 H, sept, ^3J = 6.8 Hz, C$\underline{\text{H}}\text{Me}_2$), 1.97 (3 H, s, C_6H_4-$\underline{\text{Me}}$), 1.28 (12 H, d, ^3J = 6.8 Hz, CH$\underline{\text{Me}}_2$), 1.20 (12 H, d, ^3J = 6.8 Hz, CH$\underline{\text{Me}}_2$) ppm. **^{13}C{^{1}H} NMR (C_6D_6, 100.6 MHz):** δ 146.8 (*o*-$\underline{\text{C}}_6\text{H}_3{}^i\text{Pr}_2$), 137.6 (*i*-$\underline{\text{C}}_6\text{H}_3{}^i\text{Pr}_2$), 137.1 (*i*-$\underline{\text{C}}_6\text{H}_4\text{Me}$), 133.1 (*m*-$\underline{\text{C}}_6\text{H}_4\text{Me}$), 130.1 (*p*-$\underline{\text{C}}_6\text{H}_4\text{Me}$), 130.0 (*o*-$\underline{\text{C}}_6\text{H}_4\text{Me}$), 129.4 (N=C=N), 125.6 (*p*-$\underline{\text{C}}_6\text{H}_3{}^i\text{Pr}_2$), 124.0 (*m*-$\underline{\text{C}}_6\text{H}_3{}^i\text{Pr}_2$), 118.2 (NCH), 28.9 ($\underline{\text{C}}\text{HMe}_2$), 24.5 (CH$\underline{\text{Me}}_2$), 24.1 (CH$\underline{\text{Me}}_2$), 20.8 ($C_6H_4\underline{\text{Me}}$) ppm. ^{11}B{^{1}H} NMR (C_6D_6, 128.4 MHz): δ 18.7 ppm. **IR (NaCl plates, Nujol mull, cm^{-1}):** 2728 (w), 2292 (w), 2185 (s, N=C=N as stretch), 1586 (w), 1495 (m), 1460 (s), 1403 (m), 1377 (m), 1364 (w), 1324 (m), 1260 (m), 1190 (w), 1173 (w), 1103 (w), 1058 (w), 1119 (m), 865 (m), 805 (m), 762 (m), 723 (w), 660 (w), 649 (w). **HR-ESI-MS:** *m*/*z* = 519.36585 $[M]^+$ (1%).

NMR tube scale synthesis of PhNCNB(NDippCH)$_2$ (3.27). To a C_6D_6 solution (0.5 mL) of Cp*Ti(HPP){NB(NDippCH)$_2$} (**1.83**, 15.0 mg, 0.0208 mmol) in an NMR tube equipped with

a J. Young Teflon valve was added PhNCO (2.3 μL, 0.0208 mmol). The reaction was monitored by ^{1}H NMR spectroscopy. After 7 d at 90 °C, full conversion was achieved and a mixture of 65% (**3.27**) and 35% of free borylamine $H_2NB(NDippCH)_2$ decomposition was observed, as measured by integrations of the NCH resonances in **3.27** and borylamine**. ^{1}H NMR (C_6D_6, 400 MHz):** δ 7.17 (6 H, overlapping 2 × m, *m*- and *p*-$C_6\underline{H}_3{}^{i}Pr_2$), 6.89 (2 H, m, *m*-$C_6\underline{H}_5$), 6.76 (1 H, m, *p*-$C_6\underline{H}_5$), 6.36 (2 H, m, *o*-$C_6\underline{H}_5$), 6.02 (2 H, s, NCH), 3.25 (4 H, sept., ^{3}J = 6.9 Hz, C<u>H</u>MeMe), 1.30 (12 H, d, ^{3}J = 6.9 Hz, CH<u>Me</u>$_2$), 1.21 (12 H, d, ^{3}J = 6.9 Hz, CH<u>Me</u>$_2$) ppm. **^{13}C{^{1}H} NMR (C_6D_6, 100.6 MHz):** δ 146.7 (*o*-$\underline{C}_6H_3{}^{i}Pr_2$), 139.9 (*i*-$\underline{C}_6H_5$), 137.5 (*i*-$\underline{C}_6H_3{}^{i}Pr_2$), 129.4 (*m*-$\underline{C}_6H_5$), 128.7 (N=C=N), 127.9 (*p*-$\underline{C}_6H_3{}^{i}Pr_2$), 124.0 (*m*-$\underline{C}_6H_3{}^{i}Pr_2$), 123.8 (overlapping, *m*- and *p*-$\underline{C}_6H_5$), 118.3 (NCH), 28.9 (<u>C</u>HMeMe), 24.4 (CH<u>Me</u>$_2$), 24.1 (CH<u>Me</u>$_2$) ppm. **^{11}B{^{1}H} NMR (C_6D_6, 128.4 MHz):** δ 18.7 ppm.

Cp*Ti(HPP)N{B(NDippCH)$_2$}C(H)(Tol)O) (**3.28**). To a stirred solution of Cp*Ti(HPP){NB(NDippCH)$_2$} (**1.83**, 300 mg, 0.415 mmol) dissolved in benzene (7 mL), a solution of *p*-tolyl aldehyde (49 μL, 0.415 mmol) in benzene (5 mL) was added. The resulting solution was continued to stir at RT, and changed color from brown to orange within 2 minutes. After 30 min, the volatiles were removed under reduced pressure. The product was triturated using pentane (2 x 5 mL) and then dried *in vacuo* to yield the product as light-orange powder. Yield: 0.168 g (48%). **^{1}H NMR (C_6D_6, 400 MHz):** δ 7.64 (2 H, d, ^{3}J = 4.3 Hz, *o*-$C_6\underline{H}_4CH_3$), 7.35 (1 H, s, C<u>H</u>-$C_6H_4CH_3$), 7.24-7.16 (8 H, m, overlapping *p*-, *m*-$C_6\underline{H}_3{}^{i}Pr_2$ and *m*- $C_6\underline{H}_4CH_3$, 5.94 (2 H, s, NCH), 3.81 (2 H, sept, ^{3}J = 6.9 Hz, CHMe$_2$), 3.73 (2 H, sept, CHMe$_2$), 2.57-2.51 (2 H, m, overlapping TiNCH$_2$ and N_2CNCH_2), 2.49-2.41 (2 H, m, overlapping TiNCH$_2$ and N_2CNCH_2), 2.37-2.26 (2 H, m, overlapping TiNCH$_2$ and N_2CNCH_2), 1.98 (16 H, app. s, overlapping Cp* and TiNCH$_2$), 1.75-1.68 (1 H, m, N_2CNCH_2), 1.94 (3 H, s, $C_6H_4C\underline{H}_3$), 1.60 (6 H, d, ^{3}J = 6.9 Hz, CH<u>Me</u>$_2$), 1.34 (6 H, d, ^{3}J = 6.8 Hz, CH<u>Me</u>$_2$), 1.26 (6 H, d, ^{3}J = 6.8 Hz,

CH$\underline{Me}_2$), 1.23 (6 H, d, ^3J = 6.8 Hz, CH$\underline{Me}_2$), 1.18-1.13 (1 H, m, $CH_2C\underline{H}_2CH_2$), 1.11-1.03 (2 H, m, $CH_2C\underline{H}_2CH_2$), 1.00-0.95 (1 H, m, $CH_2C\underline{H}_2CH_2$). **$^{13}C\{^1H\}$ NMR (C_6D_6, 100.6 MHz):** δ 157.3 (N_2CN), 147.5 (*o*-$\underline{C}_6H_3{}^iPr_2$), 147.1 (*o*-$\underline{C}_6H_3{}^iPr_2$), 142.8 (*i*-$\underline{C}_6H_3{}^iPr_2$), 137.4 (*i*-$\underline{C}_6H_4CH_3$), 129.0 (*m*-$\underline{C}_6H_3Me$), 126.1 (*p*-$\underline{C}_6H_3{}^iPr_2$), 123.3 (*m*-$\underline{C}_6H_3{}^iPr_2$), 123.0 (*m*-$\underline{C}_6H_3{}^iPr_2$), 118.8 ($\underline{Cp^*}$), 118.4 (*p*-$\underline{C}_6H_3Me$), 116.7 (NCH), 88.8 ($\underline{C}HC_6H_4CH_3$), 47.5 ($N_2CN\underline{C}H_2$), 43.2 ($TiN\underline{C}H_2$), 41.4 ($TiN\underline{C}H_2$), 28.9 ($\underline{C}HMe_2$), 28.5($\underline{C}HMe_2$), 26.2($CH\underline{Me}_2$), 25.0($CH\underline{Me}_2$), 24.3($CH_2\underline{C}H_2CH_2$), 24.3($CH\underline{Me}_2$), 23.6($CH\underline{Me}_2$), 23.2($CH_2\underline{C}H_2CH_2$), 12.1 (Cp*), 12.0 ($C_6H_3\underline{Me}$) ppm. **$^{11}B\{^1H\}$ NMR (C_6D_6, 128.4 MHz):** 15.7 ppm. **IR (NaCl plates, Nujol mull, cm^{-1}):** 2723 (w), 1710 (w), 1570 (s), 1512 (m), 1462 (s), 1377 (s), 1308 (m), 1272 (m), 1203 (m), 1168 (m), 1115 (m), 1086 (m), 1063 (m), 1002 (m), 934 (w), 889 (w), 872 (m), 803 (m), 764 (m), 722 (m), 647 (m). **EI-MS:** *m*/*z* = 722 $[M]^+$ (1%). **Anal. found (calcd. for $C_{51}H_{71}BN_6OTi$):** C, 72.77 (72.68); H, 8.57 (8.49); N, 9.88 (9.97)%.

Synthesis of [Cp*Ti(HPP)(μ-O)]$_2$ (3.22) and N(CHTol){B(NDippCH)$_2$} (3.29). To a stirred solution of Cp*Ti(HPP){NB(NDippCH)$_2$} (**1.83**, 300 mg, 0.415 mmol) dissolved in benzene (10 mL), a solution of *p*-tolyl aldehyde (49 μL, 0.415 mmol) in benzene (5 mL) was added at RT. The resulting solution was heated to 60 °C and stirred for 18 h, after which time it had turned bright yellow. The volatiles were removed under reduced pressure, and the organic extrusion product N(CHTol)(B{NDippCH}$_2$) (**3.29**) extracted into hexanes (2 x 10 mL). The resulting solid phase was dried *in vacuo* to afford [Cp*Ti(HPP)(μ-O)]$_2$ (**3.22**) as bright yellow powder (80 mg, 60%). The organic phases were combined and then dried *in vacuo* to afford N(CHTol)(B{NDippCH}$_2$) (**3.29**) as orange solid (180 mg, 85%).

***Data for N(CHTol)(B{NDippCH}$_2$) (3.29).* ^{1}H NMR (C_6D_6, 400MHz):** δ 8.66 (1 H, s, NCH), 7.43 (2 H, d, ^3J = 7.8 Hz, *o*-$C_6\underline{H}_4CH_3$), 7.23-7.14 (6 H, overlapping 2 × m, *m*- and *p*-$C_6\underline{H}_3{}^iPr_2$), 6.68 (2 H, d, ^3J = 7.8 Hz, *m*-$C_6\underline{H}_4CH_3$), 6.20 (2 H, s, $N(CH)_2N$), 3.45 (4 H, sept, ^3J = 6.9 Hz,

C<u>H</u>Me$_2$), 1.86 (3 H, s, C$_6$H$_4$C<u>H</u>$_3$), 1.31 (12 H, d, CH<u>Me</u>Me, ^3J = 6.8 Hz), 1.28 (12 H, d, CHMe<u>Me</u>, ^3J = 6.8 Hz) ppm. **^{13}C{^{1}H} NMR (C$_6$D$_6$, 100.6 MHz):** δ 167.6 (NCH), 147.6 (*p*-<u>C</u>$_6$H$_3$^{i}Pr$_2$), 146.6 (*o*-<u>C</u>$_6$H$_3$^{i}Pr$_2$), 141.4 (*p*-<u>C</u>$_6$H$_4$CH$_3$), 138.9 (*i*-<u>C</u>$_6$H$_3$^{i}Pr$_2$), 136.8 (*i*-<u>C</u>$_6$H$_4$CH$_3$), 129.3 (*m*-<u>C</u>$_6$H$_4$CH$_3$), 128.8 (*o*-<u>C</u>$_6$H$_4$CH$_3$), 123.7 (*m*-<u>C</u>$_6$H$_3$^{i}Pr$_2$), 118.9 (NCHCHN), 28.9 (<u>C</u>HMe$_2$), 24.5 (CH<u>Me</u>Me), 24.2 (CHMe<u>Me</u>), 21.2 (C$_6$H$_4$<u>C</u>H$_3$) ppm. **^{11}B{^{1}H} NMR (C$_6$D$_6$, 128.4 MHz):** δ 24.3 ppm. **IR (NaCl plates, Nujol mull, cm^{-1}):** 2723 (w), 1706 (w), 1661 (C=N st, m), 1607 (m), 1576 (m), 1460 (s), 1378 (s), 1329 (s), 1301 (s), 1260 (s), 1217 (m), 1103 (m), 1057 (m), 1018 (m), 935 (w), 908 (w), 853 (w), 805 (s), 761 (m), 722 (m), 660 (m). **ESI$^+$-HR-MS** found (calcd for [C$_{34}$H$_{45}$BN$_3$, M + H$^+$] $^+$): 506.3707 (506.37065).

Condensation methodologies reacting tolylaldehyde with *tert*-butylamine or H$_2$NB(NDippCH)$_2$. For all reactions *p*-tolyl aldehyde (5.85 µL, 0.0496 mmol) was introduced into a 3 mL glass vial equipped with a stir bar, dissolved in the appropriate solvent (total 1 mL) and then subjected to either *tert*-butylamine (5.21 µL, 0.0496 mmol) or H$_2$NB(NDippCH)$_2$ (20 mg, 0.0496 mmol), respectively. The conversion was checked by regular ^{1}H NMR aliquots. The three specific reaction conditions including used solvents, temperatures and time conditions are listed below:

A) DCM (1 mL), NEt$_3$ (50 µL), MgSO$_4$, 1 h reflux;

B) Diethylether (1 mL), Mol. Sieves (4 Å), 16 h, RT;

C) Toluene (1 mL), MgSO$_4$, 16 h, 100 °C.

After the indicated times the reactions using *tert*-butylamine showed quantitative conversion to N(CHTol)^{t}Bu (**3.30**), while none of the reactions using H$_2$NB(NDippCH)$_2$ showed any traces of condensation product N(CHTol)(B{NDippCH}$_2$) (**3.29**) and neither prolonged reaction times nor increasing reaction temperature lead to detectable product formation.

Cp*Ti(HPPH)N{B(NDippCH)$_2$})OC(CH$_2$)(Ar^{CF_3}) (**3.31**). To a Schlenk tube containing Cp*Ti(HPP){NB(NDippCH)$_2$} (**1.83**, 300 mg, 0.415 mmol) dissolved in benzene (3 mL) was transferred a solution of MeC(O)-4-$C_6H_4CF_3$ (78.1 mg, 0.415 mmol) dissolved in benzene (3 mL). The Schlenk tube that contained the ketone was rinsed with benzene (1.5 mL), and was transferred to the dark red reaction mixture as well. The reaction mixture was stirred at RT for 8 h, after which time it had turned deep red. The volatiles were removed *in vacuo*, and then the product was washed with hexanes (3 x 10 mL). Yield: 200 mg (53%). Diffraction-quality crystals were grown from a saturated hexane solution at -30 °C. **^{1}H NMR (C_6D_6, 400MHz):** δ 7.89 (2 H, d, ^3J = 8.1 Hz, *o*-$C_6\underline{H}_4CF_3$), 7.53 (2 H, d, ^3J = 8.1 Hz, *m*-$C_6\underline{H}_4CF_3$), 7.23-7.15 (6 H, m, overlapping *p*-, *m*-$C_6\underline{H}_3{}^i Pr_2$), 6.08 (1 H, broad, s, NH), 5.94 (2 H, s, N(CH$_2$)$_2$N), 5.09 (1 H, s, OC=CH$_2$), 5.00 (1 H, s, OC=CH$_2$), 3.61 (4 H, m, C$\underline{H}$Me$_2$), 2.87 (1 H, m, HNC$\underline{H}_2$CH$_2$CH$_2$), 2.63 (1 H, m, HNC$\underline{H}_2$CH$_2$CH$_2$), 2.53 (1 H, m, C=NC$\underline{H}_2$CH$_2$CH$_2$), 2.35 (2 H, m, HNCH$_2$CH$_2$C$\underline{H}_2$), 2.18 (2 H, m, C=NCH$_2$CH$_2$C$\underline{H}_2$), 1.94 (1 H, m, C=NC$\underline{H}_2$CH$_2$CH$_2$), 1.85 (15 H, s, Cp*), 1.38 (6 H, d, ^3J = 6.8 Hz, CH$\underline{Me}_2$), 1.32 (6 H, d, ^3J = 6.8 Hz, CH$\underline{Me}_2$), 1.28 (12 H, d, ^3J = 6.8 Hz, CH$\underline{Me}_2$), 1.23-1.17 (2 H, m, HNCH$_2$C$\underline{H}_2$CH$_2$), 1.11 (1 H, m, C=NCH$_2$C$\underline{H}_2$CH$_2$), 0.98 (1 H, m, C=NCH$_2$C$\underline{H}_2$CH$_2$) ppm. **^{13}C{^{1}H} NMR (C_6D_6, 125.8 MHz):** δ 162.7 (OC), 154.7 (N$_2$CN), 147.9 (*o*-$\underline{C}_6H_3{}^i Pr_2$), 147.7 (*o*-$\underline{C}_6H_3{}^i Pr_2$), 145.4 (*i*-$\underline{C}_6H_4CF_3$), 142.1 (*i*-$\underline{C}_6H_3{}^i Pr_2$), 130.0 (1 C, q, $^2J_{C\text{-}F}$ = 31.2 Hz, *p*-$\underline{C}_6H_4CF_3$), 126.9 (*p*-$\underline{C}_6H_3{}^i Pr_2$), 126.2 (*o*-$\underline{C}_6H_4CF_3$), 125.0 (1 C, q, $^3J_{C\text{-}F}$ = 3.9 Hz, *m*-$\underline{C}_6H_4CF_3$), 123.7 (*m*-$\underline{C}_6H_3{}^i Pr_2$), 123.6 (*m*-$\underline{C}_6H_3{}^i Pr_2$), 121.8 ($\underline{Cp^*}$), 118.0 (N(CH$_2$)$_2$N), 92.1 (OC=$\underline{C}H_2$), 46.8 (HNCH$_2CH_2\underline{C}H_2$), 46.5 (C=NCH$_2CH_2\underline{C}H_2$), 44.5 (HN$\underline{C}H_2CH_2CH_2$), 41.7 (C=N$\underline{C}H_2CH_2CH_2$), 28.8 ($\underline{C}HMe_2$), 28.5 ($\underline{C}HMe_2$), 26.6 (CH$\underline{Me}_2$), 26.0 (CH$\underline{Me}_2$), 23.7 (HNCH$_2\underline{C}H_2CH_2$), 23.7 (CH$\underline{Me}_2$), 23.5 (CH$\underline{Me}_2$), 23.0 (C=NCH$_2\underline{C}H_2CH_2$), 12.2 (Cp*) ppm. **^{19}F{^{1}H} NMR (C_6D_6, 282.1 MHz)**: δ -61.7 ppm. **^{11}B{^{1}H} NMR (C_6D_6, 128.4 MHz):** δ 20.8 ppm. **IR (NaCl plates, Nujol mull, cm^{-1}):** 3229 (NH st., w), 2723 (w), 2360 (w), 2342 (w), 1926 (w), 1607 (C=C st, s), 1594 (m), 1557 (s), 1463 (s),

1376 (s), 1344 (s), 1320 (s), 1309 (s), 1301 (s), 1286 (s), 1163 (m), 1124 (m), 1114 (s), 1065 (m), 1013 (w), 998 (m), 937 (m), 876 (m), 851 (m), 814 (m), 804 (m), 763 (m), 741 (m), 722 (m). **Anal. found (calcd. for $C_{52}H_{70}BF_3N_6OTi$):** C, 68.12 (68.57); H, 7.47 (7.75); N, 9.27 (9.23)%.

Characterisation data for Cp*Ti(HPPH)(N{B(NDippCH)$_2$})(OC(CH$_2$)(Ph)) (3.32), in the equilibrium with Cp*Ti(HPP){NB(NDippCH)$_2$} (1.83) and MeC(O)Ph. ^{1}H NMR (C_6D_6, 400 MHz): δ 7.98 (2 H, d, ^3J = 6.9 Hz, *o*-$C_6\underline{H}_5$), 7.30 (2 H, app t., app. ^3J = 7.6 Hz, *m*-$C_6\underline{H}_5$), 7.24-7.18 (7 H, m, overlapping *p*-, *m*-$C_6\underline{H}_3{}^i Pr_2$, *p*-$C_6\underline{H}_5$ and starting material), 6.08 (1 H, s, NH), 5.95 (2 H, s, $N(CH_2)_2N$), 5.14 (1 H, s, $OC=CH_2$), 5.05 (1 H, s, $OC=CH_2$), 3.72 (2 H, m, $C\underline{H}Me_2$), 3.65 (2 H, m, $C\underline{H}Me_2$), 2.95 (1 H, m, $HNC\underline{H}_2CH_2CH_2$), 2.57 (1 H, m, $HNC\underline{H}_2CH_2CH_2$), 2.54 (1 H, m, overlapping $C=NC\underline{H}_2CH_2CH_2$ and starting material), 2.36 (2 H, m, $HNCH_2CH_2C\underline{H}_2$), 2.20 (2 H, m, $C=NCH_2CH_2C\underline{H}_2$), 1.98 (2 H, m, $C=NC\underline{H}_2CH_2CH_2$), 1.90 (15 H, s, Cp*), 1.43 (6 H, d, ^3J = 6.9 Hz, overlapping $CH\underline{Me}_2$ and starting material), 1.43 (6 H, d, ^3J = 6.8 Hz, $CH\underline{Me}_2$), 1.31-1.29 (13 H, app d, ^3J = 5.2 Hz, overlapping $CH\underline{Me}_2$, $HNCH_2C\underline{H}_2CH_2$ and starting material), 1.22-1.08 (2 H, m, overlapping $HNCH_2C\underline{H}_2CH_2$ and $C=NCH_2C\underline{H}_2CH_2$), 1.01 (1 H, m, $C=NCH_2C\underline{H}_2CH_2$) ppm. **^{13}C{^{1}H} NMR (C_6D_6, 125.8 MHz):** 164.1 (O-C), 154.3 (N_2CN), 148.0 (*o*-$\underline{C}_6H_3{}^i Pr_2$), 147.8 (*o*-$\underline{C}_6H_3{}^i Pr_2$), 142.4 (*i*-$\underline{C}_6H_3{}^i Pr_2$), 141.9 (*i*-$C_6H_5$), 127.2 (*p*-$C_6H_5$), 126.8 (*p*-$\underline{C}_6H_3{}^i Pr_2$), 126.2 (*o*-$C_6H_5$), 123.5 (*m*-$C_6H_3{}^i Pr_2$), 123.3 (*m*-$C_6H_3{}^i Pr_2$), 121.3 ($\underline{Cp^*}$), 117.8 ($N(CH_2)_2N$), 90.6 ($OC=\underline{C}H_2$), 46.9 ($HNCH_2CH_2\underline{C}H_2$), 46.7 ($C=NCH_2CH_2\underline{C}H_2$), 44.9 ($HN\underline{C}H_2CH_2CH_2$), 41.3 ($C=N\underline{C}H_2CH_2CH_2$), 28.8 ($\underline{C}HMe_2$), 28.5 ($\underline{C}HMe_2$), 25.9 ($CH\underline{Me}_2$), 23.8 ($CH\underline{Me}_2$), 23.7 ($HNCH_2\underline{C}H_2CH_2$), 23.5 ($CH\underline{Me}_2$), 22.9 ($C=NCH_2\underline{C}H_2CH_2$), 12.2 (Cp*) ppm. **^{11}B{^{1}H} NMR (C_6D_6, 128.4 MHz):** 20.3 ppm. $K_{eq}^{298K} = 86\ L\ mol^{-1}$.

Characterisation data for Cp*Ti(HPPH)(N{B(NDippCH)$_2$})(OC(CH$_2$)(Ar^{OMe}) (3.33), in the equilibrium with Cp*Ti(HPP){NB(NDippCH)$_2$} (1.83) and MeC(O)Ar^{OMe}. ^{1}H NMR (C$_6$D$_6$, 400MHz): δ 7.93 (2 H, d, ^3J = 8.8 Hz, *o*-C$_6$H$_4$OMe), 7.24-7.19 (6 H, m, overlapping *p*-, *m*-C$_6$H$_3$^{i}Pr$_2$ and starting material), 6.92 (2 H, d, ^3J = 8.7 Hz, *m*-C$_6$H$_4$OMe), 6.07 (1 H, s, NH), 5.95 (2 H, s, N(CH$_2$)$_2$N), 5.08 (1 H, s, OC=CH$_2$) , 4.98 (1 H, s, OC=CH$_2$), 3.74 (2 H, m, CHMe$_2$), 3.55 (2 H, m, CHMe$_2$), 3.39 (3 H, s, OMe), 2.99 (1 H, m, HNCH$_2$CH$_2$CH$_2$), 2.63 (1 H, m, HNCH$_2$CH$_2$CH$_2$), 2.56 (1 H, m, C=NCH$_2$CH$_2$CH$_2$), 2.37 (2 H, m, HNCH$_2$CH$_2$CH$_2$), 2.22 (2 H, m, C=NCH$_2$CH$_2$CH$_2$), 2.00 (1 H, m, C=NCH$_2$CH$_2$CH$_2$), 1.92 (15 H, s, Cp*), 1.47-1.38 (12 H, m, overlapping CHMe$_2$ and starting material), 1.33-1.27 (12 H, m, overlapping CHMe$_2$ and starting material), 1.31 (2 H, m, overlapping HNCH$_2$CH$_2$CH$_2$ and starting material), 1.13 (1 H, m, overlapping C=NCH$_2$CH$_2$CH$_2$ and starting material), 1.02 (1 H, m, C=NCH$_2$CH$_2$CH$_2$) ppm. **^{13}C{^{1}H} NMR (C$_6$D$_6$, 125.8 MHz):** 163.9 (O-C), 159.5 (*p*-C$_6$H$_4$OMe), 148.0 (*o*-C$_6$H$_3$^{i}Pr$_2$), 147.9 (*o*-C$_6$H$_3$^{i}Pr$_2$), 147.5 (N$_2$CN), 142.5 (*i*-C$_6$H$_3$^{i}Pr$_2$), 134.7 (*i*-C$_6$H$_4$OMe), 127.3 (*o*-C$_6$H$_4$OMe), 126.8 (OMe), 123.7 (*m*-C$_6$H$_3$^{i}Pr$_2$), 123.5 (*m*-C$_6$H$_3$^{i}Pr$_2$), 121.3 (Cp*), 117.8 (N(CH$_2$)$_2$N), 113.5 (*m*-C$_6$H$_4$OMe), 89.3 (OC=CH$_2$), 54.8 (OMe), 47.0 (HNCH$_2$CH$_2$CH$_2$), 47.8 (C=NCH$_2$CH$_2$CH$_2$), 45.0 (HNCH$_2$CH$_2$CH$_2$), 41.3 (C=NCH$_2$CH$_2$CH$_2$), 28.8 (CHMe$_2$), 28.5 (CHMe$_2$), 26.7 (CHMe$_2$), 23.7 (HNCH$_2$CH$_2$CH$_2$), 23.6 (CHMe$_2$), 23.0 (C=NCH$_2$CH$_2$CH$_2$), 12.2 (Cp*) ppm. **^{11}B{^{1}H} NMR (C$_6$D$_6$, 128.4 MHz):** 20.1 ppm. $K_{eq}^{298K} = 21\ M^{-1}$.

Reaction of MeCO$_2$Me with Cp*Ti(HPP){NB(NDippCH)$_2$} (1.83) to form Cp*Ti(HPP)(NH{B(NDippCH)$_2$})(OMe) (3.35). To a brown solution of Cp*Ti(HPP){NB(NDippCH)$_2$} (**1.83**, 250 mg, 0.346 mmol) dissolved in toluene (6.5 mL), was added methylacetate (29.0 µL, 0.346 mmol) at RT. The reaction was heated to 70 °C for 3 d, by which time the solution has turned dark red. The volatiles were removed under reduced pressure, and the product was obtained *via* recrystallization in hexanes at 0 °C. Yield: 51 mg

(20 %). Diffraction-quality crystals were grown from a saturated hexane solution at 5 °C. **^{1}H NMR (C_6D_6, 400MHz):** δ 7.28-7.21 (6 H, m, overlapping *p*- and *m*-$C_6\underline{H}_3{}^{i}Pr_2$), 6.00 (2 H, s, NCH), 5.29 (1 H, s, NH), 3.66 (2 H, sept, ^{3}J = 6.8 Hz, C$\underline{H}$Me$_2$), 3.53 (2 H, sept, ^{3}J = 6.8 Hz, C$\underline{H}$Me$_2$), 3.37 (3 H, s, OMe), 3.13-3.04 (3 H, m, TiNCH$_2$), 3.01-2.94 (1 H, m, TiNCH$_2$), 2.67 (2 H, m, N_2CNCH_2), 2.50 (2 H, m, N_2CNCH_2), **1.83** (15 H, s, Cp*), 1.61-1.45 (4 H, m, $CH_2C\underline{H}_2CH_2$), 1.43 (6 H, d, ^{3}J = 6.8 Hz, CH$\underline{Me}_2$), 1.41 (6 H, d, ^{3}J = 6.8 Hz, CH$\underline{Me}_2$), 1.32 (12 H, app. t, app. ^{3}J = 6.7 Hz, CH$\underline{Me}_2$). **^{13}C{^{1}H} NMR (C_6D_6, 125.8 MHz):** 156.3 (N_2CN), 147.7 (*o*-$\underline{C}_6H_3{}^{i}Pr_2$), 147.2 (*o*-$\underline{C}_6H_3{}^{i}Pr_2$), 142.2 (*i*-$\underline{C}_6H_3{}^{i}Pr_2$), 126.6 (*p*-$\underline{C}_6H_3{}^{i}Pr_2$), 123.5 (*m*-$\underline{C}_6H_3{}^{i}Pr_2$), 123.4 (*m*-$\underline{C}_6H_3{}^{i}Pr_2$), 121.0 (Cp*), 118.2 (NCH), 61.4 (OMe), 46.8 ($N_2CN\underline{C}H_2$), 46.6 ($N_2CN\underline{C}H_2$), 45.0 (TiNCH$_2$), 42.8 (TiNCH$_2$), 28.7 (C$\underline{H}$Me$_2$), 28.6 (C$\underline{H}$Me$_2$), 26.2 (CH$\underline{Me}_2$), 25.9 (CH$\underline{Me}_2$), 24.5 ($CH_2\underline{C}H_2CH_2$), 24.5 ($CH_2\underline{C}H_2CH_2$), 23.7 (CH$\underline{Me}_2$), 23.5 (CH$\underline{Me}_2$), 11.7 (Cp*) ppm. **^{11}B{^{1}H} NMR (C_6D_6, 128.4 MHz):** 24.0 ppm. **IR (NaCl plates, Nujol mull, cm^{-1}):** 3329 (w), 3058 (w), 2727 (w), 1927 (w), 1859 (w), 1789 (w), 1656 (w), 1568 (s), 1536 (s), 1459 (s), 1406 (s), 1379 (s), 1353 (s), 1296 (s), 1206 (s), 1148 (s), 1132 (s), 1112 (s), 1068 (s), 1023 (m), 962 (m), 937 (m), 874 (m), 803 (s), 766 (m), 741 (s), 721 (m), 701 (m), 651 (s), 570 (m). **Anal. found (calcd. for $C_{51}H_{64}BF_5N_6Ti$):** C, 69.90 (70.02); H, 9.08 (8.95); N, 11.02 (11.14)%.

Alternative NMR tube scale synthesis of Cp*Ti(HPP)(NH{B(NDippCH)$_2$})(OMe) (3.35). Cp*Ti(HPP){NB(NDippCH)$_2$} (**1.83**, 15 mg, 0.0208 mmol) was dissolved in C_6D_6 (0.4 mL) in a NMR tube equipped with a J. Young Teflon valve, and dry MeOH (0.84 µL, 0.0208 mmol) was added *via* microsyringe. The reaction was left at RT and monitored *via* ^{1}H NMR spectroscopy. The reaction is complete within 1.5 h and quantitative formation of Cp*Ti(HPP)(NH{B(NDippCH)$_2$})(OMe) (**3.35**).

Reaction of Cp*Ti(HPP){NB(NDippCH)$_2$} with ethanol to form Cp*Ti(HPP)(NH{B(DippCH)$_2$})(OEt) (3.36). To a brown solution of Cp*Ti(HPP){NB(NDippCH)$_2$} (200 mg, 0.277 mmol) dissolved in toluene (5 mL), was added ethanol (29.0 µL, 0.277 mmol) at RT. After 1.5 h of stirring at RT, after which time the color turned deep red, the volatiles were removed *in vacuo*. Yield: 190 mg (90 %). Diffraction-quality crystals were grown from a saturated hexane solution at 0 °C. **^{1}H NMR (C$_6$D$_6$, 400 MHz):** δ 7.28-7.21 (6 H, m, overlapping *p*- and *m*-C$_6$H$_3$^{i}Pr$_2$), 5.98 (2 H, s, NCH), 5.42 (1 H, s, NH), 3.96 (1 H, m, OCH$_2$), 3.67 (2 H, sept, ^3J = 6.7 Hz, CHMe$_2$), 3.49 (2 H, m, CHMe$_2$), 3.39 (3 H, m, OCH$_2$), 3.08 (3 H, m, TiNCH$_2$), 2.81 (1 H, m, TiNCH$_2$), 2.68 (2 H, m, N$_2$CNCH$_2$), 2.50 (2 H, m, N$_2$CNCH$_2$), 1.80 (15 H, s, Cp*), 1.60-1.48 (4 H, m, CH$_2$CH$_2$CH$_2$), 1.46 (6 H, d, ^3J = 6.8 Hz, CHMe$_2$), 1.42 (6 H, d, ^3J = 6.8 Hz, CHMe$_2$), 1.33 (6 H, d, ^3J = 6.8 Hz, CHMe$_2$), 1.31 (6 H, d, ^3J = 6.8 Hz, CHMe$_2$), 1.04 (3 H, m, OCH$_2$CH$_3$) ppm. **^{13}C{^{1}H} NMR (C$_6$D$_6$, 125.8 MHz):** 156.5 (N$_2$CN), 147.9 (*o*-C$_6$H$_3$^{i}Pr$_2$), 147.4 (*o*-C$_6$H$_3$^{i}Pr$_2$), 142.2 (*i*-C$_6$H$_3$^{i}Pr$_2$), 126.7 (*p*-C$_6$H$_3$^{i}Pr$_2$), 123.7 (*m*-C$_6$H$_3$^{i}Pr$_2$), 123.5 (*m*-C$_6$H$_3$^{i}Pr$_2$), 121.2 (Cp*), 118.2 (NCH), 68.8 (OCH$_2$), 46.8 (N$_2$CNCH$_2$), 46.6 (N$_2$CNCH$_2$), 44.7 (TiNCH$_2$), 43.0 (TiNCH$_2$), 28.7 (CHMe$_2$), 28.5 (CHMe$_2$), 26.0 (CHMe$_2$), 24.6 (CH$_2$CH$_2$CH$_2$), 24.5 (CH$_2$CH$_2$CH$_2$), 24.0 (CHMe$_2$), 23.6 (CHMe$_2$), 20.9 (OCH$_2$CH$_3$), 12.0 (Cp*) ppm. **^{11}B{^{1}H} NMR (C$_6$D$_6$, 128.4 MHz):** 24.4 ppm. **IR (NaCl plates, Nujol mull, cm^{-1}):** 3336 (w), 2724 (m), 1918 (w), 1852 (w), 1787 (w), 1701 (w), 1654 (w), 1568 (s), 1534 (s), 1460 (s), 1378 (s), 1296 (s), 1205 (s), 1108 (s), 1068 (s), 1024 (s), 965 (m), 918 (m), 874 (m), 802 (s), 761 (m), 740 (s), 701 (m), 652 (m). **Anal. found (calcd. for C$_{45}$H$_{69}$B$_1$N$_6$O$_1$Ti):** C, 67.69 (70.31); H, 8.98 (9.05); N, 10.72 (10.93)%.

NMR tube scale reaction of Cp*Ti(HPP){NB(NDippCH)$_2$} (1.83) with MeCO$_2$Et to form Cp*Ti(HPP)(N(H){B(DippCH)$_2$})(OEt) (3.36): Cp*Ti(HPP){NB(NDippCH)$_2$} (**1.83**, 15 mg, 0.0208 mmol) was dissolved in C$_6$D$_6$ (0.4 mL) in an NMR tube equipped with a J. Young

Teflon valve, and ethylacetate (2.05 µL, 0.0208 mmol) was added *via* a microsyringe. The reaction was monitored *via* ^{1}H NMR spectroscopy. No reaction was observed at RT, but the desired product started to show at 60 °C or above. After 4.5h at 60 °C the reaction mixture showed 20% product formation, and 75% starting material. Continued heating drives the reaction further as indicated by consumption of starting material. However, the reaction product is not stable under the reaction conditions and decomposes into free borylamine and unidentifiable organometallic side products.

NMR tube scale reaction of Cp*Ti(HPP){NB(NDippCH)$_2$} (1.83) with MeCO$_2$Ph to form Cp*Ti(HPP)(NH{B(NDippCH)$_2$})(OPh) (3.37) and Cp*Ti(HPP){OC(=CH$_2$)N(B{NDippCH}$_2$}) (3.42). Cp*Ti(HPP){NB(NDippCH)$_2$} (**1.83**, 15 mg, 0.0208 mmol) was dissolved in C_6D_6 (0.4 mL) in a NMR tube equipped with a J. Young Teflon valve, and phenylacetate (2.62 µL, 0.0208 mmol) was added *via* microsyringe. The reaction was left at RT and monitored *via* ^{1}H NMR spectroscopy. The starting material is fully converted after 1 h, and a mixture of 45% Cp*Ti(HPP){OC(=CH$_2$)N(B{NDippCH}$_2$}) (**3.42**) and 55% Cp*Ti(HPP)(NH{B(NDippCH)$_2$})(OPh) is observed, as determined by integration of the NCH resonances. Both the Cp*Ti(HPP){OC(=CH$_2$)N(B(NDippCH)$_2$}) (**3.42**) as well as Cp*Ti(HPP)(NH{B(NDippCH)$_2$})(OPh) (**3.37**) are unstable under the reaction conditions and decomposes over the course of a couple of days.

Data for Cp*Ti(HPP){OC(=CH$_2$)N(B(NDippCH)$_2$}) **(3.42). ^{1}H NMR (Tol-d8, 500.3 MHz):** δ 7.21-7.13 (6 H, m, overlapping *p*- and *m*-C$_6$H$_3$^{i}Pr$_2$ and Cp*Ti(HPP)(NHB(NDippCH)$_2$)(OPh), 5.91 (2 H, s, NCH), 3.81 (2 H, sept, ^{3}J = 6.9 Hz, CHMe$_2$), 3.51 (2 H, sept, ^{3}J = 6.9 Hz, CHMe$_2$, overlapping with Cp*Ti(HPP)(NHB(NDippCH)$_2$)(OPh)), 3.50 (1 H, s, overlapping OC=CH$_2$ and Cp*Ti(HPP)(NHB(NDippCH)$_2$)(OPh)), 3.29-3.24 (2 H, m, TiNCH$_2$), 3.15 (1 H, s, OC=CH$_2$),

2.56 (1 H, m, TiNC$\underline{H}_2$), 2.51-2.48 (2 H, m, $N_2NC\underline{H}_2$), 2.38-2.34 (2 H, m, $N_2NC\underline{H}_2$), 2.32-2.27 (1 H, m, TiNC$\underline{H}_2$), **1.83** (15 H, s, Cp*), 1.52 (12 H, d, ^3J = 6.8 Hz, CH$\underline{Me}_2$), 1.49 (13 H, app. d, app. ^3J = 6.8 Hz, overlapping CH$\underline{Me}_2$ and $CH_2C\underline{H}_2CH_2$), 1.17-1.11 (2 H, m, $CH_2C\underline{H}_2CH_2$), 1.02-0.97 (1 H, m, $CH_2C\underline{H}_2CH_2$) ppm. **^{13}C{^{1}H} NMR (Tol-d8, 125.8 MHz):** δ 168.1 (*i*-C_6H_5), 159.1 ($\underline{C}$=CH_2), 151.2 (N_2CN), 147.7 (*o*-$\underline{C}_6H_3{}^iPr_2$), 147.6 (*o*-$\underline{C}_6H_3{}^iPr_2$), 142.6 (*i*-$\underline{C}_6H_3{}^iPr_2$), 126.2 (*p*-$\underline{C}_6H_3{}^iPr_2$), 123.6 (*m*-$\underline{C}_6H_3{}^iPr_2$), 123.4 (*m*-$\underline{C}_6H_3{}^iPr_2$), 119.2 ($\underline{Cp^*}$), 116.3 (NCH), 63.9 (C=$\underline{C}H_2$), 48.4 ($N_2NC\underline{H}_2$), 48.3 ($N_2NC\underline{H}_2$), 45.3 (TiNC$\underline{H}_2$), 44.7 (TiNC$\underline{H}_2$), 28.9 ($\underline{C}HMe_2$), 28.4 ($\underline{C}HMe_2$), 25.5 (CH$\underline{Me}_2$), 24.9 (CH$\underline{Me}_2$), 24.3 (CH$\underline{Me}_2$), 23.9 (CH$\underline{Me}_2$), 22.4 ($CH_2\underline{C}H_2CH_2$), 22.3 ($CH_2\underline{C}H_2CH_2$), 11.6 (Cp*) ppm. **^{11}B{^{1}H} NMR (Tol-d8, 128.4 MHz):** 14.5 ppm.

***Data for Cp*Ti(HPP)(NH{B(NDippCH)$_2$})(OPh)* (3.37). ^{1}H NMR (C_6D_6, 400MHz):** δ 7.29-7.19 (6 H, m, overlapping *p*- and *m*-$C_6\underline{H}_3{}^iPr_2$), 7.13 (2 H, m, *m*-$C_6H_5$), 7.06 (2 H, m, *o*-$C_6H_5$), 6.76 (1 H, t, ^3J = 7.3 Hz, *p*-C_6H_5), 5.97 (2 H, s, NCH), 5.77 (1 H, s, NH), 3.61 (2 H, sept, ^3J = 6.7 Hz, C$\underline{H}Me_2$), 3.54 (2 H, sept, ^3J = 6.7 Hz, C$\underline{H}Me_2$), 3.43 (2 H, m, overlapping with free borylamine side product, $TiNCH_2$), 3.13 (2 H, t, ^3J = 5.7 Hz, $TiNCH_2$), 2.55-2.43 (4 H, m, N_2CNCH_2), 1.83 (15 H, s, Cp*), 1.42 (2 H, m, $CH_2\underline{C}H_2CH_2$), 1.35 (6 H, d, ^3J = 6.8 Hz, CH$\underline{Me}_2$), 1.31 (6 H, d, ^3J = 6.8 Hz, CH$\underline{Me}_2$), 1.29-1.24 (12 H, m, overlapping free borylamine side product and CH$\underline{Me}_2$), 1.11 (2 H, m, $CH_2\underline{C}H_2CH_2$) ppm. **^{13}C{^{1}H} NMR (C_6D_6, 125.8 MHz):** δ 166.6 (*i*-C_6H_5), 155.3 (N_2CN), 148.1 (*o*-$\underline{C}_6H_3{}^iPr_2$), 147.9 (*o*-$\underline{C}_6H_3{}^iPr_2$), 141.5 (*i*-$\underline{C}_6H_3{}^iPr_2$), 129.2 (*m*-$C_6H_5$), 126.9 (*p*-$\underline{C}_6H_3{}^iPr_2$), 123.6 (*m*-$\underline{C}_6H_3{}^iPr_2$), 123.3 ($\underline{Cp^*}$), 119.3 (*o*-$C_6H_5$), 118.1 (NCH), 46.4 ($N_2CN\underline{C}H_2$), 46.1($N_2CN\underline{C}H_2$), 44.4 ($TiNCH_2$), 43.8 ($TiNCH_2$), 28.6 ($\underline{C}HMe_2$), 26.5 (CH$\underline{Me}_2$), 25.9 (CH$\underline{Me}_2$), 24.0 (CH$\underline{Me}_2$), 23.9 ($CH_2\underline{C}H_2CH_2$), 23.5 ($CH_2\underline{C}H_2CH_2$), 12.2 (Cp*) ppm. **^{11}B{^{1}H} NMR (C_6D_6, 128.4 MHz):** 22.9 ppm. **IR (NaCl plates, Nujol mull, cm^{-1}):** 3524 (w), 3438 (w), 3336 (w), 3115 (w), 3059 (w), 2724 (m), 1918 (w), 1852 (w), 1787 (w), 1701 (w), 1654 (w), 1568 (s), 1534 (s), 1460 (s), 1378 (s), 1296 (s), 1205 (s), 1108 (s),

1068 (s), 1024 (s), 965 (m), 918 (m), 874 (m), 802 (s), 761 (m), 740 (s), 701 (m), 652 (m). **Anal. found (calcd. for $C_{49}H_{69}BN_6OTi$):** C, 71.97 (72.05); H, 8.41 (8.52); N, 10.17 (10.29)%.

Alternative synthesis of Cp*Ti(HPP)(NH{B(NDippCH)$_2$})(OPh) (3.37). Cp*Ti(HPP){NB(NDippCH)$_2$} (**1.83**, 300 mg, 0.415 mmol) was dissolved in toluene (4 mL, 0 °C) and a solution of phenol (43 mg, 0.46 mmol) in toluene (6 mL, 0 °C) was added dropwise. The reaction mixture was stirred and allowed to warm at RT. After 2 h the deep red solution was dried *in vacuo*. The desired Cp*Ti(HPP)(NH{B(NDippCH)$_2$})(OPh) (**3.37**) was afforded as major product (66%), together with the free borylamine H_2NB(NDippCH)$_2$ (33%) as byproduct. Yield: 292 mg (86%).

NMR tube scale reaction of Cp*Ti(HPP){NB(NDippCH)$_2$} (1.83) with $MeCO_2CAr^{CF_3}$ to form Cp*Ti(HPP)(NH{B(NDippCH)$_2$})(OAr^{CF_3}) (3.38) and Cp*Ti(HPP){OC(=CH$_2$)N(B{NDippCH}$_2$}) (3.42). Cp*Ti(HPP){NB(NDippCH)$_2$} (**1.83**, 15 mg, 0.0208 mmol) was dissolved in C_6D_6 (0.4 mL) in a NMR tube equipped with a J. Young Teflon valve, and alcohol (4.0 mg, 0.0247 mmol) was added. The reaction was left at RT and monitored *via* ^{1}H NMR spectroscopy. The reaction mixture turned red and the starting material is fully converted after 20 min. A mixture of 55% Cp*Ti(HPP)(NH{B(NDippCH)$_2$})(OAr^{CF_3}) and 45% borylamine as common side product is observed.

***Data for Cp*Ti(HPP)(NH{B(NDippCH)$_2$})(OAr^{CF_3})* (3.38). ^{1}H NMR (C_6D_6, 400 MHz):** δ 7.34 (2 H, d, ^3J = 8.4 Hz, *m*-$C_6H_4CF_3$), 7.26-7.16 (6 H, m, overlapping *p*- and *m*-$C_6\underline{H}_3{}^iPr_2$), 6.64 (2 H, d, ^3J = 8.4 Hz, *o*-$C_6H_4CF_3$), 6.12 (1 H, broad, s, NH), 5.95 (2 H, s, NCH), 3.50 (2 H, sept, ^3J = 6.8 Hz, C$\underline{H}$Me$_2$), 3.44 (2 H, sept, ^3J = 6.9 Hz, C$\underline{H}$Me$_2$), 1.76 (15 H, s, Cp*), 2.73 (2 H, m, TiNC$\underline{H}_2$), 2.46 (2 H, m, TiNC$\underline{H}_2$), 2.28-2.21 (4 H, m, N_2CNC$\underline{H}_2$), 1.40-1.33 (4 H, m, $CH_2C\underline{H}_2CH_2$), 1.28 (6 H, d, ^3J = 6.8 Hz, CH$\underline{Me}_2$), 1.26 (6 H, d, ^3J = 6.9 Hz, CH$\underline{Me}_2$), 1.24 (6

H, d, ^{3}J = 6.9 Hz, CH$\underline{Me}_2$), 1.22 (6 H, d, ^{3}J = 6.8 Hz, CH$\underline{Me}_2$) ppm. **^{13}C{^{1}H} NMR (C_6D_6, 125.8 MHz):** δ 168.5 (*i*-$\underline{C}_6H_4CF_3$), 150.3 (N_2CN), 147.7 (*o*-$\underline{C}_6H_3{}^{i}Pr_2$), 147.7 (*o*-$\underline{C}_6H_3{}^{i}Pr_2$), 141.5 (*i*-$\underline{C}_6H_3{}^{i}Pr_2$), 126.8 (2 C, q, $^{3}J_{C\text{-}F}$ = 3.8 Hz, *m*-$\underline{C}_6H_4CF_3$), 126.7 (*p*-$\underline{C}_6H_3{}^{i}Pr_2$), 123.7 (*m*-$\underline{C}_6H_3{}^{i}Pr_2$), 123.7 (*m*-$\underline{C}_6H_3{}^{i}Pr_2$), 123.3 (1 C, q, $^{2}J_{C\text{-}F}$ = 27 Hz, *p*-$\underline{C}_6H_4CF_3$), 120.5 ($\underline{Cp^*}$), 118.9 (*o*-$\underline{C}_6H_4CF_3$), 118.2 (NCH), 47.1 ($N_2CN\underline{C}H_2$), 45.9 ($N_2CN\underline{C}H_2$), 43.7 ($TiNCH_2$), 43.5 ($TiNCH_2$), 28.6 ($\underline{C}HMe_2$), 28.6 ($\underline{C}HMe_2$), 26.5 ($CH\underline{Me}_2$), 25.9 ($CH\underline{Me}_2$), 23.8 ($CH\underline{Me}_2$), 23.6 ($CH_2\underline{C}H_2CH_2$), 23.3 ($CH_2\underline{C}H_2CH_2$), 22.7 ($CH\underline{Me}_2$), 12.1 (Cp*) ppm. *CF_3 peak could not be located.* **^{19}F{^{1}H} NMR (C_6D_6, 282.1 MHz):** δ -60.4 ppm. **^{11}B{^{1}H} NMR (C_6D_6, 128.4 MHz):** δ 23.3 ppm.

Alternative synthesis of Cp*Ti(HPP)(NH{B(NDippCH)$_2$})(OAr^{CF_3}) (3.38). Cp*Ti(HPP){NB(NDippCH)$_2$} (**1.83**, 300 mg, 0.415 mmol) was dissolved in toluene (4 mL, 0 °C) and a solution of Ar^{CF_3}OH (74.6 mg, 0.46 mmol) in toluene (6 mL, 0 °C) was added dropwise. The reaction mixture was stirred and allowed to warm at RT. After 2 h the deep red solution was dried *in vacuo*. The desired Cp*Ti(HPP)(NH{B(NDippCH)$_2$})(OAr^{CF_3}) (**3.38**) was afforded as major product (53%), together with the free borylamine $H_2NB(NDippCH)_2$ (47%) as byproduct. Yield: 202 mg (54%).

TMSCH$_2$C(=O)OPh. $TMSCH_2C(=O)OH$ (2 g, 15.1 mmol) was dissolved in hexanes (5 mL) and stirred at RT when $SOCl_2$ (1.2 mL, 16.6 mmol) was added. The reaction mixture was heated to 50 °C for 2 days upon which time the reaction mixture turned red. ^{1}H NMR analysis showed quantitative conversion to $TMSCH_2C(=O)Cl$ (^{1}H NMR (C_6D_6, 400 MHz): δ 1.89 (2 H, s, CH_2), 0.06 (9 H, s, TMS) ppm) The spectral properties matched those of literature values.[37] Additional benzene (5 mL) was added to the crude mixture and cooled while stirring to 0 °C. Subsequently, phenol (1.33 g, 15 mmol) was added and the reaction mixture was allowed to

warm to RT and stirred for 16 h. The reaction mixture was purified using column chromatography on silica gel (EtOAc:Hex; 1:10), dried over $MgSO_4$. The volatiles were removed *in vacuo* to give the title compound as off-white liquid. Yield: 1.7 g (55 % in 2 steps). **^{1}H NMR ($CDCl_3$, 400 MHz):** δ 7.3-7.05 (5 H, m, Ph), 2.13 (2 H, s, CH_2), 0.1 (9 H, s, TMS) ppm. The spectral properties matched those of literature values.[38]

NMR tube scale reaction of Cp*Ti(HPP){NB(NDippCH)$_2$} (1.83) with benzamide to form phenylnitrile and [Cp*Ti(HPP)(μ-O)]$_2$ (3.22). Cp*Ti(HPP){NB(NDippCH)$_2$} (**1.83**, 15 mg, 0.0208 mmol) was dissolved in C_6D_6 (0.4 mL) in a NMR tube equipped with a J. Young Teflon valve, and benzamide (2.51 mg, 0.0247 mmol) was added. The reaction was left at RT and monitored *via* ^{1}H NMR spectroscopy. The reaction mixture turned red and the starting material is fully converted after 2 h to form [Cp*Ti(HPP)(μ-O)]$_2$ (**3.22**) which slowly precipitated to give yellow crystals, and phenylnitrile. The observed spectrocopic signature matches those of literature values of phenylnitrile.[39]

NMR tube scale reaction of Cp*Ti(HPP){NB(NDippCH)$_2$} with hexanamide to form hexylnitrile and [Cp*Ti(HPP)(μ-O)]$_2$ (3.22). Cp*Ti(HPP){NB(NDippCH)$_2$} (**1.83**, 15 mg, 0.0208 mmol) was dissolved in C_6D_6 (0.4 mL) in a NMR tube equipped with a J. Young Teflon valve, and hexylamide (2.39 mg, 0.0208 mmol) was added. The reaction was left at RT and monitored *via* ^{1}H NMR spectroscopy. The reaction mixture turned red and the starting material is fully converted after 2 h to form [Cp*Ti(HPP)(μ-O)]$_2$ (**3.22**), which slowly precipitated to give yellow crystals, and hexylnitrile. The observed spectrocopic signature matches those of literature values of hexylnitrile.[40]

5.7 Experimental details and characterising data for Chapter Four

Improved synthesis for Mes_2BN_3. Mes_2BN_3 (2 g, 7.46 mmol) was dissolved in 10 mL of Me_3SiN_3 at RT. The resulting light-yellow solution was stirred at 40 °C for 2 days. All volatiles were removed *in vacuo*, and the product washed with cold hexanes once (5 mL, 0 °C). The product was furnished in good yield as off-white powder (1.3 g, 4.48 mmol, 60%). The spectral properties matched literature values.[41]

$N_3\{B(NMe)_2C_6H_4\}$ (4.9). TMS-N_3 (0.8 mL, 5.9 mmol) was added slowly to Br-$\{B(NMe)_2C_6H_4\}$ (1 g, 4.45 mmol) dissolved in toluene (10 mL) at RT. The mixture was stirred at 50 °C for 2 days. Volatiles were removed *in vacuo* to afford the light beige product as a waxy solid. Yield: 0.756 mg (91%). **^{1}H NMR (C_6D_6, 400MHz):** δ 7.06 (2 H, m, 3,6-C_6H_4), 6.70 (2 H, m, 4,5-C_6H_4), 2.75 (6 H, s, Me) ppm. **$^{13}C\{^1H\}$ NMR (C_6D_6, 100.6 MHz):** δ 137.5 (1,2-C_6H_4), 119.6 (4,5-C_6H_4), 108.2 (3,6-C_6H_4), 27.9 (Me) ppm. **$^{11}B\{^1H\}$ NMR (C_6D_6, 128.4 MHz):** 21.0 ppm. **IR (NaCl plates, Nujol mull, cm^{-1}):** 2924 (s), 2250 (w), 2142 (s, υ(N=N=N) st), 1608 (m), 1448 (s), 1415 (s), 1297 (s), 1260 (s), 1232 (m), 1109 (m), 1018 (m), 803 (s), 734 (s), 635 (w), 616 (m). **Anal. found (calcd. for $C_8H_{10}BN_5$):** C, 51.21 (51.38); H, 5.50 (5.39); N, 37.26 (37.45)%.

$N_3\{B(NDippCH)_2\}$ (4.10). Br$\{B(NDippCH)_2\}$ (1 g, 2.14 mmol) was stirred at 50 °C for 15 days in $TMSN_3$ (20 mL, neat). The volatiles of the brown mixture were removed *in vacuo*. The product was recrystallized in hexanes at 5 °C to give colorless, diffraction-quality needles (250 mg). Yield: 58%. **^{1}H NMR (C_6D_6, 400MHz):** δ 7.24-7.18 (2 H, m, *p*-$C_6\underline{H}_3{}^iPr_2$), 7.13-7.11 (4 H, m, *m*-$C_6\underline{H}_3{}^iPr_2$), 5.98 (2 H, s, $N(CH_2)_2N$), 3.24 (4 H, sept, ^3J = 6.9 Hz, C$\underline{H}$Me$_2$), 1.33 (12 H, d, ^3J = 6.9 Hz, CH$\underline{Me}_2$), 1.23 (12 H, d, ^3J = 6.9 Hz, CH$\underline{Me}_2$) ppm. **$^{13}C\{^1H\}$ NMR (C_6D_6, 125.8 MHz):** δ 147.7 (*o*-$\underline{C}_6H_3{}^iPr_2$), 136.7 (*i*-$\underline{C}_6H_3{}^iPr_2$), 128.5 (*p*-$\underline{C}_6H_3{}^iPr_2$), 123.8 (*m*-$\underline{C}_6H_3{}^iPr_2$), 118.6 ($N(\underline{C}H_2)_2N$), 28.9 ($\underline{C}HMe_2$), 24.23 (CH$\underline{Me}_2$), 24.19 (CH$\underline{Me}_2$) ppm. **$^{11}B\{^1H\}$ NMR (C_6D_6,**

128.4 MHz): 20.0 ppm. **IR (NaCl plates, Nujol mull, cm^{-1}):** 2143 (s, υ(N=N=N) st), 2361 (w), 1948 (w), 1586 (w), 1525 (m), 1460 (s), 1406 (s), 1379 (s), 1362 (s), 1329 (m), 1192 (m), 1113 (m), 1088 (m), 1059 (m), 1020 (m), 914 (m), 805 (s), 761 (s), 652 (m). **Anal. found (calcd. for $C_{26}H_{36}BN_5$):** C, 72.65 (72.72); H, 8.62 (8.45); N, 16.15 (16.31)%.

NMR tube scale synthesis of $Cp''_2TiNB\{N(Me)_2C_6H_4\}$ (4.11). A deep blue solution of $(Cp''_2Ti)_2(\mu_2, \eta^1, \eta^1\text{-}N_2)$ (**1.16**, 20 mg, 0.020 mmol) in toluene-d8, and a 2 mL glass vial containing $N_3\{B(NMe)_2C_6H_4\}$ (7.5 mg, 0.040 mmol) were chilled in a glovebox freezer set to -35 °C. After 20 min, the blue solution was transferred to the glass vial containing the azide and mixed until all azide was dissolved at RT. The blue color immediately turned brown and the evolution of bubbles indicated formation of nitrogen. The solution was transferred to a NMR tube fitted with a J. Youngs valve, and the reaction progress was monitored using ^{1}H NMR spectroscopy. **^{1}H NMR (Toluene-d8, 400MHz):** δ 8.04 (2 H, m, 2-$C_5\underline{H}_3$), 7.05-7.04 (2 H, m, 3,4-$C_6\underline{H}_4$), 6.79-6.77 (2 H, m, 2,5-$C_6\underline{H}_4$), 6.53 (4 H, s, 4,5-$C_5\underline{H}_3$), 3.12 (6 H, s, NMe), 0.14 (36 H, s, $SiMe_3$) ppm. **^{13}C{^{1}H} NMR (Toluene-d8, 125.8 MHz):** δ 138 (1,2-C_6H_4), 134.9 (2-C_5H_3), 132.8 (1,3-C_5H_3), 127.3 (4,5-C_5H_3), 107 (3,6-C_6H_4), 29.4 (NMe), -0.07 ($SiMe_3$) ppm. **^{11}B{^{1}H} NMR (C_6D_6, 128.4 MHz):** 17.5 ppm.

NMR tube scale synthesis of $Cp''_2TiNB\{N(Dipp)CH\}_2$ (4.13). A deep blue solution of $(Cp''_2Ti)_2(\mu_2, \eta^1, \eta^1\text{-}N_2)$ (**1.16**, 15 mg, 0.015 mmol) in toluene-d8 was added to a 2 mL glass vial containing $N_3\{B(NDippCH)_2\}$ (12.8 mg, 0.03 mmol) at RT. The reagents were mixed using a glass pipette, and the color changed to red-brown. The mixture was transferred into a NMR tube fitted with a J. Youngs valve, and the reaction progress was monitored using ^{1}H NMR spectroscopy. **^{1}H NMR (Toluene-d8, 400MHz):** δ 7.32 (2 H, s, 2-$C_5\underline{H}_3$), 7.23 (6 H, app. s, overlapping *p*- and *m*-$C_6\underline{H}_3{}^iPr_2$), 7.01 (4 H, app. s, 4,5-$C_5\underline{H}_3$), 5.80 (2 H, s, $N(C\underline{H}_2)_2N$), 3.63 (4 H, sept, ^3J = 6.8 Hz, $C\underline{H}Me_2$), 1.51 (12 H, d, ^3J = 6.8 Hz, $CH\underline{Me}_2$), 1.23 (12 H, d, ^3J = 6.8 Hz, $CH\underline{Me}_2$), -0.08 (36 H, s, $SiMe_3$) ppm. **^{13}C{^{1}H} NMR (Toluene-d8, 125.8 MHz):** δ 144.6

(*o*-$\underline{C}_6H_3{}^iPr_2$), 141.9 (*i*-$\underline{C}_6H_3{}^iPr_2$), 141.5 (1,3-$C_5H_3$), 139.2 (2-$C_5H_3$), 127.5 (*p*-$C_6\underline{H}_3{}^iPr_2$), 127.4 (4,5-$C_5H_3$), 124.0 (*m*-$\underline{C}_6H_3{}^iPr_2$), 117.6 (N($\underline{C}H_2$)$_2$N), 28.9 ($\underline{C}HMe_2$), 26.2 (CH$\underline{Me}_2$), 23.9 ($\underline{C}HMe_2$), 0.72 ($SiMe_3$) ppm. **$^{11}B\{^1H\}$ NMR (C_6D_6, 128.4 MHz):** 17.5 ppm.

Cp''$_2$TiNB(Mes)$_2$ (4.1). To a deep blue solution of (Cp"$_2$Ti)$_2$(μ_2, η^1, η^1-N_2) (**1.16**, 200 mg, 0.195 mmol) dissolved in toluene (5 mL) at -78°C was added slowly N_3BMes_2 (114 mg, 0.390 mmol) dissolved in toluene (10 mL) at -78 °C. The reaction mixture was allowed to warm to RT and turned green after 30 min. The green mixture was stirred for 12 h at RT after which the volatiles were removed under reduced pressure. The green product was obtained as a green powder after extraction into hexanes (3 x 15 mL), and removal of the volatiles. Yield: 208 mg (70 %). Diffraction-quality crystals were grown from a saturated hexane solution at 4 °C. **^{1}H NMR (Toluene-d8, 400MHz):** δ 7.46 (2 H, s, 2-C_5H_3), 7.34 (4 H, s, 4,5-C_5H_3), 6.72 (4 H, s, C_6H_2), 2.62 (12 H, s, *o*-C$\underline{H}_3$-C_6H_2), 2.18 (6 H, s, *p*-C$\underline{H}_3$-C_6H_2), 0.00 (36 H, s, $SiMe_3$) ppm. **$^{13}C\{^1H\}$ NMR (Toluene-d8, 125.8 MHz):** δ 144.0 (*i*-C_6H_2), 139.9 (*o*-C_6H_2), 135.6 (*p*-C_6H_2), 134.3 (1,3-C_5H_3), 130.6 (2-C_5H_3), 130.3 (4,5-C_5H_3), 128.5 (*m*-C_6H_2), 24.4 (*o*-$\underline{C}H_3$-C_6H_2), 21.1 (*p*-$\underline{C}H_3$-C_6H_2), -0.09 ($SiMe_3$) ppm. **$^{11}B\{^1H\}$ NMR (C_6D_6, 128.4 MHz):** 44.2 ppm. **IR (NaCl plates, Nujol mull, cm^{-1}):** 2726 (w), 1607 (w), 1460 (s), 1377 (s), 1294 (m), 1249 (m), 1209 (w), 1083 (m), 1021 (w), 968 (w), 919 (m), 838 (s), 754 (m), 734 (m), 722 (m), 692 (w), 636 (w). *Despite several attempts on large, well-defined single crystals, a satisfactory elemental analysis of this extremely sensitive compound could not be obtained.*

Cp''$_2$TiN^{t}Bu (4.15). In the glovebox, a deep blue solution of (Cp"$_2$Ti)$_2$(μ_2, η^1, η^1-N_2) (**1.16**, 600 mg, 0.52 mol) in toluene (5 mL), and a colorless solution of $N_3{}^tBu$ (136 mg, 1.04 mol) were chilled to -35 °C for 30 min. The solution containing the azide was then transferred into the other solution, and the resulting mixture was removed from the glovebox and slowly allowed to warm to RT while stirring. Upon warming the formation of bubbles indicated the release of nitrogen gas, and the color changed to dark red. After 16 h of stirring at RT all

volatiles were removed *in vacuo*, and the product was extracted into pentanes. Diffraction-quality crystals were grown from a saturated pentane solution at -30 °C. Note: Azides are explosive and a blast-shield was used as a safety precaution. Yield: 443 mg (79 %). **^{1}H NMR (Toluene-d8, 400MHz, RT):** δ 8.09 (2 H, s, 2-$C_5(SiMe_3)_2\underline{H}_3$), 6.67 (4 H, s, 4,5-$C_5(SiMe_3)_2\underline{H}_3$), 1.20 (9 H, s, CMe_3), 0.22 (36 H, s, $SiMe_3$) ppm. **^{13}C{^{1}H} NMR (Toluene-d8, 125.8 MHz, RT):** δ 135.1 (1,3-$\underline{C}_5(SiMe_3)_2H_3$), 130.1 (2-$\underline{C}_5(SiMe_3)_2H_3$), 126.8 (4,5-$\underline{C}_5(SiMe_3)_2H_3$), 72.3 ($N\underline{C}Me_3$), 32.3 ($C\underline{Me}_3$), 0.63 ($SiMe_3$) ppm. **IR (NaCl plates, Nujol mull, cm^{-1}):** 2479 (w), 2364 (w), 2092 (w), 2002 (w), 1936 (w), 1876 (w), 1560 (w), 1472 (m), 1441 (s), 1403 (m), 1356 (s), 1306 (s), 1248 (s), 1210 (s), 1082 (s), 1040 (w), 1021 (w), 973 (s), 920 (s), 853 (s), 754 (s), 734 (m), 691 (m), 691 (m), 635 (m). *Several attempts to obtain a satisfactory elemental analysis from crystalline material failed, presumably due to the high sensitivity of this complex.*

Cp''{1,3-C_5H_3($SiMe_3$)($SiMe_2$(CH_2NH)BMes_2)}Ti (4.16). Cp"$_2$TiNBMes_2 (100 mg, 137 mmol) was dissolved in toluene (10 mL) and the resulting green solution was heated to 80 °C for 36 h. Volatiles were removed *in vacuo,* and the product was triturated in pentanes. After removal of the volatiles the product was afforded as a grey powder. Yield: 71 mg (71%). **^{1}H NMR (Toluene-d8, 400MHz, -10 °C):** δ 7.39 (1 H, s, 2-$C_5(SiMe_3)_2\underline{H}_3$), 6.99 (1 H, s, $C_6\underline{H}_2Me_3$), 6.89 (1 H, s, $C_6\underline{H}_2Me_3$), 6.79 (1 H, s, 2-$C_5\underline{H}_3$), 6.70 (1 H, s, $C_6\underline{H}_2Me_3$), 6.61 (1 H, s, $C_6\underline{H}_2Me_3$), 6.23 (1 H, s, 4,5-$C_5\underline{H}_3$), 5.96 (1 H, s, 4,5-$C_5(SiMe_3)_2\underline{H}_3$), 5.95 (1 H, s, 4,5-$C_5(SiMe_3)_2\underline{H}_3$), 5.87 (1 H, s, 4,5-$C_5\underline{H}_3$), 3.97 (1 H, d, ^{2}J = 9.6 Hz, $SiCH_2$), 2.55 (3 H, s, *p*-$C_6H_2\underline{Me}_3$), 2.32 (3 H, s, *p*-$C_6H_2\underline{Me}_3$), 2.25 (3 H, s, *o*-$C_6H_2\underline{Me}_3$), 2.23 (3 H, s, *o*-$C_6H_2\underline{Me}_3$), 2.08-2.05 (6 H, m, overlapping *o*-$C_6H_2\underline{Me}_3$ and residual protio toluene), **1.83** (1 H, d, ^{2}J = 9.5 Hz, $SiCH_2$), 0.28 (6 H, s, $SiMe_2$), 0.21 (9 H, s, $SiMe_3$), 0.12 (9 H, s, $SiMe_3$), 0.07 (9 H, s, $SiMe_3$) ppm. *NH peak not located*. **^{13}C{^{1}H} NMR (Toluene-d8, 125.8 MHz, -10 °C):** δ 162.0 (2-$\underline{C}_5(SiMe_3)_2H_3$), 145.3 (*i*-$C_6H_2$), 133.6 ($\underline{C}SiCH_2$), 132.4 (1,3-$\underline{C}_5(SiMe_3)_2H_3$), 130.3 (2-$\underline{C}_5(SiMe_3)_2H_3$), 128.4 (*o*-$\underline{C}_6H_2Me_3$), 128.2 (*o*-$\underline{C}_6H_2Me_3$) 127.8 (*o*-$\underline{C}_6H_2Me_3$), 127.6 (*m*-

$C_6H_2Me_3$), 127.6 (*m*-$C_6H_2Me_3$), 124.7 (*m*-$C_6H_2Me_3$), 127.4 (4,5-C_5H_3), 126.2 (*m*-$C_6H_2Me_3$), 125.8 (*o*-$\underline{C}_6H_2Me_3$), 125.6 (*p*-$\underline{C}_6H_2Me_3$), 125.5 (*p*-$\underline{C}_6H_2Me_3$), 125.0 (*i*-$\underline{C}_6H_2Me_3$), 121.8 (4,5-C_5H_3), 117.0 (4,5-$\underline{C}_5(SiMe_3)_2H_3$), 116.3 (4,5-$\underline{C}_5(SiMe_3)_2H_3$), 70.8 ($SiCH_2$), 24.9 (*p*-$C_6H_2\underline{Me}_3$), 21.7 (*o*-$C_6H_2\underline{Me}_3$), 21.4 (*p*-$C_6H_2\underline{Me}_3$), 20.9 (*o*-$C_6H_2\underline{Me}_3$), 1.09 ($SiMe_2$), 0.56 ($SiMe_3$), 0.23 ($SiMe_3$), 0.12 ($SiMe_3$) ppm. **$^{11}B\{^1H\}$ NMR (Toluene-d8, 128.4 MHz):** 44.1 ppm. **IR (NaCl plates, Nujol mull, cm^{-1}):** 3385 (w, υ(N-H) st), 2274 (w), 2137 (w), 2085 (w), 2060 (w), 1962 (w), 1595 (m), 1543 (w), 1457 (s), 1412 (w), 1377 (s), 1260 (s), 1086 (s), 1020 (s), 917 (m), 801 (s), 755 (m), 721 (w), 692 (w), 661 (w), 638 (w). **EI-HRMS found (calcd for [$C_{40}H_{64}BNSi_4Ti$, M^+]$^+$):** 726.3798 (726.3766). **Anal. found (calcd. for $C_{40}H_{64}BNSi_4Ti$):** C, 64.91 (65.82); H, 8.96 (8.84); N, 1.99 (1.92)%. The poor agreement between found and calculated carbon values might be due to incomplete combustion.

NMR tube scale synthesis of Cp''$_2$TiNBMes$_2$(DMAP) (4.17). Cp''$_2$TiNBMes$_2$ (**4.1**, 20 mg, 0.027 mmol) was dissolved in toluene-d8 (0.5 mL), and the green solution was subsequently transferred into a vial containing DMAP (3.3 mg, 0.027 mmol). The resulting red mixture was transferred into a NMR tube fitted with a J. Youngs valve, and the reaction was confirmed to be complete after 10 min *via* ^{1}H NMR spectroscopy. **^{1}H NMR (Toluene-d8, 400 MHz, RT):** δ 8.22 (2 H, d, ^3J = 6.4 Hz, *o*-$NC_5\underline{H}_4$), 7.06 (2 H, s, 2-C_5H_3), 6.82 (4 H, s, $C_6\underline{H}_2$), 6.50 (2 H, s, broad, 4,5-C_5H_3), 6.39 (2 H, s, broad, 4,5-C_5H_3), 5.88 (2 H, d, ^3J = 6.3 Hz, *m*-$NC_5\underline{H}_4$), 2.75 (12 H, s, *o*-$C_6\underline{Me}_3H_2$), 2.25 (6 H, s, *p*-$C_6\underline{Me}_3H_2$), 1.99 (6 H, s, NMe_2), 0.28 (18, s, $SiMe_3$), 0.18 (18, s, $SiMe_3$) ppm. **$^{13}C\{^1H\}$ NMR (Toluene-d8, 125.8 MHz, RT):** δ 156.6 (*o*-$N\underline{C}_5H_4$-NMe_2), 154.1 (*p*-$N\underline{C}_5H_4$-NMe_2), 144.7 (*i*-$\underline{C}_6H_2$), 140.3 (*o*-$\underline{C}_6H_2$), 135.3 (*p*-$\underline{C}_6H_2$), 128.5 (*m*-$\underline{C}_6H_2$), 128.4 (2-C_5H_2), 123.6 (1,3-C_5H_2), 121.3 (4,5-C_5H_2), 105.0 (*m*-$N\underline{C}_5H_4$), 38.0 (NMe_2), 25.5 (*o*-$C_6\underline{Me}_3H_2$), 21.2 (*p*-$C_6\underline{Me}_3H_2$), 1.1 ($SiMe_3$), 0.98 ($SiMe_3$) ppm. **$^{11}B\{^1H\}$ NMR (C_6D_6, 128.4 MHz, RT):** 43.9 ppm.

NMR tube scale reaction of Cp''$_2$TiNBMes$_2$ (4.1) with Ph$_2$CO. Cp"$_2$TiNBMes$_2$ (**4.1**, 20 mg, 0.027 mmol) was dissolved in 0.5 mL of C_6D_6 and Ph_2CO (4.9 mg, 0.027 mmol) was added. The reaction progress was monitored by ^{1}H and ^{11}B NMR spectroscopy. After 4 days at 55 °C there was full conversion, and quantitative formation of the known compounds Ph_2C=NBMes$_2$ (**4.20**)[42] and (Cp"$_2$Ti=O)$_n$ (**4.18**)[43] was observed. The spectral NMR data agreed with literature data of these compounds.[42,43]

NMR tube scale reaction of Cp''$_2$TiNBMes$_2$ (4.1) with PhHCO. Cp"$_2$TiNBMes$_2$ (**4.1**, 20 mg, 0.027 mmol) was dissolved in 0.5 mL of C_6D_6 and subsequently PhHCO (3.2 μL, 0.027 mmol) was added. After 10 minutes at room temperature, full conversion of 4.1 was observed as judged by ^{1}H NMR spectroscopy. Quantitative formation of the known compounds PhHC=NBMes$_2$ (**4.19**)[44] and (Cp"$_2$Ti=O)$_n$ (**4.18**)[43] was observed. The spectral NMR data agreed with literature data of these compounds.[43,44]

Cp''$_2$Ti(H)N(H)BMes$_2$ (4.21). Cp"$_2$TiNBMes$_2$ (**4.1**, 250 mg, 34.3 mmol) was dissolved in benzene (4 mL) in a Schlenk tube which was connected *via* a T-piece to a high vacuum line and a hydrogen lecture bottle. The green solution was freeze pump-thawed twice and subsequently pressurized with a hydrogen atmosphere of 1.2 bar. The frozen solution was subsequently thawed, and turned orange within 10 min. Stirring at RT continued for 2 h, after which the reaction mixture was filtered. The volatiles were removed in vacuo to afford an orange powder. Yield: 210 mg (83 %). Diffraction quality crystals were grown from a saturated hexane solution under 1 bar pressure of H_2 at -35 °C. **^{1}H NMR (Toluene-d8, 400MHz, RT):** 7.80 (1 H, s, br., NH), 6.80-6.71 (4 H, app. s, broad, $C_6\underline{H}_2Me_3$), 6.42-6.14 (4 H, app. s, br., 4,5-$C_5(SiMe_3)_2\underline{H}_3$), 4.78 (1 H, s, br., 2-$C_5(SiMe_3)_2\underline{H}_3$), 4.50 (1 H, s, br., 2-$C_5(SiMe_3)_2\underline{H}_3$), 3.08 (1 H, s, TiH), 2.75-2.53 (6 H, app. s, br., *o*-$C_6H_2\underline{Me}_3$), 2.43-2.12 (12 H, m, br., overlapping *o*-$C_6H_2\underline{Me}_3$, *p*-$C_6H_2\underline{Me}_3$, and residual protio-solvent), 0.44-0.15 (36 H, app. s, br., $SiMe_3$) ppm. **^{1}H NMR (Toluene-d8, 400 MHz, -60 °C):** δ 7.78 (1 H, s, br., NH), 6.89 (1 H, s, $C_6\underline{H}_2Me_3$),

6.87 (1 H, s, $C_6\underline{H}_2Me_3$), 6.67 (1 H, s, $C_6\underline{H}_2Me_3$), 6.59 (1 H, s, $C_6\underline{H}_2Me_3$), 6.37 (2 H, app. s, br., 4,5-$C_5(SiMe_3)_2\underline{H}_3$), 6.24 (1 H, s, 4,5-$C_5(SiMe_3)_2\underline{H}_3$), 6.02 (1 H, s, 4,5-$C_5(SiMe_3)_2\underline{H}_3$), 4.73 (1 H, s, 2-$C_5(SiMe_3)_2\underline{H}_3$), 4.47 (1 H, s, 2-$C_5(SiMe_3)_2\underline{H}_3$), 3.00 (1 H, s, TiH), 2.67 (3 H, s, *o*-$C_6H_2\underline{Me}_3$), 2.57 (3 H, s, *o*-$C_6H_2\underline{Me}_3$), 2.23 (3 H, s, *o*-$C_6H_2\underline{Me}_3$), 2.14 (6 H, s, *p*-$C_6H_2\underline{Me}_3$), 2.13 (3 H, s, *o*-$C_6H_2\underline{Me}_3$), 0.32 (9 H, s, $SiMe_3$), 0.29 (9 H, s, $SiMe_3$), 0.18 (9 H, s, $SiMe_3$), 0.11 (9 H, s, $SiMe_3$) ppm. **$^{13}C\{^1H\}$ NMR (Toluene-d8, 125.8 MHz, -60 °C):** δ 142.6 (4,5-$\underline{C}_5(SiMe_3)_2H_3$), 141.8 (4,5-$\underline{C}_5(SiMe_3)_2H_3$), 139.3 (*o*-$\underline{C}_6H_2Me_3$), 138.7 (*o*-$\underline{C}_6H_2Me_3$), 138.6 (*o*-$\underline{C}_6H_2Me_3$), 138.3 (*o*-$\underline{C}_6H_2Me_3$), 135.7 (*p*-$\underline{C}_6H_2Me_3$), 135.1 (*p*-$\underline{C}_6H_2Me_3$), 132.6 (1,3-$\underline{C}_5(SiMe_3)_2H_3$), 129.5 (*m*-$\underline{C}_6H_2Me_3$), 129.3 (*m*-$\underline{C}_6H_2Me_3$), 129.2 (*m*-$\underline{C}_6H_2Me_3$), 129.1 (*m*-$\underline{C}_6H_2Me_3$), 121.3 (1,3-$\underline{C}_5(SiMe_3)_2H_3$), 119.9 (1,3-$\underline{C}_5(SiMe_3)_2H_3$), 116.7 (1,3-$\underline{C}_5(SiMe_3)_2H_3$), 114.3 (2-$\underline{C}_5(SiMe_3)_2H_3$), 110.9 (2-$\underline{C}_5(SiMe_3)_2H_3$), 24.7 (*o*-$C_6H_2\underline{Me}_3$), 23.9 (*o*-$C_6H_2\underline{Me}_3$), 22.1 (*o*-$C_6H_2\underline{Me}_3$), 20.3 (*p*-$C_6H_2\underline{Me}_3$), 20.1 (*p*-$C_6H_2\underline{Me}_3$), 20.0 (*o*-$C_6H_2\underline{Me}_3$), 0.35 ($SiMe_3$), -0.58 ($SiMe_3$), -1.19 ($SiMe_3$), -1.44 ($SiMe_3$) ppm. **$^{11}B\{^1H\}$ NMR (Toluene-d8, 128.4 MHz):** 42.0 ppm. **IR (NaCl plates, Nujol mull, cm^{-1}):** 3354 (w, υ(N-H) st), 2137 (m), 2085 (m), 1646 (w, υ(Ti-H) st), 1608 (m), 1550.4 (w), 1456 (s), 1422 (m), 1377 (s), 1261 (s), 1248 (s), 1231 (m), 1210 (m), 1173 (m), 1089 (s), 1071 (m), 1034 (m), 1018 (m), 959 (w), 928 (s), 921 (s), 838 (s), 754 (m), 722 (m), 692 (m), 675 (m), 636 (m). *A satisfactory elemental analysis could not be obtained due to slow decomposition of the compound.*

General procedure for the NMR tube scale reaction of Cp"$_2$TiNBMes$_2$ with hydrogen gas: Cp"$_2$TiNBMes$_2$ (**4.1**, 15 mg, 0.0205 mmol) was dissolved in toluene in a NMR tube fitted with a J. Youngs valve. The solution was freeze pump thawed two times, and subsequently subjected to a hydrogen gas atmosphere of 1 bar while frozen. The reaction mixture was thawed and an immediate color change from green to orange indicated complete conversion of the reaction within a few minutes.

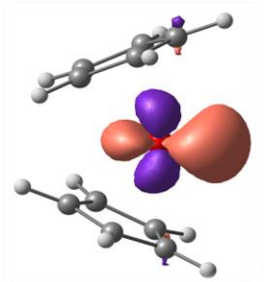
Characterising data for Cp''$_2$Ti(D)N(D)B(Mes)$_2$. **^{2}H NMR spectrum (61.4 MHz, toluene-H8, 298 K):** 7.94 (1 D, br., s, ND), 3.08 ppm (1 D, s, TiD) ppm. **IR (NaCl plates, Nujol mull, cm^{-1}):** 2409 (w, υ(N-D) st), 2137 (m), 2085 (m), 1608 (m), 1550.4 (w), 1456 (s), 1422 (m), 1377 (s), 1261 (s), 1248 (s), 1231 (m), 1210 (m), 1173 (m), 1151 (m, υ(Ti-D) st), 1089 (s), 1071 (m), 1034 (m), 1018 (m), 959 (w), 928 (s), 921 (s), 838 (s), 754 (m), 722 (m), 692 (m), 675 (m), 636 (m).

5.8 References

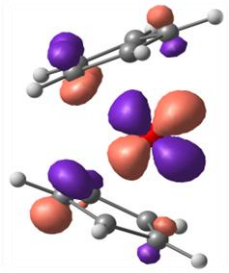
1 A. B. Pangborn, M. A. Giardello, R. H. Grubbs, R. K. Rosen and F. J. Timmers, *Organometallics*, 1996, **15**, 1518–1520.
2 J. Feng and J. A. Reimer, *J. Magn. Reson.*, 2011, **209**, 300–305.
3 T. J. Hadlington, J. A. B. Abdalla, R. Tirfoin, S. Aldridge and C. Jones, *Chem. Commun.*, 2016, **52**, 1717–1720.
4 B. A. Clough, S. Mellino, A. V. Protchenko, M. Slusarczyk, L. C. Stevenson, M. P. Blake, B. Xie, E. Clot and P. Mountford, *Inorg. Chem.*, 2017, **56**, 10794–10814.
5 D. A. Evans and J. M. Janey, *Org. Lett.*, 2001, **3**, 2125–2128.
6 M. E. Sloan, A. Staubitz, T. J. Clark, C. A. Russell, G. C. Lloyd-Jones and I. Manners, *J. Am. Chem. Soc.*, 2010, **132**, 3831–3841.
7 C. A. Jaska, K. Temple, A. J. Lough and I. Manners, *J. Am. Chem. Soc.*, 2003, **125**, 9424–9434.
8 J. N. Kirwan and B. P. Roberts, *J. Chem. Soc., Perkin Trans. 2*, 1989, **0**, 539–550.
9 J. M. Purser A N and D. B. F. Spielvogel, *Notes*, 1968, **7**, 2156–2157.
10 A. P. M. Robertson, E. M. Leitao, T. Jurca, M. F. Haddow, H. Helten, G. C. Lloyd-Jones and I. Manners, *J. Am. Chem. Soc.*, 2013, **135**, 12670–12683.
11 O. J. Metters, S. R. Flynn, C. Dowds, H. A. Sparkes, I. Manners and D. F. Wass, *ACS Catal.*, 2016, **6**, 6601–6611.
12 Natalie A. Jones, Stephen T. Liddle, A. Claire Wilson and P. L. Arnold, *Organometallics*, 2007, **26**, 755–757.
13 J. Okuda, *J. Organomet. Chem.*, 1989, **375**, C13–C16.
14 S. Wiese, M. J. B. Aguila, E. Kogut and T. H. Warren, *Organometallics*, 2013, **32**, 2300–2308.
15 T. E. Hanna, I. Keresztes, E. Lobkovsky, W. H. Bernskoetter and P. J. Chirik, *Organometallics*, 2004, **23**, 3448–3458.
16 W. Fraenk, T. Habereder, T. M. Klapötke, H. Nöth and K. Polborn, *J. Chem. Soc. Dalt. Trans.*, 1999, **0**, 4283–4286.
17 Aldo E. Guiducci, A. Catherine L. Boyd and P. Mountford, *Organometallics*, 2006, **25**, 1167–1187.
18 Z. Otwinowski and W. Minor, *Processing of X-ray Diffraction Data Collected in Oscillation Mode*, Academic press, New York, 1997.
19 A. Altomare, G. Cascarano, G. Giacovazzo, A. Guagliardi, M. C. Burla, G. Polidori and M. Camalli, *J. Appl. Crystallogr.*, 1994, **27**, 435.
20 L. Palatinus and G. Chapuis, *J. Appl. Cryst.*, 2007, **40**, 786–790.
21 P. W. Betteridge, J. R. Cooper, R. I. Cooper, K. Prout and D. J. Watkin, *J. Appl.*

Cryst., 2003, **36**, 1487.
22 S. Mellino, *DPhil Thesis, University of Oxford*, 2017.
23 M. J. Frisch, G. W. Trucks, H. B. Schlegel, G. E. Scuseria, M. A. Robb, J. R. Cheeseman, G. Scalmani, V. Barone, B. Mennucci, G. A. Petersson, H. Nakatsuji, M. Caricato, X. Li, H. P. Hratchian, A. F. Izmaylov, J. Bloino, G. Zheng, J. L. Sonnenberg, M. Hada, M. Ehara, K. Toyota, R. Fukuda, J. Hasegawa, M. Ishida, T. Nakajima, Y. Honda, O. Kitao, H. Nakai, T. Vreven, J. A. Montgomery Jr., J. E. Peralta, F. Ogliaro, M. J. Bearpark, J. Heyd, E. N. Brothers, K. N. Kudin, V. N. Staroverov, R. Kobayashi, J. Normand, K. Raghavachari, A. P. Rendell, J. C. Burant, S. S. Iyengar, J. Tomasi, M. Cossi, N. Rega, N. J. Millam, M. Klene, J. E. Knox, J. B. Cross, V. Bakken, C. Adamo, J. Jaramillo, R. Gomperts, R. E. Stratmann, O. Yazyev, A. J. Austin, R. Cammi, C. Pomelli, J. W. Ochterski, R. L. Martin, K. Morokuma, V. G. Zakrzewski, G. A. Voth, P. Salvador, J. J. Dannenberg, S. Dapprich, A. D. Daniels, Ö. Farkas, J. B. Foresman, J. V Ortiz, J. Cioslowski and D. J. Fox, *Gaussian 09, Revis. D.01, Gaussian Inc., Wallingford CT*, 2013.
24 A. D. Becke, *J. Chem. Phys.*, 1993, **98**, 5648–5652.
25 J. P. Perdew and Y. Wang, *Phys. Rev. B*, 1992, **45**, 13244–13249.
26 S. Grimme, J. Antony, S. Ehrlich and H. Krieg, *J. Chem. Phys.*, 2010, **132**, 154104–154119.
27 S. Grimme, S. Ehrlich and L. Goerigk, *J. Comput. Chem.*, 2011, **32**, 1456–1465.
28 A. Schäfer, H. Horn and R. Ahlrichs, *J. Chem. Phys.*, 1992, **97**, 2571–2577.
29 A. V. Marenich, C. J. Cramer and D. G. Truhlar, *J. Phys. Chem. B*, 2009, **113**, 6378–6396.
30 F. Weigend and R. Ahlrichs, *Phys. Chem. Chem. Phys.*, 2005, **7**, 3297–3305.
31 N. T. Coles, M. F. Mahon and R. L. Webster, *Organometallics*, 2017, **36**, 2262–2268.
32 H. C. Brown, K. K. Wang and C. G. Scouten, *Proc. Natl. Acad. Sci. U. S. A.*, 77, 698–702.
33 D. J. Nelson, J. D. Egbert and S. P. Nolan, *Dalt. Trans.*, 2013, **42**, 4105.
34 X. Chen, J.-C. Zhao and S. G. Shore, *J. Am. Chem. Soc.*, 2010, **132**, 10658–10659.
35 H. Nöth and S. Thomas, *Eur. J. Inorg. Chem.*, 1999, **1999**, 1373–1379.
36 M. E. Sloan, A. Staubitz, T. J. Clark, C. A. Russell, G. C. Lloyd-Jones and I. Manners, *J. Am. Chem. Soc.*, 2010, **132**, 3831–3841.
37 O. Tsuge, S. Kanemasa, T. Suzuki and K. Matsuda, *Bull. Chem. Soc. Jpn.*, 1986, **59**, 2851–2860.
38 A. Heydari and R. Alijanianzadeh, *Chem Lett*, 2003, **32**, 226–227.
39 E.-C. Wang, K.-S. Huang, H.-M. Chen, C.-C. Wu and G.-J. Lin, *J. Chinese Chem. Soc.*, 2004, **51**, 619–627.
40 G. Rojas and K. B. Wagener, *J. Org. Chem.*, 2008, **73**, 4962–4970.
41 P. Paetzold and R. Truppat, *Chem. Ber.*, 1983, **116**, 1531–1539.
42 D. P. Emerick, F. C. Nahm, K. Niedenzu, L. Komorowski and J. Lipinski, *ZAAC*, 1980, **468**, 44–54.
43 T. E. Hanna, E. Lobkovsky and P. J. Chirik, *Eur. J. Inorg. Chem.*, 2007, **2007**, 2677–2685.
44 C. Summerford and K. Wade, *J. Chem. Soc. A*, 1970, 2010.

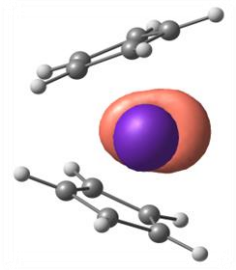
Appendix



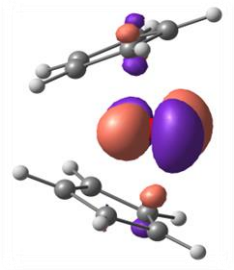
LUMO+2 ($2a_1$)



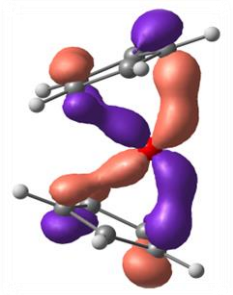
LUMO+3 ($2b_2$)



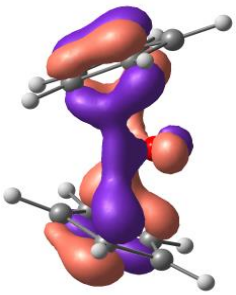
LUMO ($1a_1$)



LUMO+1 ($2b_1$)



HOMO ($1b_2$)



HOMO-1 ($1b_1$)

Figure A1 Selected frontier molecular orbitals of $[Cp_2Ti]^{2+}$ (drawn for $Cp_{cent(1)}$–Ti(1)–$Cp_{cent(2)}$=135.2°. Mulliken symbols are for the approximate C_{2v} symmetry of the fragments. Isosurfaces are drawn at the 0.032 a.u. contour level.[1]

References

1 B. A. Clough, S. Mellino, A. V. Protchenko, M. Slusarczyk, L. C. Stevenson, M. P. Blake, B. Xie, E. Clot and P. Mountford, *Inorg. Chem.*, 2017, **56**, 10794–10814.